NSTX-U FY2015 Year End Report

J. Menard, M. Ono, and the NSTX-U Team

September 11, 2015 – Version 11

Table of contents

Executive Summary of NSTX-U Year-End Report for FY2015

- **Executive Summary for FY2015 Notable Outcomes**
  - *Objective 1.2 "Perform experimental research on NSTX-U to resolve key spherical torus issues at magnetic field, plasma current, and pulse length beyond that achieved in NSTX, after completion of CD-4 for the project"*
    - NSTX-U did not operate during FY2015 due to the ohmic heating coil arc-fault that occurred in April 2015. However, substantial research program planning and operational preparation are in place to support achieving this Notable Outcome in FY2016. The NSTX-U scientific organizational structure was re-organized to have three new over-arching Science Groups: Boundary Science, Core Science, and Integrated Scenarios. This new structure and run-time-incentives were implemented to increase cross-group interaction and shot-planning to increase shot efficiency and scientific productivity. To increase the representation of Universities in NSTX-U scientific management, at least one University representative is now included in leadership of all topical science groups. This has increased the number of collaborating institutions in leadership positions from 4 to 12 from FY2014 to FY2015.
    - This new scientific organizational structure was in place for the NSTX-U 2015 Research Forum and worked very effectively. The total requested run-time for experiments is ~250 days with 55 available implying a record-high factor of 4.5 over-subscription. The 30 highest priority proposals have been identified, 23 of these proposals have been reviewed as of September 5, and all 30 will be reviewed prior to physics operations. Thus, roughly half of the entire FY2016 research campaign experiments will have been reviewed prior to operation.
  - *Objective 1.2 "Provide leadership, coordination, and support to the FES joint research target with the goal of quantifying the impact of broadened current and pressure profiles on tokamak plasma confinement and stability"*
    - NSTX-U supported the FY-15 Joint Research Target by leading and coordinating research activities on the DIII-D, C-Mod, and NSTX-U facilities. Preparation for the JRT-15 started in late CY-2013, potential goals and contributions from NSTX-U were discussed in a first meeting, initial ideas and a tentative plan for the JRT-15 were then discussed in a joint NSTX-U/DIII-D meeting to present opportunities and priorities for collaborative research. Joint work on the physics of steady-state scenarios sustained by neutral beam current drive emerged as the highest priority for NSTX-U and DIII-D to address the JRT-15 goals. C-Mod experiments with lower-hybrid current drive as a means to alter the current profile and improve plasma stability were also included.
    - The delay in NSTX-U operations motivated a shift of activities of NSTX-U researchers toward modeling work targeting specific areas of overlap with experiments conducted on the other two facilities. For NSTX and DIII-D, the modes thought to dominate fast ion transport were toroidal Alfvén eigenmodes. For typical NSTX cases studied, the critical gradient model (CGM) and the experiment were found to be in reasonable agreement and show relatively small losses of 5-10% until large TAE avalanche events. Initial simulations for DIII-D using CGM were unsuccessful with simulations under-predicting the measured deficit in neutron rate by a factor ~2. It was found that other lower-frequency instabilities are present in high q_{min} plasmas in DIII-D, and that such modes must be included in the modeling to improve agreement with measurements.

- *Outcome 3.2 "Develop a plan to continue the NSTX-U/PPPL Theory partnership within projected funding levels"*

  - The FY2015 budgets for NSTX-U and PPPL theory were sufficiently favorable that the NSTX-U/Theory partnership could be sustained. Guiding principles for the topics chosen include: (1) importance to the NSTX-U/ST/tokamak research program, (2) ability of PPPL theory to make contributions that surpass and/or complement NSTX-U non-PPPL collaborator contributions, and (3) ability to dedicate a substantial fraction of time to topic.

  - The topical areas, research, and results most consistent with the above goals include:

    - **Transport and Turbulence:** Development of the GTS gyrokinetic code continued to focus on including electromagnetic effects to be able to study finite-beta effects on turbulence. Global GTS simulations in the electrostatic limit have shown the how the strong parallel flow shear in NSTX can partially suppress low-k Ion Temperature Gradient (ITG) mode turbulence, but at the same time serve as a destabilization mechanism for the Kelvin-Helmholtz instability. Non-linear GTS calculations indicate that ion heat flux values are within a factor of two of the experimental level in the outer half of the plasma and that Dissipative Trapped Electron Modes at high collisionality yields a dependence of electron heat flux that is consistent with that observed experimentally, decreasing transport with decreasing collisionality.

    - **Energetic Particles:** Fast-ion-mode-driven thermal energy transport continued to be studied, and linear HYM simulations showed that core Compressional Alfven Eigenmodes (CAEs) can drive Kinetic Alfven Waves (KAW) at larger minor radius, resulting in energy channeling to electrons from the core to a region of the plasma just outside the main fast ion distribution. Future work will include non-linear HYM simulations to determine a better estimate for the power channeling and impact on electron temperature profiles.

    - **Boundary Physics:** Pedestal transport is a critically important topic, and a new technique to handle electromagnetic effects in the XGC1 code was implemented and benchmarked against the Cyclone case. This "hybrid" algorithm can handle tearing parity modes (i.e., microtearing). Linear electromagnetic XGC1 calculations have been performed to study edge physics in NSTX, and it showed the growth of Kinetic Ballooning Modes at a beta value of 6%, in good agreement with experimental observations of an abrupt change in turbulence correlation length at a beta value of 8%. Future development of XGC1 will include incorporation of kinetic electrons to study trapped electron modes, collisionless tearing and microtearing modes.

    - **Macroscopic Stability:** The non-linear M3D-C1 code has been extended to include a finite thickness resistive wall and full 3D nonlinear simulations of Vertical Displacement Events (VDEs) in NSTX have been performed. New synthetic diagnostics are being added to the code to enable more detailed validation with NSTX magnetics and halo current data. IPECOPT with stellarator optimization tools and also IPEC coupling matrix methods were successfully utilized to find the n=1-6 optimized configuration for neoclassical toroidal viscosity (NTV) with minimized residual resonant fields for the planned NSTX-U off-midplane non-axisymmetric control coils (NCC).

- **Executive Summary for Facility and Diagnostics**

  - NSTX Upgrade Project Accomplishments

    - **CD-4 KPP-1** - In FY 2015, the NSTX-U team continued to make very good progress on the NSTX Upgrade Project. After completion of an integrated systems test procedure (ISTP) on August 10, 2015, in shot 201085 NSTX-U achieved 100kA of plasma current satisfying the CD-4 key performance parameter (KPP) threshold of 50kA necessary for completion of the NSTX Upgrade Project. EFIT equilibrium reconstructions confirmed the plasma current and plasma shape consistent with the camera images. This achieved an important first step toward resuming research operations and using the new capabilities of NSTX-U.

    - **CD-4 KPP-2:** - On May 11, 2015, the NB2 neutral beam system successfully fired 45kV beams with 100 ms pulse lengths for multiple shots, successfully completing the NSTX Upgrade Project CD-4 KPP for Neutral Beam injection into the in-vessel armor at > 40keV beam for > 50 ms. The first cryo-panel regeneration of NB2 was successfully completed.

  - Facility and Diagnostic Milestones

    - **Milestone F(15-1)** - The high-Z tile project using molybdenum alloy "TZM" (Titanium-Zirconium-Molybdenum) is on schedule for installation following the FY16 run campaign. Initial analyses of the first design iteration have been completed. Material procurements have begun after a successful Conceptual Design Review.

    - **Milestone F(15-2)** - Conceptual layout of the divertor cryo-pump (DCP) including the refrigerator and the cryo-lines through the test cell has been performed. Drawing of cryo-system details for components that need to be fabricated has been performed. Layout of in-vessel routing of the cryo-pump has started and the size of the refrigeration system has been scoped. The detailed specification / scope of work for refrigeration systems has been started.

    - **Milestone F(15-3**) - The project for the NSTX-U ECH / EBW High Power 28 GHz RF Source is gyrotron-based and the TFTR Test cell Basement was chosen for its site due to low stray magnetic fields and availability of floor space and ample AC power and water cooling. The conceptual design review for the ECH system is to be held in late September 2015 / early October and the preliminary design completion will follow.

    - **Milestone F(15-4)** - Non-symmetric Control Coil (NCC) design and physics analysis have been continued and extended, in particular by combining the existing mid-plane coils with the off-midplane coils. High-level engineering design and analysis have been conducted. Mineral Insulated Cables (MICs) are a strong candidate for the in-vessel coil application. A procurement requisition is currently in progress to purchase test samples in order to conduct various tests and decide if the MIC can be used for these coil applications.

    - **Milestone D(15-1)** - A major NSTX-U boundary science diagnostic is the Material Analysis Particle Probe (MAPP), and MAPP installation on NSTX-U was completed. Commissioning of this instrument is expected to be finished in October 2015, when execution of the first experimental proposals requiring analysis of MAPP samples are planned.

Operations, Heating Systems, and Diagnostics

- The digital coil protection system (DCPS) has been successfully tested and utilized during the power supply commissioning and integrated testing leading to the achievement of the first plasma and KPP target.

- Substantial progress was made in commissioning the NSTX-U magnetic diagnostics. These sensors were used to support the CS KPP activity, allowing EFIT reconstructions of all discharges. A large number of upgrades to the plasma control system hardware and software were also implemented.

- The NSTX-U gas injection systems on NSTX were improved in the area of divertor heat flux mitigation, and increased levels of gas injection from high-field side. These systems were brought on-line and calibrated in support of CD-4 operations. Three Massive Gas Injection (MGI) valves with the ITER MGI double flyer plate design have been successfully tested in external magnetic fields of 1 T. The upper MGI valve has been installed on NSTX-U.

- A Lithium Safety Peer Review was held at PPPL on June 16 – 18, 2015. The review was part of a US Department of Energy "notable outcome" for the Laboratory for fiscal year 2015. The NSTX lithium evaporator (LITER) system have been remounted and checked for interferences with the upper divertor gap.

- Newly implemented boronization system will enable PFC conditioning prior to lithium, and the ability to inject boron and boron carbide will permit granule injection studies without introducing lithium into NSTX-U.

- All hardware components to enable Transient CHI operations are installed on NSTX-U. An important external system required for initiating CHI discharges is the CHI 2 kV, 40 mF Capacitor Bank. Tests were conducted by operating the system from a local computer that is located near the capacitor bank system.

- The HHFW system installation was completed and steady progress made in commissioning. Significant HHFW related diagnostic upgrades were also performed in FY 2015.

- Installation, calibration, and commissioning of the core diagnostic capabilities including MPTS and CHERS (which are needed to support the FY2016 campaign) have been completed. The Motional Stark Effect-Collisionally Induced Florescence (MSE-CIF) system and the Motional Stark Effect diagnostic based on Laser Induced Fluorescence (MSE-LIF) were commissioned. The core and edge tangential Multi-energy Soft X-ray system (ME-SXR), the midplane tangential Transmission Grating Imaging Spectrometer (TGIS), and the poloidal Ultrasoft X-ray arrays (USXR) are being readied. Both vertical and tangential Fast Ion D-Alpha (FIDA) diagnostics are ready for plasma experiments on NSTX-U. A new and innovative ssNPA system has been installed. Other fast ion diagnostics that were previously available on NSTX have also been reinstalled and tested. Over 20 boundary physics diagnostic systems on NSTX-U are operational and additional ones are being readied.

- **Executive Summary of Research Results – FY15 Milestones**
  - *R(15-1): Assess H-mode energy confinement, pedestal, and scrape off layer characteristics with higher B_T, I_P and NBI heating power*
    - A number of experiments were submitted to the NSTX-U 2015 Research Forum to investigate how increased plasma current, field strength and heating power will influence H-mode energy confinement, local transport, pedestal and scrape-off layer structure, and divertor heat flux width. These experiments will rely upon a number of enhanced diagnostic measurements, and together will be coupled with modeling efforts to expand our physics understanding of core, pedestal, scrape-off-layer (SOL) and divertor physics at higher field, higher power, and presumably reduced collisionality.
    - Recent global nonlinear gyrokinetic simulations using GTS predict a distinct dissipative trapped electron mode (DTEM) in NSTX H-modes with large density gradients. A unique feature of the DTEM is that predicted transport increases with increasing collision frequency in the range relevant for NSTX-U and could be at least partially responsible for the observed energy confinement scaling in NSTX ($\tau_E \sim 1/\nu_*$).
    - Plasma current scans contained in the above transport experiments will also provide new data on the scaling of SOL and divertor heat flux widths at increased plasma current. In addition to Langmuir probes, the divertor measurements will exploit three infrared cameras, including one wide-angle, slow frame rate camera and two dual-band fast frame rate cameras.
  - *R(15-2): Assess the effects of neutral beam injection parameters on the fast ion distribution function and neutral beam driven current profile*
    - In preparation for dedicated experiments on NSTX-U activities focused on the development of improved modeling/analysis tools and of diagnostics to characterize the fast ion distribution function and its evolution as a function of NB injection parameters.
    - Several numerical tools have been improved and validated against NSTX and DIII-D data to provide a more accurate description of the fast ion evolution. Those models have been developed to provide quantitative results also for scenarios with instabilities causing enhanced fast ion transport. Instabilities range from toroidal Alfvén eigenmodes (TAEs) and other Alfvénic instabilities to lower frequency MHD and energetic particle-driven modes such as long-lived kink modes, fishbones and EPMs.
      1. Starting from the ORBIT code, an "hybrid" model has been developed to compute self-consistently the evolution of instabilities and fast ion distribution. Phase and amplitude of each mode are evolved based on the energy exchanged with fast ions. Growth rates and relaxed fast ion profiles are computed dynamically, providing a quantitative estimate of the mode stability and saturation amplitude.
      2. A second approach relies on the notion of a "critical gradient" in the fast ion profile resulting from fast ion transport by instabilities. Required inputs are growth and damping rates, which are obtained for example from linear stability analysis through the NOVA-K and HINST.
      3. A reduced model for fast ion transport ("kick" model) has been implemented in TRANSP and tested against NSTX and DIII-D data. Initial results compare well with experimental results and with predictions from the "critical gradient" model. Extensive validation is ongoing, suggesting further improvements to the model.

- *R(15-3): Develop the physics and operational tools for obtaining high-performance discharges in NSTX-U*

  - Modeling, control tools and experimental planning were conducted in FY2015 to prepare for the realization of high-performance discharges on NSTX-U in FY16. A significant accomplishment was the commissioning of the NSTX-U magnetic field sensors, including the new sensors on the center-stack. This enabled off-line equilibrium reconstructions during the first plasmas on NSTX-U and the ability to qualify the calibrated signals in the real-time plasma control system. This activity is a critical step in actively controlling the plasma shape to achieve high-performance discharges.

  - The realtime EFIT (rtEFIT) code in the plasma control system was updated to incorporate the latest version released by General Atomics and the new magnetic measurement locations on NSTX-U. This new version was tested using input data created by NSTX-U TRANSP simulations where the magnetic field at the location of the magnetic sensors was a constraint to rtEFIT. The reconstruction based on the synthesized magnetic sensor information was in good agreement with the plasma shape from TRANSP providing confidence that an essential tool for active shape control in the PCS is ready to support operations in FY16.

  - A number of experimental proposals that commission control tools necessary for high-performance discharges on NSTX-U completed a full review in FY15, and two XPs that integrate control tools and operational scenarios to develop high-performance plasmas on NSTX-U in FY16 were also approved.

  - Many experiments were also submitted to directly address MHD mode stabilization and control, aiming to directly exploit the new capabilities of NSTX-U in this role. The proposals spanned a large range of topics, all which must be addressed in the new NSTX-U device, and many which will examine the latest advances in mode control capabilities in magnetic fusion as a whole. The proposals range from error field correction to state-space control of key plasma profiles including current profile peaking and beta, plasma rotation, tearing mode stabilization, and passive and active control of unstable RWMs.

- **Executive Summary for Additional Research Highlights**

Boundary Science

➢ Executive Summary of Research Highlights for Pedestal Structure and Control

- The evolution of the H-mode pedestal profiles between edge-localized mode cycles has been studied in-depth in collaborative experiments on Alcator C-Mod and DIII-D. Multiple diagnostics show the onset of quasi-coherent fluctuations during recovery of the edge pressure gradient after an edge-localized mode. Theory suggests that the onset of kinetic ballooning modes is the mechanism that clamps local pressure gradients. The measured gradients are in good agreement with calculations of the kinetic ballooning mode critical gradient in the EPED1 model.

- A detailed comparison between the gas-puff imaging and beam emission spectroscopy diagnostics shows a high degree of similarity in the trends of poloidal correlation lengths, de-correlation times, and velocity estimates for boundary turbulence measured at the same normalized radius. One outstanding difference is a factor of ~7 different in fluctuation levels, with the higher values approaching 15-20% observed in the gas-puff imaging. Resolution of these differences likely requires sophisticated time-dependent modeling and synthetic diagnostics.

- Pedestal modeling studies have advanced, primarily using the XGC suite of kinetic codes. A new formula for the bootstrap current in spherical tokamaks has been derived. Deviation from the well-known Sauter neoclassical formula occurs because of large gyro-radius, large banana-orbit trapped particle fraction, and some unconventional guiding center orbit effects. The suite of codes was also used to better understand Enhanced Pedestal H-modes, an attractive high confinement scenario from NSTX, which will also be explored in NSTX-U.

➢ Executive Summary of Research Highlights for Divertor and Scrape-Off Layer

- Comparisons of the heat flux footprints in ohmic discharges with scrape-off layer turbulence calculations showed that the length and time scales of the turbulence is consistent with resistive ballooning modes; furthermore, H-mode discharges occupy a theoretically expected region of parameter space for profiles very close to the separatrix. Validation of the model predictions is critical, as the model has previously indicated that the inverse scaling of the heat flux footprint width with plasma current may be dominated by turbulence. During transient events, new analysis showed that the heat flux footprint narrowed in NSTX with increasing amplitude of edge-localized modes, qualitatively consistent with NSTX operation along the current-driven kink-peeling mode branch of edge stability space.

- In preparation for experiments with the innovative snowflake divertor configuration, additional equilibrium calculations with new NSTX-U coils were conducted, showing the feasibility of generating desirable magnetic topologies. Edge plasma transport calculations with the UEDGE code were used to determine that the injected argon gas concentration needed to reduce divertor heat flux below 5 MW/m^2 in snowflake and standard configurations

should be ~1-2%. In addition the effect of applied 3-D magnetic perturbations on the snowflake topology, particularly near the X- and strike-point regions, was assessed.

- The effect of externally applied 3-D magnetic fields on the magnetic field line topology near the divertor strike zones was assessed with the IPEC ideal plasma response code. Overall plasma response reduces the amplitude of the stochastic field, but can in some cases amplify the field for low-n perturbations, which is qualitatively consistent with strong striations of divertor heat flux observed in such cases.

- Preparation for NSTX-U operations with a number of new boundary diagnostic capabilities has accelerated. The upgraded and new diagnostics include resistive and infrared imaging bolometry, divertor spectroscopy for impurity evolution from plasma facing components, divertor cameras for radiation and feedback control and thermography, and measurements of edge neutral density and imaging of the lithium granule injector ablation.

➢ Executive Summary of Research Highlights for Materials and Plasma Facing Components

- Substantial progress was made on understanding the behavior of lithium films and interactions on a number of high-Z materials. Deuterium retained in lithium on molybdenum substrates could be reduced by 75% as temperature was increased to 180^{o} C. The presence of oxygen impurities increased the overall retention, and required a temperature of 380^{o} C for desorption. Progress was also made on wetting of liquid lithium on stainless steel substrates.

- The Material Analysis Particle Probe (MAPP) made measurements on the LTX device, in preparation for use in NSTX-U. The new results suggested that lithium-coated stainless steel might be retaining hydrogen in a more weakly-bound state than expected. This is similar to the weaker oxide-bonding observed in laboratory experiments, i.e. that the hydrogen is not bound as Li-H. In addition, material migration and mixed-material evolution studies using the WALLDYN code package for NSTX and NSTX-U were initiated.

- Collaborative experiments conducted on the Magnum-PSI experimental plasma device strongly suggest the 'accepted' temperature limits associated with lithium PFCs, typically ~ 400^{o} C, may be overly pessimistic. In these experiments, lithium layers were evaporated onto TZM samples, and pre-filled liquid metal targets were also tested. It was found that the inferred lithium erosion yield was approximately two orders-of-magnitude less than an adatom-evaporation model in previous studies conducted on the PISCES-B device. These results point to higher acceptable temperature operating windows for lithium on high-Z substrates, as envisioned for NSTX-U.

Core Science

- Executive Summary of Research Highlights for Macroscopic Stability

  - The ideal magnetohydrodynamic (MHD) stability limits of kink modes in tokamak plasmas have been explored in detail for NSTX. Calculations with the DCON code for a large number of experimental equilibria showed that previous estimates of the no-wall limit on the plasma beta and internal inductance were relatively accurate. The no-wall beta limit also decreased with increasing aspect ratio and increasing broadness of the pressure profile. These no-wall beta limit dependencies have implications for NSTX-U which has a larger aspect ratio and new neutral beams that may increase the broadness of pressure and current profiles.

  - The MISK code has been further validated by detailed comparison with experimental results from NSTX. In several discharges the code predicted a transition from damping of the mode to growth as the time approaches the experimental time of plasma disruption via an unstable resistive wall mode (RWM). The main stabilization mechanism is through rotational resonances with the motions of thermal particles in the plasma, though energetic particles also contribute to stability.

  - Joint experiments in NSTX and DIII-D have unified kinetic resistive wall mode physics between the two devices. Analysis of kinetic RWM marginal stability points using the same computational tools (MISK code) show good quantitative agreement between experiment and theory over a wide range of plasma rotation, with RWMs becoming unstable at high as well as low rotation in both devices. Near zero rotation, the linear kinetic calculation can overestimate the plasma stability as non-linear effects can cause destabilization below the computed linear stability points – an important consideration for ITER.

  - Following the call by DOE placing tokamak disruption prediction and avoidance as one of two highest priority research elements in the US fusion program, a new analysis code (DECAF) has been developed for characterization and forecasting of tokamak plasma disruptions. Initial results have produced automated analysis of disruption event chains, and an NSTX-U Working Group has been formed to continually improve analysis performance.

  - The first NSTX-U plasmas that have surpassed DOE CD-4 goals have been reconstructed using a new NSTX-U EFIT model and analysis and a capable set of magnetic diagnostic and coil current input. The model and diagnostics proved to be sufficiently complete and with sufficient stray field compensation to allow reconstructed ohmically heated equilibria with reconstructed wall current significantly larger than the reconstructed plasma currents.

  - The joint efforts to quantify 3D plasma response in tokamaks across theory and experiments in US devices have been extended, and show that ideal MHD approximations are widely valid but kinetic and rotational effects can be important especially in high-β operational regimes. The ideal responses measured by upgraded sensors in DIII-D below the no-wall β limit were successfully reproduced by IPEC, MARS-F, VMEC, and M3D-C1, with only minor differences, and the responses across and beyond no-wall limit for both DIII-D and NSTX were also quantitatively explained by kinetically self-consistent calculations using MARS-K.

- The self-consistent calculations with drift-kinetic effects using MARS-K were numerically verified with a new code – the general perturbed equilibrium code (GPEC), by showing good agreement between computed eigenfunctions. GPEC applications to NSTX-U predicted the well-known trend of resonant field amplification (RFA) across the no-wall limit, and further a new trend near the kinetic no-wall limit with finite response amplitude. The two important aspects of kinetic response, modified amplitude and toroidal phase shift due to the torque, can be efficiently studied by Nyquist diagram by scanning applied field frequency. MARS-K applications to NSTX-U reveal the characteristic shapes and poles of the diagram depending on kinetic and fluid models, and will be tested in DIII-D and NSTX-U experiments.

- A state-space algorithm for plasma rotation control was expanded to include actuation by neutral beam injection and the unique use of NTV torque in closed-loop feedback on a target rotation profile. The capabilities of the control algorithm and the dynamics and steady-state capabilities were examined for an improved NTV model including the observed strong dependence on ion temperature. The controller is projected to achieve steady-state rotation profiles for a wide range of ion temperatures.

- NSTX-U Non-axisymmetric Control Coil (NCC) physics design has continued and extended, in particular by including the existing midplane coils with the planned off-midplane coils. The three rows of coils can produce highly coherent perturbations at the outboard section without a gap between the coils, and thus better align and control the perturbation relative to the field lines. For resistive wall mode (RWM) control capability by NCC, the sensors were successfully optimized, and VALEN3D predicts that the active RWM control can stabilize plasma even near the ideal wall limit if the optimized sensors and gains are combined with NCC. TRIP3D analysis shows 2x6 partial NCC should achieve ELM suppression and interesting combinations of high-n islands when more coils are added.

- The nonlinear 3D Extended MHD code M3D-C1 has been extended to include a finite thickness resistive wall. Full 3D nonlinear simulations of Vertical Displacement Events (VDEs) in NSTX have been performed. New synthetic diagnostics are being added to the code to enable detailed validation with NSTX magnetics and halo current data.

- NSTX-U will employ three Massive Gas Injection (MGI) valves that are very similar to the double flyer plate design being considered for ITER. NSTX-U will be the first device to operate this valve design in plasma discharges. These valves have been tested off-line and deliver the required amount of gas to support NSTX-U experiments, which will offer new insight to the MGI data base by studying gas assimilation efficiencies for MGI gas injection from different poloidal locations, with emphasis on injection into the private flux region. The valve has also been successfully operated in external magnetic fields of 1 T.

- A novel disruption mitigation system based on the rail-gun concept has been designed, and plans for an off-line experimental test are in progress. This device - referred to as an Electromagnetic Particle Injector (EPI) - is fully electromagnetic, with no mechanical moving parts, which ensures high reliability after a long period in standby. Scoping studies conducted during 2015 show that in addition to responding on the required fast time scale, its performance substantially improves when operated in the presence of high magnetic fields. The system is also suitable for installation in close proximity to the reactor vessel.

- Executive Summary of Research Highlights for Transport and Turbulence

  - In some NSTX H-mode plasmas, the high-k fluctuation power (measured by coherent microwave scattering) was observed to decrease and shift to higher perpendicular wave-number with increasing density gradient, even though the electron temperature gradient remained well in excess of the linear ETG threshold. Nonlinear gyrokinetic simulations (GYRO) show that increasing the density gradient reduces the predicted transport and shifts the nonlinear turbulent spectra to higher poloidal wave number, qualitatively supporting the experimental observation of nonlinear density gradient stabilization of ETG turbulence (i.e. beyond well-known linear threshold effects). (Collaboration with MIT)

  - Global nonlinear gyrokinetic simulations (GTS) predict a distinct dissipative trapped electron mode (DTEM), with transport increasing with increasing collision frequency, in some NSTX H-mode discharges where large density gradients locally suppress ETG turbulence. While these DTEM simulations are based on discharges somewhat different than those used for energy confinement scaling studies, they provide an additional theoretical microturbulence mechanism (in addition to microtearing modes) that could be at least partially responsible for the observed energy confinement scaling in NSTX, $\tau_E \sim 1/\nu_*$ (to be tested in FY2016).

  - Recent ORBIT modeling indicates that compressional and global Alfven eigenmodes (CAE, GAE) can cause a net radial convection (due largely to trapped electrons), in addition to the previously predicted diffusion by orbit stochastization. In core regions where large χ_e has been inferred, the predicted convection can dominate electron thermal diffusion.

  - "Stiff" electron thermal transport (large changes in transport and turbulence for small changes in driving gradients) was observed in a set of RF-heated L-mode plasmas. Electron-scale fluctuation amplitudes, as measured by the high-k scattering system at r/a~0.6, were reduced significantly following the cessation of RF heating. Gradient-driven nonlinear gyrokinetic simulations investigating local stiffness (GYRO) or finite-ρ_* global effects like turbulence spreading (GTS) are unable to reproduce the observed behavior. It is hypothesized that flux-driven simulations may be required to explain the apparent stiffness.

  - Recent analysis of perturbative momentum transport experiments in MAST L-modes indicate the existence of a momentum pinch comparable to values inferred in NSTX H-modes. Gyrokinetic calculations are being used to assess whether the pinch is consistent with the Coriolis pinch mechanism. This mechanism was unable to explain the pinch in the NSTX H-modes due to the predicted dominance of fundamentally electromagnetic microtearing and kinetic ballooning modes (KBM), motivating the lower beta MAST L-mode and planned NSTX-U L-mode experiments for FY2016. Additional linear gyrokinetic simulations for NSTX H-modes predict that the influence of centrifugal effects on momentum transport can rival the Coriolis pinch for unstable ITG-KBM modes, an effect that will be explored further.

  - Recent analysis has shown that the previously observed deviation in intrinsic carbon transport from neoclassical theory (near r/a~0.7) in lithiated ELM-free discharges is eliminated when ELMs are triggered using externally applied 3D fields. This is due to the recovery of main ion profiles similar to natural ELMy H-mode discharges. To further investigate the anomaly in the lithiated ELM-free cases, gyrokinetic predictions of quasilinear carbon flux for unstable ITG-KBM modes were investigated (using GKW, collaboration with U-Bayreuth). Most

notably, these predictions indicate that both roto-diffusion (impurity flux driven by rotation gradient) and centrifugal effects for the unstable ITG-KBM modes can cause a large outward convection and corresponding locally hollow carbon profile comparable to experiment.

- A new python-based interface to the STRAHL impurity transport code, including a model for neo-classical/anomalous transport in combination with atomic data from the ADAS database, has been developed to predict synthetic core/edge multi-energy soft X-ray (ME-SXR) for comparison with measurements planned for FY2016. Modeling of edge electron density and temperature measurements using the ratio of helium line emission has been tested on RFX-mod, using the system that will be installed for future NSTX-U experiments (FY2016 or FY2017). Models have also been developed to quantify impurity densities from beam plasma charge-exchange and background Bremsstrahlung emission, measured in the XUV spectral range using the upgraded Transmission Grating Imaging Spectrometer (TGIS).

- NSTX-U researchers contributed to analysis and gyrokinetic simulations of the DIII-D National Fusion Science Campaign experiment "Controlling H-mode particle transport with ECH". NSTX researchers were also instrumental in the development and implementation of a synthetic Doppler Back Scattering (DBS) diagnostic to apply to gyro-kinetic simulations for comparison to experiment. This work has provided substantial experience and basis for (i) studying density profile control in NSTX-U using RF heating, (ii) investigating parallel velocity gradient driven instabilities in NSTX-U, and (iii) analysis of DBS measurements expected to be developed during NSTX-U operations.

➢ Executive Summary of Research Highlights for Energetic Particles

- New modeling tools have been developed and validated to provide an accurate description of the fast ion evolution even when instabilities cause substantial fast ion transport. Two models are available, based on a "Critical Gradient" approach for the relaxed fast ion profile and on a "transport probability" for fast ion evolution in phase space. A preliminary comparison between the two models for NSTX and DIII-D data shows satisfactory agreement. This work addresses Research Milestone R(15-2) and JRT-15.

- A database has been compiled to characterize stability boundaries for several classes of energetic particle driven instabilities in NSTX. Recent work has focused on including MSE-constrained q-profile and rotational shear information in the database. This contributes to separate stability regions for different instabilities. The database will be further expanded for the new operating regimes accessible on NSTX-U as operations resume.

- The onset of a so-called "bursting/chirping" regime for Alfvénic instabilities is typically associated with enhanced fast ion transport. A theory based on hole-clump formation in phase space has been tested for NSTX plasmas, based on mode stability analysis performed through the NOVA-K code. The results indicate that the theory, which is based on a single-resonance idealized scenario, is not enough to properly predict the onset of strongly unstable regimes. Work is in progress to extend the previous theory to account for the presence of multiple resonances over fast ion phase space.

- Non-linear, self-consistent simulations of TAE and fishbone instabilities for NSTX have been performed through the M3D-K code. The simulations show a strong interaction between

TAEs and the fishbone, resulting in either increase or decrease of the mode saturation level depending on the mode spectrum and frequencies. As beam beta increases above a threshold, saturation levels increase sharply and global fast ion transport occurs, similarly to what is observed experimentally.

- A new method to investigate the saturation level for Alfvénic modes has been developed. Starting from ORBIT code simulations, energy exchange between fast ions and the instabilities is computed and used to feed-back on mode evolution and the fast ion distribution. The method is being applied to TAE modes on NSTX and will then be extended to DIII-D and ITER scenarios.

- Suppression of Alfvénic modes by High Harmonic Fast Wave heating has been investigated. Modes were reproducibly stabilized for long periods of time for injected HHFW power in excess of 1.5MW. The abrupt return of mode activities at HHFW turn-off suggests that modifications to the fast ion distribution, resulting in mode suppression, were relatively small, or that HHFW directly interferes with the resonant drive of the modes.

- Analysis tools for the interpretation of fast ion diagnostics data have been improved. A new "3D Halo" model implemented in TRANSP provides more accurate estimates of the halo neutrals distribution around the Neutral Beam volume, and a technique has been developed for the analysis of FIDA and ssNPA data through the FIDAsim code for extended data sets. The new technique has been applied to a NSTX database, suggesting measurable flattening of the fast ion profile by Alfvénic and other fast ion driven MHD instabilities.

Integrated Scenarios

➢ Executive Summary of Research Highlights for Solenoid-Free Start-up and Ramp-up

- All hardware components to enable Transient CHI operations have been installed on NSTX-U and the re-furbished CHI capacitor bank systems has undergone full power tests into a dummy load to prepare it for CHI plasma operations.

- Modeling that combines TRANSP with TORIC and GENRAY suggest, among other things, that start-up should begin using longer wavelength fast wave antenna phasing during the EC pre-heating to maximize electron heating and then transitioning to shorter wavelength phasing to reduce absorption by fast ions and to maximize absorption by electrons.

- NIMROD simulations aimed at better understanding of the reconnection processes during transient CHI discharges have identified a new mechanism for reconnection in NSTX CHI discharges. In this mechanism, an elongated current sheet that forms during CHI can spontaneously break up into plasmoids through a mechanism known as "Plasmoid Instability" could play an important role in large volume closed flux formation.

- In an effort lead by the NSTX-U CHI Team, during the past year all necessary CHI hardware, including the US procured primary ceramic insulators, were successfully installed on the QUEST vacuum vessel in Kyushu University.

- During FY15 a Topical Review Paper on solenoid-free plasma start-up in spherical tokamaks was written that summarizes the state of research for solenoid-free plasma start-up methods.

- Executive Summary of Research Highlights for Wave Heating and Current Drive

  - Four experimental proposals were allocated runtime: characterizing the scrape-off layer losses of high harmonic fast wave (HHFW) power in H-mode plasmas, the absorption of HHFW power by fast and thermal ions, generating low-current fully non-inductive plasmas heated with HHFW, and a novel technique for obtaining 2D images of the HHFW wavefield.

  - NSTX-U HHFW system sources 3 – 6 have been recommissioned for operation, and steady progress is being made in restoring Sources 1 and 2. The new compliant center conductors have been installed, and vacuum tuning was successful.

  - Diagnostic upgrades are underway: (1) divertor Langmuir probes to measure RF rectification, (2) an IR camera to monitor heat loads to the antenna (3) the ORNL SOL reflectometer for density profile measurements, and (4) various midplane probes in the vicinity of the antenna.

  - Recent analysis suggests that RF rectification is playing a role in the deleterious SOL losses of HHFW power. Experiments on NSTX-U have been planned around this work, and an experiment on the UCLA Large Plasma Device (LAPD) is also being proposed.

  - The full-wave code AORSA shows higher SOL power losses when the FW cut-off is moved away from the antenna. These previous 2D results were verified using 3D simulations and extended to tokamaks with conventional geometry. DIII-D results agree with NSTX results and previous experiments, but results for Alcator C-Mod and EAST, which use hydrogen minority heating, differ.

  - A cylindrical cold-plasma model of fast-wave propagation in NSTX-like conditions has been benchmarked against previous models. The computed RF voltage in the SOL is roughly consistent with Langmuir probe data. The model also computes significant wave power propagating in the edge of the plasma similar to experimental observations and full-wave simulations using the AORSA code.

  - Predicting the heating of future devices such as ITER depends on accurate calculations of the ICRF power absorption partition by different plasma species. A detailed comparison between four European ICRH codes plus AORSA shows that power absorption trends (as a function of minority concentration) agree reasonably well and improve for low electron absorption.

  - A megawatt-level 28 GHz electron cyclotron (EC) heating system is planned for NSTX-U, and scoping studies have sited the gyrotron in the TFTR Test Cell Basement where magnetic fields (measured during full coil field tests) will not affect the gyrotron operation. The gyrotron design development has advanced from 1.2 MW for 0.1 sec to >1.5 MW for 2 seconds. The waveguide design has been completed and is expected to deliver 90% or more of the gyrotron power to the antenna input.

- Executive Summary of Research Highlights for Advanced Scenarios and Control

  - Coil currents for plasma startup on NSTX-U were developed using time-dependent modeling of the magnetic fields with the LRDFIT code including the new vessel geometry and conducting structures. The startup scenario that produced first plasma was in good agreement with the target scenario developed using time-dependent modeling.

  - XMP-100 and XMP-131 produced the first plasma operation on NSTX-U in order to satisfy the KPP CD-4 upgrade milestone. Plasma currents up to 140 kA and lasting up to 40ms were achieved using pre-programmed coil currents. This demonstrated the integrated readiness of many critical systems, including the plasma control system.

  - Advanced Scenarios and Control TSGs will lead a large number of XMP and XPs that commission operational plasma control tools on NSTX-U. These activities including active vertical stability, X-point position, and neutral beam injection control will occur early in the upcoming NSTX-U campaign and many of these proposals have completed the necessary reviews and are approved to run.

  - ASC run time priorities for FY16 include the development of scenarios that utilize the new capabilities of NSTX-U. These include high non-inductive fraction plasmas, discharge lengths lasting many seconds and a stable snowflake configuration.

  - Fully non-inductive startup, ramp-up and sustainment scenarios for NSTX-U have been explored using time-dependent free-boundary simulations with TRANSP. The results motivate development of an electron cyclotron RF source and dynamic antenna phasing on the existing higher-harmonic fast wave system on NSTX-U to maximize the available non-inductive current drive early in the discharge when the plasma density is too low for efficient neutral beam coupling.

  - Advances in integration of plasma control algorithms with TRANSP and the free-boundary equilibrium ISOLVER calculation in a robust, user-friendly closed-loop software architecture allowed for verification of updates and improvements to the real-time EFIT (rtEFIT) code in the plasma control software.

  - The platform integrating control tools with TRANSP has been used to develop viable current profile control algorithms that utilize the second neutral beam on NSTX-U. Experiments are planned for the upcoming run that will inform and test the simulation of this advanced control capability.

  - A large effort toward improving the consistency, maintainability and reliability of the plasma control software was completed in FY15 in order to incorporate new control capabilities on NSTX-U and enable future growth of the software.

Performance of FY2015 Notable Outcomes:

Objective 1.2 *"Perform experimental research on NSTX-U to resolve key spherical torus issues at magnetic field, plasma current, and pulse length beyond that achieved in NSTX, after completion of CD-4 for the project"*

NSTX-U did not operate during FY2015 due to the ohmic heating coil ground-plane lead arc-fault that occurred in April 2015. However, substantial research program planning and operational preparation were in place to support operations in FY2015. This preparation places NSTX-U in a very good position to carry out a comprehensive research program in FY2016 and to meet all FY2016 research milestones including the FY2016 notable outcome Objective 1.2 which is identical to this FY2015 notable outcome. The preparation for experimental scientific research is summarized here, and the extensive facility, diagnostic, and operational preparation is describe in later sections of this year-end report.

The first major change to the FY2015-16 research program was to re-organize the scientific leadership and management structure as shown in Figure NO-1-1. In particular, the previous 7-8 semi-independent Topical Science Groups (TSGs) were re-organized to be elements of three new over-arching Science Groups (SGs): Boundary Science, Core Science, and Integrated Scenarios. This new structure and run-time-incentives were implemented to increase cross-TSG interaction

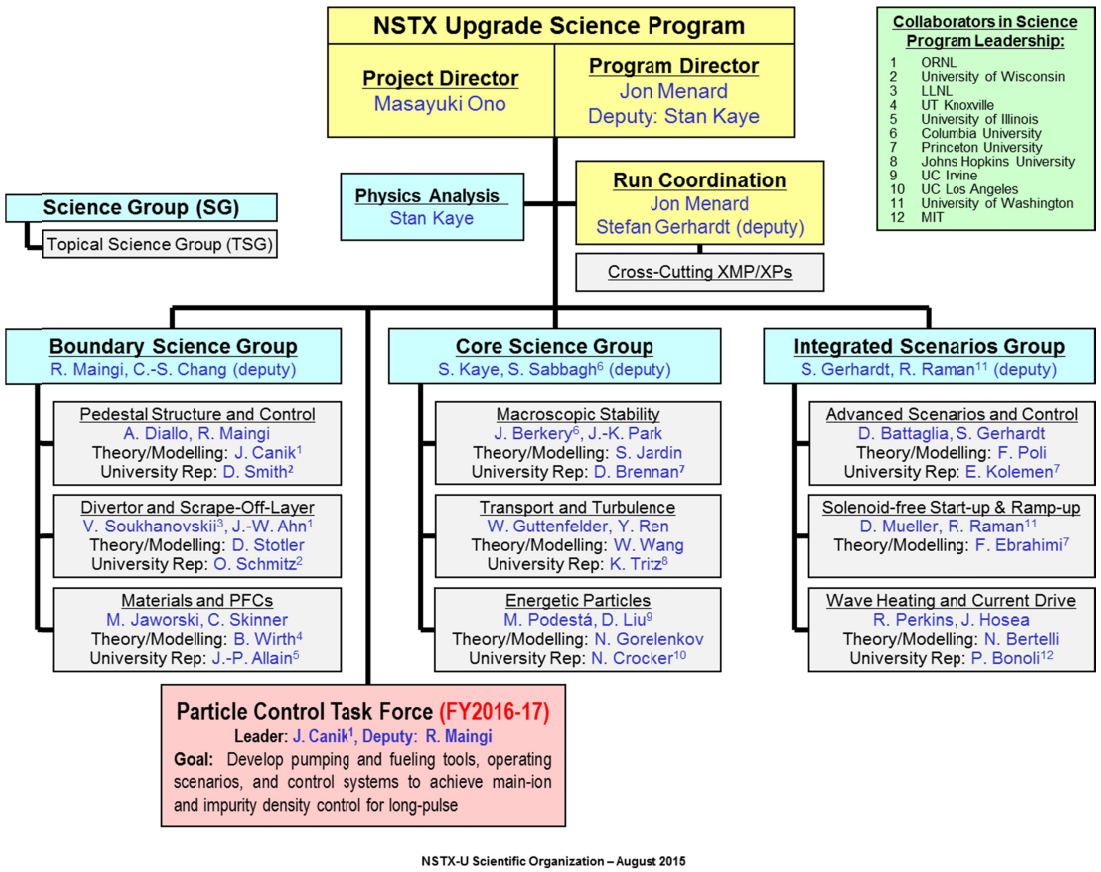

Figure NO-1-1: *NSTX-U Scientific Organization as of September 2015.*

and shot-planning and sharing to increase shot efficiency and scientific productivity. This new structure also placed top NSTX-U scientific leaders in positions of increased authority and accountability, and thus far has significantly increased coherence within the SGs. For example, the core SG has developed several experimental proposals that will each provide data for several TSGs and other SGs in support of FY2016 research milestones. This new organizational structure is also reflected in the structure of this FY2015 year-end report.

The new organizational structure also now provides optional "Task Forces" (TFs) which have a specific operational and/or scientific goal that cuts across several SGs, have a 2-3 year life-span, and reports directly to the NSTX-U Program and Project Directors. Given the critical need for improved density and impurity control for long-pulse operation in NSTX-U, a Task Force was created to directly address this issue. Finally, in order to increase the representation of Universities in NSTX-U scientific management, at least one University representative is now included in leadership of all TSGs, and this has substantially increased the number of collaborating institutions in leadership positions from 4 to 12 from FY2014 to FY2015.

Baseline (12+4 weeks) # run weeks:	16											
Estimated total # run days:	80											
Estimated XMP run-days	25	Cross-cutting commissioning, shot development, calibrations (may not include TSG-specific XMPs)										
Reserve for multi-TSG XPs	10											
Contingency / director's reserve	5											
Nominal total days for TSG/TFs to prioritize	50											
Minimum # run days per TSG / TF	2.5										Priority #1 fraction	
Milestone weighting for FY15-early FY16 run	0.75	0.25									0.75	
	TSG / Task Force	FY 15 Milestones	FY16 Milestones	FY15 count	FY16 count	Milestone additional runtime	Forum Idea Count Increment	Nominal TSG / TF run days for single TSG XPs	Nominal TSG / TF run days for multi-TSG XPs	Nominal TSG / TF run days for all XPs	Nominal Priority 1 XP run time	Nominal Priority 2 XP run time
Boundary	Pedestal	R15-1		1	0	0.75	0.5	3.5	1	4.5	3.5	1
	Divertor and SOL	R15-1	R16-1	1	1	1	1	4.5	1	5.5	4	1.5
	Materials and PFCs		R16-2		1	0.25	0	2.5	1	3.5	2.5	1
Core	Macroscopic Stability	JRT-15, R15-3	JRT-16	2	1	1.75	1	5	1	6	4.5	1.5
	Transport & Turbulence	JRT-15, R15-1		2	0	1.5	0.5	4.5	1	5.5	4	1.5
	Energetic Particles	JRT-15, R15-2	R16-3	2	1	1.75	0.5	4.5	1	5.5	4	1.5
Scenarios	Advanced Scenarios and Control	Notable, JRT-15, R15-2, R15-3	JRT-16, R16-4	4	2	3.5	1	7	1	8	6	2
	Solenoid-Free Start-up		R16-4	0	1	0.25	0	2.5	1	3.5	2.5	1
	Wave Heating and Current Drive		R16-3	0	1	0.25	0	2.5	1	3.5	2.5	1
Task Forces	Particle Control	R15-3		1	0	0.75	0.5	3.5	1	4.5	3.5	1
						Total:		40	10	50	37	13

Figure NO-1-2: *Run-time guidance at 2015 Research Forum*

This new scientific organizational structure was in place for the NSTX-U 2015 Research Forum and worked very effectively. At the Forum, and following the plenary session which outlined forum goals and defined the Science Group meeting agendas, all 9 topical science groups met in 3 parallel sessions, while the cross-cutting particle control task-force was stand-alone to enable participation by all forum participants. All TSGs and TFs were requested to follow the run-time guidance shown in Figure NO-1-2. Following the TSG parallel sessions, the SGs then met in 3 parallel sessions to identify overlap and possible consolidation among the three TSGs of each SG. From these discussions resulted several experimental proposal ideas to generate data that could be shared across multiple TSGs and SGs. The meeting concluded with Science Group summaries and a draft Run Plan presented by the run coordinator based upon the draft prioritization.

As shown in Figure NO-1-2, it is expected there will be approximately 55 run days available in the FY2016 run campaign dedicated to experimental proposals. As evident in Figure NO-1-3 the total requested run-time for experiments is ~250 days implying a record high request in run-time by a factor of 3.4× including commissioning time and 4.5× for dedicated scientific experiments.

Topical Science Group or Task Force	Run Days Requested	Fraction
Macroscopic Stability (MS)	40.75	14.9%
Cross-cutting and Enabling (CC)	34.85	12.8%
Divertor and Scrape-off-layer (DS)	33.5	12.3%
Advanced Scenarios and Control (ASC)	33	12.1%
Pedestal Structure and Control (PS)	25	9.2%
Particle Control Task Force (PC)	23	8.4%
Energetic Particles (EP)	22.5	8.3%
Turbulence and Transport (TT)	21	7.7%
Materials and PFCs (MP)	15.5	5.7%
Solenoid-free Start-up and Ramp-up (SR)	14.5	5.3%
Wave Heating and Current Drive (RF)	9	3.3%
	272.6	100%

#	Institution	Run Days Requested	Fraction
1	Princeton Plasma Physics Laboratory	112.1	41.1%
2	Oak Ridge National Laboratory	28.5	10.5%
3	Princeton University	20.5	7.5%
4	Lawrence Livermore National Laboratory	18	6.6%
5	General Atomics	17	6.2%
6	ITER (France)	12	4.4%
7	University of Washington	11.5	4.2%
8	Columbia University	10.5	3.9%
9	University of Wisconsin	9	3.3%
10	University of California - Irvine	7.5	2.8%
11	Nova Photonics	6	2.2%
12	University of Illinois	4	1.5%
13	Massachusetts Institute of Technology	4	1.5%
14	University of California - San Diego	3	1.1%
15	Johns Hopkins University	3	1.1%
16	University of Tennessee	2	0.7%
17	Lehigh University	1	0.4%
18	Florida International University	1	0.4%
19	University of California - Los Angeles	1	0.4%
20	University of York (United Kingdom)	1	0.4%
		272.6	100%

Requested / Available Run Time:
Total: 273 / 80 = 3.4×
Research: 248 / 55 = 4.5×

84 unique lead author names

Figure NO-1-3: *Run-time requested by topic (left) and by institution (right)*

	XP number	XP title	Responsible Group	XP author first name	XP author last name	XP author e-mail	Priority	Run Weeks 1-4	Run Weeks 5-8	Run Weeks 9-12	Run Weeks 13-16
▶	1501	Optimization of vertical control algorithm	ASC-TSG	Dan	Boyer	mboyer@pppl.gov	P1a	1			
	1502	Tuning of the Automated Rampdown Software	ASC-TSG	Stefan	Gerhardt	sgerhard@pppl.gov	P1c	1			
▶	1503	X-point control integration with shape control	ASC-TSG	Egemen	Kolemen	ekolemen@princeton.edu	P1a	1			
▶	1504	Beam power and beta-N control	ASC-TSG	Dan	Boyer	mboyer@pppl.gov	P1b	0.5	0.5		
▶	1505	Optimizing Boronization XMP	MP-TSG	Charles	Skinner	cskinner@pppl.gov	P1a	0.5	0.5		
▶	1506	Low-beta, low-density locked mode studies	MS-TSG	Clayton	Myers	cmyers@pppl.gov	P1a	0.25	0.75		
▶	1507	Maximizing the non-inductive current fraction in NSTX-U H-modes	ASC-TSG	Stefan	Gerhardt	sgerhard@pppl.gov	P1a		0.5	0.25	0.25
▶	1508	Controlled Snowflake Studies	ASC-TSG	Egemen	Kolemen	ekolemen@pppl.gov	P1b		0.25	0.5	0.25
▶	1509	Combined betaN and li feedback control	ASC-TSG	Dan	Boyer	mboyer@pppl.gov	P1b		0.25	0.25	0.5
	1510	Characterizing the SOL Losses of HHFW Power in H-Mode Plasmas	RF-TSG	Rory	Perkins	rperkins@pppl.gov	P1a		0.5	0.25	0.25
	1511	Multi-machine studies of the L-H power threshold dependence on aspect ratio	PS-TSG	Michael	Bongard	mbongard@wisc.edu	P1b		1		
▶	1512	Characterization of the Pedestal Structure as function Ip, BT, and Pnbi	PS-TSG	Ahmed	Diallo	adiallo@pppl.gov	P1a		0.5	0.5	
	1513	Effects of B-> Li transition on the pedestal structure	PS-TSG	Rajesh	Maingi	rmaingi@pppl.gov	P1a		0.5	0.5	
	1514	Heat flux and SOL width Scaling in NSTX-U	DS-TSG	Travis	Gray	tkgray@pppl.gov	P1a		0.25	0.5	0.25
▶	1515	High-beta n=1,2,3 feed-forward error field correction	MS-TSG	Clayton	Myers	cmyers@pppl.gov	P1a		0.5	0.5	
▶	1516	Optimization of PID dynamic error field correction	MS-TSG	Clayton	Myers	cmyers@pppl.gov	P1a		0.5	0.5	
▶	1517	Neoclassical toroidal viscosity at reduced collisionalty (independent coil control)	MS-TSG	S.A.	Sabbagh	sabbagh@pppl.gov	P1a		0.25	0.5	0.25
▶	1518	RWM PID control optimization based on theory and experiment	MS-TSG	S.A.	Sabbagh	sabbagh@pppl.gov	P1a		0.25	0.5	0.25
	1519	Massive Gas Injection Studies on NSTX-U	MS-TSG	Roger	Raman	raman@aa.washington.edu	P1a			0.5	0.5
▶	1520	Ip/Bt scaling	TT-TSG	Stan	Kaye	kaye@pppl.gov	P1a		0.5	0.25	0.25
▶	1521	Validation of gyrokinetic codes in NSTX-U NBI-heated L-mode plasmas	TT-TSG	Yang	Ren	yren@pppl.gov	P1a		0.5	0.25	0.25
▶	1522	Beam ion confinement of 2nd NBI	EP-TSG	Deyong	Liu	deyongl@uci.edu	P1a		0.75	0.25	
▶	1523	Characterization of 2nd NBI line	EP-TSG	Mario	Podesta	mpodesta@pppl.gov	P1a		0.25	0.5	0.25
▶	1524	AE Critical Gradient	EP-TSG	Bill	Heidbrink	wwheidbr@uci.edu	P1a		0	0.25	0.75
▶	1525	Rotation effects on CAEs and GAEs	EP-TSG	Neal	Crocker	ncrocker@physics.ucla.edu	P1a				1
	1526	Establish heat transmission pathways in high-Z reference shape	MP-TSG	Michael	Jaworski	mjaworsk@pppl.gov	P1a		0.25	0.25	0.5
▶	1527	ELM pacing via multi-species granule injection and 3D field application for main ion c	PC-TF	Robert	Lunsford	rlunsfor@pppl.gov	P1a		0.75	0.25	
▶	1528	Characterize plasma near planned plenum entrance position	PC-TF	John	Canik	canikjm@ornl.gov	P1a		0.75	0.25	
▶	1529	Controlled introduction of Lithium into NSTX-U	PC-TF	Rajesh	Maingi	rmaingi@pppl.gov	P1a		0.5	0.5	
▶	1530	Triggering ELMs with LGI and 3-D fields in lithiated discharges	PC-TF	Robert	Lunsford	rlunsfor@pppl.gov	P1a			0.75	0.25

Figure NO-1-4: *Summary of the 30 highest priority experimental proposals for the NSTX-U FY2016 research campaign including title, TSG/TF responsible, proposal author information, and when during the campaign the experiment is likely to be run. Proposals already reviewed are indicated by the black triangle ▶.*

The 30 highest priority experimental proposals (XPs) identified at the research forum and in subsequent planning meetings are summarized in Figure NO-1-4 and many of these XPs are described in later parts of this report. 23 XPs have been reviewed as of September 5, and all 30 will have been reviewed prior to starting physics operations. Thus, the NSTX-U program is very well prepared for scientific research, as roughly half of the entire FY2016 research campaign experiments will have been reviewed prior to operation.

Objective 1.2 *"Provide leadership, coordination, and support to the FES joint research target with the goal of quantifying the impact of broadened current and pressure profiles on tokamak plasma confinement and stability"*

NSTX-U supported the FY-15 Joint Research Target by leading and coordinating research activities on the DIII-D, C-Mod and NSTX-U facilities. The Coordination Committee was composed by M. Podestà and S. Gerhardt (NSTX-U, leader and deputy), C. Holcomb and W. Solomon (DIII-D, leader and deputy), G. Wallace and S. Scott (C-Mod, leader and deputy).

Preparation for the JRT-15 started in late CY-2013 with two meetings at PPPL. Potential goals and contributions from NSTX-U were discussed in a first meeting, based on previous brainstorming sessions of the NSTX-U Topical Science Groups. Initial ideas and a tentative plan for the JRT-15 were then discussed in a joint NSTX-U/DIII-D meeting, in which opportunities and priorities for collaborative research were presented. From these initial meetings, joint work on the physics of steady-state scenarios sustained by Neutral Beam current drive emerged as the highest priority for NSTX-U and DIII-D to address the JRT-15 goals. Once C-Mod operations were also confirmed for FY-15, the experimental plans have been naturally extended to include lower-hybrid current drive as a means to alter the current profile and improve plasma stability and performance.

The initial scoping activities to identify possible experiments and analysis tasks resulted in the definition of the 4 Quarterly Milestones in early FY-14, followed by teleconferences of the Coordination Committee and by Team meetings at the three facilities throughout FY-15 to assess progress and future plans. Plans for specific experiments on NSTX-U and DIII-D were discussed at Research Forums during the Second Quarter and finalized in the following months. C-Mod plans were defined through the FY-15. Figure JRT-15-1 shows an overview of the JRT-15 calendar.

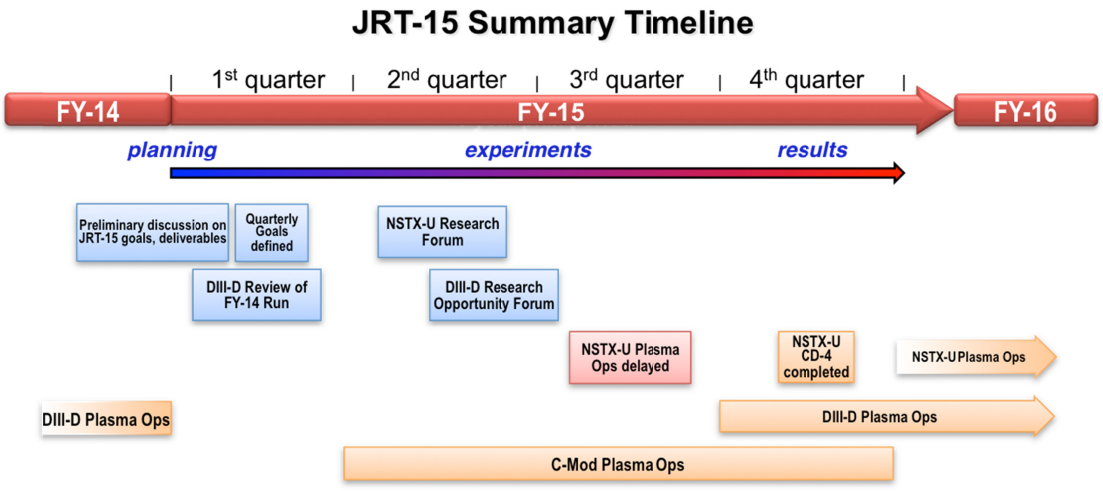

Figure JRT-15-1: *Summary timeline of JRT-15 related activities on the 3 facilities during FY-15.*

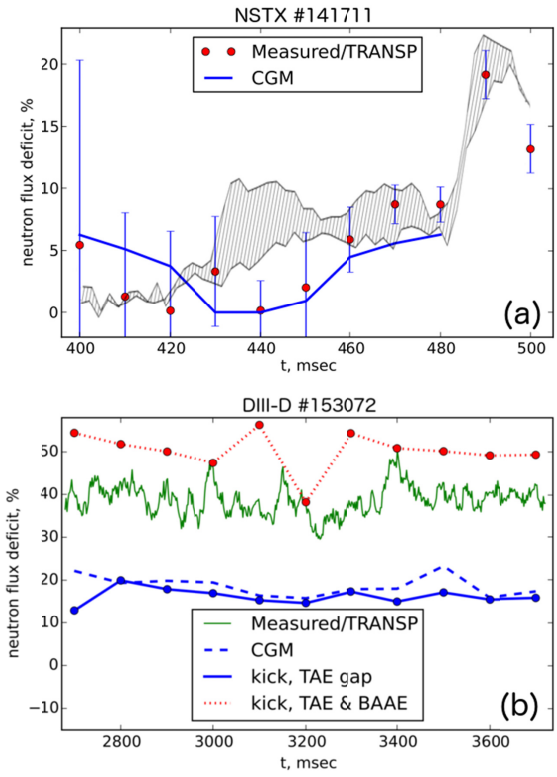

Figure JRT-15-2: *Validation of fast ion transport models for NSTX discharge #141711 and DIII-D discharge #153072. Red dots show the measured neutron rate deficit with respect to "classical" TRANSP simulations. Solid blue line shows results from a "critical gradient" model. The dashed region shows results from a "kick" model recently implemented in NUBEAM/TRANSP.*

In general, the goals for the four Quarters transitioned from organization/planning to experimental activities and analysis with all three facilities expected to contribute with experimental results. However, a hardware failure (OH arc fault) during NSTX-U re-commissioning in the third Quarter led to a revision of the NSTX-U plans for the remainder of FY-15. The delay in machine start-up motivated a shift of activities towards modeling work, targeting specific areas of overlap with experiments conducted on the other two facilities. An example of the achievements for a joint NSTX-U and DIII-D modeling activity is given below.

The example refers to the validation of improved tools to model fast ion transport in NB-heated plasmas. The necessity of modeling accurately the fast ion evolution has been confirmed by recent experiments on both DIII-D and NSTX. For those experiments, the role of fast ions is crucial to quantify overall plasma performance (e.g. in terms of confinement factor *H* and NB current drive efficiency), in particular when instabilities may affect the fast ion distribution. Two models have been developed to account for the effects of instabilities, see "Milestone R(15-2)" and "Summary of EP Research" for more details. Figure JRT-15-2 shows results of the validation of the two models, which are in reasonable agreement for both machines.

For the NSTX case, the model and the experiment show relatively small losses of 5-10% until the large TAE avalanche event around t=480ms (Figure JRT-15-2a), and both showed larger losses after this time. Initial simulations for the DIII-D case using the CGM were, instead, unsuccessful, with simulations under-predicting the measured deficit in neutron rate by a factor ~2 (Figure JRT-15-2b). For both NSTX and DIII-D, the only modes that were thought to cause substantial fast ion transport, and that were therefore included in the simulations, were toroidal Alfvén eigenmodes. The search for a reason of discrepancy between experiment and modeling revealed that, in fact, other lower-frequency instabilities are present in those high q_{min} plasmas. Their inclusion in the modeling results in a better match with the experiments (for the so-called "kick model"), see red curve in Figure JRT-15-2b.

The availability of these new simulation tools is expected to provide improved results for the analysis of the effects of broadened current and pressure on plasma performance and stability. Figure JRT-15-3 shows TRANSP results from a reduced database from NSTX and DIII-D discharges featuring different levels of AE activity. Results obtained using the new "kick" model agree better with the measurements, e.g. in terms of neutron rate and stored energy (reconstructed from experimental data through the EFIT code) than results assuming classical beam behavior. Moreover, the estimated NB current drive efficiency is shown to depend quite strongly on the level of AE activity (roughly proportional to the neutron rate deficit), with a substantial decrease of up to ~50% of efficiency with respect to simulations assuming "classical" fast ion physics only.

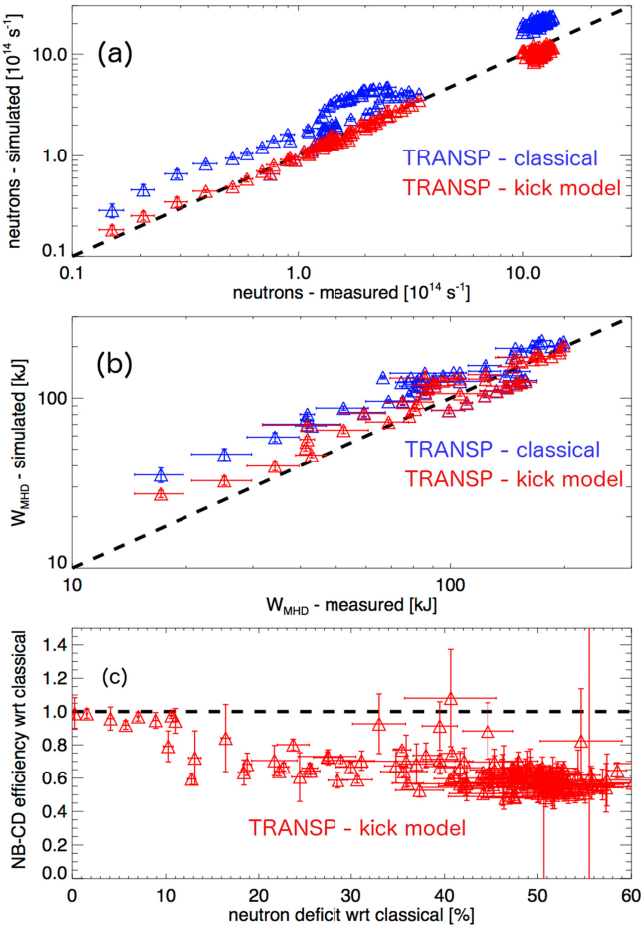

Figure JRT-15-3: *Comparison of TRANSP analysis of NSTX and DIII-D discharges with unstable AEs assuming "classical" fast ion physics and with the new "kick" model. (a) Neutron rate. (b) Stored energy, W_{MHD}. (c) NB current drive efficiency (normalized to the "classical" case) vs. neutron rate deficit.*

A complete list of experiments, other modeling/theory activities and results fulfilling the JRT-15 goals will be provided to DoE-FES in a separate report by the end of the 4th Quarter of FY-15. For NSTX-U, a partial list of activities can be found in the Summary of Milestone R(15-2) whose goal partially overlaps with the JRT-15 goals.

Outcome 3.2 *"Develop a plan to continue the NSTX-U/PPPL Theory partnership within projected funding levels"*

FY2015 budgets for NSTX-U and PPPL theory were sufficiently favorable that the previously established partnership could be sustained. Guiding principles for the topics chosen for the partnership include: (1) importance to the NSTX-U research program and the broader ST/tokamak community, (2) ability of PPPL theory to make leading contributions that surpass and/or complement contributions from NSTX-U non-PPPL collaborators, and (3) ability to dedicate a substantial time-fraction (30% minimum, 50% preferable) to reach a scientific conclusion and publication. The partnership facilitates collaboration and dedicated activities over a range of topics critical to understanding ST physics and projecting to future devices, including Transport and Turbulence, Energetic Particles, Boundary Physics, and Macroscopic Stability.

In the area of Transport and Turbulence, global gyrokinetic simulations using the GTS code in the electrostatic limit have shown how the strong parallel flow shear in NSTX can suppress to some extent the low-k Ion Temperature Gradient mode, but at the same time serve as a destabilization mechanism for the Kelvin-Helmholtz instability. Non-linear GTS calculations indicate that this low-k turbulence and neoclassical transport combined yields ion heat flux values that are within a factor of two of the experimental level in the outer half of the plasma [NT-1, 2]. The simulations also found that the relatively large density gradients often observed in NSTX discharges can destabilize Dissipative Trapped Electron Modes at high collisionality, and yields a collisionality dependence of electron heat flux that is consistent with that observed experimentally, decreasing transport with decreasing collisionality [NT-1, 2]. Development of GTS has focused on including electromagnetic effects to be able to study finite-beta effects on turbulence, most specifically the micro-tearing mode and its effect on electron transport. At present, these effects have been incorporated and benchmarked in the cylindrical limit, and further work over the next year will extend this capability to general toroidal geometry.

Energetic Particle work, in part has also addressed the issue of what was originally inferred to be highly anomalous electron transport related to the presence of CAEs in the plasma core. This inference was based on the assumption of classical behavior of beam particle confinement. However, recently published work [NT-3] has shown that the fast ion physics may not be classical; linear HYM simulations have shown that the core CAEs can drive Kinetic Alfven Waves (KAW) farther out, resulting in an energy channeling from the very core to a region of the plasma just outside the main fast ion distribution. The KAW damps primarily on electrons, with a power channeling estimate of approximately 0.4 MW over a range of realistic, inferred mode amplitudes. The amount of channeling could impact the electron temperature by several hundred eV. Further work on this topic will include non-linear HYM simulations to determine a better estimate for the power channeling and impact on electron temperature profiles. EP studies have also involved the implementation of two models into TRANSP that calculate anomalous fast ion diffusion in the presence of Alfven Eigenmodes. The Critical Gradient Model and Kick models have been validated against data from both NSTX and DIII-D, and show reasonable agreement for both machines. Further work in this area will include incorporating the effects on the fast ions from lower frequency MHD modes, as well as assessing the effect on neutral beam current drive.

In the area of Boundary Physics, atomic and molecular density data in the outer midplane of NSTX were inferred from tangential camera data via a forward modeling procedure using the DEGAS 2 Monte Carlo neutral transport code [NT-4]. The study assessed the sensitivity of the simulated camera image and neutral densities to uncertainties in the data input to the model. The simulated camera image is sensitive to the plasma profiles and virtually nothing else. The neutral densities at the vessel wall depend most strongly on the spatial distribution of the source; simulations with a localized neutral source yield densities within a factor of two of the baseline, uniform source, case. The uncertainties in the neutral densities associated with other model inputs and assumptions are ~50%. A new technique to handle electromagnetic effects in the XGC1 code has been implemented and benchmarked against the Cyclone case. This "hybrid" algorithm can handle tearing parity modes (i.e., microtearing). Linear electromagnetic XGC1 calculations have been performed to study edge physics in NSTX, and it showed the growth of Kinetic Ballooning Modes at a beta value of 6%, in good agreement with experimental observations of an abrupt change in turbulence correlation length at a beta value of 8%. Future development of XGC1 will include incorporation of kinetic electrons to study trapped electron modes, collisionless tearing and microtearing modes.

In the area of Macroscopic Stability, the non-linear M3D-C1 code has been extended to include a finite thickness resistive wall. Full 3D nonlinear simulations of Vertical Displacement Events (VDEs) in NSTX have been performed. In addition studies of both soft- and hard-beta limits have started. At present, new diagnostics are being added to the code to enable more detailed validation with NSTX magnetics and halo current data. The formation of an elongated Sweet-Parker current sheet and a transition to plasmoid instability has for the first time been predicted by simulations in a large-scale toroidal fusion plasma in the absence of any preexisting instability [NT-5]. Plasmoid instability is demonstrated through resistive MHD simulations of transient coaxial helicity injection experiments in NSTX. Motivated by the simulations, experimental camera images have been revisited and suggest the existence of reconnecting plasmoids in NSTX. Global, system-size plasmoid formation observed here should also have strong implications for astrophysical reconnection, such as rapid eruptive solar events. The NCC design and physics analysis have been continued and extended, in particular by combining the midplane coils. The three rows of coils can produce highly coherent perturbations at the outboard section without a gap between the coils, and thus better align and control the magnetic perturbations relative to the field lines. IPECOPT with stellarator optimizing tools and IPEC coupling matrix methods were utilized to find optimized configurations for NTV minimizing residual resonant fields.

References

[NT-1] Wang, W. et al, Submitted to Phys. Rev. Lett. (2015)
[NT-2] Wang, W. et al., Submitted to Phys. Plasmas (2015)
[NT-3] Belova, E. et al. Phys. Rev. Lett. **114** 015001 (2015)
[NT-4] Stotler, D. et al., Phys. Plasmas **22**, 082506 (2015)
[NT-5] Ebrahimi, F. et al., Phys. Rev. Lett. **114**, 205003 (2015)
[NT-6] Lazerson, S. et al., submitted to Plasma Phys. Cont. Fusion (2015)

NSTX-U FY2015 Year End Report: Facility and Diagnostics

In FY 2015, the NSTX-U team continued to make a good progress on the NSTX Upgrade Project. After the completion of an integrated systems test procedure (ISTP), on August 10, 2015, in shot 201085 NSTX-U achieved 100kA of plasma current satisfying the CD-4 key performance parameters (KPP) threshold of 50kA necessary for completion of the NSTX Upgrade Project. The preliminary EFIT equilibrium reconstructions confirmed the plasma current and plasma shape consistent with the camera images. This achieved an important first step toward resuming research operations and using the new capabilities of NSTX-U. It took over 250 people, 574,000 hours, over the last 5+ years to bring this project to bring the construction project to this culminating achievement. The NSTX-U Facility Operations team maintained the NSTX-U device, auxiliary systems, and site infrastructure to support the planned research efforts when NSTX-U starts plasma operations in FY2016. The team also initiated the preparation for the NSTX-U facility commissioning and subsequent plasma operations. Onsite support for equipment provided by other collaborating institutions was provided through the collaboration diagnostic interface budget. There were a number of important facility operation related enhancements carried out in FY 2015 which are needed to take full advantage of the NSTX-U device capabilities. With the enhanced plasma control requirements for longer duration plasmas expected in NSTX-U, an upgrade to the existing plasma control system is being implemented as part of the base program. After the completion of the first plasma and CD-4 KPP project milestone, the work is now shifted to the preparation for the NSTX-U research operation. The recent NSTX-U Test Cell aerial view taken in April 2015 is shown in Figure FD-1. The installation and commissioning for the modifications to the Multi-Pulse Thomson Scattering (MPTS) diagnostic required for the NSTX-U were completed in FY 2015. To provide capabilities needed to carry out the NSTX-U scientific research, the NSTX Team identified high priority facility and diagnostic enhancements for post upgrade operations as the part of the successful DOE NSTX-U Five Year Plan Review. These included diagnostics and physics capabilities provided by NSTX Research Team members from U.S. laboratories other than PPPL.

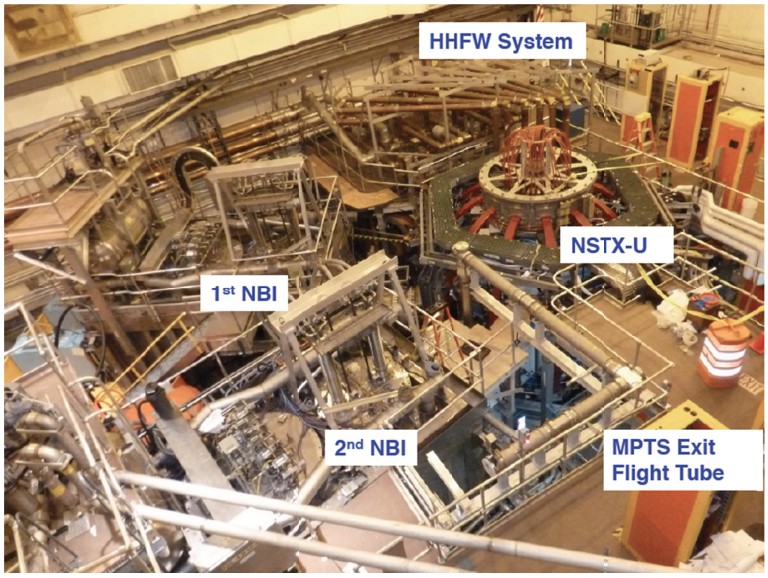

Figure FD-1: *Aerial view of the NSTX-U Test Cell. The newly commissioned 2nd NBI beam box can be seen in the foreground.*

Facility and Diagnostic Milestones for FY2015

Facility Milestone F(15-1): Complete high-Z tile design and begin procurement. (July 2015)

Description: For future facilities such as FNSF, it is important to investigate the viability of a high-Z metallic divertor in NSTX-U. After making an assessment of all graphite plasma facing component (PFC) plasma operations, a row of high-Z tiles will be installed on lower outboard divertor region.

Milestone F(15-1) Report: The purpose of the NSTX-U Divertor Upgrade-1 (DU1) is to provide operational experience and design evaluation prior to a larger, more comprehensive machine upgrade in future years. Following a similar logic as used for the NSTX Liquid Lithium Divertor system, the DU1 will be installed in the outboard divertor target in an effort to minimize operational risks during high-triangularity, high-performance discharges. In order to make a design assessment relevant to future upgrades of the high power divertor surfaces within NSTX-U, however, specific plasma discharges will be developed in the FY2016 run campaign to challenge the DU1 PFCs with heat and particle flux approaching levels expected during full, high-power operation of the NSTX-U. A study has been carried out to develop discharge shapes that will provide heat and particle flux to different areas of the outboard divertor in order to accomplish these tests. A compromise is made in shaping because it is not possible to produce plasma discharges with arbitrary amounts of input power for a given discharge shape and divertor strike-point location due to plasma stability. As a result, a 0D analysis was conducted to estimate the maximum amount for a given discharge shape and then a peak heat flux "Figure-Of-Merit" (FOM) was developed as a basis of comparison. As with other engineering FOMs, the peak heat flux calculated from this FOM is not informed by a multitude of effects present during actual experiments and only provides guidance for design and experimental planning.

The present design scheme aims to provide a 1:1 replacement of the existing graphite tiles. These will also rely on inertial cooling to minimize the required installation time. In order to achieve as broad a temperature range as possible, the design features a castellated surface that relieves thermo-mechanical stresses. The temperature limits that remain are derived from material limitations only. The molybdenum alloy "TZM" (Titanium-Zirconium-Molybdenum) is planned for usage owing to its greater ease of manufacturing than tungsten. The project scope includes several experimental tiles that will be used to further evaluate design variations including the use of tile shaping to eliminate leading edge effects and the possible use of bulk tungsten. Initial analyses of the first design

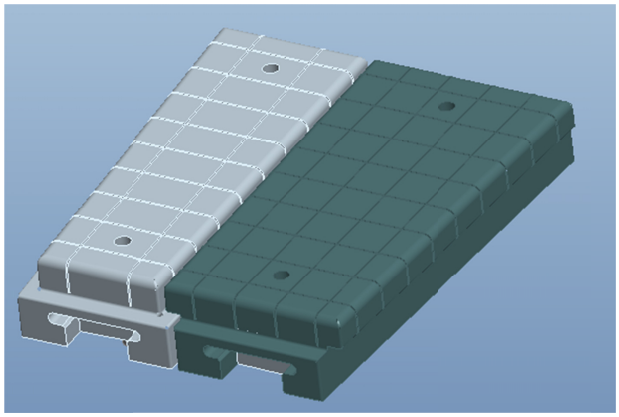

Figure FD-2: *Conceptual design of the outboard high-Z tiles. The surface castellations are clearly shown and the overall geometry mimics that of the existing tiles providing a 1:1 replacement.*

iteration have been completed. Material procurements have begun after a successful Conceptual Design Review. The initial design is shown in Figure FD-2. Final design review of the overall project is expected to be completed in early December. The NSTX-U DU1 is on schedule for installation following the FY16 run campaign.

Facility Milestone F(15-2): Develop cryo-pump system engineering design. (September 2015)

Description: For steady-state NSTX-U operations, an effective particle control tool is required. The divertor cryo-pump (DCP) has been used widely in conventional tokamak operations including DIII-D. On NSTX-U, a physics design study was performed on a closed divertor cryo-pump system in collaboration with ORNL. The initial indications are promising for providing divertor pumping for a relatively broad divertor parameter space including the snow-flake configuration. The cryo-pump system is a high priority major enhancement for the NSTX-U Five Year Plan. It is critical to develop an engineering design to start the long-lean procurement. The DCP is planned to be installed in mid-FY 2018 where a long outage is planned to start.

Milestone F(15-2) Report: The divertor cryo-pump (DCP) engineering design has two major components; in-vessel and ex-vessel. Layout of in-vessel routing of the cryo-pump has started as shown in Figure FD-3. The size of the refrigeration system has been scoped, and conceptual layouts of the cryo-system including refrigerator and cryo-lines through the test cell have been performed as shown in Figure FD-4. The specification and scope of work for the refrigeration system has been initiated. The regeneration system has been identified as a long-lead-time (~ 18 months) procurement item.

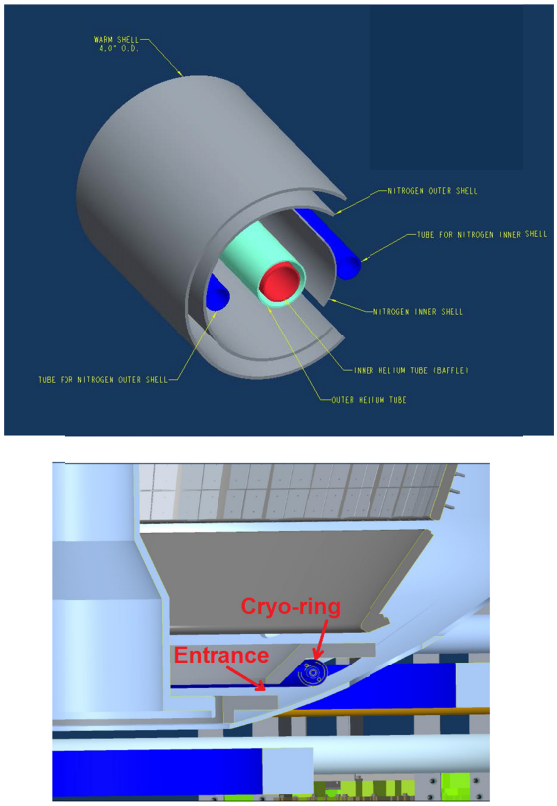

Figure FD-3: *(Top) Cryo-ring components, (bottom) layout of divertor cryo-pump in NSTX-U showing cryo-ring and plenum entrance*

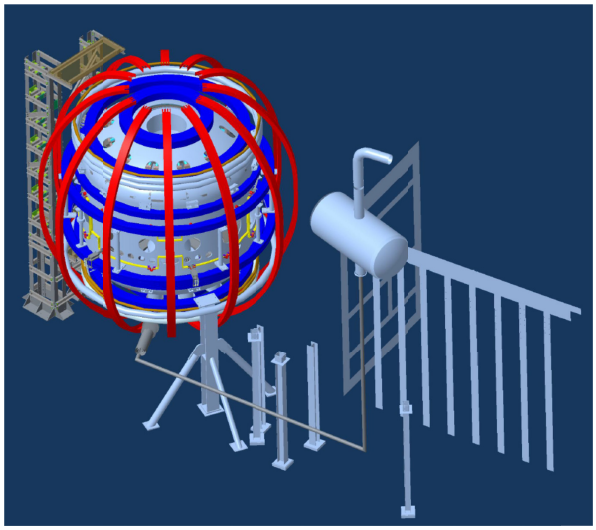

Figure FD-4: *A layout in the test cell that shows the transfer line routed from the compressor room to the north-east quadrant (bay B/C area).*

Facility Milestone F(15-3): Develop electron cyclotron heating (ECH) system engineering design. (September 2015)

Description: ECH/EBW is a promising tool to initiate STs and tokamaks without a central solenoid. It could also provide a means to control the plasma current profile. For NSTX-U, initially the ECH/EBW system will provide electron heating during non-inductive plasma start-up, later it will be used for off-axis EBW heating and current drive. The ECH system is a high priority major enhancement for the NSTX-U Five Year Plan. A 28 GHz high-power electron cyclotron/electron Bernstein wave (EC/EBW) heating system is planned in collaboration with the Tsukuba University, Japan. The engineering design includes a site-specific plan for the gyroton location and power supply/control. The initiation of procurement of the 28 GHz tube is high priority because of the long manufacturing and qualification testing. The ECH system is planned to be operational in FY2017 or FY2018 (depending on resource availability).

Milestone F(15-3) Report: The current ECH/EBW engineering design project began in November 2014. The project for the NSTX-U ECH / EBW High Power 28 GHz RF Source is gyrotron-based and after a site selection process, it was decided that the optimum location is the TFTR Test cell Basement as shown in Figure FD-5. The more-than one megawatt RF power will be routed to an antenna at NSTX-U torus at Bay E mid-plane through a low-loss waveguide system. Siting the gyrotron and its high voltage power supply in the TFTR Basement looks promising as the availability of floor space and ample AC power and water cooling are already available. After various routing studies, a routing with minimal interferences for running the waveguide to the NSTX-U Test Cell was also identified. Low-loss, corrugated circular waveguide will be used along with high performance waveguide components. Even though the waveguide path is more than 200-feet long, it is expected that 90% or more of the Gyrotron's output will be delivered to the antenna's input. Considerable progress has been made to date on the engineering design:

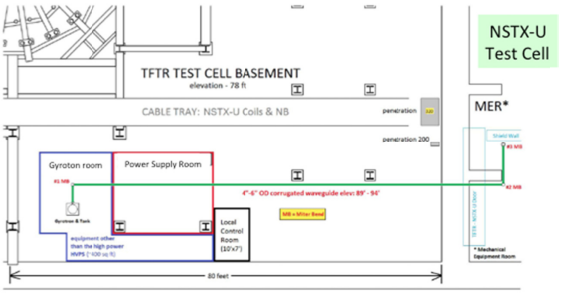

Figure FD-5: *Gyrotron site location schematic.*

a. The conceptual design of the overall system was presented and accepted by Management in February 2015.
b. The gyrotron design development being conducted by the Tsukuba University in Japan has advanced from 1.2 MW for 0.1 sec to >1.5 MW for 2 seconds
c. The waveguide system's preliminary design and all waveguide components' design descriptions have been completed
d. The ambient and dynamic magnetic fields have been measured during full coil field tests. Ambient magnetic field is about 2 Gauss (G) with < 0.2 G variation during coil pulses at ten to fifteen feet away from the NSTX field coil cable tray. The gyrotron will be installed about 15-20 feet from the tray and therefore will not be affected by the magnetic field.

The conceptual design review for the ECH system is to be held in September 2015 and the preliminary design completion will follow.

Facility Milestone F(15-4): Develop non-axi-symmetric control coil (NCC) system engineering design. (September 2015)

Description: NCC is a promising tool to for NSTX-U MHD studies including for improved control of RWMs, ELMs, and disruptions. This effort is in collaboration with Columbia University and General Atomics. The NCC system is a high priority major enhancement for the NSTX-U Five Year Plan. The engineering design includes the specification of the NCC coil configuration, back-plate (if any), and possible PFC modifications.

Milestone F(15-4) Report: NCC design and physics analysis have been continued and extended, in particular by combining the existing mid-plane coils as shown in Figure FD-6. These effectively three rows of coils can produce highly coherent perturbations at the outboard section without a gap between the coils, and thus better align and control the perturbation relatively to the field lines. IPECOPT with stellarator optimizing tools and also IPEC code were successfully utilized to find the n=1-6 optimized configuration for NTV with minimizing residual resonant fields. For RWM control capability by NCC, the sensors were successfully optimized, and VALEN3D predicts that the active RWM control can stabilize plasma even near the ideal wall limit if the optimized sensors and gains are combined with NCC. The investigation of RMP characteristics by NCC has also been continued based on vacuum island overlap width (VIOW) criterion. TRIP3D analysis showed 2x6 partial NCC can achieve thick enough VIOW for ELM suppression and interesting combinations of high n islands when more coils are added.

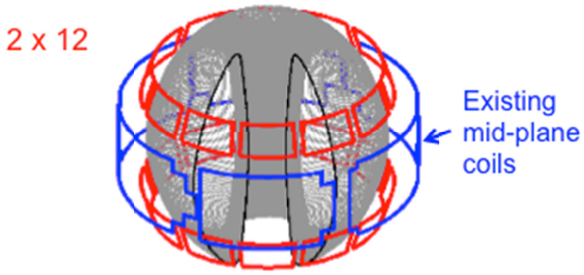

Figure FD-6: *2x12 NCC configuration in red and existing 6 RWM mid-plane coils in blue.*

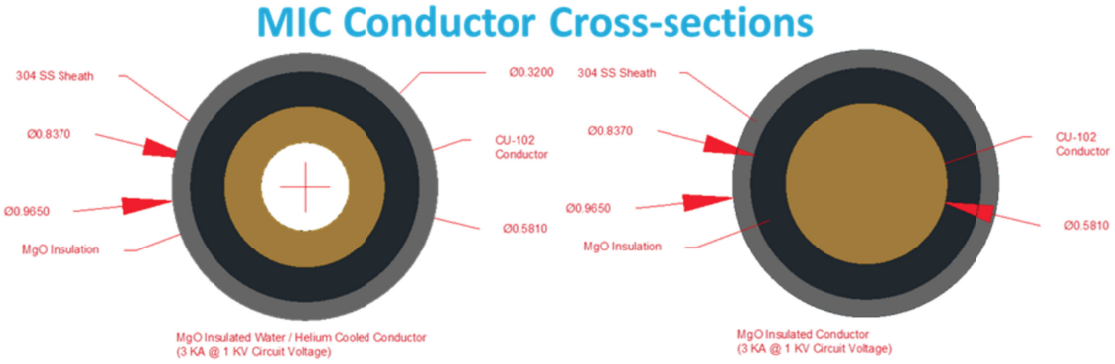

Figure FD-7: Candidate mineral-insulated conductor (MIC) cross-sections for NCC.

The scope of the NCC engineering design project is defined at a Conceptual Design Review (CDR) level. The project is divided into the following subsections: NCC Coils, Passive Plates Modifications, PFC Modifications, Vessel Penetrations, Cooling Systems, Power Supply, Metrology and Project Management. A high-level engineering design and analysis have been conducted. Mineral Insulated Cable (MIC) as shown in Figure FD-7 has been a strong candidate

for the in-vessel coils applications. A procurement requisition is currently in progress to purchase test samples in order to conduct various tests and decide if the MIC can be used for these coil applications. The MIC End Terminations design using Ceramic Break is in progress. A procurement requisition is submitted to purchase test samples of the ceramic breaks. A radiation-cooled, helium-cooled and water-cooled coil design alternatives have been evaluated. Considering the in-vessel lithium use in NSTX-U, the options maybe narrowed to radiation-cooled and helium-cooled designs. Vessel penetration and vacuum interface design options are being developed. Combinations of the NCC and RWM Coil power supply alternatives were prepared. A general understanding of the power supply units and coaxial cables requirements are being developed. The objective is to narrow down the various design alternatives and prepare a WAF as part of the CDR.

Diagnostic Milestone D(15-1): Install and commission Material Analysis Particle Probe (MAPP) (September 15)

Description: To support boundary physics operation, the MAPP diagnostic system will be installed and commissioned. MAPP is an in-vacuo inter-shot diagnostic capable of correlating surface chemistry evolution with plasma response to PMI conditioning. A unique MAPP capability is an in-situ, between-shots sample analysis following plasma exposure where samples are retracted *in-vacuo* into an adjoining chamber, and a variety of analysis techniques are performed during the in-between shots window.

Milestone D(15-1) Report: A major NSTX-U PMI diagnostic addition is the Material Analysis Particle Probe (MAPP). The MAPP system was developed by personnel from Purdue University and the University of Illinois at Urbana-Champaign (UIUC). It is an in-vacuo inter-shot diagnostic capable of correlating surface chemistry evolution with plasma response to PMI conditioning. MAPP utilizes multiple surface-science measurement techniques to characterize a sample material exposed to NSTX-U conditions and assess plasma-surface interactions near the divertor strike point. A unique sample head has been designed for MAPP to allow simultaneous exposure of up to four samples to plasma discharges. The surface of each sample is positioned (via shims or custom machining) colinear to the top surface of the retaining stems in order to avoid self sputtering. Independently controlled heaters are contained beneath each sample and radiative and conductive cross-talk heating is reduced using perforated sample stems and vertical heat baffle shields. Following plasma exposure, samples are retracted *in-vacuo* into an adjoining chamber, where a variety of analysis techniques are performed during the in-between shot window. Analysis techniques include X-ray photoelectron spectrscopy (XPS) – used to assess the chemical

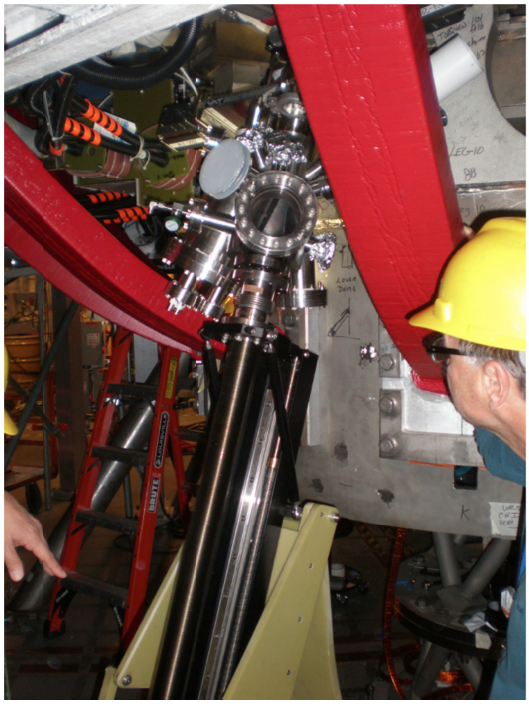

Figure FD-8: *MAPP system installed on NSTX-U*

interactions of the top ~10 nm, ion scattering spectroscopy (ISS) – interrogates the top 1-2 monolayers to determine surface chemical composition, and direct recoil spectroscopy (DRS) – uniquely capable of measuring the surface hydrogen content in samples. In addition, thermal desorption spectroscopy (TDS) can be performed at the end of each day in order to measure and quantify bulk deuterium retention. The MAPP installation on NSTX-U has been completed as showin in Figure FD-8. The analysis chamber and probe drive has been mounted on the NSTX-U lower dome port and connected to vacuum pumping system. Connections to AC power have been made to the electronics rack, and cables have been installed between it and the analysis chamber, probe drive, and vacuum pumping system. A communications link has been established and tested for remote control between the NSTX-U Control Room and the electronics rack in NSTX-U Test Cell. The initial set of MAPP diagnostics needed for NSTX-U experiments are XPS and TDS. Commissioning of these instruments is expected to be fnished in October 2015, when execution of the first experimental proposals requiring analysis of MAPP samples are planned.

NSTX Upgrade Project Accomplishments

The NSTX Upgrade (NSTX-U) Project which has two major components, new center stack, and 2nd NBI, has made excellent progress in FY 2014. The 2nd NBI CD-1 KPP was achieved in May 2015 and the new center-stack CD-1 KPP was achieved in August 2015. With the DOE reviews held in September 2015, the NSTX Upgrade Project is expected to successfully close ahead of the CD-2 base schedule and under cost.

New Center Stack (CS) Upgrade – The CS components were fabricated by the end of FY14. The completed OH/TF/PF1 bundle and CS casing were then transported to the NSTX-U test cell south bay. After wrapping the TF/OH/PF1 bundle with Micro-therm thermal insulation, the CS casing was lowered onto the bundle to complete the CS assembly. The assembled CS was then lowered into the NSTX-U vacuum chamber in November 2014 as shown in Figure FD-9. To complete the TF coil, the inner TF bundle was connected to the outer TF legs using high strength Cu–Zr alloy flex joints. The completed upper TF joint configuration is shown in Figure FD-10.

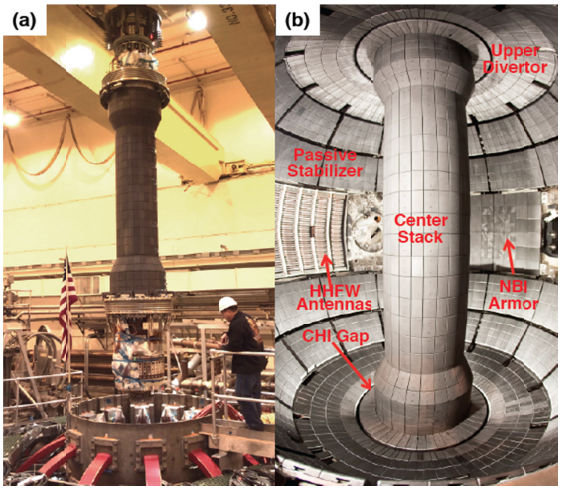

Figure FD-9: *(a) NSTX-U center-stack lowering into vacuum vessel. (b) NSTX-U Center-stack installed.*

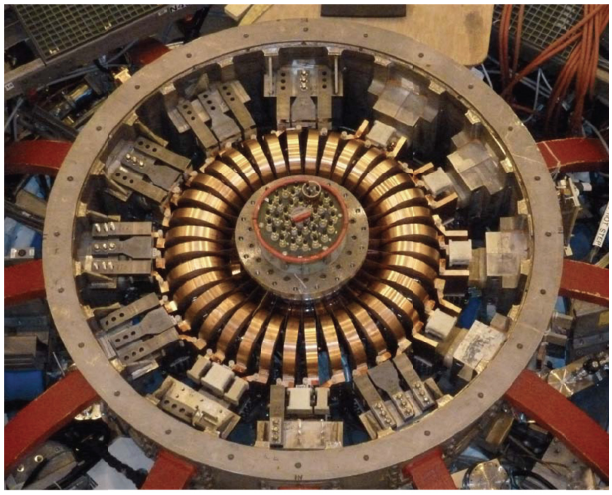

Figure FD-10: *Upper TF flex bus installed on NSTX-U.*

Digital Coil Protection System – To protect NSTX-U from unintended operational conditions due to the power supplies delivering current combinations and consequential forces or stresses beyond the design-basis, a digital coil protection system (DCPS) was implemented. The DCPS is designed to prevent accidental (either human or equipment failure) overload beyond the design conditions of the structure which the power supply system could generate, even while each individual power supply is operating within its allowable current range. In the initial instance of DCPS, the algorithms will test approximately 125 force and stress calculations against limit values, using both two models for the plasma shape and two models for potential post-disruption currents; this results in 500 total force/stress calculations in addition to 14 thermal limit calculations. The update rate of each type will be 200 μs for both the force-based and the thermal-based signals. Redundant current measurements for each coil and plasma current will be provided as inputs. This type of sophisticated coil protection system if fully demonstrated could be utilized for safe operation of future fusion devices including ITER. The DCPS has been successfully tested and utilized during the power supply commissioning and integrated testing leading to the achievement of the first plasma and KPP target.

Power system upgrades – The NSTX-U power systems include 68 identical rectifiers (Transrex AC/DC Convertors) providing a total pulsed power capability of 1650 MVA for 6 seconds every 300 seconds. New firing generators (FG) were installed for the precise control of thyrister firing angles needed for NSTX-U operations particularly critical for the 8-parallel, 130kA TF system configuration. The new FG delivers firing pulses with far greater resolution, precision, and repeatability than the previous ones in NSTX. In addition, the NSTX-U 650 MVA / pulse motor generator with weld cracks was also repaired. The motor generator repair brought the motor generator to its original specifications, and the repair will enable the full operation of NSTX-U.

Neutral Beam Injection (NBI) Systems – This fiscal year, all of the NSTX Upgrade NBI final construction work was completed for beam line, services, power, controls, and armor. Additionally a concrete shield wall was installed in the North gallery to replace the block removed from the NTC. Rework was required on the water lines and the beam line control cabling but the jobs were completed in time to support the effort to perform the KPP beam shots into armor. The Liquid Helium refrigerator was reactivated and resumed operation in support of the effort to achieve the NSTXU NBI KPP. Full Beamline 2 operations began with water flow, vacuum, pneumatics, and cryogenics. Power supplies were reactivated and fully tested prior to source installation. Beamline 2 ion sources were then conditioned using standard operating procedures. Several sources experienced electrical faults and were removed and replaced with spares.

2nd NBI CD-4 KPP achievement – On May 11, 2015, the NB2 neutral beam system successfully fired 45kV beams at 100ms pulse lengths for multiple shots, successfully completing the NSTX Upgrade Project CD-4 KPP for Neutral Beam injection into the in-vessel armor at > 40keV beam for > 50 milliseconds. The first cryo-panel regeneration of NB2 (and for NSTX-U) was successfully completed.

After completing the NSTX-U NBI KPP on Beamline 2, the Beamline 1 reactivation effort began. The beam line systems were restored to full service and source conditioning began. Several

sources experienced failures during the years of storage. The Source Shop returned to full operations in support of repair and refurbishment tasks to replenish our supply of sources and spares. Efforts to repair and replace source grid modules has started with repairs to existing modules underway and fabrication of new parts under evaluation. To support ongoing NBI operations, the SF6 skid was refurbished to allow full control of our SF6 inventory with 6 NBI systems back in use. Additional resources have been added to handle electronics and mechanical repairs and source shop and decontamination efforts to fully support NBI operations in the future.

OH Ground Fault – On April 24th, 2015 during the execution of the coil power tests the NSTXU OH circuit suffered arc damage from a short created by the movement of a grounding conductor on the OH Ground Plane across energized OH water connections. The arc damaged the conductor water connections, caused a water leak and tripped off the power supplies. The cause was quickly identified as a grounding conductor on the OH ground plane that was installed without the required electrical break. The resulting circulating currents in the conductor interacted with the OH field propelling it into the water connections. The lack of a proper ground on the OH compression ring to which the water connections were mounted was identified as a contributing cause. Subsequent inspection and investigation identified the cause as well as other areas of the design that can be improved to avoid a recurrence of the fault. These items include redesign of the grounding clamp on the OH ground plane, grounding of the OH compression ring, and redesign of the water connections on the OH coil. Disassembly and inspection of all of the TF and OH components in the upper and lower umbrella identified other areas that can be improved upon including TF finger supports, OH Coaxial connector, and Bussbar support grounding. In parallel, an internal as well as an external review were conducted to identify the cause of the fault and review the recovery plan. In addition, a review committee to look into the extent of condition and a review committee to perform root cause analysis of the fault were conducted. The necessary repair and improvements were completed in July 2015, and the first plasma and subsequent plasmas satisfying the CD-4 KPP target were successfully achieved on August 10, 2015. The repaired and improved upper umbrella section is shown in Figure FD-11.

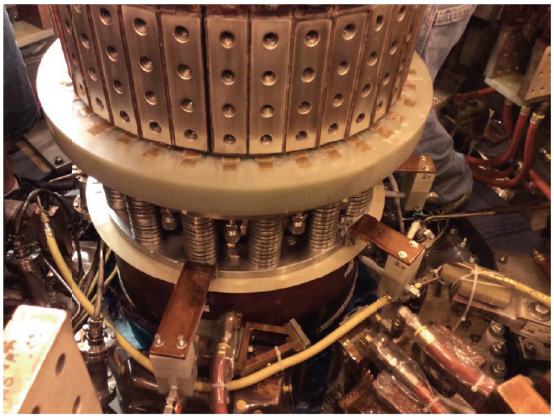

Figure FD-11: *Photo of the restored and improved upper umbrella section.*

Plasma Control System development in preparation for research plasma operations – A key capability required for the achievements of the CD-4 KPP targets and the research plasma operation is the plasma control system. FY-2015 saw a large number of upgrades to the plasma control system hardware and software. These upgrades have been oriented to improve both the maintainability and reliability of the system, and to prepare for both the CS-Upgrade KPP and subsequent research operations. A number of key elements of the plasma control system are provided below.

New control computers – In FY-15, new real-time Linux computers featuring the Concurrent RedHawk OS replaced the Sunfire v40z hardware from FY-06. These come complete with vendor support for the real-time performance of the hardware and software, including the interface card drivers. These new systems use a modern serial FPDP interface instead of the previously employed parallel FPDP interface, providing enhanced data acquisition capabilities and room for future expansion. The two new systems mirror the previous two systems in terms of having a dedicated "active" computer for normal operations, and a standby "development" computer to facilitate building and deploying new control software in-situ. Each new system has 64 available processing cores, upgraded from the 8 available in the v40z. Note that these computers must run not only the plasma control system, but also one (of two) instances of the Digital Coil Protection System (DCPS).

Deployment of new real-time hardware – In FY-15, additional real-time hardware has been deployed. A second generation of the Stand Alone Digitizer, called the SAD II, has been deployed to measure both magnetics signals and coil currents. These digitizers were designed by PPPL, and incorporate both a 32 channel digitizer and hardware to multiplex a series of digitizers. Three of these SAD II digitizers have been deployed.

Improvements to the power supply control code – In NSTX, the transrex power supplies, which power the TF, OH, and PF coils, were controlled via a stand-alone program called PSRTC (Power Supply Real Time Control). This code was first written in FORTRAN, then converted to C, and as a consequence was hard to maintain and improve. During the later stages of the construction outage, this code was rewritten as a module within the plasma control system. This upgrade allows the code to be more easily maintained and upgraded, and couples it more closely with the physics algorithms that generate the current or voltage requests. As an example of an upgrade facilitated by this code rewrite, a new feature was added where the code checks the measured values of dI_{coil}/dt against that predicted by a simple model, and turns off the power supply in the event of a significant discrepancy as occurred during the OH fault.

Additional magnetic sensors available in real-time – As part of the CS upgrade project, approximately 20 additional magnetic field sensors and 15 additional poloidal flux loops were added to the CS. These signals have been brought into the real-time system. Additionally, eight more magnetic field sensors in the outboard divertor have been brought into the real-time system. Collectively, it is anticipated that these additional sensors will better constrain the divertor magnetic structure in rtEFIT, thus benefiting the research program in control of advanced divertors (snowflake, X-divertor, etc)

Preparing rtEFIT for research operations – The rtEFIT code, which resides within PCS, computes the full 2D magnetic equilibrium in real-time, constrained by various real-time measurements. This code is thus critical for all efforts in profile control and shape/position control. In order to bring this code up to the requirements for NSTX-U, a senior PPPL physicist and a PPPL post-doc visited GA in January for training on the code and to learn about future updates. Following this visit, an updated version of rtEFIT was placed in the NSTX-U PCS. This version has been tested using input data created by NSTX-U TRANSP simulations; the magnetic

field at the location of sensors was computed based on the TRANSP simulations, and then provided as constraints to rtEFIT. The updated PCS code was then used to reconstruct the equilibrium based on the synthetic measurements; this is described in more detail in the Advanced Scenarios and Control section of the report. This is a significant step toward commissioning the code for research operations.

Shape Control Development – The convention on NSTX was to use an algorithm called day0 to provide simple pre-programmed current control of the PF coils during the plasma breakdown phase. Around 20ms, when the plasma current was about 200 kA, the PF current control would transition to the plasma current and control (PCC) algorithm that provided active feedback of the outer gap, Z position and vertical stability, as well as the option to scale the PF request with plasma current. Finally, control of at least the PF3 and PF5 coils would transition to the ISOFLUX algorithm, with a separate vertical stability algorithm applied as a final step. This capability was restored for NSTX-U within the PCS code, however an alternative scheme was also implemented that provides more flexibility and simplicity.

In the new scheme, the PCC algorithm provides pre-programmed current control, active feedback of the outer gap, and the option to make the PF request proportional to Ip (for plasma equilibrium) and ohmic current (to account for the larger ohmic fringe field variation on NSTX-U). Active control of the Z-position and vertical stability is handled in the separate Vertical Position category (VPC) that can operate in conjunction with either PCC or ISOFLUX control; this capability is described below. This architecture removes a number of algorithm transitions that often limited flexibility in scenario development and simplifies the flow of control. The PCC algorithm was also improved by removing a number of hard-coded parameters, such as the choice of magnetic sensors, in order to increase the code flexibility.

Updates to the ISOFLUX algorithm, which provides shape control based on the results of rtEFIT reconstructions are also underway. The modifications are being tested using rtEFIT reconstructions of synthetic data from TRANSP simulations as described in the previous section. An additional “add-on” to ISOFLUX will allow for control of advanced divertors; see description below.

Improved vertical control capability – The NSTX vertical control system was based on a single pair of poloidal flux loops, whose voltage was used to infer a quantity roughly proportional to the plasma vertical velocity; as noted above, those calculations were essentially an add-on following the ISOFLUX calculations. For NSTX-U, this code has been broken out into its own category (called VPC), with dedicated algorithms. This new code has been improved to include 18 flux loop voltages. Capability has been included to correct the observed voltage signals for variations in the coil current, allowing a more accurate estimate of the plasma velocity. Furthermore, an observer for the plasma position has been included, based on poloidal flux measurements. Finally, code has been added to disable vertical control algorithm is control is observed to be lost. This will help limit the forces on NSTX-U.

Neutral beam injection control from PCS – A category for PCS control of the six neutral beam sources has been developed. The algorithm allows the PCS operator to pre-program sources to be on or off at selected intervals during the discharge, or to let the algorithm determine a modulation pattern for the source to achieve an operator requested time-averaged power. To avoid source faults and limit the fatigue on neutral beam components, minimum on and off times, as well as a maximum number of modulations per discharge are enforced for each beam in determining. The power requests can be made on an individual per source basis, or the sources can be grouped together. For example, all of the sources could be combined into one group, enabling the operator to provide a single request for total beam power. The order in which sources are modulated within a group by the real-time code is determined by an operator specified `batting order'. Finally, the power for request for each group of sources can be communicated to the NBI category in real-time from other PCS categories, for example, those responsible for β_N or rotation profile control, allowing the neutral beams to be used for feedback control.

Progress towards β and l_i/q_o control – A software specification has been written for a PCS category to post-process the results of rtEFIT, enabling the use of smoothing filters and dynamic observers to make the estimates of parameters like β_N, l_i, and the q-profile more suitable for use in feedback control algorithms. A software specification has also been written for a flexible control category that will be used for simultaneous feedback control of the scalar quantities like β_N, l_i, q_0 in the near-term, and will later be used to control spatial profiles, like q and rotation. Two algorithms have been specified within the category: one for PID control, and another for implementing more general state-space control algorithms. The algorithms will generate actuator requests (like beam power, plasma current, and shape descriptors) that will be distributed to the dedicated PCS categories for each physical actuator (e.g., the beam power request will be sent to the NBI category).

Advanced Divertor Control – Additional capabilities are currently being added to the ISOFLUX algorithm which will enable real-time feedback control of snowflake divertor (SFD) magnetic configurations in NSTX-U. The SFD is an alternative magnetic divertor concept that is characterized by a second-order null formed by two x-points in close proximity. The SFD, which has increased flux expansion and a larger plasma-wetted area, is an attractive option for heat flux mitigation in NSTX-U in which unmitigated peak heat fluxes in a standard divertor configuration may reach 20 MW/m^2 and compromise plasma-facing components. The real-time SFD control system at NSTX-U will be capable of simultaneous control of multiple SFD parameters, such as the separation between the two x-points in the divertor region and their orientation. The system is currently designed to use the upper and lower PF-1a, PF-1c, and PF-2 coils for control and is intended to work in conjunction with the other shape control functionality within ISOFLUX. The capabilities for SFD control that will be implemented include a non-iterative algorithm that is capable of approximating the locations of two x-points in real-time using input data from rtEFIT. The specified algorithm then calculates the PF coil currents required to minimize the errors between the two calculated and desired x-point locations, operates on these errors with a PID controller, and then outputs the appropriate voltage requests to the PF coils. The new snowflake algorithm in ISOFLUX will enable control of upper, lower, or combined upper-lower SFD

configurations. Future work will focus on integration of SFD control with control of additional plasma shape parameters such as strike point and flux expansion.

Preparation toward full operationsl capability – We are formulating the operational plan toward full operational capability for NSTX-U. A draft plan is shown based on assessment of physics needs for first year of operations. The 1st year goal is to operate NSTX-U with the electromagnetic forces (I_pB_T) at halfway between NSTX and NSTX-U limits and 50% of the NSTX-U design-point of heating of any coil. This still allows NSTX to operate at $B_T \sim 0.8$ T, $I_p \sim 1.6$ MA, and the maximum flat-top duration of 3.5 s in the first year which is far beyond the achieved NSTX parameters. The device will be inspected and refurbished as needed at the end of the each operating year. For the second year, the toroidal magnetic field will be increased to its full field value of 1 T but keeping the heating of the coil to 75% of the design-point of any coil. This will allow 3 sec discharges at full field and current. The same limits should allow the full 5 sec discharges at $B_T \sim 0.8$ T, $I_p \sim 1.6$ MA. The device will be brought to full operational capability in the third year of NSTX-U operation.

HHFW Heating and Current Drive Systems – The NSTX RF heating and current drive (CD) systems will consists of the existing 6 MW high harmonic fast wave (HHFW) system and the new ECH/EBW system, which is an important element of the NSTX five year facility upgrade plan. The HHFW system is expected to perform better with higher toroidal field of NSTX-U. After the initial HHFW operation with the NSTX-U plasmas, an upgrade of the HHFW antennas is envisioned to increase the heating power and heating / CD efficiency. As a part of the NSTX-U five year plan, a MW-class ECH/EBW system is planned. The ECH/EBW system is particularly crucial for the non-inductive start-up research where it can be effectively bridge the temperature gap between the CHI based start-up plasmas which tends to be below 50 eV and the HHFW heating and CD regime which tends to be above ~ 200 eV. It is estimated that about 0.5 to 1 MW to ECH/EBW power would be sufficient to heat the CHI plasmas to ~ 200 eV range. The ECH/EBW system could also provide an efficient off-axis CD needed for advanced ST operations.

HHFW Antenna Upgrade – In the HHFW area, while the system is basically unchanged, the HHWF feed-thru conductor must be modified to be able to handle the higher disruption loads (~ x 4) in NSTX-U. To handle those disruption loads, compliant connectors were designed, tested and installed between the feed-throughs and antenna straps for the NSTX-U operations. In order to increase the power from the existing 12-strap HHFW antenna, RF voltage stand-off was tested on an RF test stand with the new compliant feeds. The test demonstrated the rf voltage stand-off of 46 kV which is about twice the value required. The HHFW antennae with compliant feeds and improved back plate grounding were installed in NSTX as shown in Figure FD-12. The tests also showed RF-induced arc-prone areas behind the

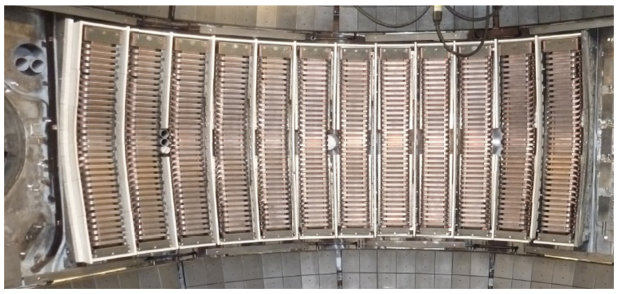

Figure FD-12: *Enhanced HHFW antenna installed in NSTX-U with compliant feeds and improved back-plate*

back-plate. The HHFW system installation was completed and steady progress has been made in commissioning. The HHFW system; sources 3 – 6 are ready for operation, and progress is being made in restoring Sources 1 and 2. Major efforts included improved weatherproofing of outdoor transformer-rectifiers, commissioning of PLC controls on Sources 2 and 3, and refurbishment of the water-cooling systems of Sources 3, 5 and 6 and the high-voltage protection systems of Sources 1 and 2. Vacuum tuning was successful. Vacuum commissioning is planned to commence in September.

Significant HHFW related diagnostic upgrades have been performed in FY 2015. Two arrays of divertor Langmuir probes were installed in the NSTX-U vessel specifically for HHFW studies. Circuitry is being built to directly measure the RF (30 MHz) component of the collected current to determine the process underlying the SOL loss of HHFW power. Recent analysis suggests that RF rectification is driving the heat flux to the surface. Measuring the RF voltage at the divertor, along with a new wide-angle IR-camera view provided by ORNL, will test this hypothesis in great detail. A SOL reflectometer, upgraded by ORNL to be compatible with the higher magnetic fields in NSTX-U, is being reinstalled. A mid-plane probe shaft, situated in the middle of the HHFW antenna, is being fitted with two Langmuir probes and double-Langmuir probe designed by ORNL.

Coaxial Helicity Injection (CHI) System – Supporting TSC simulations have identified the required coil currents to initiate transient CHI discharges on NSTX-U. All hardware components to enable Transient CHI operations are installed on NSTX-U. An important external system required for initiating CHI discharges is the CHI 2 kV, 40 mF Capacitor Bank. Worn out components were replaced, and the design for the capacitor bank current limiting resistor assembly was revised and improved. Discharging the charged bank at full voltage into a dummy load then successfully tested the re-furbished capacitor bank.

Resistive Wall Mode (RWM) control system – While NSTX-U is a modification of NSTX, changes to the device conducting structure (e.g. new 2nd NBI port structure), mid-plane RWM control coils, and equilibria require re-computation of n = 1 active RWM control performance using proportional gain, and RWM state space control. The upgrade also adds new capability, such as independent control of the 6 RWM coils. This new capability, combined with the upgrade of the RWM state space controller will also allow simultaneous n = 1 and n = 2 active control, along with n = 3 dynamic error field correction. Finally, the active control performance of the proposed off-mid-plane non-axisymmetric control coils (NCC) also needs to be evaluated, A significant increase in controllable β_N is expected with the RWM state space control in NSTX-U, as was found for NSTX.

Disruption Mitigation Systems – Predicting and controlling disruptions is an important and urgent issue for ITER. Methods to rapidly quench the discharge after an impending disruption is detected are also essential to protect the vessel and internal components of an ST-FNSF. In support of this activity, NSTX-U will employ three Massive Gas Injection (MGI) valves [OMS1] that are very similar to the double flyer plate design being considered for ITER. NSTX-U will be the first device to operate this valve design in plasma discharges. These valves have been tested

off-line and deliver the required amount of gas (~ 200 – 400 Torr.L) to support NSTX-U experiments, which will offer new insight to the MGI data base by studying gas assimilation efficiencies for MGI gas injection from different poloidal locations, with emphasis on injection into the private flux region. The valve has also been successfully operated in external magnetic fields of 1 T. The upper MGI valve has been installed on NSTX-U. All of the necessary piping connections for the lower valve have been installed. Details of the piping connections for the mid-plane valve are in progress.

Electromagnetic Particle Injector (EPI) – While the MGI system may be adequate for most disruptions, the warning time for the onset of some disruptions could be much less than the MGI system response time. To address this important issue, a novel system based on the rail-gun concept has been designed, and plans for an off-line experimental test are in progress. The device referred to as an EPI is fully electromagnetic, with no mechanical moving parts, which ensures high reliability after a period of long standby. In addition to responding on the required fast time scale, its performance substantially improves when operated in the presence of high magnetic fields. The system is also suitable for installation in close proximity to the reactor vessel.

Fueling Tools – NSTX-U plasma operations will require the capability for gas injection from numerous locations. The gas injection systems on NSTX were not adequate to meet the physics program needs of NSTX-U as improvements are needed in the area of divertor heat flux mitigation, and increased levels of gas injection from high-field side to meet the up to 10s discharge pulses planned for in NSTX-U. These are briefly summarized.

For normal inductive plasma operation, NSTX-U will rely on three outboard gas injectors as on NSTX. However, Injectors 2 and 3 are being relocated to bays I and G as their original locations on the vessel were eliminated by the modifications providing the 2nd neutral beam port. NSTX relied on two high-field side gas injectors, one injecting near the midplane and one injecting at the "shoulder" of the center stack near the PF-1aU coil. These were used for H-mode triggering, and the high-field mid-plane injector was routinely used on most of the H-mode discharges. In NSTX-U, the system will have the capability for injection from two mid-plane locations and two "shoulder" locations at the top of the center stack. At each location, these injectors will be toroidally displaced by 180 degrees. Furthermore, for both the midplane and shoulder locations, one installation will have a larger diameter tube, while the other installation will have a small diameter tube; this variation in tube size will provide a measure of control over the flow rates. The higher gas delivery capability from these injectors may be required during Li conditioned operation on NSTX-U as the injectors on NSTX were at some times (such as during the diffusive Li coating experiments) were found to be inadequate to maintain the required electron densities in NSTX.

For CHI start-up, in addition to the existing gas injector on bay K bottom, a Tee will be added at Bay G bottom port, which is the location of lower divertor Penning gauge, and this too used to provide more control and improved toroidal gas injection symmetry.

The glow discharge conditioning (GDC) system will use one of the mid-plane injectors as on NSTX. The boronization system, based on deuterated Tri-Methyl-Boron (dTMB) in a He carrier gas, is being significantly modified, by adding a new gas delivery system with improved safety features. In addition to the mid-plane injection, provisions will be provided for gas injection from both the upper and lower divertor regions. This is based on results from DIII-D that suggest that spatially distributed injectors will provide more uniform coverage of the boron coatings.

For divertor heat flux mitigation studies, NSTX relied on a single low-conductance gas injection location beneath the lower divertor plate on Bay-E. Initial NSTX-U capabilities will replace this injector with two high-conductance injectors in the lower divertor, separated by 180 degrees toroidally. This capability can be extended to additional toroidal angles, and to the upper divertor, in subsequent years once experience is gained with the new system.

Commissioning of the gas injection system for NSTX-U – The legacy gas injection code from NSTX, while functional, had reached a state where maintenance and upgrades were difficult. Therefore, the control algorithms were redesigned and rewritten to improve its clarity, consistency and the ability to introduce new capabilities (such as density or radiation feedback) that employ the NSTX-U gas injectors. A number of the gas lines and vessel pressure measurements were changed or upgraded during the outage, and these systems were brought on-line and calibrated in support of CD-4 operations. Note that unlike NSTX, all gas injectors will now be programmed from the PCS.

Boronization – Boronization is a conditioning technique for reducing oxygen that will be applied to NSTX-U plasma-facing components after bakeout and helium glow discharge cleaning (GDC). The boronization process involves GDC with a mixture of 95% helium and 5% deuterated trimethylborane (dTMB) which is followed by another period of helium GDC. During the past year, a new dTMB system was installed on NSTX-U. A PLC is used to control the flow of dTMB through coaxial lines from a specially-designed gas cabinet inside the NSTX-U Test Cell to the vacuum vessel. The boronization system will be available for plasma operations in FY16.

Preparations for NSTX-U Lithium Operations – The safe handling of lithium is essential for supporting the technologies required for lithium conditioning of plasma-facing components (PFCs) and ELM control. As part of the process of evaluating practices and procedures for lithium use at PPPL facilities including NSTX-U, a Lithium Safety Peer Review was held at PPPL on June 16 – 18, 2015. The review was part of a US Department of Energy "notable outcome" for the Laboratory for fiscal year 2015. The reviewers included representatives from Environmental Health and Safety group at Princeton University, Applied Research Laboratory at the Pennsylvania State University, Corrosion Science and Technology Group at Oak Ridge National Laboratory, and Sandia National Laboratories in New Mexico. The reviewers visited PPPL facilities that included the NSTX-U Test Cell and areas for lithium technology development and storage. They also examined lithium handling procedures, and interviewed members of the staff who work with lithium. The reviewers observed that PPPL personnel and their safety practices were appropriate and adequate for present lithium-related activities.

Granule Injector for Investigation of Multi-species Particle Injection and ELM Control – The mechanical assembly and testing was completed for the NSTX-U granule injector (GI). A new control system for remote GI operation has been designed, and its components have been procured. The initial motivation for the GI was to inject lithium granules for ELM control ("ELM pacing"). This was successfully demonstrated on EAST and DIII-D, and ELM pacing experiments with lithium injection are planned for NSTX-U. An outstanding question is the effect of other granule materials on plasmas, and this will be investigated in the upcoming NSTX-U run. Laboratory tests of the LG have been performed with boron and boron carbide granules. Boronization will precede PFC conditioning with lithium, and the ability to inject boron and boron carbide will permit granule injection studies without introducing lithium into NSTX-U.

Lithium Evaporator – The NSTX lithium evaporator (LITER) system will be reused on NSTX-U. Each LITER is a temperature controlled stainless steel container filled with liquid lithium (LL), with a nozzle to direct the lithium vapor for coating PFCs at desired locations. As on NSTX, the nozzle will be aimed on NSTX-U toward the middle of the inner divertor to maximize the lithium deposition on the divertor plates. The LITER passes through a PFC gap in the upper divertor region. Changes to the upper umbrella structure (for NSTX-U) necessitated modifications to the LITER mounting brackets. The LITERs have been remounted and checked for interferences with the upper divertor gap. The liquid lithium filler for LITER (LIFTER) was also successfully tested. The station where the LIFTER is used load the LITERs has been reinstalled in the NSTX-U South High Bay. Two layers of stainless steel protect the concrete floor from accidental exposure to liquid lithium.

Liquid lithium technology development – The implementation of a flowing liquid lithium divertor is a long-term goal for NSTX-U. However, the challenge of developing a system that requires lithium flow through the vacuum boundary from an external reservoir to an in-vessel divertor is daunting. Recent experiments with lithium coatings on high-Z plasma-facing components (PFCs) under high-flux plasma bombardment in the Magnum PSI linear plasma device indicated that the erosion rate of deuterium-saturated lithium was much lower than lithium alone. This suggests that the properties of liquid lithium PFCs could be investigated with significantly reduced lithium inventories. For example, tiles could be "preloaded" with internal reservoirs of lithium that could flow to the surface during plasma operations. Several concepts were developed in collaboration with the Eindhoven University of Technology in the Netherlands. They are the basis for a test tile under consideration for installation as part of the high-Z divertor tile upgrade planned in FY16.

NSTX-U Diagnostic System Status and Plans - Diagnostic installation was an active area of NSTX-U operational preparation in FY2015. A list of the existing diagnostic systems expected to be available during the first year of operation is shown in Table FD-1. An exception is the poloidal FIR high-k scattering system, which will be installed during the shutdown following the FY2016 campaign. Over half of those diagnostic systems are provided by collaborators, with installation support provided by PPPL. The in-vessel diagnostic installation and related calibration tasks were completed in FY2014, so diagnostic work in FY2015 focused on completion of vacuum interfaces that did not require vessel entry for installation and on installation of diagnostic hardware outside the vessel. Installation, calibration, and

commissioning of core diagnostic capabilities needed to support the FY2016 campaign have been completed. The status of these key systems at the end of FY2015 is briefly summarized below.

MHD/Magnetics/Reconstruction
- Magnetics for equilibrium reconstruction
- *Halo current detectors*
- *High-n and high-frequency Mirnov arrays*
- Locked-mode detectors
- RWM sensors

Profile Diagnostics
- MPTS (42 ch, 60 Hz)
- T-CHERS: $T_i(R)$, $V_\phi(r)$, $n_C(R)$, $n_{Li}(R)$, (51 ch)
- P-CHERS: $V_\phi(r)$ (71 ch)
- *MSE-CIF (18 ch)*
- *MSE-LIF (20 ch)*
- *ME-SXR (40 ch)*
- Midplane tangential bolometer array (16 ch)

Turbulence/Modes Diagnostics
- *Poloidal FIR high-k scattering (installed in 2016)*
- *Beam Emission Spectroscopy (48 ch)*
- Microwave Reflectometer,
- *Microwave Polarimeter*
- Ultra-soft x-ray arrays – multi-color

Energetic Particle Diagnostics
- *Fast Ion D_α profile measurement (perp + tang)*
- Solid-State neutral particle analyzer
- Fast lost-ion probe (energy/pitch angle resolving)
- Neutron measurements

Edge Divertor Physics
- Gas-puff Imaging (500kHz)
- Langmuir probe array
- Edge Rotation Diagnostics (T_i, V_ϕ, V_{pol})
- *1-D CCD H_α cameras (divertor, midplane)*
- *2-D divertor fast visible camera*
- Metal foil divertor bolometer
- AXUV-based Divertor Bolometer
- IR cameras (30Hz) (3)
- *Fast IR camera (two color)*
- Tile temperature thermocouple array
- *Divertor fast eroding thermocouple*
- Dust detector
- Edge Deposition Monitors
- Scrape-off layer reflectometer
- Edge neutral pressure gauges
- *Material Analysis and Particle Probe*
- *Divertor VUV Spectrometer*

Plasma Monitoring
- FIReTIP interferometer
- Fast visible cameras
- Visible bremsstrahlung radiometer
- *Visible and UV survey spectrometers*
- *VUV transmission grating spectrometer*
- *Visible filterscopes (hydrogen & impurity lines)*
- Wall coupon analysis

Table FD-1 *- Initial NSTX-U Diagnostic Systems*

Multi-Pulse Thomson Scattering (MPTS) – Modification of the MPTS system was required to reorient the laser beams to accommodate the larger diameter of the new center stack while maintaining the necessary spatial resolution. A new laser beam input flight tube, new exit flight tube, new beam dump, and modifications of the light collection optics were required. These new components were fabricated, installed, and aligned. The system was commissioned and a calibration based on Rayleigh and Raman scattering from nitrogen and argon gases in the vessel was completed. Ten of the MPTS polychromators were rebuilt to improve their optical performance. The MPTS system is ready to support the FY2016 campaign.

CHERS – Reinstallation and calibration of the following charge-exchange recombination spectroscopy (CHERS) diagnostics was completed: CHERS (toroidal and poloidal), Edge Rotation Diagnostic (ERD, toroidal and poloidal) and Real-Time Velocity (RTV). An upgrade of the operating system for the control and data acquisition PCs was completed. Modification of the control and data acquisition software to be compatible with the new PC operating systems was completed and the CHERS diagnostics were commissioned to be ready to support the FY2016 experimental campaign.

Far Infrared Tangential Interferometer/Polarimeter – UC-Davis is in the process of reconfiguring and upgrading the Far Infrared Tangential Interferometer/Polarimeter (FIReTIP) on NSTX-U. The seven-channel FIReTIP system employed previously on NSTX is being reconfigured into a three-chord system. Chord #1 will be employed for core plasma density monitoring as well as density feedback control and density calibration of the Thomson scattering system, while subsequent channels (as additional vacuum windows and retro-reflectors are installed) will monitor core and edge fluctuations. The FIReTIP lasers will be placed just outside the NSTX-U test cell, necessitating the fabrication of long lengths of over-moded waveguide to transport the FIReTIP beams to Bay G. A 3-level laser table has been fabricated which will house not only the FIReTIP lasers, but also the CO_2 and CO_2-pumped FIR lasers for the poloidal high-k scattering system.

Constraints imposed by the new location of FIReTIP chord #1 has necessitated the design and fabrication of internal retro-reflectors (decision pending on subsequent chords). As internally-mounted retro-reflectors are subject to high levels of mechanical vibrations (attached, as they are, to the vacuum vessel rather than placed on a vibration isolation mount), this has required the addition of a vibration monitoring system consisting of a HeNe interferometer coupled to a field programmable gate array (FPGA) to provide real-time vibration compensated density information.

UC Davis has successfully overhauled the CO_2 and CO_2-pumped FIR lasers that generate the FIReTIP beams. Dielectric-coated waveguides and support flanges have been developed to couple the beams to/from the NSTX-U vacuum vessel. The in-vessel retro-reflector was installed in FY2014 and the beam input/output window structure was installed in FY2015. In FY2015, the UC-Davis group prepared the new FIR laser and detector systems and they will be installed on NSTX-U in early FY2016. The 3-level laser tower has been completed as shown in Figure FD-13, and is due to be installed on NSTX-U in late 2015 along with the optics, phase comparator electronics, digitizers etc. that make up the full system. Chord #1 is expected to be operational for research plasmas in early 2016, with additional chords to follow in succeeding years.

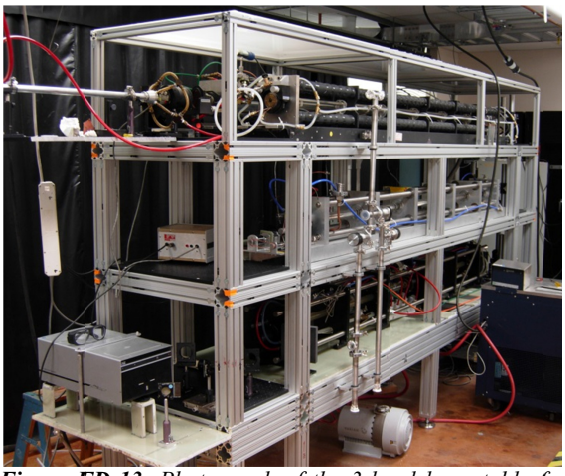

Figure FD-13: *Photograph of the 3-level laser table for FIReTIP and the poloidal high-k scattering system.*

Soft X-Ray Diagnostics – The primary focus of the Johns Hopkins University group this year was diagnostic preparation for NSTX-U, comprised of the core and edge tangential Multi-energy Soft X-ray system (ME-SXR), the mid-plane tangential Transmission Grating Imaging Spectrometer (TGIS), and the poloidal Ultrasoft X-ray arrays (USXR). The new core/edge ME-

SXR system was built and installed at Bay-G, currently sharing a port with the PPPL AXUV diode-based bolometer system. The core system provides a total of 100 channels of soft X-ray detection covering the entire plasma outboard mid-plane with a spatial resolution of ~3cm. In addition, the edge ME-SXR adds another 100 channels at high resolution, ~ 1cm, covering the plasma pedestal and outer edge, r/a ~ 0.6-1.1. These channels are grouped into 5 sets of 20 channels each viewing the plasma tangentially through a separate filtered pinhole, while a remotely activated shutter will protect the filters and diodes from lithium deposition during LITER operation. The data from the ME-SXR system is used as input to a JHU-developed Neural Network analysis code that will provide electron temperature profiles with high time resolution, of ~10kHz, on a routine between-shot basis. The NSTX-U ME-SXR array design and the Neural Network analysis method were implemented and tested also at the EAST tokamak, using a JHU built edge ME-SXR system. The EAST diagnostic tests demonstrated good agreement between the ME-SXR and the TS electron temperature profile, as well as stable in-vessel operation. The ME-SXR system will also be a main diagnostic for the assessment of impurity transport, and will be used in conjunction with gas impurity injection and with the laser blow-off diagnostic to be built within the PPPL-LLNL collaboration. For analysis of the impurity transport, the STRAHL transport code was modularized and inserted into a Python user interface, to streamline data handling and calculation of the transport coefficients. Finally, the ME-SXR system will be also used for fast boundary position measurements to assess the viability of non-magnetic sensors for equilibrium boundary detection and feedback position control.

The new Transmission Grating Imaging Spectrometer (TGIS) diagnostic with a direct-detection VUV/XUV sensor for increased sensitivity was also evaluated on LTX, where it was used to study the comparison between recycling of solid and liquid lithium surfaces. For NSTX-U, the TGIS with a direct-detection CCD will significantly reduce the complexity of the diagnostic as well as provide measurements with a significantly higher SNR. The JHU group is now also evaluating the direct-detection TGIS for analysis of the upper divertor on NSTX-U using a new, state-of-the-art atomic physics modeling code. The measurements from the divertor TGIS will provide spatially and spectrally resolved estimates of radiated power as well as the concentration and transport of impurities. These data will be used in conjunction with the OEDGE and DIVIMP codes for validation of divertor models. The JHU advanced atomic physics code was also used in support of a collaboration with PPPL and RFX-mod, by modeling the He-I line ratio emission for use as a plasma SOL/edge temperature and density diagnostic.

Motional Stark Effect – Collisionally Induced Fluorescence (MSE-CIF) – The MSE-CIF system was commissioned and is ready to support the FY2015 experimental campaign. The beam-into-gas calibration of the system will be performed early in the FY2016 campaign. Testing and optimizing of the algorithms for real-time capability (rt-MSE) was completed and rt-MSE will be available for the FY2016 campaign. A study was performed to optimize the width of the light collection aperture to provide larger signals with the higher toroidal field of NSTX-U.

Motional Stark Effect – Laser Induced Fluorescence (MSE-LIF) – The MSE-LIF will provide measurements of the field line pitch angle profile without requiring injection of the heating neutral beam needed for the present MSE-CIF system on NSTX-U. This system was installed and commissioned prior to the NSTX upgrade outage and utilizes a small diagnostic neutral beam

and a laser to excite the fluorescence. The light collection optics were reinstalled and optical and optical fibers for 32 spatial channels were installed. The detectors and filters needed to support these channels were installed and tested. The laser and diagnostic neutral beam are in the process of being re-commissioned. Initial experimental results will be obtained during the FY2016 campaign. It is expected that that combined measurements from the MSE-LIF and MSE-CIF diagnostics will allow radial profiles of the radial component of the electric field and the pressure to be measured.

Turbulence Diagnostics – For turbulence diagnostics systems, the high-k scattering system detector array presently located at Bay K will have to be relocated to Bay L after the 2nd NBI installation at Bay K. By re-aiming the microwave beam, it is possible to measure both the radial and poloidal components of the high-k turbulence. The existing 280 GHz system will be replaced by a 693GHz system. The higher frequency system is designed to improve high-k resolution and SNR. For low-k turbulence, the beam emission spectroscopy (BES) system with a new generation of BES detector has been developed by the University of Wisconsin group. The group is planning to expand the BES system from 28 spatial channels to 48 channels for NSTX-U. For magnetic fluctuations, a promising diagnostic appears to be the cross polarization system presently being tested on DIII-D. A preliminary feasibility study is planned on NSTX-U. For the edge region, an enhanced gas puff imaging (GPI) diagnostic will be implemented.

High-k Scattering System – The 290 GHz high-k tangential scattering system of NSTX is being replaced by a 693 GHz poloidal scattering system for NSTX-U, thereby considerably enhancing planned turbulence physics studies by providing a measurement of the k_θ-spectrum of both ETG and ITG modes. The probe beam in this case will enter the plasma from Bay G while a tall exit window located on Bay L will be employed to collect the radially- and poloidally-scattered beams and image them onto an array of waveguide mixers. The reduced wavelength will result in less refraction and extend the poloidal wavenumber coverage from the previous 7 cm^{-1} up to >40 cm^{-1}. Measuring the k_θ as well as the k_r spectrum is crucial for identifying the source of turbulence, since the 2D k-spectra driven by different instabilities have different anisotropies.

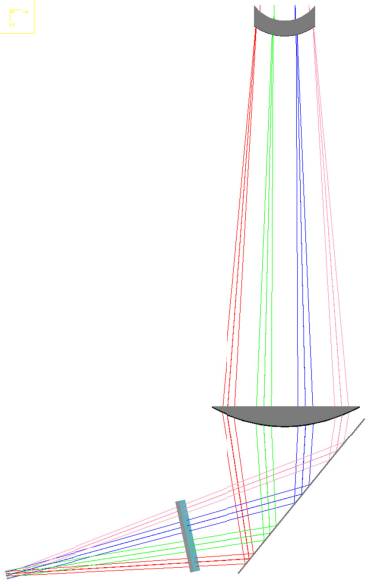

Figure FD-14: *Optics simulation of the high-k scattering system, showing how the scattered beams pass through the Bay L window to be focused onto a multi-element mixer array.*

Supplemental funds from DoE have been used for the purchase of a high power CO_2 laser from Edinburgh Instruments, which will pump a 693 GHz FIR laser recently overhauled by UC Davis. The lasers and supporting equipment will be housed in the "mezzanine" area just outside the NSTX test cell. A three level, 12 foot long table supports both high-k scattering lasers, as well as four FIReTIP lasers, and is enclosed in Lexan panels for a dry air environment. The laser table will be installed in Fall 2015 together as part of the FIReTIP system. Low loss corrugated waveguides, re-machined by UC Davis from the previous 290 GHz waveguide, bring the FIR

beam to launch optics on Bay G. A system of mirrors and HDPE lenses have been designed to direct and focus the probe beam to the scattering region, while a steerable mirror aims the probe beam ±2.5° to target various scattering volumes. The receiver system is placed outside a large exit window on Bay L, with the scattered beams tilted up and then focused on to a 4-pixel mixer array as shown in Figure FD-14. The tip/tilt angle of the large mirror is remotely controlled, as is the distance between the mirror and the focusing optics, thereby allowing placement of the scattering volume along the line-of-sight of the launch beam from the plasma core out to the pedestal region. While a single 4×1 mixer array is being fabricated by VDI for initial plasma operation, the system can be easily upgraded to an 8×2 configuration. The High-k Scattering system is scheduled to be completed by the end of 2015, after which it will undergo laboratory testing and characterization at UC Davis. After testing is complete, it will be shipped to PPPL, installed, and commissioned in 2016.

Beam Emission Spectroscopy – The Beam Emission Spectroscopy (BES) diagnostic on NSTX-U is based upon observing the Dα emission of collisionally-excited neutral beam atoms and provides spatially-resolved measurements of longer wavelength density fluctuations in the plasma core. These measurements play a key role in elucidating the physics of ion transport and MHD instabilities. In FY15, BES sightlines were reconfigured for 2D measurements spanning the outer plasma and pedestal region. The 2D fiber assembly was designed and fabricated by U. Wisconsin with support from PPPL, and the new configuration contains 54 sightlines in an approximate 9x7 grid, as shown in Figure FD-15. The new 2D configuration opens scientific opportunities for multi-field turbulence measurements with flow fields from velocimetry techniques. Flow field observations can shed light on E×B flow and shear flow, zero-mean-frequency zonal flows, and geodesic acoustic mode (GAM) zonal flows. Also, turbulence-induced particle transport can be directly inferred from 2D BES measurements of density and flow field. Finally, the U. Wisconsin collaboration completed a 16-channel expansion of the BES detection system for a total of 48 detection channels available for the FY2016 campaign.

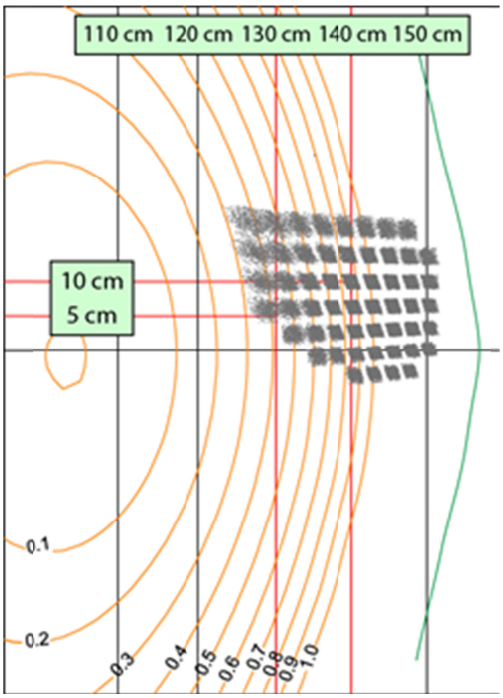

Figure FD-15: *Projected sightlines for updated BES configuration.*

Magnetics For Equilibrium Reconstruction, Boundary Control, and RWM Suppression – There are many more magnetic sensors in NSTX-U than NSTX, largely due to the increase in the number of sensors on the newly fabricated center column. Substantial progress was made in commissioning the NSTX-U magnetic diagnostics, as described below.

The poloidal field and flux measurements are used to constrain both off-line and realtime equilibrium reconstructions. The analog integrators for these systems were all checked, and repairs made. All sensors were then cabled to their integrators, and then to the transient and real-time digitizers. The sensors were then calibrated using single coil discharges. Updated sensor gains were determined, and errant pickup of the TF and OH fringing fields was corrected in the data. These sensors were used to support the CS KPP activity, allowing EFIT reconstructions of all discharges.

Progress was also made on other magnetic diagnostic systems. A rogowski sensor was installed on one the TF outer legs, allowing a measurement of the time-derivative of the TF current. This measurement, combined with a toroidal flux loop, will used to measure the diamagnetic flux in the plasma. The resistive wall mode (RWM) sensor signals were examined during these magnet shots, and a number of cabling errors resolved. Finally, the plasma current measurement system was refurbished, with some major hardware upgrades. These were successfully commissioned, and the data that was collected will be used to improve the vessel-current compensation in the plasma current measurement.

Boundary Physics Diagnostics – The NSTX facility has been investing strongly in boundary physics related diagnostics in the past several years, and a major activity has been to insure that port space is available on NSTX-U to accommodate them. There are over 20 boundary physics diagnostic systems on NSTX-U and additional ones are being readied. They include Gas-Puff Imaging (500kHz), a new poloidal Langmuir probe array, Edge Rotation Diagnostics (T_i, V_ϕ, V_{pol}), 1-D CCD H_α cameras (divertor and midplane), 2-D fast visible cameras for divertor and overall plasma imaging, divertor bolometer, IR cameras (30Hz), fast IR camera (two color), tile temperature thermocouple array, divertor fast eroding thermocouples, dust detector, Quartz Microbalance Deposition Monitors, scrape-off layer reflectometer, edge neutral pressure gauges, Material Analysis and Particle Probe (MAPP) [see Milestone D(15-1) Report**]**, Divertor Imaging Spectrometer, Lyman Alpha (Ly_a) Diode Array, visible bremsstrahlung radiometer, visible and UV survey spectrometers, VUV transmission grating spectrometer, visible filterscopes (hydrogen & impurity lines), and wall coupon analysis. Major upgraded boundary physics diagnostics are described in more detail below.

SOL and divertor diagnostic development for NSTX-U – Two new diagnostics are being developed by LLNL to support radiative divertor feedback control. In a conceptual form, both spectroscopic diagnostics would provide a semi-localized electron temperature estimate in the divertor in real time, which can be used in the plasma control system to control the gas seeding rate. These diagnostics are the divertor SPRED vacuum ultraviolet spectrometer, and the divertor imaging Balmer line spectromer (DIBS). The divertor SPRED spectrometer will use real-time carbon or nitrogen spectral line intensities as proxies of radiated power, as well as boron-like, beryllium-like, and lithium-like line intensity ratios that are highly sensitive to electron

temperature in the range 1-10 eV. The DIBS diagnostic will provide a multi-chordal coverage of the divertor legs. Temperature-sensitive high-n Balmer line intensity ratios (n=6-12) will be used in real-time for electron temperature evaluation. Both diagnostics are being installed on NSTX-U for initial testing in FY2016.

Design of Resistive and Infrared Imaging Bolometers for NSTX-U – Measurement of the power radiated from the plasma support a range of activates from informing day-to-day tokamak operations to in-depth physics studies. Excessive power radiated from the core can have a negative impact on performance, while emission in the boundary plasma can be used as an efficient means of spreading heat exhaust, thus making spatial coverage and resolution important. Power can be lost over a wide range of photon energies, and specialized sensor technologies must be used to make accurate measurements. Through collaboration with ORNL, key upgrades and improvements to NSTX-U radiated power measurements will work to enhance upcoming research in the areas of transport and boundary plasma physics through the use of resistive bolometers. Additional efforts through ORNL and NIFS collaborations will explore using novel infrared imaging bolometers.

Resistive bolometers are a conventional proven technology for radiated power measurement used on nearly all large-scale magnetically confined plasma devices. Small thermally isolated metallic foils, 4 μm Au, absorb radiation emitted from the plasma resulting in a rise in temperature which can be detected via a resistance change and used to infer the radiated power. Prior implementation on NSTX was challenging, and work in FY15 by ORNL and PPPL looked to understand and overcome the shortcomings of previous designs as well as adapt them for NSTX-U. Testing of existing sensor stock is underway and conceptual design activities are nearing completion in an effort to develop resistive bolometer tools to be installed following the FY16 campaign. Both core and lower divertor regions are being considered as priorities for initial diagnostic deployments, and a strategy for more comprehensive coverage beyond FY17 is being developed.

Infrared imaging bolometers offer a novel means of measuring radiated power by observing a foil's temperature via infrared emission rather than its resistance. This technique leverages technological advancements in high-resolution IR imaging cameras to improve spatial coverage and has been demonstrated on large-scale fusion devices such as LHD and JT-60U. On-site collaboration by NIFS, Japan along with colleagues from ORNL, and PPPL performed laboratory testing and developed a conceptual design of an infrared imaging bolometer to view the lower divertor of NSTX-U. Expected for testing during FY16 operations, this will be the first imaging bolometer designed specifically for divertor and boundary physics research. Results will impact future developments of radiated power measurements, both at NSTX-U and within the tokamak community, helping to complement existing resistive bolometer tools.

Upper and lower divertor cameras – Full poloidal/toroidal coverage of impurity emission from the PFCs is achieved via a combination of bandpass-filtered fast cameras viewing upper and lower PFCs and line-scan cameras. Two wide-angle fast visible cameras (Bay E and Bay J top) were used in NSTX for the full toroidal imaging of the lower divertor. These cameras will be re-

installed in NSTX-U and will be complemented with a symmetric view of the upper divertor from Bay H bottom. Two image-intensified radiation-hardened CIDTEC cameras expand these capabilities with the ability to image weaker visible lines and a custom-built two-color system (TWICE) for the simultaneous imaging of different wavelengths. Intensified camera views include the lower divertor (from Bay I top) and a close-up of the surface analysis sample system MAPP (from Bay J top).

TWICE diagnostic for NSTX-U – A two-color imaging system being developed by ORNL based on a charge injection device (CID) radiation-hardened intensified camera was built for studies of plasma-surface interactions on PFCs in NSTX-U. The two-color imaging system (TWICE, Two-Wavelength Imaging Camera Equipment) shown in Figure FD-16 was developed to image the lower divertor PFCs and expand the capabilities available from fast visible cameras with the ability to image weaker visible lines (via an image intensifier) and the simultaneous imaging of the same field of view at different wavelengths. By means of commercially-available mechanically-referenced optical components, the two-color setup images the light from the plasma, relayed by a fiber optic bundle, at two different wavelengths side-by-side on the same detector. Remotely-controlled filter wheels are used for narrow bandpass and neutral density filters on each optical path allowing for simultaneous imaging of emission at wavelengths differing in brightness up to 3 orders of magnitude.

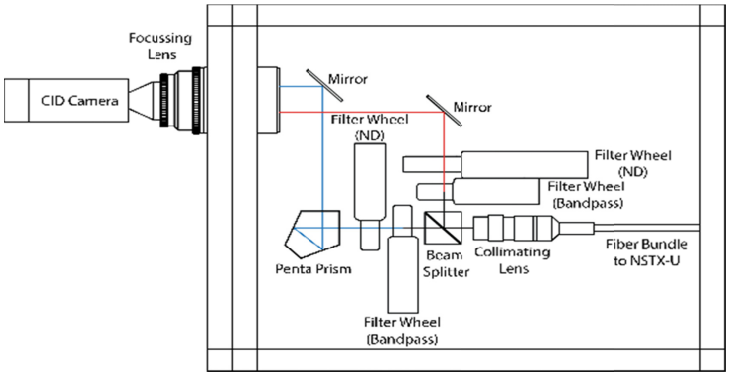

Figure FD-16: *Layout of optical and mechanical components in the TWICE image splitter box.*

Divertor camera for churning mode, turbulence, and radiative divertor real-time feedback control - A new divertor imaging diagnostics was implemented to:

- Improve understanding of turbulent transport and its relation to the divertor heat flux width
- Improve understanding of snowflake divertor transport and the presence of the theorized 'churning mode' in the null-point region
- Implement divertor plasma temperature feedback for radiative divertor real-time control

The new LLNL Vision Research Phantom v1211 camera will be dedicated to the imaging of the lower divertor via a lower dome radial re-entrant divertor port on Bay B. The choice in the optics was driven by the needed field of view and magnification, the conservation of etendue and the minimization of filter bandpass shift while a Schott coherent bundle with 8/10 micron (core/clad) 1000x800 fibers will be used as optical guide. The resulting resolution of 360x288 pixels leads to a maximum frame rate of 76.6 kHz (200 kHz with cropping in the toroidal direction) and a 2 s recording time. Imaging via D-alpha and Li I is envisioned for turbulence studies. Imaging via C

III is envisioned for the development of a radiative divertor feedback signal derived from the change in location of the C III radiation shell along the divertor leg as a result of changes in the divertor temperature in the transition to detachment.

Edge neutral density diagnostic – The Edge Neutral Density Diagnostic (ENDD) was used in recent years coupled to the Monte-Carlo neutral code DEGAS2 to infer neutral densities in the low field side SOL in discharges from the last year of NSTX operations. The ENDD diagnostics was upgraded for NSTX-U. ENDD was relocated to a re-entrant viewport on the Bay G midplane port cover with the shutter acting as a mirror. ENDD lines of sight are now tangential to the outer mid-plane in front of the NBI armor graphite tiles. Direct imaging on the camera sensor was substituted with imaging via a coherent fiber bundle allowing for the positioning of the DALSA camera farther away from NSTX-U. ENDD will monitor hydrogenic emission via a D-α narrow-bandpass interference filter. The choice of D-α instead of D-β was driven by the higher confidence in the knowledge of molecular contribution to D-α emissivity.

Divertor Spectrometers – Progress has been made with three LLNL high spectral resolution extreme ultraviolet (EUV) grating spectrometers that will be used to infer impurity densities in the plasma core and pedestal. The two previously existing spectrometers, the X-ray and Extreme Ultraviolet Spectrometer (XEUS) and the Long-Wavelength and Extreme Ultraviolet Spectrometer (LoWEUS) and the new spectrometer, the Metal Monitor and Lithium Spectrometer Assembly (MonaLisa), have been calibrated on the Livermore EBIT facility to cover the wavelength range between 5 – 440 Å. The design is such that the spectrometers will cover overlapping wavelength ranges to ensure no gaps in impurity monitoring (XEUS, 5 – 65 Å; MonaLisa, 50 – 220 Å; LoWEUS, 190 – 440 Å). All three spectrometers have been successfully mounted on NSTX-U (see Figure FD-17). The port is located at Bay E midplane with the spectrometers stacked on top of one another, providing near-midplane radial views.

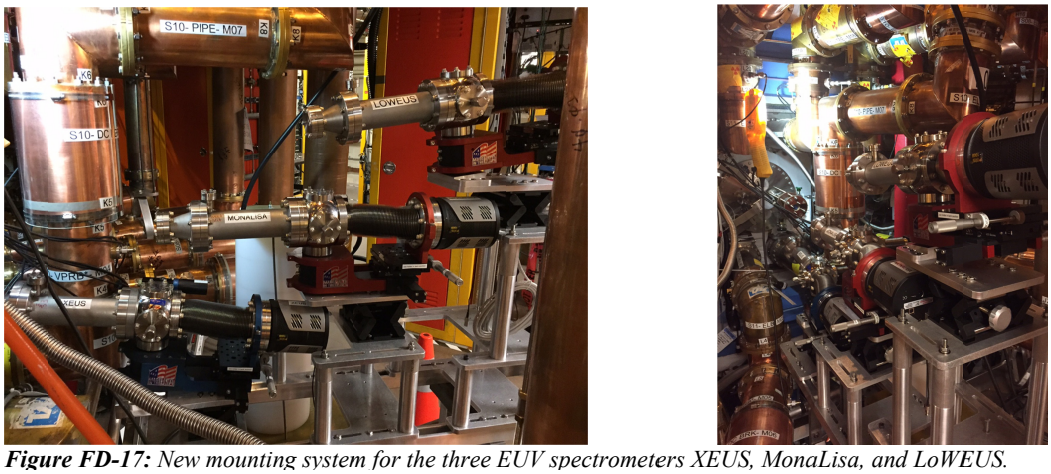

Figure FD-17: *New mounting system for the three EUV spectrometers XEUS, MonaLisa, and LoWEUS.*

Improved spectroscopic diagnostic coverage of upper divertor and center stack of NSTX-U
In order to diagnose the in-situ behavior of lithium coatings and the impact of lithium on poloidal and toroidal asymmetries in lithium coatings, and correspondingly, on plasma conditions and stability; new high-resolution UV-VIS-NIR spectroscopic diagnostics are being installed in NSTX-U by University of Tennessee at Knoxville (UT-K) and ORNL teams to monitor the

previously uncovered upper divertor and central stack region. The diagnostics consist of a high-speed ProEM-HS 512 camera, an IsoPlane SCT320 spectrometer and 32 sightlines: 16 sightlines on the upper divertor and 16 sightlines on the central stack. These spectroscopic views of the center-stack are obtained from one port at the Bay J equatorial plane for spectroscopy. A port at the Bay G bottom has been allocated to this project to provide views of the upper divertor. During the past year, a spectrometer, the Princeton instrument IsoPlane SCT320, was procured. This spectrometer can work with up to 3 different gratings: one low resolution grating (1200 G/mm) to monitor wide regions of the spectrum; one high resolution grating (3600 G/mm optimized for UV) to measure fine spectral features of selected spectral lines (i.e. to measure temperature); one intermediate resolution (2400 G/mm optimized for visible light) to monitor the intensity of multiple impurity lines at once. A ProEM:512B camera will be coupled to this spectrometer. The diagnostic support and optical design for the Bay J mid-plane and Bay G are complete, and the machine shop is manufacturing the fiber holder and other mechanical part. The second fiber optic bundles will be delivered at the early of September. These new diagnostic capabilities of the central stack and upper divertor will enable us to address outstanding questions regarding the dependence of the effectiveness of lithium evaporation on the poloidal and toroidal asymmetries in the coating.

Laser blow-off impurity injection system – Significant progress has been made in the laser blow-off (LBO) impurity injector development in FY2015. The LLNL group worked with PPPL on developing and installing a laser blow-off impurity injection system on NSTX-U. The LLNL LBO team presented a Conceptual Design Review of the system. The laser blow-off impurity injection system will be used for low- and high-Z impurity transport studies in the core, pedestal, and edge of NSTX-U plasmas. The system comprises of a 10-Hz, 1 J laser, beam delivery optics, and a target chamber that will be mounted on the NSTX-U vacuum vessel. The laser to be utilized is an infrared 1064 μm Q-switched Nd:YAG laser with a 16 ns pulse duration which has previously been used as a laser ablation system on EBIT-I and SuperEBIT. A preliminary beam path has been drawn out by LLNL and is awaiting approval and implementation. A new laser room location has been chosen and will be built on the mezzanine above the South Bay entrance. The laser room specifications for operation have been worked out. The target chamber has been designed and will be located on Bay J at 109' elevation. The system was designed and components are being fabricated. Installation is planned for early FY2016 and operational in FY 2016.

Pulse Burst Laser System – During FY2015, good progress was made on fabrication of the Pulse Burst Laser System (PBLS) being provided as an upgrade to the MPTS diagnostic under a DOE Early Career Research Project. Delivery of the laser to PPPL is expected in early FY2016. The high time resolution measurements enabled by this capability will play a key role in exploration of H-mode pedestal and ELM physics. The fast data acquisition system required for the MPTS detectors to be able to follow the rapid laser pulses from the PBLS was acquired, installed, and commissioned.

Energetic Particle Diagnostics – In preparation for the upcoming NSTX-U Run, both vertical and tangential Fast Ion D-Alpha (FIDA) diagnostics by UCI have been reinstalled, aligned and calibrated. Improvements have been made in the control modules and stray-light blocking to help make the measurements more accurate and reliable. Both FIDA systems are ready for plasma

experiments on NSTX-U. A new and innovative ssNPA system by UCI, which uses stacks arrays of silicon diodes with different foil thickness to get spatial profile measurements and some energy information, has been installed. Arrays mounted at different ports around the NSTX-U vessel provide both radial and tangential views to enable measurements of the fast ion distribution at different values of radius, energy and pitch. The electronics have been successfully tested on bench and they are able to measure fluctuations up to 150 kHz, which is suitable to study fast ion driven instabilities and transport. The final integration test of ssNPA detectors and electronics is currently underway. Other fast ion diagnostics that were previously available on NSTX have also been reinstalled and tested. This includes neutron counters and a scintillator-based lost-ion probe (sFLIP), which measured lost fast ions reaching the vessel wall, and a new charged fusion product (CFP) profile diagnostic.

Neutron Diagnostics – Three fission chamber neutron detectors and two scintillator detectors were installed on NSTX in FY2015. The absolute calibration of the fission chambers was determined through use of a Cf-252 neutron source in the vessel. This source is one that PPPL obtained from ANL to replace an old TFTR-era source that had become too weak to provide in-vessel calibrations within an operationally acceptable amount of time. These fission chamber detectors were operational for the NSTX-U first plasma KPP. A transfer of the fission chamber calibrations to a much higher range of neutron rates will be performed early in the FY2016 campaign.

A scintillator-based Fast Lost Ion probe (sFLIP) contributes to the NB characterization by providing energy and pitch resolved spectra of lost fast ions, e.g. from prompt losses, as the NB tangency radius is varied. sFLIP is being upgraded with a faster CCD detector capable of frame rates up to 100 kHz. A set of photo-multiplier tubes is also being installed on sFLIP for energy and pitch integrated measurements at rates up to 250 kHz from 6-10 sub-regions of the sFLIP scintillator plate. Major modifications to the vacuum vessel and two large diagnostic ports to accommodate the new neutral beam lines for NSTX-U has resulted in displacement of sFLIP from the port it had used during NSTX operations. A suitable alternate port for this diagnostic was identified, and that port was enlarged and substantially reinforced to accommodate the diagnostic. The in-vessel part of this diagnostic was then installed at the new location, while at the same time extending its range of pitch angle acceptance. This latter change should allow for additional physically valuable information to be obtained about beam ion losses in the forthcoming campaigns.

Charged Fusion Product (CFP) Diagnostic – The fusion rate profile diagnostic (also known as the ‘proton detector’ or ‘PD’) has been designed by collaborators at Florida International University. It provides direct measurements of the fusion reactivity profile. Because both the 3 MeV protons and 1 MeV tritons produced by DD fusion reactions are largely unconfined for NSTX-U parameters, they quickly escape the plasma. When these ions are measured by the PD detector array, their orbits can be tracked backward into the plasma. Such orbits are equivalent to curved sightlines for each detector, so that multiple signals can be inverted to infer a radial profile of the high-energy fast ions. A 4-channel CFP prototype has been tested in FY2013 on the MAST device (see the Energetic Particle Research Section). The 3 MeV protons and 1 MeV tritons produced by DD fusion reactions in MAST have been clearly observed. Given the

successful observations on MAST, a similar system for with 6 channels) has passed its final design review. Construction and installation on a probe drive on NSTX-U is anticipated in early FY16. The data obtained on NSTX-U will be used in a proposal for a future 16-channel system for NSTX-U.

Energetic-Particle-Induced Mode Diagnostics – A recently-developed UCLA 16-channel comb quadrature reflectometry system has been utilized on NSTX to study the eigenmode structure of fast-ion driven Alfven as well as other MHD modes. This unique system has also provided a wealth of additional information including investigation of three-wave coupling processes and identification of the potential role of Compressional Alfven Eigenmodes (CAEs) in contributing to core anomalous transport. In order to prepare for higher density operation in NSTX-U it is proposed to expand operation to 100GHz through the installation of 8 additional channels. This upgrade to 24 channels will allow detailed eigenmode structure measurements in high performance NSTX-U plasmas. Similarly to NSTX, several arrays of high-frequency Mirnov coils will provide routine measurements of the fluctuations spectrum on NSTX-U. Two sets of coils are toroidally displaced to enable the computation of the toroidal mode number of the modes from the phase of the complex spectrum. A reduced set of coils is displaced poloidally to provide information on the poloidal mode structure. The bandwidth of the magnetic fluctuation measurements will be extended on NSTX-U from the present 2-2.5 MHz up to 4 MHz, to account for the expected frequency up-shift of the modes as the toroidal field is increased. Another quantity of great relevance for EP studies is the radial structure of *AE modes. Several complementary systems will be available to this end on NSTX-U, including beam emission spectroscopy (BES) arrays, reflectometers, interferometers, polarimeters, and X-ray detectors. A proposal for installing a Doppler back-scattering (DBS) system will be also considered based on the available funds (see below). The BES system will provide low-k density fluctuation measurements near the mid-plane for normalized radii $0.1 < r/a < 1$. The number of channels will be increased from 32 up to 64 to simultaneously sample a wide region of the plasma. The measurement region will extend poloidally to cover a ~10 cm broad strip along the mid-plane. Further improvements may include a toroidally-displaced set of viewing channels, possibly limited to the edge region, to measure background emission (in the absence of the 2nd NB source) or the toroidal mode number of the instabilities. Density fluctuations are also derived from a multi-channel reflectometer system. The 16 channels available on NSTX will be complemented by 8 new channels at higher frequency, which will enable fluctuation measurements up to densities $\sim 10^{20}$ m^{-3}. Line-integrated measurements of density fluctuations will also be available from 3-4 far-infrared interferometer with sampling frequency ~4MHz. Beside density fluctuations, other quantities such as magnetic field and velocity fluctuations are important for a thorough identification and characterization of the different instabilities. A new radial polarimeter system will provide direct measurement of magnetic fluctuations along the mid-plane. Pending incremental funding for diagnostics development, flow fluctuations will be measured through a millimeter-wave Doppler back-scattering (DBS) system operating in the 80-100 GHz frequency range. This new measurement capability represents an alternative, substantially independent tool for identifying fast-ion modes that would significantly strengthen comparison with theory, expanding previous internal measurements of fast-ion modes previously restricted to perturbed density on NSTX. Additional information on fluctuations with frequency < 100 kHz will be

provided by a multi-energy SXR array with two toroidally displaced sets of views. Spatial resolution varies from ~1cm at the outboard mid-plane (R > 150 cm) to ~3 cm in the core and inboard mid-plane region (40 < R < 140 cm). Faster measurements with up to ~500 MHz bandwidth will be available from a system of two poloidal SXR arrays. Each array contains 16 channels viewing poloidally through two variable selected filters, with 2-3 cm resolution.

Doppler backscattering system (DBS) – UCLA collaborators will be installing a 96 GHz DBS before the end of the calendar year It recently underwent and passed a design review. Fabrication of the antenna mounting structure is proceeding (the electronics are already finished). It will probe density fluctuations with k_θ~10–15 cm^{-1}. It can penetrate to equilibrium densities as high as ~$1.1x10^{20}$ m^{-3}. (There is a tradeoff between penetration and achievable k_θ. Penetrating to high equilibrium density reduces k_θ). The system can also function as a reflectometer, in which chase it will reflect at $1.1x10^{20}$ m^{-3}. A four channel 81-87 GHz system is currently being fabricated and is expected to replace the 96 GHz system early next year. As a reflectometer, it will extend the existing capability for measuring MHD or fast-ion mode amplitude in the core to higher density (the current reflectometer array penetrates to $7x10^{19}$ m^{-3}). As a DBS system, it will measure the Doppler shift of the turbulent fluctuations, which can be used to determine plasma equilibrium and fluctuation **E**x**B** velocity. That may allow direct determination of the **E** fluctuation associated with fast- ion driven modes. Currently, on the density perturbation associated fast-ion modes can be directly measured.

Alfven Eigenmode Antenna for AE Stability Measurements – Simple antennae have been used in several machines (JET, C-Mod) to study TAE stability. The linear damping rate can be measured by sweeping the antenna frequency through the mode frequency. It will be useful to extend these studies to low aspect ratio tokamaks (MAST and NSTX). This would also help to validate ITER projections by challenging our fundamental understanding of the physics in the drive and stability of these modes. For low aspect ratio the antenna can also be used to study higher frequency Alfvén modes such as GAE and CAE. The "MHD active spectroscopy" plan begins with relatively simple antenna design. As operational experience builds up, more ambitious designs will be tried. In years 1&2 several proto-type antenna designs will be evaluated to optimize the coupling to TAE and CAE. The NSTX-U prototype AE antenna system consists of up to 4 compact modules, each of which is a single, 5-turn 'window-frame' coil, similar in principle to those used on JET, C-Mod and MAST. In parallel, the external power supplies for driving the antenna, the coupling networks and control hardware and software will be developed. While the highest priority will be to develop the capability to study TAE, time will be devoted to evaluating the antenna and coupling network at frequencies up to 2MHz, as will eventually be needed for Global and Compressional Alfvén eigenmode studies. A four-element *AE antenna was designed and installed on NSTX-U to test selectivity of the toroidal / poloidal mode number, as well as improving the coupling of the antenna to the modes. The low power (≈1kW) experiments will provide important information on antenna coupling and natural damping rates for each of the eigenmodes. This information will be used to determine the potential benefits of higher power experiments. If the natural eigenmode damping rates are small, there is the possibility of driving them to amplitudes where stochastic heating of thermal ions occurs.

NSTX-U FY2015 Year End Report: Research Results

In FY2015, the NSTX-U research team contributed experimental data and analysis in support of the 2015 DOE Joint milestone*: "Conduct experiments and analysis to quantify the impact of broadened current and pressure profiles on tokamak plasma confinement and stability. Broadened pressure profiles generally improve global stability but can also affect transport and confinement, while broadened current profiles can have both beneficial and adverse impacts on confinement and stability. This research will examine a variety of heating and current drive techniques in order to validate theoretical models of both the actuator performance and the transport and global stability response to varied heating and current drive deposition."*

The NSTX-U research contributions to the 2015 Joint Milestone are described in a separate report, and the NSTX-U contributions to *"Provide leadership, coordination, and support to the FES joint research target with the goal of quantifying the impact of broadened current and pressure profiles on tokamak plasma confinement and stability"* are summarized above.

Summary descriptions of the results of research milestones are provided below. Several of these milestones were originally written assuming experimental results from NSTX-U would be obtained in FY2015. However, as a result of the delay in NSTX-U research operation until FY2016, the milestone reports below provide information on planned experiments rather than experimental results. Descriptions of additional selected research highlights are also provided in subsequent sections.

FY2015 Research Milestone R(15-1): Assess H-mode energy confinement, pedestal, and scrape off layer characteristics with higher B_T, I_P and NBI heating power **(Target - September 2015. Initiated – September 2015)**

Milestone Description: *Future ST devices such as ST-FNSF will operate at higher toroidal field, plasma current and heating power than NSTX. To establish the physics basis for future STs, which are generally expected to operate in lower collisionality regimes, it is important to characterize confinement, pedestal and scrape off layer trends over an expanded range of engineering parameters. H-mode studies in NSTX have shown that the global energy confinement exhibits a more favorable scaling with collisionality ($B\tau_E \sim 1/\nu^*_e$) than that from ITER98y,2. This strong ν^*_e scaling unifies disparate engineering scalings with boronization ($\tau_E \sim I_p^{0.4} B_T^{1.0}$) and lithiumization ($\tau_E \sim I_P^{0.8} B_T^{-0.15}$). In addition, the H-mode pedestal pressure increases with $\sim I_P^2$, while the divertor heat flux footprint width decreases faster than linearly with I_P. With double B_T, double I_P and double NBI power with beams at different tangency radii, NSTX-U provides an excellent opportunity to assess the core and boundary characteristics in regimes more relevant to future STs and to explore the accessibility to lower collisionality. Specifically, the relation between H-mode energy confinement and pedestal structure with increasing I_P, B_T and P_{NBI} will be determined and compared with previous NSTX results, including emphasis on the collisionality dependence of confinement and beta dependence of pedestal width. Coupled with low-k turbulence diagnostics and gyrokinetic simulations, the experiments will provide further evidence for the mechanisms underlying the observed confinement scaling and pedestal structure. The scaling of the divertor heat flux profile with higher I_P and P_{NBI} will also be measured to characterize the peak heat fluxes and scrape off layer widths, and this will provide the basis for eventual testing of heat flux mitigation techniques. Scrape-off layer density and temperature profile data will also be obtained for several divertor configurations, flux expansion values, and strike-point locations to validate the assumptions used in the FY2012-13 physics design of the cryopump to inform the cryo-pump engineering design to be carried out during FY2016.*

Milestone R(15-1) Report:

A number of experiments were submitted to the NSTX-U 2015 Research Forum to investigate how increased plasma current, field strength and heating power will influence H-mode energy confinement, local transport, pedestal and scrape-off layer structure, and divertor heat flux width. These experiments will rely upon a number of enhanced diagnostic measurements, and together will be coupled with modeling efforts to expand our physics understanding of core, pedestal, scrape-off-layer (SOL) and divertor physics at higher field, higher power, and presumably reduced collisionality.

Experiment XP1520 “Ip/Bt scaling” will provide first data on the scaling of H-mode global energy confinement, as well as local transport and turbulence properties, as plasma current and toroidal field are increased beyond those achieved with NSTX. In addition to dedicated engineering scans in I_p and B_T (important for comparison with traditional empirical confinement scalings), a coupled current and field scan (at fixed $q \sim I_p/B_T$) will allow us to text access to lower collisionality plasma (at relatively constant β and $\rho_* = \rho_i/a$) to determine whether the favorable $\tau_E \sim 1/\nu_*$ confinement scaling observed in NSTX remains at even lower collisionality. As wall conditioning was shown to play a significant role in confinement and transport in NSTX, elements of this XP will be run during both the early boronized phase of NSTX-U operation, as well as repeated later on with lithium wall conditioning. This XP will also allow us to assess differences from changes in aspect ratio by comparing to previous NSTX data over similar I_p and

B_T values, as well as differences due to using the 2nd NBI at larger tangency radii. Additional XPs ("Core impurity transport measurements using new ME-SXR", "Perturbative momentum transport in NSTX-U L and H-modes") will investigate impurity and momentum transport for similar discharges, providing further insight into the changes in transport characteristics at increased I_p and B_T.

A key component of this XP will be to obtain low-k core turbulence measurements using the upgraded University of Wisconsin beam emission spectroscopy (BES) diagnostic, which has 16 additional detector channels (for a total of 48) reconfigured in a 2D array spanning core and edge views. The UCLA 16 channel reflectometer will also be available, and later in the year a Doppler backscattering (DBS) diagnostic is planned, possibly allowing intermediate-k fluctuation measurements. Both transport and turbulence measurements will be used, coupled with gyrokinetic analysis (e.g. GYRO, GTS), to infer the dominant core theoretical turbulence mechanism and whether it changes at higher I_p, B_T and reduced collisionality.

As an example, recent global nonlinear gyrokinetic simulations using GTS predict a distinct dissipative trapped electron mode (DTEM) in NSTX H-modes with large density gradients. A unique feature of the DTEM is that predicted transport increases with increasing collision frequency in the range relevant for NSTX-U (Figure R15-1-1). While these simulations are based on discharges somewhat different than those used for energy confinement scaling studies, they provide an additional theoretical microturbulence mechanism (in addition to microtearing modes) that could be at least partially responsible for the observed energy confinement scaling in NSTX ($\tau_E \sim 1/\nu_*$).

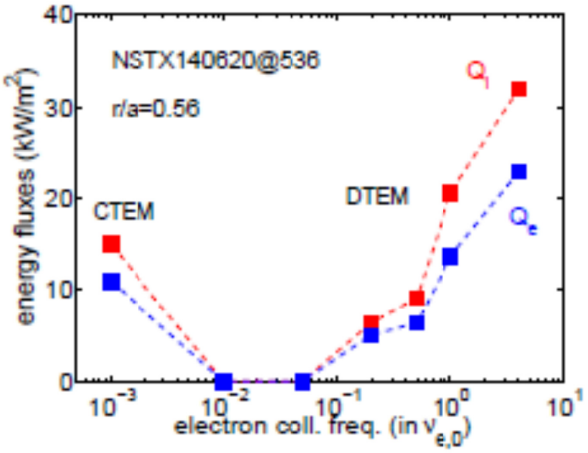

Figure R15-1-1: *Simulated TEM-driven energy fluxes as a function of electron collision frequency. Increasing electron collision frequency causes a turbulence transition from CTEM (at unrealistically low collision frequency) to DTEM (relevant to NSTX/NSTX-U).*

Experiment XP1512 "Characterization of the pedestal structure as a function of Ip, Bt, and Pnbi" will expand upon XP1520 by focusing on more thoroughly characterizing the change in pedestal structure at increased current, field and heating power (including use of the 2nd NBI). This XP will exploit the enhanced edge spatial resolution of the upgraded Thomson scattering system to determine how the pedestal height and width scale with poloidal beta, and results will be compared to corresponding theoretical modeling (e.g. EPED1) to determine how this relates to the onset of ELMs. The inter-ELM pedestal dynamics and associated turbulence will also be measured using both BES and 16 channel reflectometer, and comparison will be made with modeling using gyrokinetic codes (e.g. GS2, XGC-1). As the pedestal structure in NSTX was shown to be sensitive to wall conditioning, this XP will also take advantage of discharges using both boronized and lithiated wall conditioning.

Current scans contained in the above XPs will also provide new data on the scaling of SOL and divertor heat flux widths at increased plasma current. In addition to Langmuir probes, the divertor measurements will exploit three infrared (IR) cameras (ORNL), including one wide-angle, slow frame rate camera (30 Hz, viewing the lower divertor) and two dual-band fast frame rate cameras (1.6 kHz, viewing upper and lower divertors). IPEC modeling will be used to compare to the visible and IR footprints images. In addition, XP1514 "Heat flux and SOL width scaling in NSTX-U" will add to this understanding by investigating how the change in SOL and divertor heat flux widths is correlated with measurements of SOL turbulence. In addition to BES and reflectometry, this XP will exploit gas puff imaging (GPI) to characterize changes in SOL turbulence, especially with the addition of lithium wall conditioning and increased beam power through the use of the 2nd NBI. These results with be compared with modeling from SOLT, XGC1 and SOLPS to determine if changes in pedestal and SOL density gradient are related to changes in SOL turbulence. An additional XP1528 "Characterize plasma near planned plenum entrance position" will provide additional data on the density, temperature and particle flux in the SOL and divertor to validate the assumptions used in the design of the planned cyropump.

In NSTX-U, discharges with Ip ~2 MA and P_{NBI} ~12 MW and up to 5 s duration are projected to produce steady-state peak divertor heat fluxes in excess of 10 MW/m^2 , thereby challenging thermal limits of divertor graphite PFCs. The leading heat flux mitigation candidates for NSTX-U are the snowflake (SF) divertor geometry and the impurity-seeded radiative divertor technique, applied to the lower and upper divertors.

Research is planned on NSTX-U to demonstrate steady-state SF configurations as well as radiative divertors with reduced heat flux, compatible with high-beta, low collisionality H-mode scenarios. Several XPs have been accepted at the Research Forum to initiate research in these areas. Initial divertor experiments planned on NSTX-U in the first year will address radiative divertor operational space (current, power, density), neutral and impurity compression; calibration of control diagnostic signals without feedback; X-point MARFE characterization and avoidance; and studies of toroidal asymmetries of impurity radiation due to gas injection port locations. Several new diagnostics have been developed to study two-dimensional divertor impurity radiation distribution and support radiative divertor feedback control.

In preparation to experiments, modeling of the divertor transport and radiation in the standard and SF geometry has been performed. The modeled SF equilibria were also used in predictive edge transport modeling with multi-fluid code UEDGE. The model used NSTX-like transport coefficients, a neutral model using diffusive treatment in cross-field directions and a full Navier-Stokes treatment in the parallel direction, a fixed fraction (3 % carbon) impurity and the ion recycling coefficients R = 1 at the wall, and R = 0.99 at the divertor plates. Effects of the classical electromagnetic particle drifts were not included. The power flowing into the SOL was equally split between electrons and ions. The model did not include any special transport modifiers in the null region of the SF configuration, hence, it mostly showed effects of the SF geometry on heat and impurity radiation. The geometric factors were very favorable: in the outer strike point region, both the connection length and the poloidal flux expansion were increased by factors of 2-3 w.r.t. the standard divertor geometry.

The most challenging case with P_{SOL} = 9 MW representative of the 12 MW, 2 MA NBI-heated plasma discharge was studied in detail. It was found that a highly radiative scenario occured in the SF configuration at a much lower density, enabling a greater power loss (w.r.t. the standard divertor), and a larger operating window with reduced peak divertor heat flux at lower electron density. In the outer divertor, high peak divertor heat flux (7 MW/m^2) was obtained with the standard divertor, and a rediuced flux (3-4 MW/m^2) in the SF-minus configuration. Both the flux expansion and the additional radiated power loss were responsible for the heat flux reduction in the SF-minus model. The inner divertor region was found to be highly radiative (possibly with a detached strike point) in both configurations. Impurity-seeded divertors (with neon and argon) were also analyzed. It was found that 50% less argon was needed in the SF-minus configuration to achieve similar peak heat flux reduction factors (cf. standard divertor). The UEDGE modeling results supported the SF divertor as a leading steady-state divertor power exhaust solution for NSTX-U, and provided guidance for further radiative divertor development, including real-time feedback control.

FY2015 Research Milestone R(15-2): Assess the effects of neutral beam injection parameters on the fast ion distribution function and neutral beam driven current profile **(Target - September 2015. Initiated – September 2015)**

Milestone Description: *Accurate knowledge of neutral beam (NB) ion properties is of paramount importance for many areas of tokamak physics. NB ions modify the power balance, provide torque to drive plasma rotation and affect the behavior of MHD instabilities. Moreover, they determine the non-inductive NB driven current, which is crucial for future devices such as ITER, FNSF and STs with no central solenoid. On NSTX-U, three more tangentially-aimed NB sources have been added to the existing, more perpendicular ones. With this addition, NSTX-U is uniquely equipped to characterize a broad parameter space of fast ion distribution, Fnb, and NB-driven current properties, with significant overlap with conventional aspect ratio tokamaks. The two main goals of the proposed Research Milestone on NSTX-U are (i) to characterize the NB ion behavior and compare it with classical predictions, and (ii) to document the operating space of NB-driven current profile. Fnb will be characterized through the upgraded set of NSTX-U fast ion diagnostics (e.g. fast-ion D-alpha: FIDA, solid-state neutral particle analyzer: ssNPA, scintillator-based fast-lost-ion probe: sFLIP, and neutron counters) as a function of NB injection parameters (tangency radius, beam voltage) and magnetic field. Well controlled, single-source scenarios at low NB power will be initially used to compare fast ion behavior with classical models (e.g. the NUBEAM module of TRANSP) in the absence of fast ion driven instabilities. Diagnostics data will be interpreted through the "beam blip" analysis technique and other dedicated codes such as FIDASIM. Then, the NB-driven current profile will be documented for the attainable NB parameter space by comparing NUBEAM/TRANSP predictions to measurements from Motional Stark Effect, complemented by the vertical/tangential FIDA systems and ssNPA to assess modifications of the classically expected Fnb. As operational experience builds up during the first year of NSTX-U experiments, additions to the initial Fnb assessment will be considered for scenarios where deviations of Fnb from classical predictions can be expected. The latter may include scenarios with MHD instabilities, externally imposed non-axisymmetric 3D fields, and additional High-Harmonic Fast Wave (HHFW) heating.*

Milestone R(15-2) Report

In preparation for dedicated experiments on NSTX-U (see below), activities related to Milestone R(15-2) have focused on the development of improved modeling/analysis tools and of diagnostics to characterize the fast ion distribution function and its evolution as a function of NB injection parameters.

Several numerical tools have been improved and validated against NSTX and DIII-D data to provide a more accurate description of the fast ion evolution. Those models have been developed to provide quantitative results also for scenarios with instabilities causing enhanced fast ion transport. Instabilities range from toroidal Alfvén eigenmodes (TAEs) and other Alfvénic instabilities to lower frequency MHD and energetic particle-driven modes such as long-lived kink modes, fishbones and EPMs.

XP/XMP	Title	Goals
110	FIDA/ssNPA/sFLIP checkout	Commissioning of main fast ion diagnostics. Test background subtraction techniques for FIDA. Compare phase space response of different systems. Test sFLIP diagnostic.
107	Neutron diagnostic calibration	Obtain low-NB-power plasmas with low neutron count rate. Transfer calibration from pulse-counting to current-counting mode for fission chamber counter. Transfer calibration to scintillators.
1522	Beam ion confinement of 2nd NB line	Checkout confinement properties of fast ions from 2nd NB line in quiescent conditions. Investigate confinement vs. beam source, injection energy, plasma current, toroidal field. Compare with classical predictions from NUBEAM/TRANSP.
1523	Characterization of 2nd NB line	Assess operating regimes achievable with combinations of 1st + 2nd NB lines. First characterization of NB-CD with 2nd NB line. Dedicated discharges will explore pressure profile modifications vs. NB source mix. This XP complements the Ip/Bt scan XP by Kaye et al.
1524	AE critical gradient	Explore applicability of "critical gradient" model for fast ion profile in the presence of instabilities. Validate numerical models. Characterize EP transport vs. NB power, fast ion pressure with unstable AE modes.

Table R15-2-1: *Summary of approved XMPs and XPs to address R15-2 Milestone after the beginning of NSTX-U operations.*

Starting from the ORBIT code, an "hybrid" model has been developed to compute self-consistently the evolution of instabilities and fast ion distribution [R15-2-1]. Phase and amplitude of each mode are evolved based on the energy exchanged with fast ions. Growth rates and relaxed fast ion profiles are computed dynamically, providing a quantitative estimate of the mode stability and saturation amplitude. A second approach relies on the notion of a "critical gradient" in the fast ion profile resulting from fast ion transport by instabilities [R15-2-2]. Required inputs are growth and damping rates, which are obtained for example from linear stability analysis through the NOVA-K and HINST codes (cf. Section on Energetic Particle Research highlights for more details). This model has been applied to several NSTX and DIII-D cases, showing reasonable agreement with experimental data, e.g. in terms of predicted vs. measured neutron rate deficit (cf. Figs. JRT-15-1 and 2 in the "JRT-15 Notable Outcome" Section). Finally, a reduced model for fast ion transport ("kick" model) has been implemented in TRANSP [R15-2-3] and tested against NSTX and DIII-D data. Initial results compare well with experimental results and with predictions from the "critical gradient" model. Extensive validation is ongoing, suggesting further improvements to the model. One key issue to resolve is to improve the model implementation in the NUBEAM module of TRANSP. For instance, in its first implementation the model was applied in between macroscopic NUBEAM time steps. This resulted in under-estimated losses for particles that are near a loss boundary. Work is in progress to merge the model in the "orbiting" section of NUBEAM, so that classical mechanisms (scattering, slowing down) and additional transport can be treated on similar time scales. Once validated, this model is expected to provide more accurate simulations of the fast ion phase space evolution, which enables more quantitative predictions of quantities such as NB current drive and power exchange between fast ions and thermal populations.

The improved modeling capabilities are expected to be ready for validation with data from dedicated NSTX-U experiments. Experimental plans have been finalized to cover the most

important aspects of NSTX-U re-commissioning, with emphasis on the new, 2nd NB injection line, see Table R15-2-1. The initial characterization will start with an asssessment of fast ion confinment and dynamic for "MHD-quiescent" scenarios for which classical fast ion physics applies. Data from those experiments will be compared to predictions from numerical tools such as the NUBEAM module in TRANSP. Experiments will then be extended to higher-performance, H-mode plasma cenarios with a variety of NB injection mixes. Under these conditions, with injected NB power exceeding 2-4MW, Alfvénic and other MHD instabilities are likely to be excited. This will provide the opportunity to test and validate the fast ion transport models described above, in order to obtain accurate modeling of the fast ion distribution function and of its temporal evolution. Finally, planned experiments for the coming Run include dedicated sessions to explore scenarios which maximize the non-inductive NB-driven current fraction, up to fully non-inductive scenarios, and to explore the range of validity of "critical gradient" models for fast ion transport and profile evolution.

Key diagnostics for the experimental characterization of the fast ion distribution function on NSTX-U are fast-ion D-alpha (FIDA) systems and arrays of solid-state neutral particle analyzers (ssNPA). Analysis and interpretation of FIDA and ssNPA data is challenging, since the systems sample only a portion of the entire distribution. The FIDAsim code [R15-2-4] is used for forward-modeling of experimental data to infer the actual distribution function based on predictions from the TRANSP/NUBEAM code and comparison to experimental data. Recent development of a FIDA analysis technique will enable accurate interpretation of data from the upgraded FIDA and ssNPA systems available on NSTX-U (see below for details on the diagnostics). To test the technique, measured fast-ion D-alpha (FIDA) data from an extensive NSTX database have been compared to "classical" predictions that neglect transport by instabilities [R15-2-5]. Even in the absence of detectable MHD, in virtually all cases, the profile peaks at smaller major radius and the profile is broader than the predictions. Abrupt large-amplitude MHD events flatten the FIDA profile, as do most toroidal Alfven eigenmode (TAE) *avalanche* events. Generally, the onset of a long-lived mode also flattens the FIDA profile. There is a shortfall of high-energy ions at large major radius in discharges with repetitive TAE bursts.

To improve the interpretation of both FIDA and ssNPA data, a new 3D "halo" model previously implemented in TRANSP has undergone extensive verification for NSTX and projected NSTX-U scenarios [R15-2-6]. The 3D halo neutral code uses a "beam-in-a-box" model that envelopes both injected beam neutrals and resulting halo neutrals. Upon deposition by charge exchange, a subset of the beam energy components produces first generation halo neutrals that are tracked through successive generations until an ionization event occurs or the descendant halos exit the box. The 3D halo neutral model and Neutral Particle Analyzer (NPA) simulator in the TRANSP code have been benchmarked with the Fast-Ion D-Alpha simulation (FIDAsim) code. When using the same atomic physics database, TRANSP and FIDAsim simulations get excellent agreement on the spatial profile and magnitude of beam and halo neutral densities, as well as the NPA energy spectrum. The simulations show that halo neutrals remain in the vicinity of the neutral beam footprint as expected and that halo neutral density can be comparable with beam neutral density. Future comparisons between measurements, FIDAsim and TRANSP modeling will benefit from this important improvement for NSTX-U scenarios with complex NB injection patterns.

In preparation for the upcoming NSTX-U Run, both vertical and tangential FIDA diagnostics have been reinstalled, aligned and calibrated. Improvements have been made in the control modules and stray-light blocking to help make the measurements more accurate and reliable. Both FIDA systems are ready for plasma experiments on NSTX-U. A new and innovative ssNPA system, which uses stacks arrays of silicon diodes with different foil thickness to get spatial profile measurements and some energy information, has been installed. Arrays mounted at different ports around the NSTX-U vessel provide both radial and tangential views to enable measurements of the fast ion distribution at different values of radius, energy and pitch. The electronics have been successfully tested on bench and they are able to measure fluctuations up to 150 kHz, which is suitable to study fast ion driven instabilities and transport. The final integration test of ssNPA detectors and electronics is currently underway. Other fast ion diagnostics that were previously available on NSTX have also been reinstalled and tested. This includes neutron counters and a scintillator-based lost-ion probe (sFLIP) which measured lost fast ions reaching the vessel wall.

An important addition to the NSTX-U set of fast ion diagnostics is an array of fusion product detectors, recently tested on MAST [R15-2-7]. Professor Werner Boeglin, of the Physics Department of Florida International University (FIU) in Miami, Florida, has been collaborating with the NSTX-U group to implement an array of surface barrier diode detectors to measure the emission rate and radial profile of the 3 MeV protons and 1 MeV tritons produced by DD fusion reactions in NSTX-U plasmas [R15-2-8]. These particles' gyro orbits are unconfined even at maximum magnetic field in NSTX-U. Consequently, this diagnostic can provide details of the spatial extent of the NB ion population through tomographic reconstruction of the fusion reaction rate profile along the curved orbits that reach each detector in the array. The result aids in determining the profile of the neutral beam driven current. The instrument is also capable of measuring the effects of MHD activity on the beam ion density profile. In the past year, Prof. Boeglin and co-workers analyzed an extensive set of data from a prototype of this system that had been fielded on MAST in 2013. The data confirmed the feasibility of the measurement and preliminary results are similar to those of the MAST neutron camera, which measures the DD fusion reactivity profile by means of the neutrons emitted from the reaction. Prof. Boeglin's student, Ramona Perez, successfully defended her Ph.D. dissertation, entitled "A Charged Fusion Product Diagnostic for a Spherical Tokamak", on this instrument and data in April 2015 [R15-2-9]. Another Ph.D. student has joined Prof. Boeglin's research group and has completed the design of the detector array for NSTX-U, based upon the results from MAST. This design has passed its Final Design Review at PPPL and is under construction, for use in forthcoming NSTX-U campaigns.

Finally, UCLA collaborators will be installing a 96 GHz Doppler backscattering system before the end of the calendar year. It recently underwent and passed a design review. Fabrication of the antenna mounting structure is proceeding (the electronics are already finished). It will probe density fluctuations with k_θ~10–15 cm^{-1}. It can penetrate to equilibrium densities as high as ~$1.1x10^{20}$ m^{-3}. (There is a tradeoff between penetration and achievable k_θ. Penetrating to high equilibrium density reduces k_θ). The system can also function as a reflectometer, in which case it will reflect at $1.1x10^{20}$ m^{-3}. A four channel 81-87 GHz system is currently being fabricated and is expected to replace the 96 GHz system early next year. As a reflectometer, it will extend the

existing capability for measuring MHD or fast-ion mode amplitude in the core to higher density (the current reflectometer array penetrates to $7x10^{19}$ m^{-3}). As a DBS system, it will measure the Doppler shift of the turbulent fluctuations, which can be used to determine plasma equilibrium and fluctuation **E**x**B** velocity. That may allow direct determination of the **E** fluctuation associated with fast- ion driven modes. Currently, only the density perturbation associated with fast-ion modes can be directly measured.

References

[R15-2-1] R. B. White et al., to be presented at 57th APS-DPP Meeting, Savannah GA (2015)
[R15-2-2] N. Gorelenkov et al., TH/P1-2, 25th IAEA-FEC, Saint Petersburg RU (2014)
[R15-2-3] M. Podestà et al., Nucl. Fusion **55**, 053018 (2015)
[R15-2-4] W. W. Heidbrink et al., Commun. Comput. Phys. **10**, 716 (2011)
[R15-2-5] W. W. Heidbrink et al., in preparation (2015)
[R15-2-6] S. Medley et al., submitted to Plasma Phys. Control. Fusion (2015)
[R15-2-7] M. Cecconello et al., Plasma Phys. Control. Fusion **57**, 014006 (2015)
[R15-2-8] W. U. Boeglin et al., Rev. Sci. Instrum. **81**, 10D301 (2010)
[R15-2-9] R. Perez et al., Rev. Sci. Instrum. **85**, 11D701 (2014)

FY2015 Research Milestone R(15-3): *Develop the physics and operational tools for obtaining high-performance discharges in NSTX-U* **(Target - September 2015. Initiated – September 2015)**

Milestone Description: *Steady-state, high-beta conditions are required in future ST devices, such as a FNSF/CTF facility, for increasing the neutron wall loading while minimizing the recirculating power. NSTX-U is designed to provide the physics knowledge for the achievement of such conditions by demonstrating stationary, long pulse, high non-inductive fraction operation. The ultimate toroidal field (1.0 T) and plasma current (2.0MA) capability of NSTX-U is twice that in NSTX. NSTX-U has a capability for >5 second discharges, and it has an additional beamline which doubles the available heating power and provides much greater flexibility in the beam current drive profile. The aim for studies during the first year of operation of NSTX-U is to lay the foundation for the above operational scenario goals by developing needed physics and operational tools, using toroidal fields up to ~0.8 T, plasma currents up to ~1.6 MA, improved applied 3D field capabilities from additional power supplies, a variety of plasma facing component (PFC) conditioning methods, and advanced fueling techniques. As an example of the latter, supersonic gas injection provides higher fueling efficiency, and will be used to develop reliable discharge formation with minimal gas loading. Differing PFC conditioning techniques, including boronization and lithium coatings, will be assessed to determine which are most favorable for longer pulse scenarios. Impurity control techniques, an example of which is ELM pacing, will be developed for the reduction of impurity accumulation in otherwise ELM-free lithium-conditioned H-modes. The higher aspect ratio, high elongation ($2.8 < \kappa < 3.0$) plasma shapes anticipated to result in high non-inductive fraction in NSTX-U will be developed, and the vertical stability of these targets will be assessed, with mitigating actions taken if problems arise. An initial assessment of low-n error fields will be made, along with expanding the RWM control and dynamic error field correction strategies using both proportional and state-space $n \geq 1$ feedback schemes, taking advantage of the spectrum flexibility provided by the 2nd SPA power supply. Resonant field amplification measurements, ideal MHD stability codes, and kinetic stability analysis will be used to evaluate the no-wall and disruptive stability limits in these higher aspect ratio and elongation scenarios. These physics and operational tools will be combined to make an initial assessment of the non-inductive current drive fraction across a range of toroidal field, plasma density, boundary shaping, and neutral beam parameters.*

Milestone R(15-3) Report:

Modeling, control tools and experimental planning were conducted in FY15 to prepare for the realization of high-performance discharges on NSTX-U in FY16.

One significant accomplishment in FY15 was the commissioning of the NSTX-U magnetic field sensors, including the new sensors on the center-stack. This enabled off-line equilibrium reconstructions during the first plasmas on NSTX-U and the ability to qualify the calibrated signals in the realtime plasma control system. This activity is a critical step in actively controlling the plasma shape to achieve high-performance discharges.

The realtime EFIT (rtEFIT) code in the plasma control system was updated to incorporate the latest version released by General Atomics and the new magnetic measurement locations on NSTX-U. This new version was tested using input data created by NSTX-U TRANSP simulations where the magnetic field at the location of the magnetic sensors was a constraint to rtEFIT. The reconstruction based on the synthesized magnetic sensor information was in good

agreement with the plasma shape from TRANSP (see Figure IS-ASC-6) providing confidence that an essential tool for active shape control in the PCS is ready to support operations in FY16.

An ongoing effort to upgrade the hardware and software in the plasma control system (PCS) made significant progress in FY15. The upgrades improve the maintainability and reliability of the system, and facilitate an expansion of the control tools. A number of critical capabilities (such as coil current and gas control) operated within the new architecture and code organization during the first plasma campaign in August 2015. Additional capabilities, such as shape control, vertical stability control and neutral beam injection control, were extensively tested and are ready to support FY16 operations.

A number of experimental proposals (XPs) that commission control tools necessary for high-performance discharges on NSTX-U completed a full review in FY15. The following summarizes key experiments that develop control capabilities that contribute to the FY15-3 milestone:

- XP-1501 "Optimization of vertical control algorithm" will determine the plasma elongation limit imposed by vertical stability as a function of the plasma inductance (li) and identify limitations in the active vertical control system on NSTX-U. The second half of the experiment will use the previous results coupled with control models to examine the expansion of the elongation limits as a result control model development and optimization.

- XP-1503 "X-point control integration with shape control" will test the functionality of controlling the locations of the upper and lower x-point position using the upgraded set of poloidal field coils. Verification of acceptable x-point control is an essential first step toward implementing full plasma shape control capabilities such as advanced magnetic divertor geometries.

- XP-1504 "Beam power and beta-N control" demonstrates expanded capability to control the timing of the neutral beam injection within the plasma control system to deliver a requested heating power or achieve a particular beta-N.

- XP-1509 "Combined betaN and li feedback control" will gather a dataset needed to inform model-based control algorithms under development. Plasma current, total and individual beam powers, and mid-plane outer gap size will be considered as actuators. Results will be compared to predictions of closed loop TRANSP simulations to verify the predictive capability of these simulations.

- "Current profile controllability scoping study" this XP will generate data to validate models of the current profile evolution that will be used for designing current profile feedback control algorithms. Actuator modulations (individual beams, outer-gap size, density) will be done in several shots to assess the current profile dynamic response to these changes and the effect of beam pulse-width modulation. Variations in actuator

trajectories during the ramp-up will also be done to assess controllability and the applicability of TRANSP and control-oriented reduced models to this phase of the discharge.

Two XPs that integrate control tools and operational scenarios to develop high-performance plasmas on NSTX-U in FY16 are:

- XP-1507 “Maximizing the non-inductive current fraction in NSTX-U H-modes” aims to operate with nearly 100% non-inductive current drive. Global plasma models provide guidance for the non-inductive plasma current expected for a given toroidal field (TF) and confinement assumptions. This experiment will assess those predictions against the available TF operating space.

- “Develop long pulse H-mode for NSTX-U” will aim to make the longest possible H-mode plasma (> 4.5 seconds). This requires scenario development within the constraints of coil heating and neutral beam operation, development of stable plasma shape control through the full swing of the ohmic fringe field, and integrating tools and scenarios that provide adequate MHD stability, particle control and impurity control.

Many experiments were also submitted to the NSTX-U Research Forum to directly address MHD mode stabilization and control, aiming to directly exploit the new capabilities of NSTX-U in this role. The proposals spanned a large range of topics, all which must be addressed in the new NSTX-U device, and many which will examine the latest advances in mode control capabilities in magnetic fusion as a whole. The following summarizes some of these proposals, which span from error field correction to state-space control of key plasma profiles including current profile peaking and beta, plasma rotation, tearing mode stabilization, and passive and active control of unstable RWMs.

In the area of error field corection, three relevant experiments from were proposed and accepted at the research forum. The corresponding experimental proposals have also been reviewed.

- XP 1506 “Low-beta, low-density locked mode studies” the goal is to provide an initial assessment of n=1 error fields in NSTX-U, obtain optimal feed-forward n=1 correction (compass scans), connect to the NSTX locked mode database, and possible to address transient error fields during startup.
- XP 1515 has the goal of assessing the n=1,2,3 error fields at high-β, starting with the technique of ramping error field amplitudes and performing a so-called compass scan in phase space.
- XP 1516 “Optimization of PID dynamic error field correction”, the mode ID upgrade (miu) algorithm corrects for static and AC pickup on the RWM/EF sensors will be tested. The sensors, phases, and gains in the miu-based PID feedback algorithm will be tuned, and the low pass filter (already available in PCS) will be utilized to isolate the effect of DEFC from fast RWM control.

In the areas of neoclassical toroidal viscosity (as applied to plasma rotation control for global mode stability, and resistive wall mode active control, experiments were proposed and accepted at the research forum. The corresponding experimental proposals for the first two experiments have also been reviewed.

- XP 1517 "Neoclassical toroidal viscosity at reduced collisionality (independent coil control)" will test the dependence of neoclassical toroidal viscosity (NTV) on ion collisionality in the new NSTX-U plasma conditions to vary the plasma density and temperature where NTV torque is maximized in the plasma, focusing on the NTV scaling and comparison to theory at the lowest collisionality possible. The increase in NTV strength in these regimes are important to understand from a physics perspective for extrapolation to future devices, but it also has more near-term practical importance in developing more accurate simple models for the expected rotation damping to be used in NSTX-U state-space rotation feedback control. This rotation control capability will be used for global mode control in NSTX-U. To further support closed-loop rotation feedback, the present experiment will apply the planned $n = 2$ and $n = 3$ applied field configurations (as shown in Figure R15-3-1 below - and potentially their combination) expected for non-resonant braking, with and without n = 1 field correction.

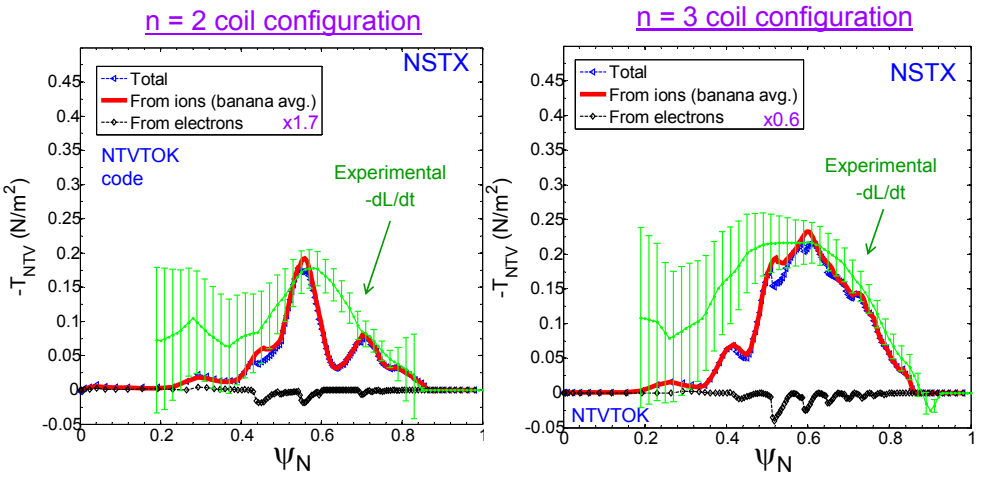

Figure R15-3-1: *NTV torque density profiles computed for NSTX plasmas with n = 2 and n = 3 applied field 'configurations' compared to experiment using a perturbative technique to isolate the NTV torque.*

- XP 1518 "RWM PID control optimization based on theory and experiment". NSTX experiments using n = 1 RWM control in 2010 and subsequent analysis using the VALEN code showed that some settings for control using Br and Bp sensors were optimal, while others could be improved. In particular, the Bp feedback phase, and Br feedback gain presently differed the most from the experimental settings for NSTX. Given the changes to the device hardware (e.g. the vacuum vessel), the n = 1 RWM PID control system parameters such as feedback phase and gain need to be determined. The dual component sensor gains and feedback phases will be examined in this experiment for the first time in NSTX-U.

Another proposed XP, the RWM state space controller (RWMSC) will be applied to high performance plasmas (high normalized beta, low li, etc.) to examine several aspects of mode control physics, as a logical next step to the initial experiments of 2010. The present experiment moves beyond the initial experiments in the following ways: (i) eigenfunctions of different target plasmas will be introduced, and several target plasmas will be used (high triangularity, high li-low A, snowflake divertor), (ii) eigenfunctions with $n > 1$ will be introduced to the controller, (iii) independent control of the 6 RWM coils will allow control of $n > 1$ perturbations, (iv) a more careful comparison of control with/without wall states will be conducted, (v) an initial set of shots will test compatibility with plasma rotation reduction by NTV, (vi) proportional feedback using Br sensors will be added. Gains and feedback phase will be adjusted as needed. NTV magnetic braking will be compatible if the eigenfunction and wall states used do not conflict with the applied field. This has never been tested. Proportional gain using RWM Br sensors has also never been used with the state space controller, and will be tested in this experiment.

Finally, in the area of assessing passive stability limits, another proposed experiment in which NSTX-U plasmas with various on- and off-axis neutral beam injection will be used to produce a variety of rotation profiles and energetic particle distribution functions (changing both the radial (Ψ) profile and the pitch angle dependence). Then standard techniques of determining the stability of the plasma will then be employed for these different EP distribution function plasmas. These include using n=3 non-resonant magnetic braking to slow the plasma rotation to the marginal stability point, or using n=1 AC fields to measure resonant field amplification (RFA) which indicates proximity to the marginal stability point.

I. Boundary Science Research Highlights

In 2014, three topical science groups (TSGs) were organized under a new boundary science group. The three TSGs include (a) pedestal structure and control, (b) divertor and scrape-off layer, (c) and materials and plasma facing components. Each of these TSG areas is covered as a sub-section in the boundary science group report below.

A. Pedestal Structure and Control TSG Research Highlights

A major goal of the NSTX-U Pedestal Structure and Control TSG is to characterize H-mode access and L-H power threshold, characterize the pedestal structure, understand the turbulence in pedestal and identify common characteristics in phenomenology of different ELM types, and develop control approaches to improve the plasma performance.

1. Collaborative studies

a. Pedestal Saturation and the onset of the Quasi-Coherent fluctuations on DIII-D and C-Mod

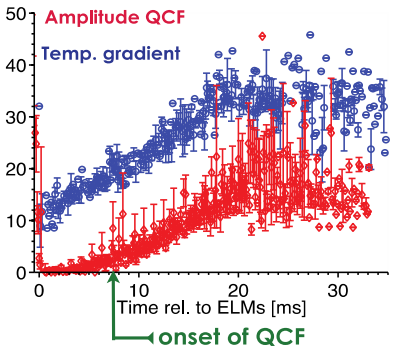

Figure BP-PED-1: *Evolution of magnetic signal of the QCF and the pedestal temperature gradient.*

State-of-the-art measurements of the edge transport barrier recovery following edge-localized modes (ELMs) on C-Mod and DIII-D reveal new evidence that turbulent fluctuations play an important role in the saturation of the edge gradient in the inter-ELM period [BPR-PED-1, BPR-PED-2, BPR-PED-3]. Identification of edge quasi-coherent fluctuations (QCFs) on multiple diagnostics is observed when the pressure gradient in the edge pedestal region of the plasma saturates following the ELM. This supports the hypothesis advanced in recent theoretical models that the threshold for the onset of kinetic ballooning modes (KBMs) sets the criteria for the saturation of the pressure gradient. Figure BP-PED-1 shows a correlation between the onset of QCFs and the saturation of the edge temperature gradient following the ELM. The fluctuations are of the order of the ion gyroradius and are localized to the plasma edge based on beam emission spectroscopy (BES) measurements on DIII-D. Similarly on C-Mod [BPR-PED-3], the QCFs are determined to be edge localize based on the reflectometry and the gas-puff-imaging measurements. Magnetic measurements confirm the MHD nature of the fluctuations as expected for KBMs. The pedestal predictive EPED model indicates that the pedestal pressure gradient reaches KBM critical gradient when the

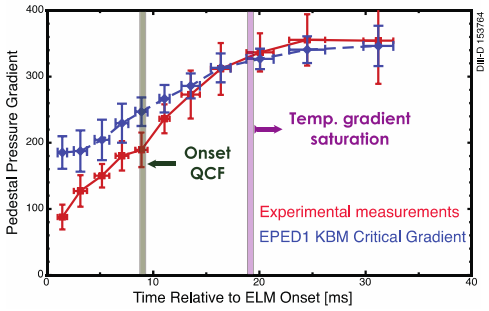

Figure BP-PED-2: *EPED1 KBM calculations in blue symbols. The red squares represent the pedestal pressure gradient evolution. The vertical lines indicate, respectively, the QCF onsets and the temperature gradient saturation.*

fluctuations are observed. In addition the EPED [BPR-PED-3] model predicts saturation of the pressure gradient, i.e., the observed gradient does not exceed the prediction after the onset of the instability (Figure BP-PED-2). These results provide additional data toward validation of key theoretical predictions for the physics of the pedestal, which is essential for performing reliable predictions for the fusion performance of ITER plasmas.

b. Investigation of L-H transition physics on NSTX using GPI velocimetry

A new collaboration on NSTX GPI data analysis was begun with Dr. Santanu Banerjee of the Institute for Plasma Research in India. A paper was completed and submitted to *Nuclear Fusion* this fiscal year: "Analysis of edge turbulence imaging data in NSTX Ohmic plasmas" by S. Banerjee and S.J. Zweben. Two dimensional turbulence velocity fields were derived from particle image velocimetry (PIV) based on orthogonal dynamic programming algorithm, and the turbulence velocity and turbulence Reynolds stress profiles are compared for L-mode and H-mode time periods. The work on NSTX was motivated by recent results from Cziegler on C-Mod [BPR-PED-5] that showed that the time sequence of the L-H transition can be described by the peaking of the Reynolds work, then the collapse of the turbulence, and finally the rise of the diamagnetic electric field shear. Researchers on NSTX in collaboration with IPR researcher have implemented a velocimetry analysis using GPI data [BPR-PED-6] to investigate the L-H transitions on 17 L-H transitions in ohmic, RF and NBI heated discharges. Initial work is focusing on the dynamic of the radial and vertical velocity fields across the L-H transition. So far, it is clear that that vertical velocity measured at edge and outside the separatrix reverses propagation direction across the L-H transition in all three types of discharges. Such reversal becomes less consistent for the vertical velocity inside the separatrix. Further work is underway to determine potential causes of such discrepancies. In addition, the time resolved Reynolds stress and its impact on turbulence for the set of discharges would be computed and compared with observations from C-Mod [BPR-PED-5].

2. Cross diagnostic comparison between GPI and BES on NSTX

Fluctuation measurements from Gas Puff Imaging (GPI) and Beam Emission Spectroscopy (BES) have been compared, and generally good agreement is found [BPR-PED-5]. Measurements are compared primarily near the 0.85 normalized flux position where both diagnostics are expected to predominantly measure density fluctuations. The diagnostic views are closely positioned in R and Z, but are toroidally separated by approximately 16 degrees. Peak cross-diagnostic correlation values often exceed R=0.6, and time traces visually exhibit a high degree of similarity as seen in Figure BP-PED-3. Typical measures of turbulence characteristics (i.e.

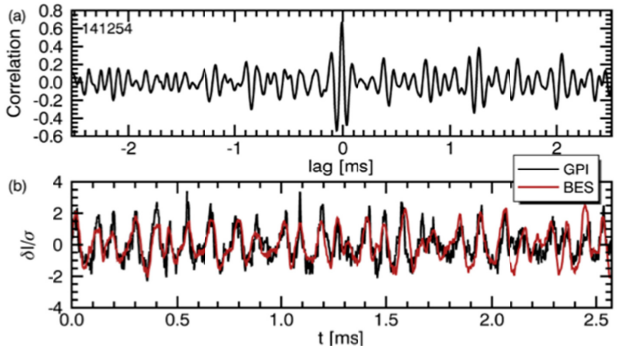

Figure BP-PED-3: *Traces of (a) time-lagged cross-correlation between GPI and BES and (b) time traces of GPI and BES intensity.*

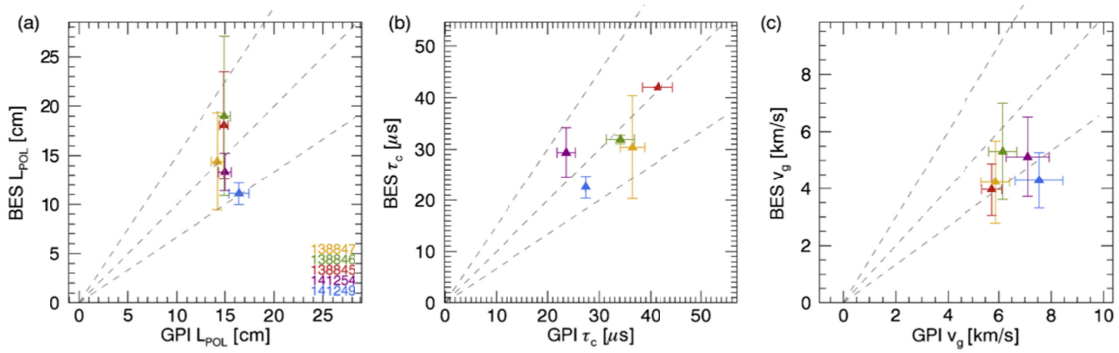

Figure BP-PED-4: *Scatterplots comparing (a) poloidal correlation lengths estimates, (b) de-correlation time estimates, and (c) TDE velocity estimates.*

poloidal correlation length, de-correlation time, and statistical velocity) also agree at the +/-40% level as demonstrated by the scatterplots of these quantities shown in Figure BP-PED-4. In addition, cross-diagnostic cross-coherence for frequencies between 5 and 15 kHz is strong, and skewness and kurtosis values for fluctuation PDFs are consistent with a Gaussian distribution within the sample deviations for both diagnostics.

Some discrepancies are also observed. Autopower spectra exhibit differences above ~20 kHz, but these are likely attributable to the lower signal-to-noise ratio of GPI. Most notably, fluctuation levels measured by GPI were typically 15-20% of the mean while BES values were 2-3% of the mean. DEGAS-2 simulations suggest neutral density fluctuations could have an impact on GPI fluctuation levels, but a more sophisticated, time-dependent modeling effort is needed to resolve the issue.

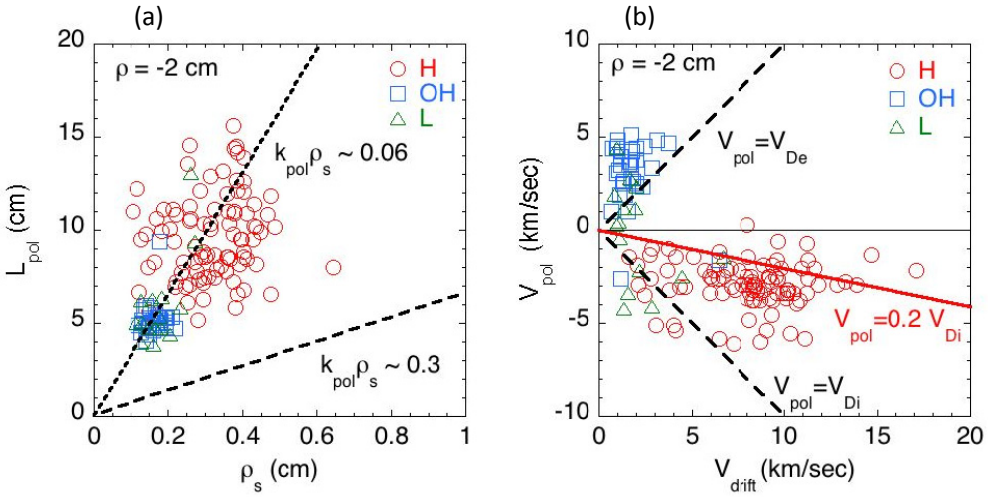

Figure BP-PED-5: *Examples of these results for the 140 shot GPI database. In the left figure are the variations of the poloidal turbulence correlation length L_{pol} just inside the separatrix with respect to the drift-wave gyroradius parameter ρ_s, showing a fairly clear scaling $k_{pol}\rho_s$ ~0.06 (using the B field on axis). The higher L_{pol} in H-mode plasmas is consistent with the higher edge temperature and ρ_s. In right figure are the poloidal turbulence velocities V_{pol} at the same radius with respect to the calculated diamagnetic drift velocity. The Ohmic shots are consistent with the expected electron diamagnetic drift velocity, but the H-mode shots, are most consistent with V_{pol} ~0.2 x the ion diamagnetic speed.*

3. Turbulence studies in NSTX edge using GPI

A new paper, accepted for publication by *Nuclear Fusion*, describes the range of variations in edge and SOL turbulence observed using a gas puff imaging (GPI) diagnostic in NSTX discharges. The database consists of 140 shots including Ohmic, L-mode, and H-mode plasmas measured during steady-state conditions (e.g. without ELMs). Turbulence quantities were evaluated using both cross-correlation analysis and blob tracking. Relative fluctuation levels varied from $\delta I/I \sim 0.15–1.0$, autocorrelation times were $\tau_{auto} \sim 15– 40$ μs, correlation lengths were $L_{pol} \sim L_{rad} \sim 5– 10$ cm, and turbulence velocities were $V_{pol} \sim 2 \pm 1$ km/s and $V_{rad} \sim 0.5 \pm 0.5$ km/s outwards. These variations were evaluated with respect to both the global and local edge plasma parameters, and compared with simplified theoretical models (see Figure BP-PED-5).

4. BES measurements reveal connections between pedestal structure and ELM evolution patterns

An investigation of sub-millisecond ELM burst events captured by BES measurements on NSTX revealed three characteristic evolution patterns that notably correlate with confinement and pedestal parameters [BPR-PED-11, BPR-PED-12]. Automated machine learning analysis of BES time-series data identified short duration (<0.1 ms), non-oscillatory ELM events, intermediate duration (0.1-0.5 ms) ELM events, and long duration (0.5-1 ms), oscillatory ELM events, as shown in Figure BP-PED-6. The short and intermediate ELM events correlate with lower plasma current and lower confinement time, and conversely for the longer ELM events. Also, the short and intermediate ELM events correspond to the double-null topology, and longer ELM events correspond to the lower-single-null topology. Finally, the short and intermediate ELM events correlate with smaller density gradients and larger temperature gradients, and conversely for the longer ELM events. Linear ELM stability models and heuristic ELM classification schemes do not address the nonlinear dynamics that influence ELM intensity, saturation mechanisms, or filament dynamics, but the results of this investigation suggest connections between nonlinear ELM dynamics and confinement and pedestal parameters.

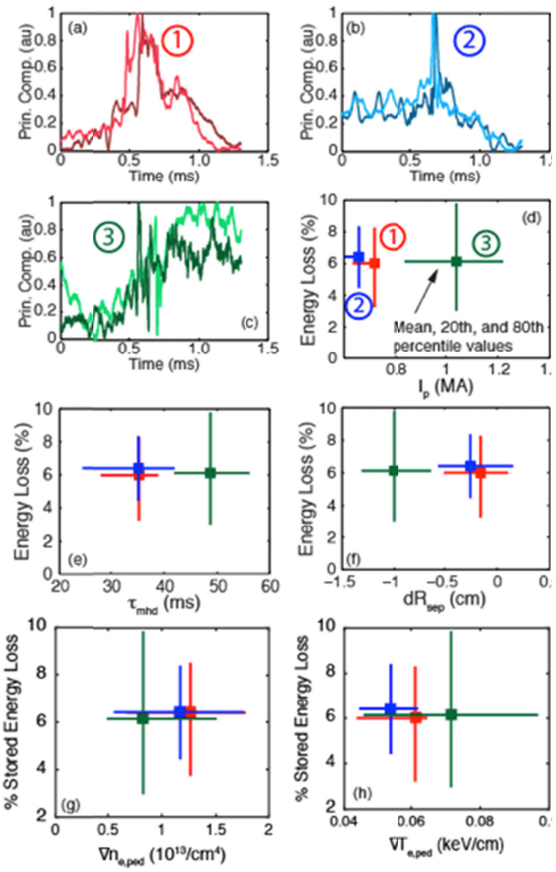

Figure BP-PED-6: *Characteristic evolution patterns for (a) intermediate, (b) short, and (c) long duration ELM events; (d-h) Characteristic parameter regimes for the identified ELM evolution patterns.*

5. EHO observations and the impact of EHOs on confinement

An investigation of EHO (edge harmonic oscillations) observations in BES data revealed that higher amplitude EHOs occurred only at lower confinement times, as show in Figure BP-PED-7, and the observation is consistent with a picture of EHO-enhanced particle transport. The analysis was performed by a 2015 SULI intern (J. Weberski (U. Illinois) working with D. Smith (U. Wisconsin)). EHOs are a key feature of the Quiescent H-mode regime on DIII-D, but a similar operation regime was not been observed on NSTX. Other results indicated that higher EHO toroidal mode numbers were accessible at lower collisionality, lower elongation, higher triangularity, and lower toroidal rotation.

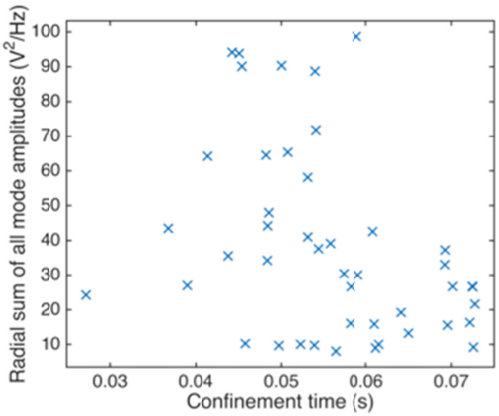

Figure BP-PED-7: *Radially-integrated EHO amplitudes from BES measurements suggest the largest EHO amplitude observations only occur at smaller confinement times.*

6. Diagnostics enabling pedestal studies

a. Gas-puff imaging

An upgrade for the GPI hardware was done in collaboration with a first-year graduate student, Noah Mandall. A new variable zoom lens was mounted on the front of the GPI optics, which is now capable of imaging objects of 0.1 cm diameter in the region of the GPI gas cloud (the previous resolution was ~0.5-1 cm). This improved spatial resolution, along with a x5-10 increase light transmission expected from a new fiber optic imaging bundle and a new Dα filter, will allow a search for small-scale modes such as ETG or microtearing modes in the plasma edge of NSTX-U.

b. Impurity Granule Injection for ELM pacing and impurity control

Prior to the upgrade outage, a Lithium Granule Injector (LGI) was developed and built for NSTX. This device was designed to utilize a mechanically rotating impeller to inject sub-millimeter sized particles radially into the NSTX discharge as shown in the figure below. These granules ablate upon impact with the edge plasma and generate a high density flux tube leading to the creation of an ELM. The underlying motivation behind this stimulated ELM triggering was the observation [BPR-PED-15] of an inverse relationship between ELM frequency and the peak divertor heat flux. Thus if the rate of ELM events can be increased (a concept known as “pacing”) then there should be a commensurate reduction on the thermal stresses endured by the plasma facing components. The ability to modify or control this parameter would be advantageous for next step burning plasma devices such as ITER. In addition, while the application of lithium coatings on NSTX led to ELM-free discharges [BPR-PED-8], there was a concomitant increase in the core impurity content [BPR-PED-16] that occurred within this ELM-free regime. The controlled re-

introduction of a series of regular ELM events at a perturbative level is therefor designed to flush these core impurities without significant degradation of plasma performance parameters.

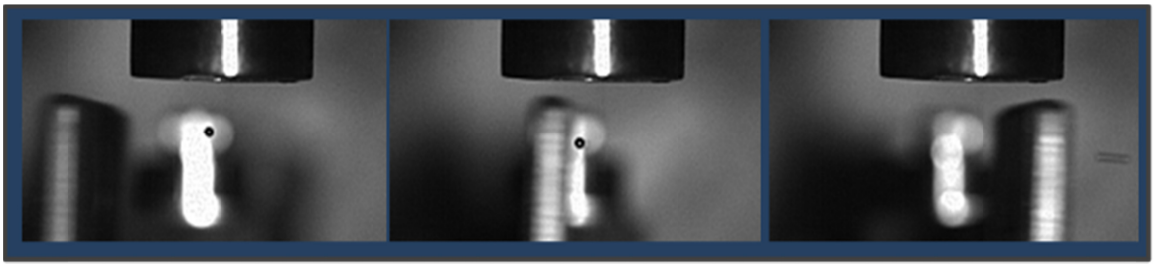

Figure BP-PED-8: *Impeller impact with a carbon granule. The above filmstrip shows a 700 micron carbon microsphere being radially driven towards the edge of the NSTX-U plasma which is located ~ 0.7m off-frame to the right. The resulting blur of the accelerated granule (right frame) can be used to calculate an estimated 45 m/sec granule velocity.*

While the LGI was not implemented on NSTX prior to the upgrade, the design was successfully fielded on the EAST tokamak to generate and pace ELMs [BPR-PED-17]. Utilizing 600 micron lithium spheres the LGI demonstrated pacing frequencies at up to 100 Hz with high triggering efficiencies. Following this successful test, a modified version of the granule injector was also installed on DIII-D in 2014. In these experiments [BPR-PED-18] ELMs were triggered at 3-4 times their natural frequency and there was a noted decrease in the accumulation of Nickel impurities within the core plasma.

A new upgraded version of the granule injector has been constructed and tested for the upcoming NSTX-U research campaign. In contrast to previous LGI designs, the upgraded system has been expanded to utilize additional species of non-fueling impurity granules for experiments in ELM pacing, ablation physics and impurity transport. Laboratory experiments have been conducted with boron carbide and vitreous carbon, materials similar in density and sublimation energy to the ITER first wall component beryllium. Both species have been injected into test chambers at frequencies exceeding 300 Hz and injection velocities of 50 m/sec (e.g. Figure BP-PED-8). Experiments focused on the injection of all three species, the above two as well as the original lithium, are planned for the upcoming experimental campaign. Tests are also envisioned injecting high-Z (tungsten, molybdenum) dust.

Imaging of the pellet ablation will help determine the penetration depth of injected pellets and collaboration with the UCSD group and the DUSTT-UEDGE code [BPR-PED-19] is envisioned for simulations of particle trajectories and ablation dynamics. For the imaging of the pellet ablation, two cameras will be set-up. The main view will be from the 12 o'clock port on the Bay J midplane port cover, looking at the injected granules from above. The new LLNL Vision Research Phantom camera (v1211) will be dedicated to this view during LGI experiments. The chosen field of view and the resolution of 360x288 pixels will lead to a spatial resolution of ~0.5 mm/pixel with a maximum frame rate of 76.6 kHz and a 2 s recording time. An additional view from the side (Bay F midplane) is currently being planned to enable the 3D particle tracking. The Bay H bottom Miro4 camera would be dedicated to this view with a temporary re-routing of the imaging bundle during LGI experiments.

A NSTX-U LRDFIT high-triangularity equilibrium reconstruction and the ray tracing code POV-Ray [BPR-PED-20] were used to guide in the choice of views and optics. In Figure BP-PED-9, POV-Ray renderings of the entire vessel (left) and of the two LGI views (Bay J on right-top, Bay F on right bottom) are shown. Three granules were positioned at the limiter location (red), separatrix (green) and Ψ_N=0.6 (blue). The choice in collection optics will provide a field of view covering this full radial range and thus the entire trajectory of the granules.

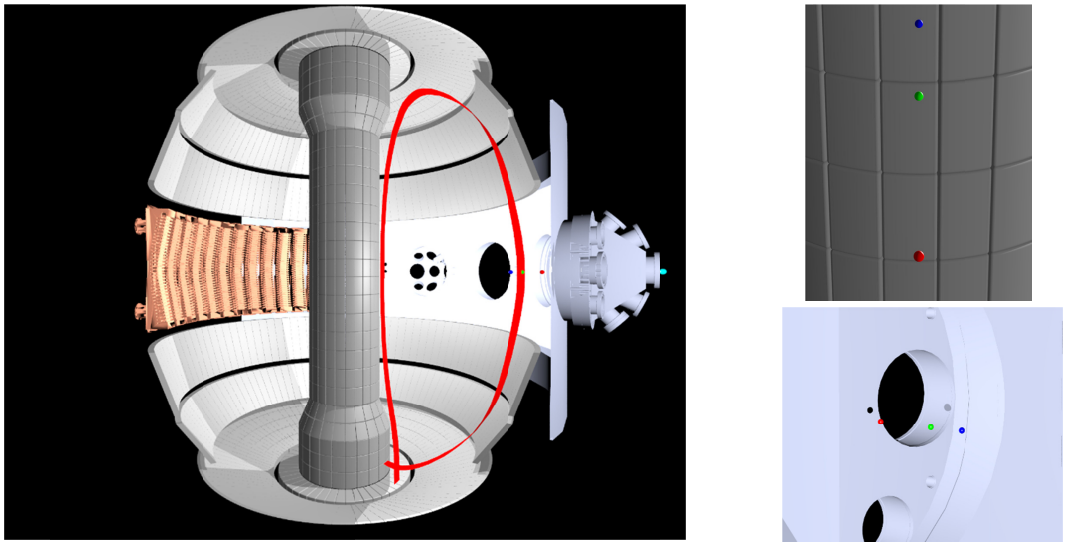

Figure BP-PED-9: *POV-Ray renderings of entire vessel (left), Bay J (right-top) and Bay F (right-bottom) views. Three granules were positioned at limiter radius (red), separatrix (green) and Ψ_N=0.6 (blue) based on an NSTX-U LRDFIT reconstruction.*

7. Modeling work

a. Pedestal gyrokinetic studies

A new pedestal gyrokinetic modeling effort was initiated by Dr. M. Coury. These efforts are motivated by recent experimental work published by R. Maingi JNM 2015 that shows that ELMs are suppressed at the highest lithium doses. Gyrokinetic calculations using GS2 code are being carried out to identify micro-instabilities (the fastest growing unstable mode) at several radii within the pedestal region, based on fits to experimental profiles and equilibria. The effect of increasing Li doses on these micro-instabilities will, thus, be investigated. Profiles and kinetic EFITs from the experimental scan above [BPR-PED-24] were generated using the python analysis tool developed at DIII-D. Initial results including modes scan over a wide range of wavenumbers and radii for increasing Li doses are being validated using convergence tests.

b. Enhanced Pedestal H-mode studies

Experiments on NSTX established that the bifurcation from H-mode (H_{98} < 1.2) to the ELM-free Enhanced Pedestal (EP) H-mode (H_{98} = 1.2 - 2.0) occurs when the ion thermal (χ_i) and momentum transport become decoupled from particle transport, such that T_i and rotation

pedestals increase independent of the density pedestal [BPR-PED-8, BPR-PED-9, BPR-PED-10]. Recent work comparing discharges operating near the threshold for transitioning to EP H-mode reveal that the onset of the EP H-mode transition is found to correlate with reduced ion pedestal collisionality (ν^*_{ped}) and an increased broadening of the density fluctuation ($\delta n/n$) spectrum in the pedestal as measured with beam emission spectroscopy. The spectrum broadening at decreased ν^*_{ped} is consistent with GEM simulations that indicate the toroidal mode number of the most unstable instability increases as ν^*_{ped} decreases [BPR-PED-9, BPR-PED-10]. The shifting of the ion-scale turbulence to higher frequencies (spectrum broadening) may describe the decrease in the thermal and momentum transport relative to particle transport. The lowest ν^*_{ped}, and thus largest spectrum broadening, on NSTX is achieved with low pedestal density via lithium wall conditioning and when Z_{eff} in the pedestal is significantly reduced via large edge rotation shear from external 3D fields or a large ELM. This is consistent with the observation that EP H-mode is often triggered by a large ELM event and most often occurred when using lithium-conditioned walls. Preliminary kinetic neoclassical transport calculations using XGC0 [BPR-PED-13] confirm that Z_{eff} is reduced when edge rotation braking leads to a more negative E_r that shifts the impurity density profiles inward relative to the main ion density. These calculations also describe the role kinetic neoclassical and anomalous transport effects play in the decoupling of energy, momentum and particle transport [BPR-PED-14] at the bifurcation to EP H-mode.

c. A new bootstrap current formula for H-mode pedestal plasma

Existing analytic bootstrap current formulas, such as the Sauter formula [BPR-PED-21], and numerical codes, such as NEO [BPR-PED-22] and CQLP [BPR-PED-23], rely on the "local" assumption that the ion banana orbit width is much smaller than the gradient scale lengths of the plasma density and temperature. However, this assumption is not valid in an H-mode pedestal. The code PERFECT [BPR-PED-24] allows the density gradient scale length to be comparable to the ion banana width, but does not allow a realistic ion temperature gradient.

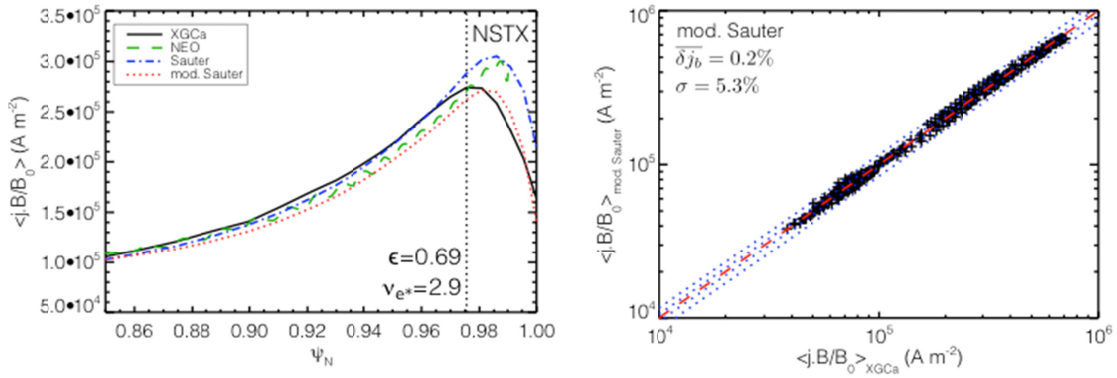

Figure BP-PED-10: *Left: Bootstrap current in a NSTX pedestal (discharge #128013) from the nonlocal gyrokinetic particle code XGCa (black), the local drift-kinetic code NEO (green), and the local Sauter formula (blue). It can be seen that the bootstrap current in NSTX pedestal from the "local" approximation is noticeably higher than that without such an approximation. Right: Accuracy of the new analytic formula compared to numerous XGCa simulation results in various geometry and plasma parameters including tight aspect ratios.*

Nonlocal effects in NSTX-U pedestal are expected to be greater than that in a conventional tokamak pedestal due to the unconventional guiding center orbit effect, the largeness of the ion

gyroradius, and the dominance of the banana fraction. A newly developed global gyrokinetic neoclassical code XGCa, which is equipped with a fully non-linear Fokker-Planck-Landau collision operator [BPR-PED-25] without the local assumption, has been used to study the bootstrap current in realistic edge conditions and to develop a new bootstrap current formula that is much more accurate in the H-mode pedestal. In the local regime with weak collisionality, the local (NEO) and global neoclassical (XGCa) codes and the Sauter formula show excellent agreement. In an H-mode pedestal, XGCa generally finds smaller bootstrap current than that obtained using the local approximation. This difference is particularly distinct in a spherical tokamak (Figure BP-PED-10, left panel). A new bootstrap current formula has been obtained as a modification to the existing Sauter formula, which reproduces various XGCa results with good accuracy, and can be used for pedestal physics in NSTX-U with greater confidence (Figure BP-PED-10, right panel).

References

[BPR-PED-1] A. Diallo et al., Physics of Plasmas, 22(5) 05611 (2015).
[BPR-PED-2] A. Diallo et al., Nucl. Fusion 55 053003 (2015)
[BPR-PED-3] A. Diallo et al., Phys. Rev. Lett., 112:115001 (2014).
[BPR-PED-4] P. Snyder et al., Nucl. Fusion 51 103016 (2011).
[BPR-PED-5] Y. Sechrest et al., Physics of Plasmas, 22, 052310 (2015)
[BPR-PED-6] I. Cziegler et al., PPCF, 56 075013 (2014)
[BPR-PED-7] Banerjee et al., RSI 86, 033505 (2015)
[BPR-PED-8] R. Maingi et al., 2009 J. Nucl. Mater. 390–391 440
[BPR-PED-9] R. Maingi et al., 2010 Phys. Rev. Lett. 105 135004
[BPR-PED-10] S.P. Gerhardt et al., 2014 Nucl. Fusion 54 083021
[BPR-PED-11] D. Smith et al., 2013 Phys. Plasmas 20 055903
[BPR-PED-12] D. Smith et al., 2013 Nucl. Fusion 53 113029
[BPR-PED-13] C. S. Chang et al., 2004 Phys. Plasmas 11, 2649
[BPR-PED-14] D.J. Battaglia et al., 2014 Phys. Plasmas 21, 072508
[BPR-PED-15] L.R. Baylor et al., Phys. Rev. Lett. **110** (2013) 245001
[BPR-PED-16] F. Scotti et al., Nucl. Fusion, **53** (2013) 083001
[BPR-PED-17] D.K. Mansfield et al., Nucl. Fusion **53** (2013) 113023
[BPR-PED-18] A. Bortolon et al., "ELM Pacing by injection of low-Z impurity pellets" FES Community Input Workshop on Transients, San Diego, CA, Mar 30 - Apr 1, 2015.
[BPR-PED-19] R.D. Smirnov et al., JNM 415 (2011) S1067.
[BPR-PED-20] Persistence of Vision Raytracer Pty, Ltd., P.O. Box 407, Williamstown, Victoria 3016, Australia, http://www.povray.org/.
[BPR-PED-21] O. Sauter et al., Physics of Plasmas **6**, 2834 (1999)
[BPR-PED-22] E. Belli and J. Candy, PPCF **50**, 095010 (2008) and PPCF **54**, 015015 (2012)
[BPR-PED-23] O. Sauter et al., Contrib. Plasma Phys., 34 (1994)
[BPR-PED-24] M. Landreman and D. Ernst, PPCF **54**, 115006 (2012)
[BPR-PED-25] E. S. Yoon and C. S. Chang, Phys. Plasmas **21**, 032503 (2014)

B. Divertor and Scrape-Off-Layer TSG Research Highlights

1. SOL turbulence and transport

In collaboration with NSTX-U team members [S. Zweben, W. Davis], work at Lodestar is underway to analyze a 14-shot database of Ohmic and H-mode NSTX discharges with high quality gas-puff imaging (GPI) and edge plasma profile data. Ongoing analysis, presented at the TTF workshop [BPR-DSOL-1] is focused on relating recent theoretical work [BPR-DSOL-2] on the SOL heat flux width λ_q with experimental observations. The work, funded by a separate Lodestar theory grant, studied the scaling of λ_q under various assumptions about the edge/SOL turbulence such as the drift-interchange character of the modes and the saturation mechanisms. Theory results [BPR-DSOL-2] projected to ITER suggests that turbulence mechanisms may dominate the $1/I_p$ scaling of λ_q observed in present-day machines. The validation of the theoretical model assumptions is thus critical, and well suited to the available NSTX GPI database. Preliminary results [BPR-DSOL-1] suggest that: (i) the length and time scales of the turbulence are consistent with drift-resistive ballooning modes, driven at least in part by curvature, and possibly affected by sheared flows; (ii) saturation levels are near the wave-breaking limit for Ohmic and L-mode discharges and may be below that limit for H-mode discharges; (iii) H-modes occupy the theoretically expected region of parameter space in terms of near-separatrix scale lengths of pressure, major radius, and ion-sound radius. Ongoing work is verifying these conclusions and addressing their implications for theory and modeling.

Finally, previous turbulence code simulation work addressing the effect of lithium on the SOL heat flux width in two complementary NSTX discharges has been completed, written up for publication [BPR-DSOL-3], and is now in the review process.

2. Survey of midplane neutral density data

Profiles of the neutral deuterium atom density at midplane are essential for studies of the H-mode pedestal, edge plasma turbulence, and power lost by charge exchange loss of neutral beam ions. The conventional experimental technique for determining the neutral density via the imaging of light emission is effective only over a limited spatial range. Direct modeling of neutral transport in the scrape-off layer and edge plasma is extremely difficult, time consuming, and inadequately constrained. The hybrid method described in [BPR-DSOL-4] provides a convenient alternative to these approaches, providing both deuterium atom and molecule density profiles over a wide range in radius via forward modeling of data from the Edge Neutral Density Diagnostic (ENDD) tangentially viewing visible camera. The range of variation of neutral densities in the 2010 NSTX run campaign has been determined by applying this technique to twelve time slices from seven discharges [BPR-DSOL-5]. The method has now been thoroughly tested and the uncertainties have been quantified.

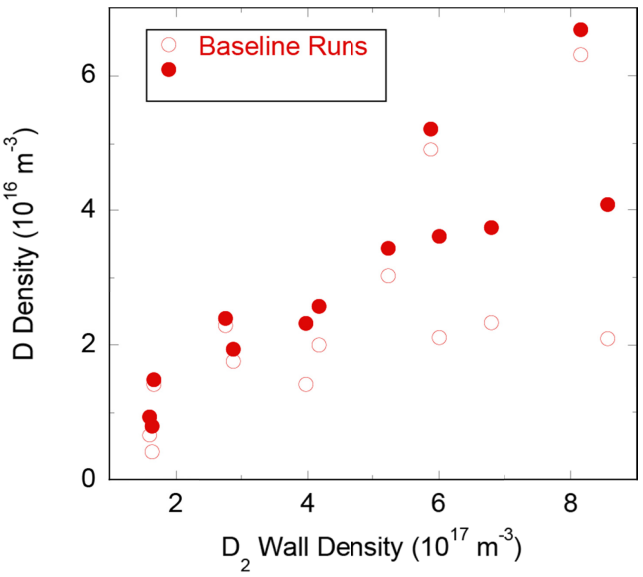

Figure BP-DSOL-1: *Range of atomic (vertical axis) and molecular (horizontal axis) densities for twelve simulations. Both the atomic densities at the wall (open symbols) and profile maxima (closed symbols) are depicted [BPR-DSOL-5].*

The resulting survey of neutral densities near the vacuum vessel wall is depicted in Figure BP-DSOL-1. Molecular densities range from 2 to $8x10^{17}$ m^{-3}; the atomic deuterium densities are roughly an order of magnitude smaller, 1 to $7x10^{16}$ m^{-3}. The former is similar to the range inferred from midplane micro-ion gauge data [BPR-DSOL-4]. No clear correlation of these values with other discharge parameters, such as the divertor Balmer-α emission or edge deuterium ion density is apparent; the same is true of the peak Balmer-β emissivities obtained by Abel inversion of the ENDD data.

The accuracy of the simulations in reproducing the experimental light emission is quantified by the radial distance between observed and simulated peaks of the ENDD profiles [BPR-DSOL-5]. The location of the simulated peak is sensitive to the shape of the electron density and temperature profiles, taken from Thomson scattering data, and little else. This includes the spatial distribution of the source, demonstrating that the results are insensitive to the principal assumption of this method, that the source of neutral deuterium can be described by a uniform molecular flux coming from the vessel wall. The inferred neutral densities do vary with the source's spatial distribution, and with other input quantities, resulting in an overall factor of two uncertainty in their magnitude.

The insensitivity of the simulated ENDD image to the source distribution, combined with the lack of correlations between the neutral densities and other parameters, prohibits any inferences regarding the nature of the actual source of neutral atoms and molecules in the experiments. Plausible sources include neutral leakage from the divertor, main chamber recycling, and outgassing from nearby material surfaces. Gaining some insight into this question in future experiments will require a more extensive survey. This is now possible since this method provides the basis for a routine neutral density profile diagnostic since it can be automated, given reasonable plasma profiles near midplane.

3. Effect of pedestal stability regime on the behavior of ELM heat flux footprints

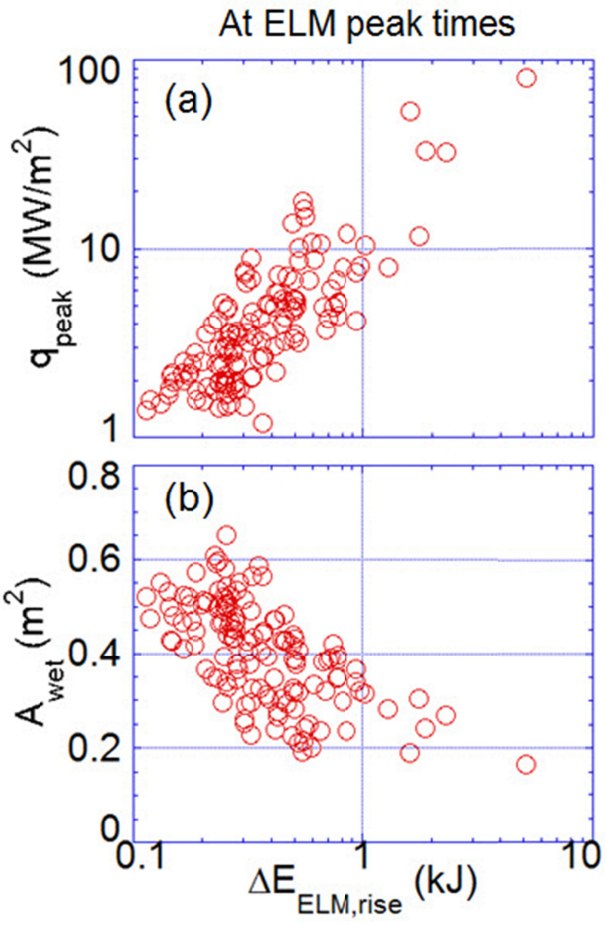

Figure BP-DSOL-2: *Peak heat flux (a) and wetted area (b) at ELM peak times, i.e. at maximum total power, as a function of ejected energy during the ELM rise time calculated from the measured IR heat flux in NSTX. This dataset is for kink/peeling ELMs dominantly found in NSTX.*

Following the first demonstration in NSTX that divertor heat flux profile by ELMs can either broaden or contract, depending on the number of ELM filaments found in the profile [BPR-DSOL-6], it is found that pedestal plasma regime plays an important role in the behavior of ELM heat flux footprints. The effective area at the divertor surface that accommodates total power expelled by ELMs, the wetted area (A_{wet}), is crucial for the determination of ELM mitigation requirements for ITER. A_{wet} has been observed to broaden significantly during the ELM, compared to the inter-ELM values, in several tokamaks [BPR-DSOL-7] in which the pedestal plasma is usually against the peeling-ballooning stability boundary with intermediate to high toroidal mode number (n=10–20). However, in NSTX [BPR-DSOL-6] and DIII-D, cases of significant contraction of A_{wet} by ELMs have been observed when the pedestal plasma is against the current driven kink/peeling boundary with low toroidal mode number (n=1–5). Figure BP-DSOL-2 shows the behaviour of A_{wet} and peak heat flux (q_{peak}) as a function of measured ELM energy loss, which illustrates the reduction of A_{wet} with the increase of ELM size, leading to the rapid increase of q_{peak}. Data in DIII-D have shown that increasing pedestal collisionality (ν_e*=0.3 → 0.9 → 3.5) leads to more favorable ELM footprints behavior, *i.e.* from contraction toward broadening, being consistent with an ELITE analysis that shows movement of the operating point in the stability diagram from the peeling toward the ballooning side, i.e. most unstable for n=5 → 10 → 25, respectively. NSTX pedestal plasma is found to be dominantly on the peeling side [BPR-DSOL-8], with ELMs usually reducing A_{wet}, although the pedestal ν_e* is generally higher than ~1 contrary to DIII-D. It is suspected that strong shaping in the ST geometry may have played an important role in determining pedestal stability in NSTX. Non-linear ELM simulation using BOUT++ is in progress to compare to the observed footprints behavior.

4. Plasma response to the applied 3D fields and its impact on divertor footprints

Plasma response to the applied 3D fields and its impact on divertor footprints have been investigated in the framework of ideal plasma shielding and amplification in NSTX. A full ideal plasma response code, IPEC, was used to calculate current induced by the plasma response in the pedestal region and the resulting B-fields in addition to the externally imposed 3D fields. This information was then put in a field line tracing simulation to produce divertor footprints pattern, to be compared to the measured footprints by visible and IR cameras. For the case of n=3 perturbations, ideal plasma shielding is found to prevent magnetic islands from opening as consistently shown in the field line connection length (L_c) profile and magnetic footprints on the divertor target. It is also found that the ideal plasma shielding modifies the degree of stochasticity but does not change the overall helical lobe structures of the vacuum field for n = 3 [BPR-DSOL-9, [BPR-DSOL-10], see figure BP-DSOL-3. On the other hand, amplification of vacuum fields by the ideal plasma response is predicted for the case of n = 1 perturbations [BPR-DSOL-10], better reproducing measurements of strong striation of divertor footprints. However, some local discrepancies between measurements and simulations still remain. Strong amplifications of n=1 fields cause a significant mixing of the ideal plasma and the vacuum layers. They produce significant amount of new field line connections from edge to divertor plates that are not captured in the vacuum field line tracing, and therefore modify footprints at the divertor surface compared to the vacuum case.

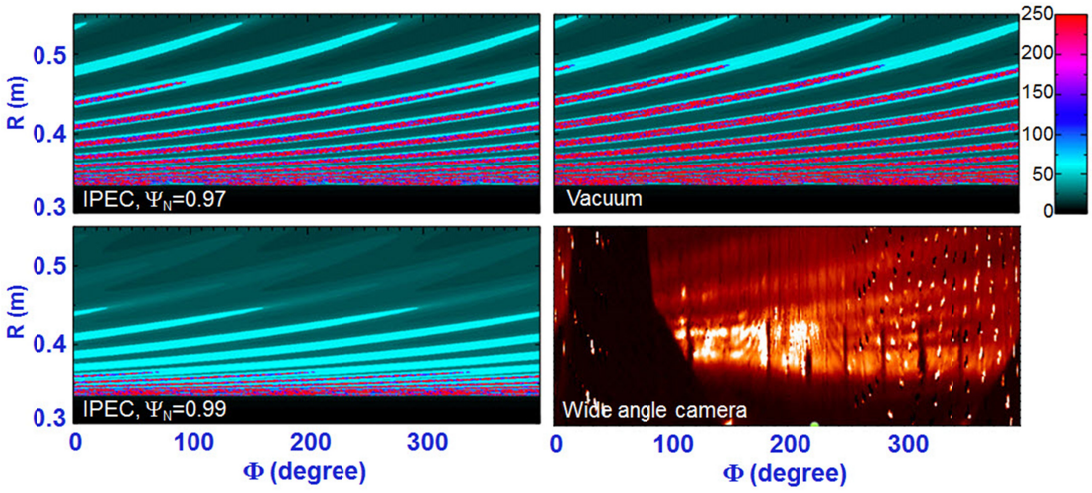

Figure BP-DSOL-3: *Comparison of simulated divertor footprints from field line tracing from to the 2-D wide angle visible camera image (Li-I, λ=670.9nm). The left two plots are with inclusion of ideal plasma response and the upper right plot is for the vacuum case. The visible camera image was re-mapped from (x, y) to (r, Φ) coordinate (the dark portion on the left hand side represents the center column).*

5. Snowflake divertor research on NSTX-U

In NSTX-U, discharges with $I_p \sim 2$ MA and P_{NBI} ~12 MW and up to 5 s duration are projected to produce steady-state peak divertor heat fluxes in excess of 10 MW/m^2, thereby challenging thermal limits of divertor graphite PFCs [BPR-DSOL-11]. One of the four elements of the NSTX Upgrade research mission is the development of advanced plasma-material interface solutions. The leading heat flux mitigation candidates for NSTX-U are the snowflake (SF) divertor geometry and the impurity-seeded radiative divertor technique, applied to the lower and upper divertors. Research is planned on NSTX-U to test snowflake magnetic feedback control, and demonstrate steady-state SF configurations with reduced heat flux, compatible with high-beta, low collisionality H-mode scenarios. A new set of divertor coils has been installed in NSTX Upgrade, as compares to NSTX.

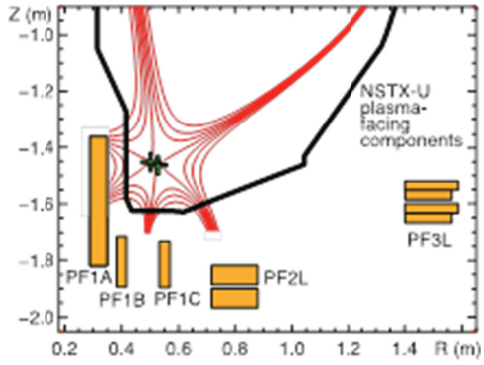

Figure BP-DSOL-4: *An upgraded NSTX-U divertor coil set. A modeled SF equilibrium that uses all four divertor coils is shown.*

To enable flexibility in divertor configuration and shaping control, an additional divertor coil PF1C has been installed in NSTX-U, as shown in Figure BP-DSOL-4. However, in the initial plasma operations period, three coils will be connected to power supplies: the up-down symmetric PF1A, PF1C, and PF2 coils. A number of magnetic equilibria with SF configurations have been modeled successfully using the predictive free-boundary Grad-Shafranov code ISOLVER.

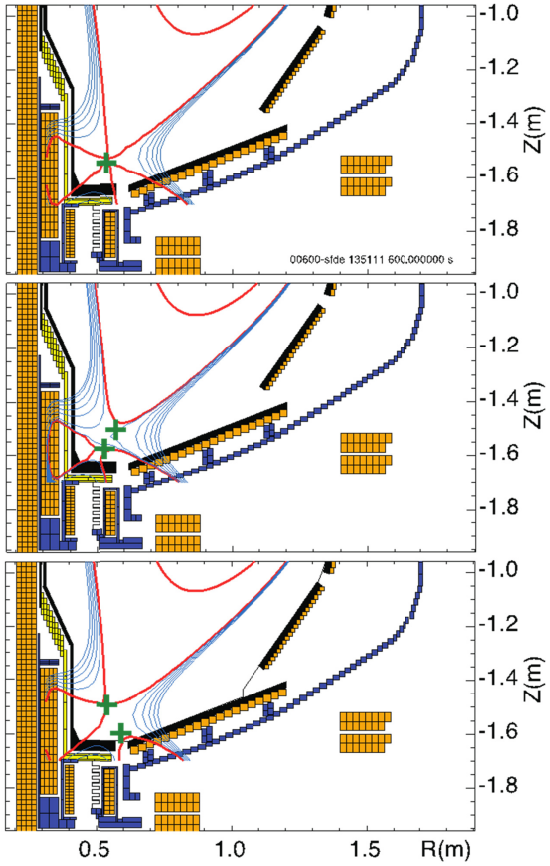

Figure BP-DSOL-5: *Modeled SF equilibria using the divertor coil set (PF1A, PF1C and PF2L as shown in Figure BP-DSOL-4) available in initial NSTX-U experiments. (a) Near-exact SF, (b) SF-plus, and (c) SF-minus configuration.*

The exact SF, SF-minus and SF-plus configurations in the lower and upper divertor regions could be realized with the up-down symmetric set of divertor coils operated below their respective current limits, and with plasma currents up to 2 MA. Four divertor coils should enable control of up to four independent parameters, e.g., positions of the null-points and strike points. Robust SF

configurations were obtained in simulations even when time-varying leakage flux from the time-evolving ohmic solenoid current was included. Examples of the standard divertor and SF-plus, SF-minus and near-exact SF configurations obtained with three divertor coils are shown in Figure BP-DSOL-5. All configurations maintained a primary X-point height at about 10 cm above the divertor surface.

The modeled SF equilibria were also used in predictive edge transport modeling with multi-fluid code UEDGE. Several key modeling results are shown in Figure BP-DSOL-6, with the details provided in [BPR-DSOL-12]. The model used NSTX-like transport coefficients, i.e., χ = 2-4 m^2/s and D = 0.5 m^2/s [BPR-DSOL-13], a neutral model using diffusive treatment in cross-field directions and a full Navier-Stokes treatment in the parallel direction, a fixed fraction (3 % carbon) impurity and the ion recycling coefficients R = 1 at the wall, and R = 0.99 at the divertor plates. Effects of the classical electromagnetic particle drifts were not included. The power flowing into the SOL was equally split between electrons and ions. The model did not include any special transport modifiers in the null region of the SF configuration, hence, it mostly showed effects of the SF geometry on heat and impurity radiation.

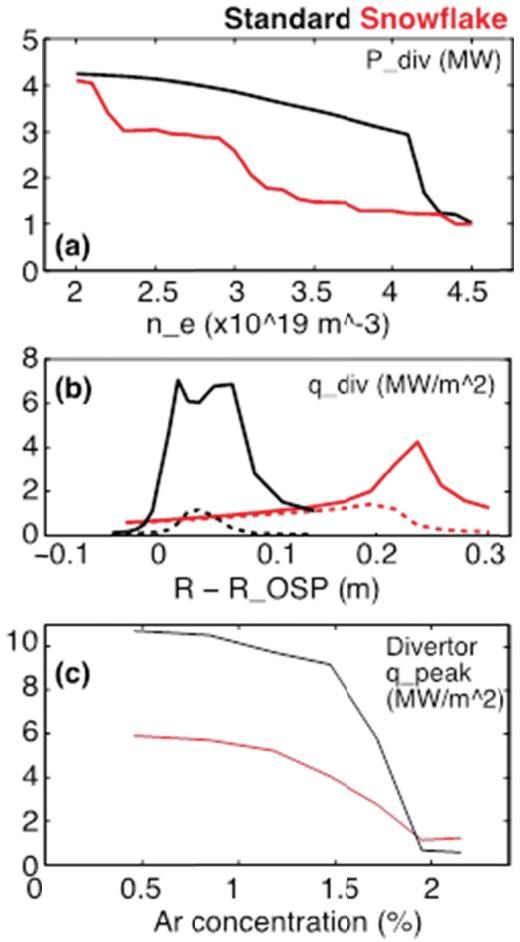

Figure BP-DSOL-6: *UEDGE modeling results for NSTX-U standard (black traces) and SF-minus (red traces) divertor configurations. (a) Divertor power as a function of electron density (n_e at the core-boundary interface); (b) Divertor heat flux profiles at $n_e = 3.5x10^{19}$ m^{-3} - total (solid lines) and without the radiative heating flux (dashed lines); (c) Peak divertor heat flux vs. Ar concentration in a radiative Ar-seeded divertor.*

The geometric factors were very favorable: in the outer strike point region, L_c ~ 20-30m (c.f. 7 - 15m in the standard divertor), and f_{exp} ~ 40 (c.f. 10-20 in the standard divertor). Results for the most challenging P_{SOL} = 9 MW case representative of the 12 MW, 2 MA NBI-heated plasma discharge are shown in Figure BP-DSOL-6. Divertor power as a function of density is plotted in Figure BP-DSOL-6a. A highly radiative scenario occurs in the SF configuration at a much lower density, enabling a greater power loss (w.r.t. the standard divertor), and a larger operating window with reduced q_{div} at lower n_e. Total divertor heat fluxes and the heat fluxes without radiative heating at $n_e = 3.5 \times 10^{19}$ m^{-3} are shown in Figure BP-DSOL-6b. In the outer divertor, high q_{peak} ~ 7MW/m^2 was obtained with the standard divertor, and only 3-4 MW/m^2 in the SF-minus configuration. The figures suggest that both the flux expansion and the additional radiated

power loss are the leading q_{peak} reduction mechanisms in the SF-minus model. The inner divertor region was found to be highly radiative (possibly with a detached strike point) in both configurations. Impurity-seeded divertors (with neon and argon) were also analyzed. Figure BP-DSOL-6c shows that 50% less argon is needed in the SF-minus configuration to achieve similar q_{peak} reduction factors (cf. standard divertor). Thus, UEDGE modeling results support the SF divertor as a leading steady-state divertor power exhaust solution for NSTX-U [BPR-DSOL-14].

6. Impact of resonant magnetic perturbation fields on snowflake divertor topology

Explorations are under way to optimize the magnetic topology in the plasma edge of NSTX-Upgrade with the goal to improve neutral and impurity fueling and exhaust characteristics. One means considered is the use of externally applied resonant magnetic perturbation fields to spread heat and particle fluxes in the divertor and at the same time adjust the level of plasma re-fueling by reduced inward transport of neutrals and impurities as well as by improving the coupling to the exhaust systems. In this note, a first of its' kind assessment of the perturbed magnetic topology of a representative NSTX snowflake configuration is discussed.

For this assessment we use a representative NSTX snowflake scenario from a scoping study of plasma equilibria for the new cryo-pump design and calculated the magnetic field line connection length L_c from wall to wall. Then, a toroidal mode number n=3 field at 3kAt nominal current was applied to investigate the impact of such 3D RMP fields on the snowflake divertor topology. The result is shown in figure BP-DSOL-7. Here the snowflake divertor field line topology with RMP fields applied is shown on the left and the RMP case on the right. Without RMP field the four divertor legs of the snowflake configuration are seen as long L_c domains surrounded by the scrape-off layer with typical L_c values of 30m.

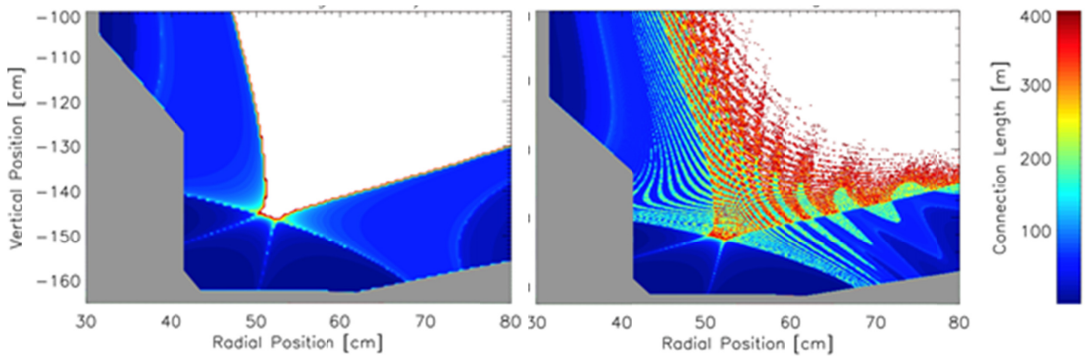

Figure BP-DSOL-7: *Calculation of the perturbed magnetic topology at the X-point of the snowflake configuration at NSTX-Upgrade: left side without RMP field and right side with RMP field. A complex 3D helical mesh of magnetic lobes departing from the two X-points is seen intersecting the divertor target plates in a strongly shaped, helical divertor footprint pattern shown in the right-hand-side panel.*

Application of RMP fields (Figure BP-DSOL-7, right side) yields decomposition of the invariant manifolds of the hyperbolic fixed points in the snowflake configuration, such that a complex mesh of helical lobes departing from the X-points towards the divertor plates is seen. Such perturbed boundary structures due to RMP field application have been predicted (e.g. [BPR-

DSOL-15]) and seen experimentally in single null plasmas at DIII-D (e.g. [BPR-DSOL-16]) and also extensively studied at NSTX (e.g. [BPR-DSOL-17, BPR-DSOL-18]). This calculation of the perturbed topology of a snowflake divertor shows that the strong magnetic shaping in the snowflake configuration and the second X-point together yield to a finer scaled mesh of the helical lobes and that they undergo at the high field side a much stronger bending compared to the disconnected double null cases studied with RMP fields predominantly so far at NSTX. Of particular interest are the short L_c field line bundles (green and light green color in figure BP-DSOL-7, right side), which extend well into the confined plasma region w/o RMP field. These magnetic field line bundles represent open field line bundles on 3-5 times the characteristic SOL length and can yield substantial parallel losses to the target. These helical SOL bundles can act as additional exhaust channel to the divertor plates and pumping systems. Exploration of these SOL channels on the edge transport characteristics will be tackled using the EMC3-EIRENE fluid plasma and kinetic neutral transport code.

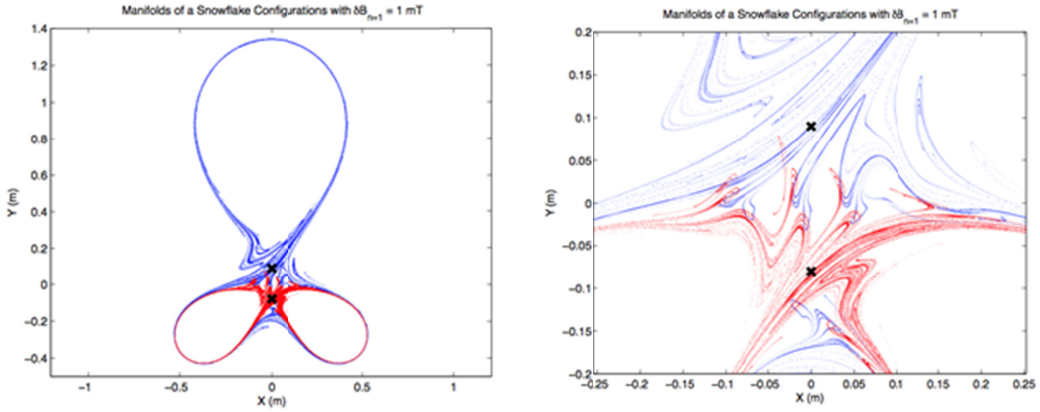

Figure BP-DSOL-8: *Perturbed structure of the invariant manifolds of both hyperbolic fixed points of a snowflake equilibrium addressed as example using a 3-wire model. Blue traces are the stable and unstable manifolds of the upper and red traces of the lower X-point. This analysis shows mixing of the chaotic traces of magnetic field lines between the different manifold branches of both X-points in the perturbed magnetic snowflake topology.*

One important aspect of transport with a perturbed snowflake topology is if the additional hyperbolic fixed point (X-point) will yield effective mixing of perturbed magnetic field lines from invariant manifolds of both snowflake X-points. This is seen in figure BP-DSOL-8 as a result of a conceptual study using a 3-wire model in order to calculate the unperturbed plasma equilibrium including the entire manifold domain (the lower part of the red traced manifolds is far outside of the regular equilibrium reconstruction for NSTX-U). This analysis that the invariant manifolds of the two snowflake X-points considered are connected by short connection length field lines inside of the skeleton spanned by the two sets of invariant manifolds. This could yield population of the lower snowflake divertor legs with heat and particle fluxes to fully exploit the capabilities of the snowflake for heat and particle flux distribution. This task is addressed collaboratively with Dr. G. Canal and Dr. T.E. Evans from General Atomics, who focus on resolution of the dynamics of the X-point invariant manifolds with RMP fields applied.

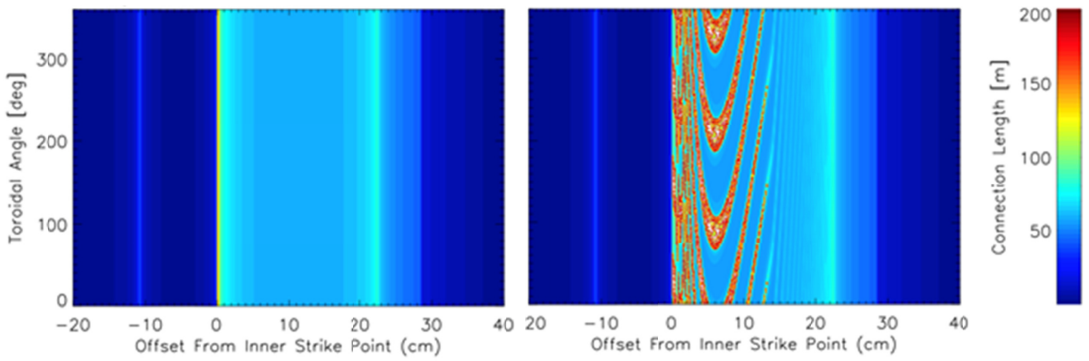

Figure BP-DSOL-9: *Perturbed magnetic footprint at the inner divertor leg with RMP field on the right and w/o RMP field on the left. Both divertor legs are clearly seen with no RMP field applied. The upper divertor leg is transformed into a pattern of highly shaped, boomerang like helical lobes while the secondary divertor leg (at d=-10 cm) is not affected. The strong bending of the helical lobes of the first strike point is distinguishable different from the pattern of typical single-null NSTX case and hence is expected to be resolvable experimentally by divertor heat and particle flux imaging at NSTX-U.*

The intersection of the helical lobes from both snowflake X-points with the divertor wall elements at the **inner divertor leg** forms a complex pattern as shown in figure BP-DSOL-9. Here, the magnetic footprint pattern at the inner strike line is depicted without RMP fields applied on the left and with RMP fields on the right. The helical lobes departing from the upper divertor leg of the snowflake configuration are strongly bent such that boomerang like structure evolves in the target footprint pattern. This pattern is distinguishable from the standard single-null configurations with RMP fields studies in the past and is expected to be resolvable experimentally using divertor heat and particle flux imaging. Also, the effective area wetted by heat flux seems to be increased with a 3D snowflake compared to a 3D standard single null divertor shape.

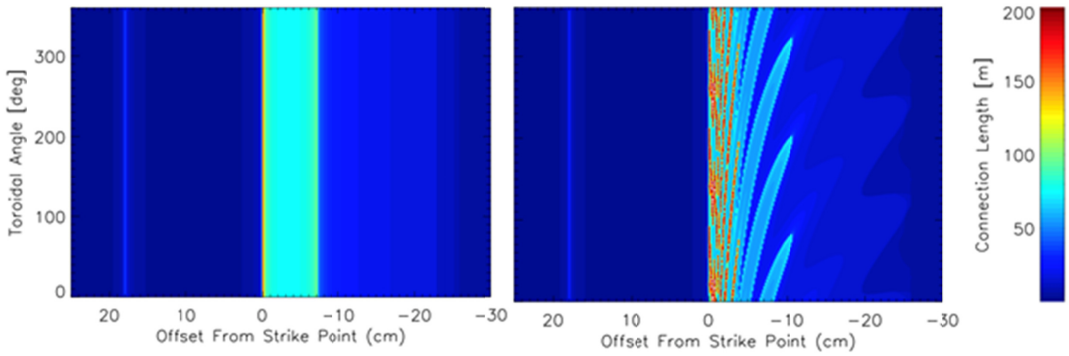

Figure BP-DSOL-10: *Perturbed magnetic footprint at the outer divertor leg with RMP field on the right and w/o RMP field on the left. Both divertor legs are clearly seen with no RMP field applied. The upper divertor leg is transformed into a pattern of helical lobes that undergo much less shaping than seen for the inner divertor leg. Still, formation of striated heat and particle flux pattern is expected which can potentially aid the heat and particle flux spreading intended with the snowflake configuration.*

For the **outer strike line**, a less pronounced impact of the RMP field on the magnetic footprint pattern in the divertor is seen. In figure BP-DSOL-10, the magnetic footprint without RMP field is shown on the left and with RMP field on the right. The helical lobes induced by the RMP field are much less separated radially and not bent into a boomerang structure. However, a dominant

helical n=3 structure is still seen for the upper leg of the snowflake configuration while the lower leg seems to be unaffected. As the connection length in the private flux region of the snowflake configuration is short, the effect of the RMP field on the snowflake structure requires more detailed analysis of the invariant manifolds. The can yield mixing of field lines from the upper to the lower snowflake divertor legs and could yield heat flux separation from the upper to the lower legs. This would be an attractive mechanism to aid heat and particle flux spreading in the snowflake configuration. Based on this first of its time analysis of the perturbed magnetic topology of a snowflake divertor, a detailed comparison of these features using EMC3-EIRENE for the snowflake divertor with and w/o 3D fields and for the standard divertor with and w/o 3D fields is being conducted.

7. Radiative divertor experiments and feedback control development

In order to mitigate steady-state divertor peak heat fluxes in excess of 10 MW/m^2 impurity-seeded radiative divertor technique is envisioned. Radiative divertors use deuterium and/or seeded impurities to reduce divertor particle and heat fluxes through volumetric momentum and energy dissipative processes - the ion-neutral elastic and inelastic collisions, recombination and radiative cooling. The critical issue for the radiative divertor is the steady-state feedback control of reduced divertor peak heat flux through the rate of impurity seeding, using some divertor parameter as a control quantity. The divertor detachment process is tokamak-specific with respect to divertor PFC material, seeding gas species, radiating impurity, onset parameters, and their relation to the core plasma. The radiative detachment of the divertor SOL is achieved when heat conduction can no longer be sustained as a result of high SOL collisionality and high volumetric power and momentum losses. The detachment signatures universally measured in present-day tokamak experiments include (1) the loss of plasma pressure $T_e n_e$ along the SOL (field line) from upstream locations to the target, increased divertor $n_e \leq 10^{15}$ m^{-3} and decreased $T_e \leq 1-2$ eV; (2) the reduction of divertor heat flux and increase in P_{rad}; and (3) reduction of ion flux density to the plate, accompanied by an increased volumetric recombination rate. In order to control radiative detachment, a diagnostic control signal should unambiguously reflect one of the detachment characteristics.

Initial radiative divertor experiments planned on NSTX-U in the first two years include

- Radiative divertor operational space (current, power, density), neutral and impurity compression
- Calibration of control diagnostic signals without feedback
- Combination with three-dimensional fields for ELM control
- Double null radiative divertor studies (not attempted in NSTX to date). The upper divertor diagnostic complex should enable characterization of the power and particle flux fractions between the lower and upper divertors.
- X-point MARFE characterization and avoidance
- Using unique 2D divertor camera coverage, toroidal asymmetries of impurity radiation due to gas injection port locations can be studied

8. SOL and divertor diagnostic development for NSTX-U

The Two Wavelength Imaging Camera Equipment (TWICE) diagnostic (Figure BP-DSOL-11) was installed on the Lithium Tokamak Experiment (LTX) to explore capabilities offered by the intensified two-wavelength imaging. Initial applications included the imaging of the MAPP head (shown in Figure BP-DSOL-12) for the determination of neutral lithium influxes via neutral lithium line ratios (460.3, 610.4, 670.9 nm) [BPR-DSOL-19] and the imaging of the LTX high field side limiter. The progressive reduction of the C-II to Li-I (Figure BP-DSOL-13) emission ratio from the unconditioned limiter with passivated lithium coatings and its correlation with the achieved peak plasma current suggested that the improvement in the plasma performance could be related to the progressive cleaning of the wall surface, which exposes the lithium underneath.

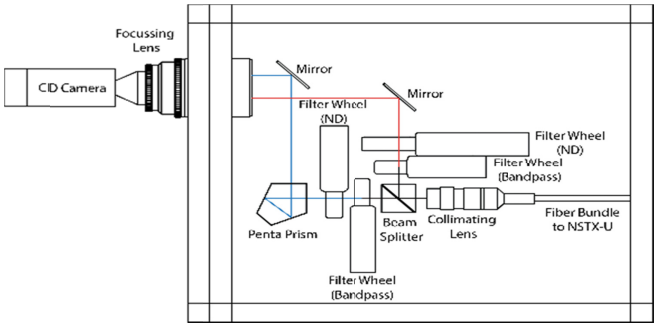

Figure BP-DSOL-11: *Layout of optical and mechanical components in the TWICE image splitter box.*

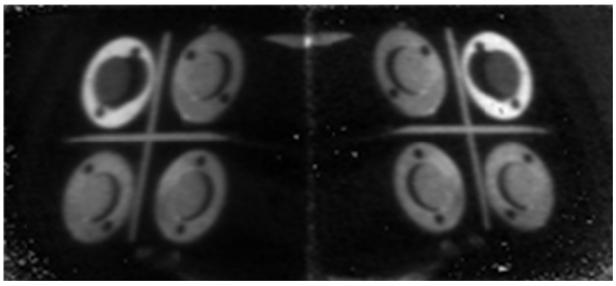

Figure BP-DSOL-12: *View of the MAPP head on LTX as imaged by TWICE and illuminated by the vessel filament.*

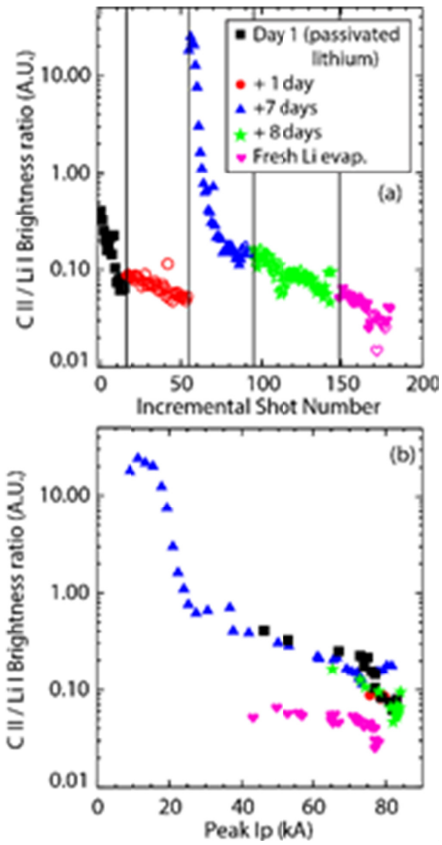

Figure BP-DSOL-13: *Evolution of the C-II (514 nm) / Li-I (670 nm) ratio with progressive discharges on unconditioned walls for consecutive run days as a function of incremental shot number (top) and peak plasma current (bottom). Filled and empty symbols represent different Ohmic coils*

References

[BPR-DSOL-1] J. R. Myra, S. J. Zweben, W. M. Davis, D. A. D'Ippolito and D. A. Russell, "*Theory based interpretive analysis of the NSTX GPI database*" , 2015 Joint US/EU Transport Task Force Workshop, Salem, MA, April 28 - May 1.

[BPR-DSOL-2] J. R. Myra, D. A. D'Ippolito, and D. A. Russell, Physics of Plasmas **22**, 042516 (2015).

[BPR-DSOL-3] D. A. Russell et al., Lodestar Report Number, LRC-15-163 (2015), submitted to Phys. Plasmas.

[BPR-DSOL-4] D. P. Stotler et al., 2015 J. Nucl. Mater. **463** 897

[BPR-DSOL-5] D. P. Stotler et al., 2015 Phys. Plasmas **22** 082506]

[BPR-DSOL-6] J-W. Ahn et al., Nucl. Fusion **54** (2014) 122004

[BPR-DSOL-7] T. Eich et al., J. Nucl. Maters. **415** (2011) S856

[BPR-DSOL-8] R. Maing, et al., Phys. Rev. Lett. **103** (2009) 075001

[BPR-DSOL-9] J-W. Ahn et al., Plasma Phys. Control. Fusion **56** (2014) 015005

[BPR-DSOL-10] K. Kim et al., accepted to Plasma Phys. Control. Fusion (2015)

[BPR-DSOL-11] T. Gray et. al., J. Nucl. Mater., vol. 415, p. S360, 2011.

[BPR-DSOL-12] E. T. Meier et al., Nucl. Fusion, to be published, 2015.

[BPR-DSOL-13] E. Meier et. al., "Modeling detachment physics in the NSTX snowflake divertor," J. Nucl. Mater., At press, 2015.

[BPR-DSOL-14] V. A. Soukhanovskii et al., "Snowflake divertor experiments in the DIII-D, NSTX and NSTX-U tokamaks aimed at the development of the divertor power exhaust solution," submitted to IEEE Transactions on Plasma Sci., July 2015

[BPR-DSOL-15] T.E. Evans et al., J. of Phys.: Conf. Series **7** (2005) 174

[BPR-DSOL-16] O. Schmitz et al. Plasma Phys. Contr. Fusion **50** (2008) 124029

[BPR-DSOL-17] J.-W. Ahn et al., JNM **415** (2011) S918

[BPR-DSOL-18] J.-W. Ahn et al., Plasma Phys. and Contr. Fusion **56** (2014) 015005

[BPR-DSOL-19] F. Scotti and V.A. Soukhanovskii, submitted to Rev. Sci. Instrum. (2015).

C. Materials and Plasma-Facing Components TSG Research Highlights

1. Introduction

The Materials and PFC (M&P) research program on the NSTX-U exists to perform the critical research needed to address the fundamental question of what materials are suitable to a fusion plasma experiment and, eventually, a fusion power plant. In the context of the NSTX-U program, this practically means gaining an understanding of the existing materials and wall-conditioning techniques (carbon PFCs + boronization and lithiumization) in use in the machine so that incremental upgrades to reactor-relevant systems (e.g. high-Z tungsten/molybdenum and flowing liquid lithium) will provide the greatest knowledge gain and minimize the operational learning-curves.

The research program in M&P has been divided into three main thrust areas: surface science to support long-pulse operation, tokamak induced material migration, and vapor-shielding physics. Each of these thrusts addresses needs of both solid and liquid plasma-facing components with-respect to future power reactors.

In the case of surface science, it is necessary to have an accurate understanding of hydrogen and impurity uptake in high-Z systems with and without low-Z coatings. The focus is on lithium coatings on high-Z substrates in order to assess fuel retention which is a critical question for the continued usage of lithium in next-step experiments such as the FNSF which is expected to make use of tritium fuel. Research highlights from laboratory studies as well as tokamak studies in the LTX device using NSTX-U diagnostics systems are given below.

The question of retention in a low-Z layer is as important as understanding where those layers are created and destroyed inside the tokamak device. In order to address this area of tokamak-induced material transport, state-of-the-art codes such as OEDGE and WallDYN have been obtained and are being modified for use with the NSTX and NSTX-U machines. These codes will provide an interpretative modeling framework which can be used to build predictive capabilities that will be tested in the NSTX-U during this 5-year plan. Improved diagnostic capabilities are also being brought online by a number of collaborators.

Finally, the ultimate temperature limits of a lithium surface greatly impacts the technological and plasma-control choices associated with the use of lithium in a future power reactor. Lower temperature limits (e.g. 400C) will necessitate the use of fast-flowing systems or alternative methods of reduced plasma power fluxes. On the other hand, higher temperatures may provide a means of accessing a self-shielding regime termed *continuous vapor-shielding*. Already experiments have demonstrated operation of a linear plasma source on a 1000C target without contaminating the plasma source. It is found that the results are consistent with the rapid formation of a deuterium-saturated lithium layer that erodes at a significantly lower rate than pure lithium. The vapor-shielding science program will be enabled by an upgrade of the NSTX-U device from the existing graphite tiles to one composed of high-Z, metallic substrates. The design for high-Z, high-heat flux components has commenced already to accomplish this upgrade. As an incremental upgrade between the bulk, high-Z tiles and fully-flowing systems, a

prototyping design activity was accomplished to examine the possibility for pre-filled liquid metal targets within the NSTX-U.

Progress in each area is continuous in the past year due in part to the capabilities present at the PPPL, collaborator institutes and the active collaboration with the Dutch Institute for Fundamental Energy Research (FOM-DIFFER). This progress is detailed below.

2. Fundamental surface science studies

Lithium is a potent wall conditioning material as demonstrated in several tokamak devices such as TFTR, CDX-U, LTX, EAST, FTU, NSTX and others. Nearly all of these experiments make use of physical vapor deposition of lithium as the conditioning technique. Understanding how experimental results obtained with this wall conditioning will translate to a future device utilizing flowing lithium (and presumably improved vacuum conditions) remains an open question and provides major motivation for fundamental surface science studies.

Experiments reported at the 56th Annual APS DPP meeting by A. Capece further demonstrate the complex picture that arises with the use of lithium [BPR-MP-2, BPR-MP-2B]. In experiments conducted in the Surface Science & Technology Laboratory at PPPL, controlled quantities of lithium were deposited on high-Z samples, exposed to precisely monitored oxygen and deuterium fluxes, and then examined with the use of temperature programmed desorption (TPD). The use of TPD provides a means of characterizing the quantity of deuterium retained in a sample as well as the desorption energy associated with evolved gases, which can be related to the surface binding energy of the retained materials.

It was found that increasing substrate temperature resulted in a reduction of the deuterium retained in 3-monolayer lithium films by a factor of four from 320 - 460K (47 - 187°C). This is shown in Figure BP-MP-1 below. Oxygen contamination was found to inhibit the formation of lithium deuteride (LiD). At low temperatures (T<130°C), the oxidized lithium was able to absorb 4-5x more deuterium than bare TZM metal (an alloy of molybdenum). However, this retained lithium was found to outgas at modest temperatures of only 470K (200°C). Pure lithium retained about half as much deuterium (as LiD) as the oxidized lithium, but this D remains bound to a significantly higher temperature of 650K (380°C).

Similar studies performed on single-crystal molybdenum, reported by Roszell, et al., provide additional insight into the complexities of ultrathin lithium films [BPR-MP-3]. Namely, it was found that single monolayers of lithium do not form LiD. Deuterium is retained by the molybdenum due to preferential bonding between the molybdenum and lithium in the first monolayer. Taken together these two results indicate the importance of the chemical interactions occurring at the surface of the plasma-facing component. Extrapolating ahead to a reactor scenario, it is possible to imagine multiple concepts that these results inform. In the case of a low temperature, absorbing surface, the results on multi-layers of lithium indicate that for pure lithium, hydrogenic fuels will be retained up to the LiD decomposition temperature of about 380 °C. On the other hand, it would appear that maintaining in-vessel structures at temperatures above 420°C or maintaining lithium coatings on the order of a single monolayer will both result in substantially reduced fuel inventory. Finally, one will need to apply some caution in

extrapolating these results performed on ultrathin lithium films to much thicker films and bulk lithium surfaces with varying amounts of C and O contamination.

A key factor in the performance of liquid lithium plasma facing components is the wetting by lithium of its container. We have observed the surface spreading of lithium from a mm-scale particle to an adjacent stainless steel surface using a scanning Auger microprobe (SAM) that has elemental discrimination [BPR-MP-3C]. The spreading of lithium occurred at room temperature (when lithium is a solid) from one location at a speed of 0.62μm/day under ultra-high vacuum (UHV) conditions. Separate experiments using TPD investigated chemical bonding between monolayer-scale films of lithium and stainless steel. A energy of 1.54 eV for multilayer lithium desorption from stainless steel was derived from a peak desorption temperature of 585 K. In contrast, sub-monolayer desorption occurred in a peak at 942 K (2.52 eV) indicating that it is energetically more favorable for lithium to bond to stainless steel in the absence of an oxidation layer than to bond to itself. To date lithium spreading originated from one corner of a lithium particle and was correlated with Ar^+ ion beam etching that removed contamination and oxide films from the surface. We have recently calibrated a pyrometer for remote temperature sensing in the SAM and plan to investigate lithium spreading as a function of surface temperature on stainless and other PFC materials such as molybdenum and tungsten. These experiments aim to elucidate the fundamental surface chemistry of reactive wetting in Li / stainless steel or Mo systems and gain an understanding that will facilitate practical issues of wetting in future liquid metal PFCs on NSTX-U.

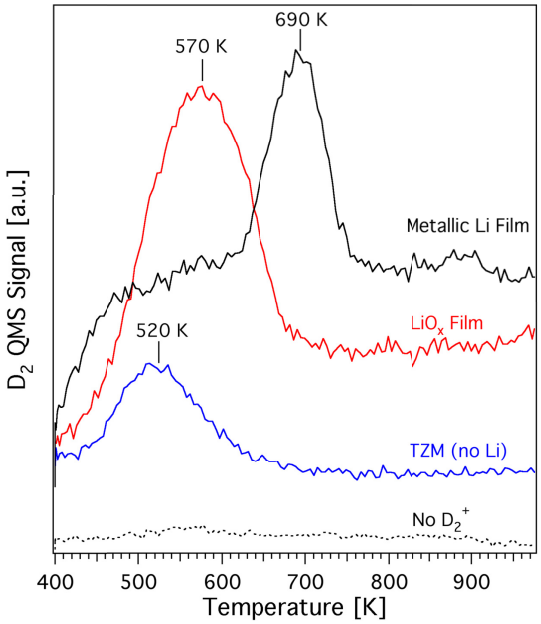

Figure BP-MP-1: *Thermal desorption of deuterium from various substrates. The area under each curve indicates the quantity of deuterium retained in the sample. While the amount retained in the metallic Li film is 2x less than for the oxide, it thermally desorbs at a higher temperature [BPR-MP-2].*

The chemical composition of a lithium surface is affected by exposure to ambient air during venting and by residual vacuum gases during tokamak operations. Previous studies using X-ray photoelectron spectroscopy (XPS) under UHV conditions have shown that thin lithium metal films were easily oxidized to a depth of at least 10 nm after exposure to 1-2 Langmuirs (1 L = $1x10^{-6}$ Torr-s) of oxygen or water vapor, corresponding to sticking coefficients of near unity[BPR-MP-1]. However oxidation of thick films can be slower than thin films due to transition from drift-dominated ionic transport for thin films to diffusion-dominated transport for thick films.

Oxidation of 0.3 - 1 mm thick layers of lithium was investigated by using a microbalance with 1 μg resolution to probe mass gain of samples exposed to air for time periods of up to two weeks [BPR-MP-3B]. Optical microscopy monitored changes in surface morphology and color during the exposures and was used to estimate the Pilling–Bedworth ratio (volume change upon oxidation). The mass gain of lithium samples with surface area ~ 1 cm^2 during exposure to ambient and dry synthetic air was measured. For ambient air, we found an initial mass gain of several mg/h declining to less than 1 mg/h after an hour and decreasing by an order of magnitude after 24 h. A 9 mg sample achieved a final mass gain corresponding to complete conversion to Li_2CO_3 after 5 days. Fissures and cracks open up in the surface from the strain resulting from volume expansion associated with the conversion of lithium to Li_2CO_3, and this facilitates oxidation. From the initial rate of mass gain we estimate a sticking coefficient of 5.7×10^{-7} for O_2 and 2.6×10^{-6} for H_2O. These values are much lower than the unity sticking coefficients measured under UHV conditions for both O_2 and H_2O molecules incident on atomically pure, ultrathin (≤ 10 nm) films of lithium. Exposure to dry air resulted in a 30 times lower initial rate of mass gain corresponding to a slower Li reaction rate in dry air.

For safe handling of lithium in NSTX-U that has been exposed to ambient laboratory air (26 °C, 760 Torr, 45% RH), our results indicate the following rule of thumb: a Li film with a 1 μm thickness requires one hour for passivation, *i.e.*, to fully convert Li to Li_2CO_3 and pose no further reactivity hazards, a 10-μm thick Li film requires one day, and a 100-μm (0.1-mm) thick Li film requires one month. Dry (synthetic) air could be considered as a breathable environment with very much reduced lithium reactivity for maintenance activities. The oxidation experiments were done in collaboration with C. Hart who was supported by US DOE Summer Undergraduate Laboratory Internship program.

3. Material Analysis and Particle Probe (MAPP)

The Materials Analysis and Particle Probe (MAPP) is a novel in vacuo surface science diagnostic that allows analysis of samples exposed to tokamak plasmas. The implementation of MAPP on NSTX-U is a collaborative effort including researchers and graduate students from both the University of Illinois at Urbana-Champaign and the Program in Plasma Physics at PPPL. Testing of MAPP on the Lithium Tokamak Experiment (LTX) continued during the past year. Stainless steel (SS) MAPP samples were exposed to direct lithium evaporation inside LTX, such that they served as proxies for the LTX plasma facing components (PFCs). MAPP was then used for XPS and thermal desorption spectroscopy (TDS) analysis of these samples.

In one interesting set of experiments, the time evolution of lithium-coated SS samples exposed to LTX plasma discharges was compared against that of control samples exposed only to the LTX residual vacuum. XPS and TDS analysis showed no statistically significant differences between these samples (Figure BP-MP-2). In conjunction with other LTX diagnostics, these MAPP results suggested that lithium-coated SS might be retaining hydrogen in a more weakly-bound state than expected. This is similar to the weaker oxide-bonding observed in laboratory experiments described above (i.e. the hydrogen is not bound as LiH). This information could be of importance

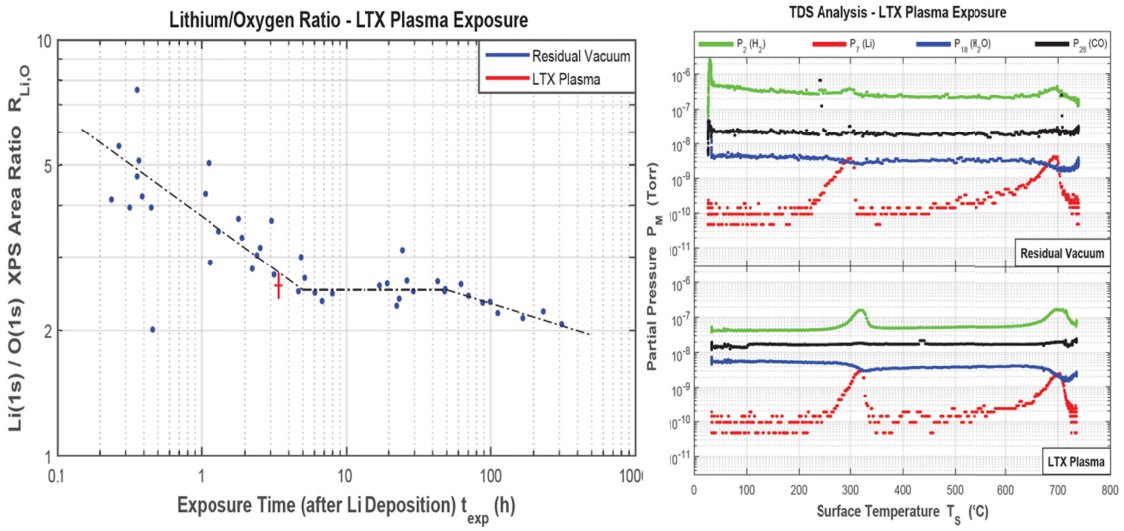

Figure BP-MP-2: *MAPP sample surfaces were statistically indistinguishable whether or not they were exposed to H+ fluence from LTX plasma discharges versus the LTX residual vacuum alone. (Left) surface lithium-oxygen ratio from XPS analysis,(right) volatile surface constituents from TDS analysis. In both cases, the important feature is the similarity between the data.*

for future MAPP experiments, particularly when the NSTX-U divertor is converted from graphite to high-Z PFCs.

MAPP has now been transferred from LTX to NSTX-U, where it will be available for sampling the divertor region during boronization and lithiumization experiments during the upcoming experimental campaign. As a result of successful testing on LTX, MAPP will have full use of its XPS, TDS, and depth profiling analysis techniques during these experiments. This includes the functionality of remote control where necessary to allow for between-shots manipulation and operation of MAPP.

4. Improved spectroscopic diagnostic coverage of upper divertor and center stack

In order to diagnose the in-situ behavior of lithium coatings and the impact of lithium on poloidal and toroidal asymmetries in lithium coatings, and correspondingly, on plasma conditions and stability; new high-resolution UV-VIS-NIR spectroscopic diagnostics are being installed in NSTX-U to monitor the previously uncovered upper divertor and central stack region. The diagnostics consist of a high-speed ProEM-HS 512 camera, an IsoPlane SCT320 spectrometer and 32 sightlines: 16 sightlines on the upper divertor and 16 sightlines on the central stack.

These spectroscopic views of the center-stack are obtained from one port at the Bay J equatorial plane for spectroscopy. A port at the Bay G bottom has been allocated to this project to provide views of the upper divertor. During the past year, we have used DOE funds to purchase a spectrometer, the Princeton instrument IsoPlane SCT320. This spectrometer is the same as the recently upgraded LLNL DIMS system. This spectrometer can work with up to 3 different gratings: one low resolution grating (1200 G/mm) to monitor wide regions of the spectrum; one high resolution grating (3600 G/mm optimized for UV) to measure fine spectral features of

selected spectral lines (i.e. to measure temperature); one intermediate resolution (2400 G/mm optimized for visible light) to monitor the intensity of multiple impurity lines at once. A ProEM:512B camera will be coupled to this spectrometer. We have now initiated the procurement of the fiber optic sight lines, using DOE project funds, and have recently received shipment of one of the two fiber bundles. Again, the fibers we are purchasing are the same as the LLNL DIMS system, which have a $480\mu m$ diameter and high transmission at wide range wavelength (350-800 μm).

The diagnostic support and optical design for the Bay J mid-plane and Bay G are complete, and the machine shop is manufacturing the fiber holder and other mechanical part. The second fiber optic bundles will be delivered at the early of September. Once the fiber holder and diagnostic bracket are completed, installation will be completed so that these two new diagnostic spectroscopic sight lines will become operational in October 2015. These new diagnostic capabilities of the central stack and upper divertor will enable us to address outstanding questions regarding the dependence of the effectiveness of lithium evaporation on the poloidal and toroidal asymmetries in the coating.

5. OEDGE and WallDYN modeling of the NSTX and NSTX-U

Significant progress has been made using the WallDYN code framework [BPR-MP-4] in developing a mixed-material evolution model for NSTX-U. WallDYN allows for the calculation of time- and poloidally-resolved surface concentrations and impurity erosion fluxes for a fully mixed C/Li/O/Mo environment. Unlike other modeling approaches that attempt to iteratively couple plasma transport and surface effects and run into computational hurdles due to the

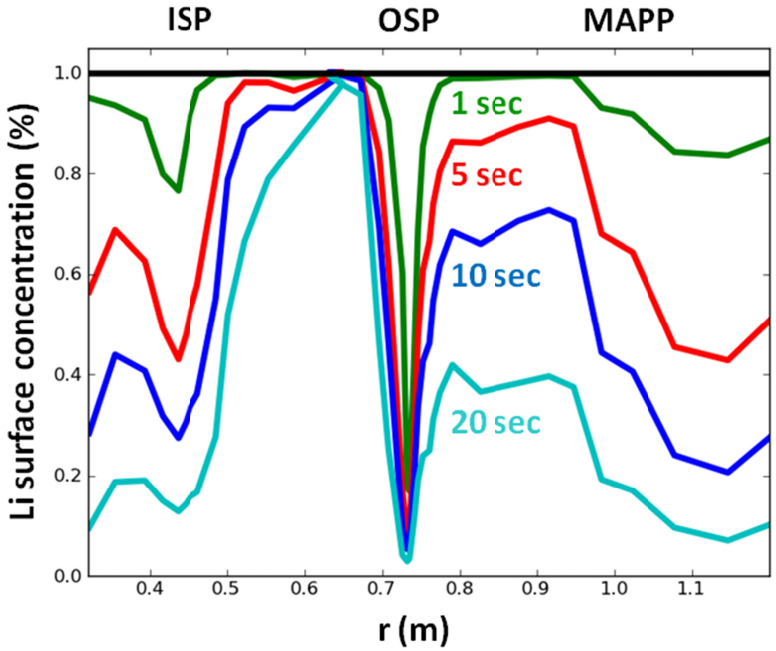

Figure BP-MP-3: *Preliminary WallDYN calculation of Li surface concentration evolution on NSTX graphite tiles during a low-triangularity discharge as a function of radius and plasma exposure time.*

disparate time and length scales, WallDYN operates by parameterizing the outputs of plasma transport and surface sputtering codes into rate equations, which can be solved simultaneously without strenuous computing requirements. Development so far has focused on the Li/C system, using plasma data from the FY2010 NSTX campaign. Figure BP-MP-3 shows a preliminary simulation of lithium migration in a low-triangularity, 0.8 MA, 4 MW NBI-heated H-mode, with the top layer Li concentration plotted versus major radius and plasma exposure time. Note that Li rapidly migrates away from the inner strike point (ISP) and outer strike point (OSP), while the concentration evolution at other locations on the wall is more gradual; this behavior was readily observed during NSTX operations. Features currently implemented in the NSTX-U WallDYN model include composition-dependent physical sputtering, chemical sputtering, realistic deuterium ion and neutral fluxes, and impurity ionization/recombination in the main SOL. Progress is ongoing on impurity ionization in the far SOL, Li diffusion into graphite, and oxide sputtering and migration.

In parallel with the computational effort, experiments have been planned on NSTX-U to test and improve the WallDYN material migration model. As seen in Figure BP-MP-3, we expect to see measurable composition changes during lithiated operations in the vicinity of the MAPP diagnostic (described elsewhere). MAPP will thus provide novel, shot-to-shot in-vacuo analysis of surface composition during migration experiments, to complement spectroscopic measurements of gross erosion and campaign-integrated measurements of deposition on witness plates. These experiments will allow for the fine-tuning of the material migration model and the eventual development of predictive capability.

6. Suppressed lithium erosion under high-flux deuterium plasma bombardment

Experiments conducted during collaborations on the Magnum-PSI experimental plasma device [BPR-MP-5] have led to results which strongly suggest the existing temperature limits associated with lithium PFCs may be overly pessimistic. In the experiments conducted at Magnum-PSI, lithium layers were evaporated onto TZM samples and pre-filled liquid metal targets were also tested. It was found that the inferred lithium erosion yield was approximately *two orders-of-magnitude less* than an adatom-evaporation model in previous studies conducted on the PISCES-B device [BPR-MP-6], shown in Figure BP-MP-4. Detailed analysis points to a particular issue in high-flux devices such as the Magnum-PSI device and future fusion divertors, that large fluxes of deuterium may exceed the diffusive transport rate within the bulk liquid. This leads to a significant concentration of LiD and deuterium at the

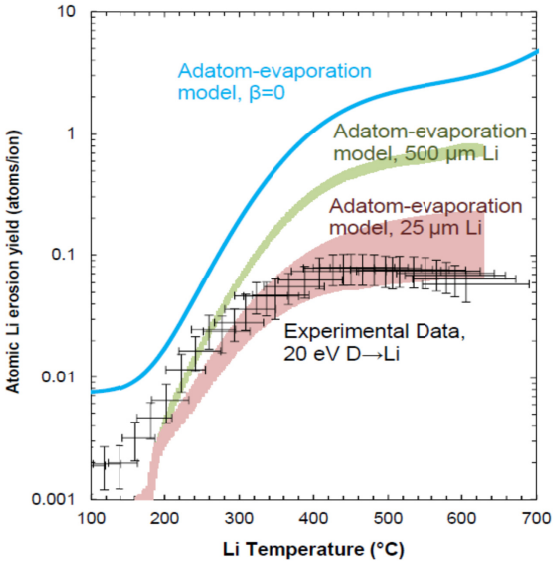

Figure BP-MP-4: *Atomic Li erosion yields vs. temperature during deuteirum plasma bombardment with D ion energies of 20eV. The predictions of the adatom-evaporation model are overlaid. A comparison is made of two lithium coating thicknesses is shown [BPR-MP-7].*

surface of the sample. The effect on erosion is enormous. First, LiD has a lower vapor pressure than pure Li resulting in less overall erosion due to evaporation. Second, the large deuterium fraction at the surface leads to preferential sputtering of the deuterium further reducing the erosion rate. Taken together, these effects explain the suppression of erosion observed in the experiment [BPR-MP-7].

The large surface fractions are consistent with suppressed deuterium diffusion in the Li-LiD sample. Deuterium diffusion was studied with the use of density-functional theory quantum computing techniques [BPR-MP-8] at Princeton University. These techniques do not rely upon model inter-atomic potentials as tradition molecular dynamics does, but rather calculates the inter-atomic potentials using an approximation of the full quantum wave equation. As shown in Figure BP-MP-5, it was found that for increasing concentrations of deuterium in a lithium sample, the deuterium diffusion rate decreases. This is partially understood by the chemical formation of LiD, a larger and slower molecule than either Li or D alone. Without the use of these suppressed diffusion rates, however, the resulting surface concentration of deuterium would be insufficient to explain the observed erosion.

In addition to the suppressed Li erosion, strong redeposition is expected at the surface. For plasma densities greater than $10^{14}cm^3$, a 10 micron coating is expected to persist approximately 500s based on redeposition modelling and the improved lithium erosion model. Comparison experiments on a carbon substrate, however, showed rapid depletion of the lithium consistent with lithium intercalation into the graphite. This result bodes well for the use of lithium as a wall conditioning technique on high-Z, metallic substrates, such as those planned in the high-Z divertor upgrade.

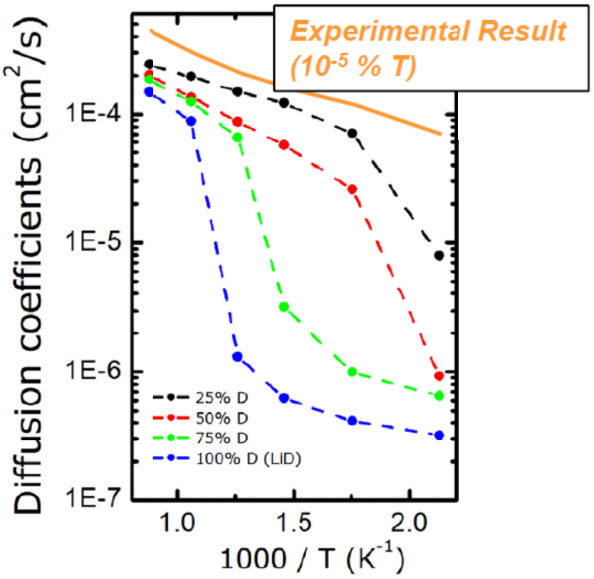

Figure BP-MP-5: *D diffusivity in Li as a function of temperature and D/Li concentration [BPR-MP-8].*

7. High-Z divertor Upgrade (Phase 1)

The purpose of the NSTX-U Divertor Upgrade-1 (DU1) is to provide operational experience and design evaluation prior to a larger, more comprehensive machine upgrade in future years. Following a similar logic as used for the NSTX Liquid Lithium Divertor system, the DU1 will be installed in the outboard divertor target in an effort to minimize operations during high-triangularity, high-performance discharges. In order to make a design assessment relevant to future upgrades of the high power divertor surfaces within NSTX-U, however, specific plasma discharges will be developed in the FY2016 run campaign to challenge the DU1 PFCs with heat and particle flux approaching levels expected during full, high-power operation of the NSTX-U.

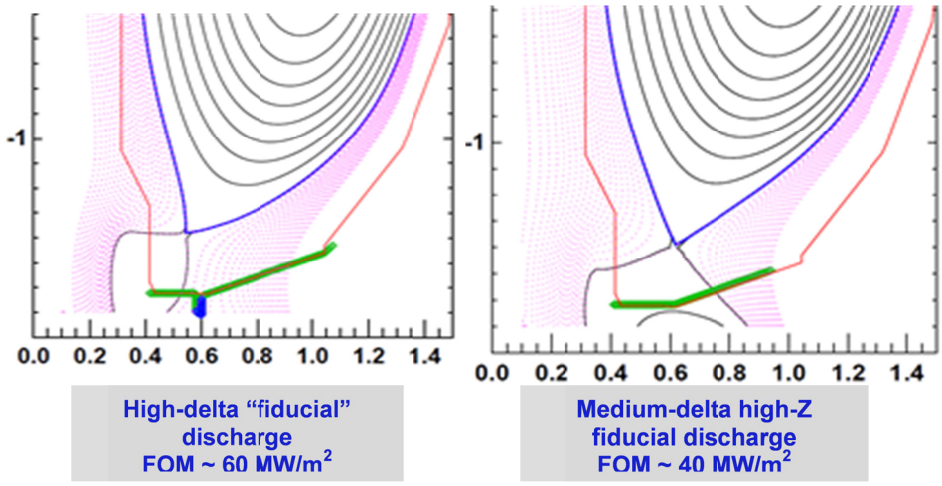

Figure BP-MP-6: *Comparison of high-delta discharge shape and figure-of-merit (FOM) heat flux with the high-Z reference discharge shape. The figure of merit does not account for heat-flux dissipation in the divertor and only provides a crude assessment of heat-fluxes. The FOM heat-fluxes on the high-Z divertor tiles would be expected to be of similar magnitude as those obtained in high-performance, high-triangularity discharges.*

A study has been carried out to develop discharge shapes that will provide heat and particle flux to different areas of the outboard divertor in order to accomplish these tests. A comparison of shapes is shown in figure BP-MP-6. A compromise is made in shaping because it is not possible to produce plasma discharges with arbitrary amounts of input power for a given discharge shape and divertor strike-point location due to plasma stability. As a result, a 0D analysis was conducted to estimate the maximum amount for a given discharge shape and then a peak heat flux "Figure-Of-Merit" (FOM) was developed as a basis of comparison. As with other engineering FOMs, the peak heat flux calculated from this FOM is not informed by a multitude of effects present during actual experiments and only provides guidance for design and experimental planning.

8. Development of pre-filled liquid metal divertor targets towards flowing-LM PFCs

Pre-filled liquid metal targets have been examined in a design study as part of a collaboration between PPPL and TU/Eindhoven. The concept of a pre-filled target is similar to how existing capillary-porous systems operate [BPR-MP-9] in that they are introduced to the fusion experiment already filled with lithium that is liquefied during operation. This scheme eliminates the need for external liquid metal recirculating loops, but tends to rely on passive forces to maintain wetted surfaces within the vessel. As such, these objects provide a potentially attractive intermediate step before implementing fully-flowing liquid metal plasma-facing components for NSTX-U.

Figure BP-MP-7 shows a concept for such a pre-filled target developed in parallel to the high-Z tiles described above. These pre-filled targets feature an internal reservoir and rely on capillary wicking effects to maintain a liquid lithium surface. This type of design would be appropriate for use as a divertor target whereas CPS-style devices have only been deployed as limiters in the past. The castellated structures reduce the surface stresses to minimal levels and the close geometry of the castellations would be expected to provide a wicking channel. Preliminary tests of the concept have been carried out with surrogate fluids indicating it is possible to replenish a surface in this way, though additional tests are needed.

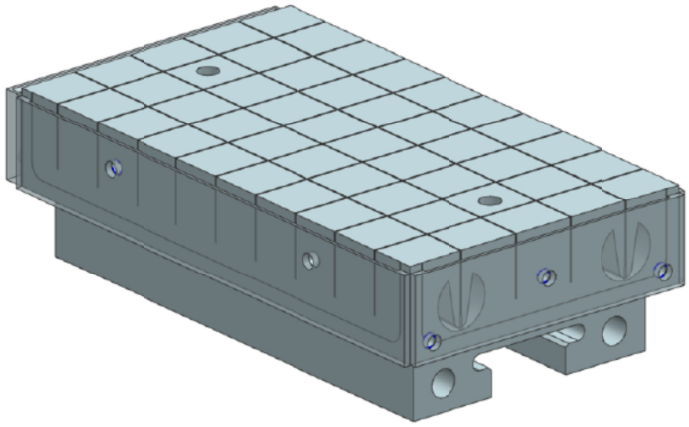

Figure BP-MP-7: *conceptual design for a pre-filled liquid metal target tile for use in the NSTX-U divertor.*

References

[BPR-MP-1] C.H. Skinner et al., *Journal of Nuclear Materials* **438** (2013) S647.

[BPR-MP-2] A.M. Capece, "The effects of temperature and oxidation on D retention in solid and liquid Li films on molybdenum plasma-facing components" Presentation at the 56th annual meeting of the APS Division of Plasma Physics, New Orleans, LA, USA, October, 2014.

[BPR-MP-2B] A.M. Capece, J.R. Roszell, C.H. Skinner and B.E. Koel, *Journal of Nuclear Materials* **463** (2015) 1177.

[BPR-MP-3] J. Roszell, A.M. Capece, C.H. Skinner and B.E. Koel, "Deuterium ion retention as lithium deuteride in thin Li films on Mo(110)" Presentation at the 56th annual meeting of the APS Division of Plasma Physics, New Orleans, LA, USA, October, 2014.

[BPR-MP-3B] C.A. Hart, C.H. Skinner, A.M. Capece, B.E. Koel, "Sorption of atmospheric gases by bulk lithium metal" *submitted to J. Nucl. Mater.*

[BPR-MP-3C] C.H. Skinner, A.M. Capece, J.P. Roszell, B.E. Koel, "Spreading of lithium on a stainless steel surface at room temperature" *to be submitted to J. Nucl. Mater.*

[BPR-MP-4] K. Schmid et al., *Journal of Nuclear Materials* **415** (2011) S284.

[BPR-MP-5] G. De Temmerman et al., *Fusion Engineering and Design* **88** (2013) 483.

[BPR-MP-6] R.P. Doerner, S.I. Krasheninnikov, *Journal of Applied Physics* **95** (2004) 4471.

[BPR-MP-7] T. Abrams, et al., "Suppressed gross erosion of high-temperature lithium via rapid deuterium implantation" *Submitted to Nuclear Fusion*; T. Abrams, "Erosion and re-deposition of lithium and boron coatings under high-flux plasma bombardment" Ph.D. Thesis, Princeton University, 2014.

[BPR-MP-8] M. Chen, T. Abrams, M.A. Jaworski and E.A. Carter, "Rock-salt structure lithium deuteride formation in liquid lithium with high-concentrations of deuterium: a first-principles molecular dynamics study" *Submitted to Nuclear Fusion*.

[BPR-MP-9] V. Evtikhin, et al., *Journal of Nuclear Materials* **271-272** (1999) 396.

II. Core Science Research Highlights

In 2014, three topical science groups (TSGs) were organized under a new core science group. The three TSGs include (a) macroscopic stability, (b) transport and turbulence, and (c) energetic particles. Each of these TSG areas is covered as a sub-section in the core science report below.

A. Macroscopic Stability TSG Research Highlights

Macroscopic stability research aimed at enabling long-pulse high performance in NSTX-U progressed in FY2015 along three main topics: (1) stability, (2) 3D fields, and (3) disruptions. A disruption characterization and avoidance system for NSTX-U, informed by passive stability understanding and active control, will allow sustainment of macroscopic stability. New equilibrium profile control capabilities will rely on understanding the physics of 3D field effects. Finally, new disruption mitigation capabilities will be implemented and greater understanding of disruption dynamics will be pursued.

1. Stability

Ideal MHD Stability of NSTX

Plasmas can operate stably above ideal magnetohydrodynamic limits to the pressure by dissipating the energy of the perturbed magnetic field into the motions of the particles via stabilizing rotational resonances. This modification to ideal stability by kinetic effects is calculated by various codes including the Modifications to Ideal Stability by Kinetic effects (MISK) code [MS-STA-1] which has been extensively developed through theory [MS-STA-2] and benchmarked against other leading codes [MS-STA-3]. Although knowledge of the ideal MHD stability is insufficient to fully understand stability in tokamaks, it is nevertheless informative as RWMs are still generally only expected to occur above the no-wall limit, and ideal fluid stability terms still underlie the necessary kinetic modifications. Therefore a real-time estimate of the no-wall limit is also useful for future disruption avoidance systems. To determine the RWM marginal point accurately requires confidence in the ideal as well as the kinetic components.

The DCON ideal MHD stability code [MS-STA-4] has been used to analyze a large database of NSTX equilibria [MS-STA-5]. For toroidal mode number n=1 and without any wall in the calculation, crossing from positive to negative $\delta W_{no\text{-}wall}$ in DCON defines exceeding the n=1 no-wall limit. In this analysis, equilibria were taken from periods during the plasma current steady-state and that had $\beta_N/l_i > 2.5$.

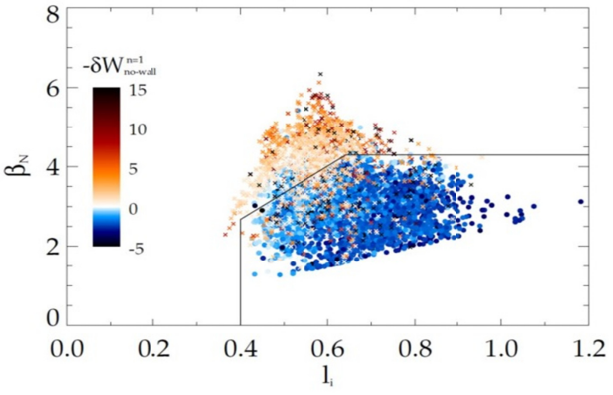

Figure MS-STA-1*: The β_N vs.l_i space of NSTX. Blue is below the no-wall limit and red is above.*

Figure MS-STA-1 shows the β_N vs. l_i space of nearly five thousand experimental equilibria from 350 NSTX discharges, with the color of each point indicating the DCON calculated $\delta W_{no\text{-}wall}$. For clarity, we have plotted the quantity - $\delta W_{no\text{-}wall}$ so that negative is ``below" (indicated with blue dots) and positive is ``above" the no-wall limit (indicated with red x's). One can see that the previously defined no-wall limit [MS-STA-6] shown with the solid lines, $\beta_N = 4.3$ above $l_i \approx 0.64$ and $\beta_N/l_i = 6.7$ from $l_i \approx 0.4$ to 0.64, does a good job describing the location of the no-wall limit in this data set. The β_N vs. pressure peaking space in NSTX is fairly similar to the β_N vs. l_i space, as might be expected since there is an experimental correspondence between broadened pressure and broadened current profiles (lower l_i). The ideal n=1 no-wall beta limit decreases with increasing aspect ratio [MS-STA-7]. This property has been previously computed for NSTX [MS-STA-8], and is now confirmed with a much larger sample of equilibria.

It is useful for purposes of disruption avoidance to have a real-time estimate of the no-wall limit, rather than running ideal stability codes after the discharges. This can be achieved by relying on quantities from real-time equilibrium reconstruction. As an example, if we combine the dependencies on β_N/l_i, $\beta_N/(p_0/\langle p\rangle)$, and A at low l_i and low $p_0/\langle p\rangle$, the following estimate can be made for the no-wall beta limit based on equilibrium quantities: $\beta_{N,no\text{-}wall} = 3^{1/3}((6.7l_i)^{-3}+(1.91p_0/\langle p\rangle)^{-3}+(14(A^{-1}-0.4))^{-3})^{-1/3}$.

The ideal stability for projected NSTX-U [MS-STA-7] equilibria has been explored in the parameter space of β_N vs. $p_0/\langle p\rangle$ previously, where a no-wall limit of $\beta_N \approx 3.5$-4 was found [MS-STA-9]. A somewhat smaller no-wall limit in NSTX-U would be consistent with its somewhat larger aspect ratio, and the scaling of $\beta_{N,no\text{-}wall}$ on aspect ratio will be further tested and refined by NSTX-U experiments. NSTX-U will also have new off-axis neutral beams that can potentially broaden the current, pressure, and plasma rotation profiles [MS-STA-9]. A broadened current profile tends to lower the no-wall and ideal-wall beta limits [MS-STA-10]. In contrast, a broadened pressure profile is beneficial in raising the ideal-wall beta limit [MS-STA-9,MS-STA-11], but it can lower the no-wall limit, opening up a large β_N range in between them. However, modifications to ideal stability by kinetic effects [MS-STA-12] should continue to enable passively stable operation in this range.

Modifications to Ideal Stability by Kinetic Effects in NSTX

To determine RWM marginal stability for use in experimental disruption avoidance, ideal stability limits like those calculated in the previous section need to be modified by kinetic effects in order to reproduce experimental marginal stability points. Specifically, reduced stability models could be developed that could employ real-time measurements (e.g. rotation) and actuation (rotation control via magnetic braking or neutral beam sources) to detect approaches to marginal stability and return the plasma to a more stable state. Here we examine the stability trajectories of several NSTX experimental RWM unstable discharges to further validate the kinetic stability calculations of the marginal point with the MISK code [MS-RWM-5].

Figure MS-STA-2 shows MISK calculated growth rates vs. time before an unstable RWM, both normalized by the wall time. The dominant rotational kinetic resonances and the mostly non-resonant influence of energetic particles are both included. One can see that in each case, the calculations trend towards instability $\gamma\tau_w = 0$ as the time approaches the time in the experiment when the RWM instability begins to grow. Additionally, MISK stability calculations for eleven time points from three discharges (taken from the same NSTX experiments) that remained stable to the RWM are also shown, on the left side of Figure MS-STA-2 (labeled as -∞ on the abscissa). All of the equilibria analyzed were predicted to be robustly stable to the RWM, with $\gamma\tau_w < -0.7$ and no discernable trends vs. time in each discharge.

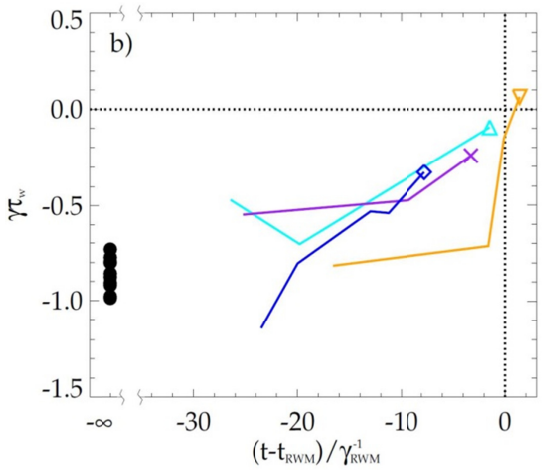

Figure MS-STA-2*: MISK calculated normalized growth rates vs. normalized time before an unstable RWM.*

The present research represents a required new stage of analysis moving toward creating an experimentally validated, reduced model of kinetic RWM stability determination for use in real-time instability prediction.

Further Comparison of NSTX and DIII-D Kinetic RWM Stabilization Physics

The 2014 NSTX-U Year-End progress report showed and described results from a joint NSTX/DIII-D experiment "*MP2014-22-07: Testing kinetic RWM stabilization theory at marginal stability in high beta, tearing mode stabilized plasmas*" (S.A. Sabbagh, J.W. Berkery, J.M Hanson, et al.). The detailed experimental and analysis results showed a unification of understanding of kinetic RWM stabilization physics between the devices. Common analysis tools, including the MISK code, were used to analyze the experimental results on both devices. Quantitative agreement was found between theory and experiment of kinetic RWM marginal stability points over a wide range of plasma rotation profile and speed. A decrement was found in the predicted marginal stability point when significant portions of the plasma had zero rotation. Extensive kinetic stability runs were completed and compiled since the last report. The MISK kinetic RWM analysis of the reconstructed DIII-D equilibrium evolutions that reach the marginal RWM stability points in the experiment described above, as well as many NSTX plasmas that either become RWM unstable, or retain stability, are summarized in Figure MS-STA-3. This single diagram contains a wealth of information that shows for the first time the unification between DIII-D and NSTX high beta plasmas regarding RWM stability and associated theoretical computations of kinetic RWM stability. First, we find that plasmas free of other MHD modes can reach linear kinetic RWM marginal stability, and also find that (as published from NSTX experiments for several years now) there is no simple "critical rotation speed" that ensures RWM stability – the plasma can become RWM unstable at high levels of plasma rotation. Trajectories of both DIII-D and NSTX plasma moving from stability to instability experimentally are

indicated by the connected dots with arrows indicating the direction of the plasma evolution. Each point represents a unique, reconstructed equilibrium, with kinetic RWM growth rates computed by the MISK code. The computation includes the effects of fast particles on plasma stability. The quantitative level of agreement between experiment and theory regarding the RWM marginal stability points is remarkable. The error in the calculation is $\Delta\gamma\tau_w \sim 0.2 - 0.3$. Figure MS-STA-3 also shows that global bursting MHD modes can lead to non-linear destabilization before linear stability limits are reached. This is shown, for example, for the lowest rotation

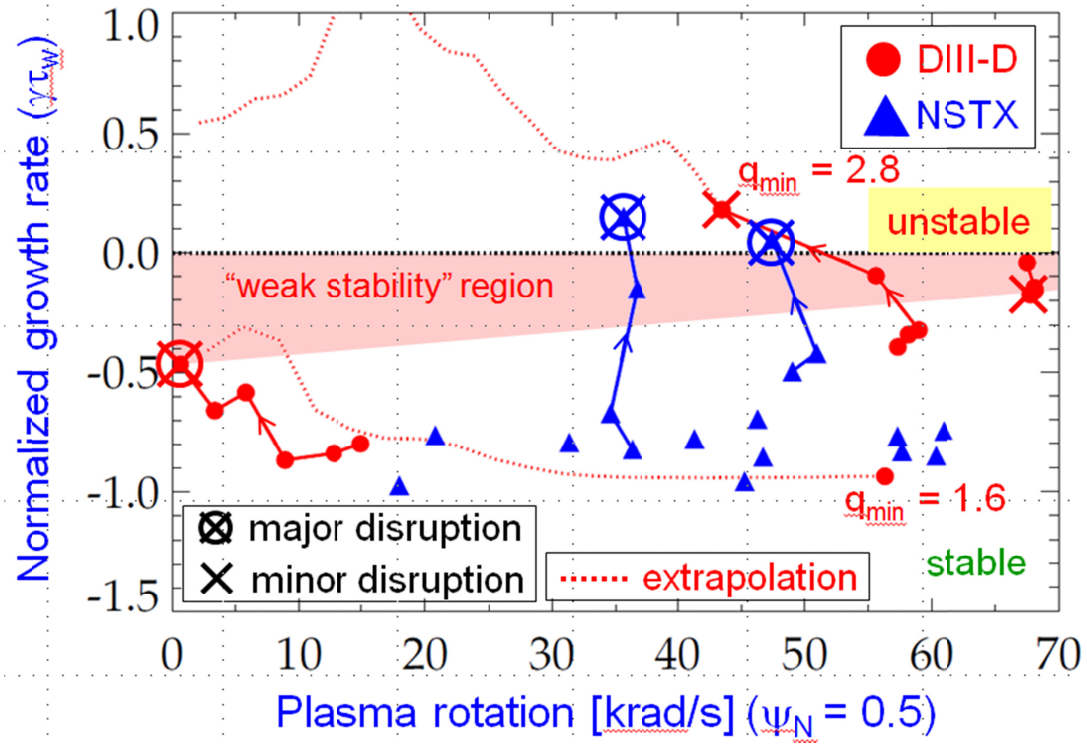

***Figure MS-STA-3**: Kinetic RWM growth rate (computed by the MISK code) normalized to the conducting wall eddy current decay time for NSTX and DIII-D plasmas suffering RWM instability, and also plasmas that are stable, as a function of plasma rotation speed.*

DIII-D case. The plasma terminates in a full current quench disruption, but at the point of the experimental disruption, the calculations shows linear kinetic RWM stability. However, the actual disruption is observed to correlate with the onset of a global bursting MHD mode. It is hypothesized that the RWM is non-linearly destabilized by this bursting event. Note that based on variations of the input equilibrium for the kinetic RWM stability calculation, it is presently not thought that the linear calculation has an error bar large enough to allow the plasma to be linearly unstable. Therefore, the actual experimental point of destabilization below the linear marginal stability point defines a region of "weak stability", which has been reported in past experimental studies on DIII-D [MS-STA-13]. The present experiment quantifies for the first time the level of $\Delta\gamma\tau_w$ that defines this weak stability region below the computed linear RWM marginal stability point. Comparing DIII-D results at the extremes of rotation in Figure MS-STA-3, is appears that the magnitude of $\Delta\gamma\tau_w$ defining the weak stability region decreases as the plasma rotation increases. Finally, the dotted lines in Figure 8 represent kinetic STA stability calculations based

on experimental DIII-D equilibrium reconstructions of the experimental high β_N, high q_{min} plasmas with the toroidal rotation profile self-similarly varied from high to low rotation. In this study, we find that these plasmas are less stable as q_{min} increases, and that marginal stability is bounded by $1.6 < q_{min} < 2.8$ over the full range of plasma rotation scanned. It is noteworthy to state that the extrapolation at $q_{min} = 1.6$ remarkably connects up smoothly from the plasma at high rotation to the plasma at low rotation – a different plasma shot – but with nearly the same q_{min} (1.7 in the experimental plasma at low rotation).

Characterization of Events Leading to Disruptions for Stability Forecasting

The FESAC 2014 Strategic Planning report defined "Control of Deleterious Transient Events" as one of two highest priority (Tier 1) initiatives of the DOE Fusion Energy Sciences (FES) strategic plan: "*Advance the fundamental science of magnetically confined plasmas to develop the predictive capability needed for a sustainable fusion energy source*". Macrostability research in the NSTX-U 5 Year Research Plan directly targets this highest priority initiative, and has already acted on it in three substantial ways. First, the NSTX-U Disruption Prediction, Avoidance, and Mitigation (DPAM) Working Group was formed to organize a focused research activity in this area. Meetings of this working group to date have emphasized the utilization of a multi-faceted approach to DPAM with quantifiable figures of merit to mark progress toward goals (most broadly stated as disruption probabilities) starting with NSTX-U, and expanding the results to other present tokamak devices. Second, NSTX-U researchers participated significantly in the recent FES Transient Events Workshops, with several talks and white papers submitted, and also with an NSTX-U collaborator leading the sub-panel on disruption prediction which produced a substantial report in this subject area.

This preparatory work stated above has led to the third element of the plan to begin to quantitatively address and solve the disruption problem in tokamaks – the creation of a general analysis code to characterize and forecast disruptions. The characterization component of the solution is critical to apply present knowledge of plasma destabilization, and to further understand how disruptions can be forecast well before they occur. Disruptions are preceded by a chain of events schematically shown in Figure MS-STA-4. By defining these "disruption event chains"

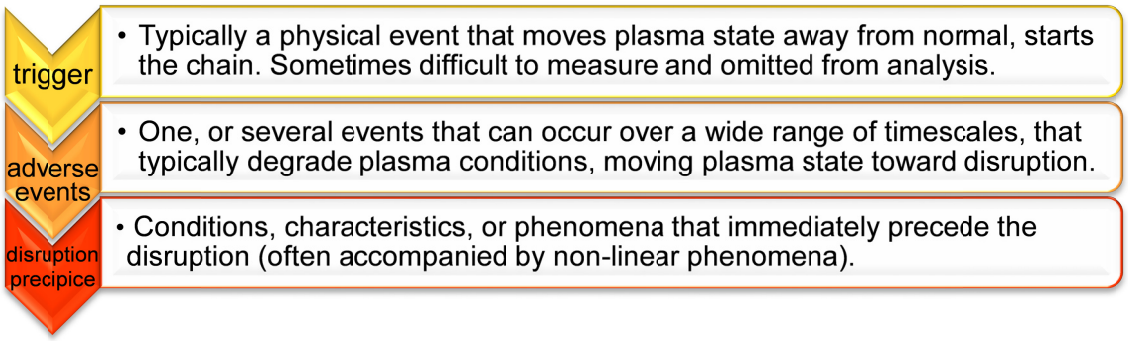

***Figure MS-STA-4**: Schematic description of a disruption event chain.*

(similar to the approach taken by De Vries, et al. [MS-STA-14]), plasma stability prediction and avoidance tools can be brought to bear on as many of the disruption chain events (DCEs) as possible, greatly increasing the opportunity to prevent the disruption from ever happening. During FY15, we developed the initial version of a computer code that automates the critical Disruption Event Characterization And Forecasting (DECAF) process. The code is written in Python and is has been designed to be both general and portable, so it can be used not only for NSTX and NSTX-U data, but also can be used to analyze data directly from other tokamaks for comparison – to maximize the applicability of results to ITER and future tokamaks. This follows the work of Gerhardt, et al. that examined the NSTX database and showed that a fairly simple algorithm processing a relatively small amount of diagnostics could predict disruptions a posteriori with high success, and with a low probability of false positives [MS-STA-15]. The present work adds the concept of, and emphasizes analysis of disruption event chains, and expands the scope of possible DCEs to bring in more physics models in the DPAM analysis to further improve results. The code will also add testing of different forecasting algorithms, and will utilize analysis results iteratively to quantitatively improve disruption forecasting. The new generalized and portable code design will make the important processing of other tokamak databases straightforward. Initial results from the DECAF code are shown in Figure MS-STA-5 for two NSTX plasmas. Ten physical disruption chain events are presently defined in the code, which will expand significantly as the code is developed as required. Figure MS-STA-5(a) shows the code results for a plasma in which the pressure profile peaking is increasing in time (a strong indicator of a potential disruption). The code issues warnings up to a point where a critical threshold is surpassed (a "PRP" event is detected, as shown in the plot). Subsequently, the code identifies three other disruption chain events leading up to the disruption – a vertical displacement event (VDE) is identified, followed by an event indicating that plasma shape control has not met expectations (SCL), followed by an event indicating that plasma current feedback control has not met expectations (IPR). Figure MS-STA-5(b) shows an example of a disruption event chain in a plasma in which the plasma current is being ramped down. First, an event is declared as the plasma fails to meet operational criteria related to the Greenwald density limit (GWL), followed by a VDE, and an IPR event. These early results of the DECAF code provide an essential starting point for which the code can be continually approved to the level of disruption forecasting required - to a few percent level, and below needed for ITER and future tokamaks.

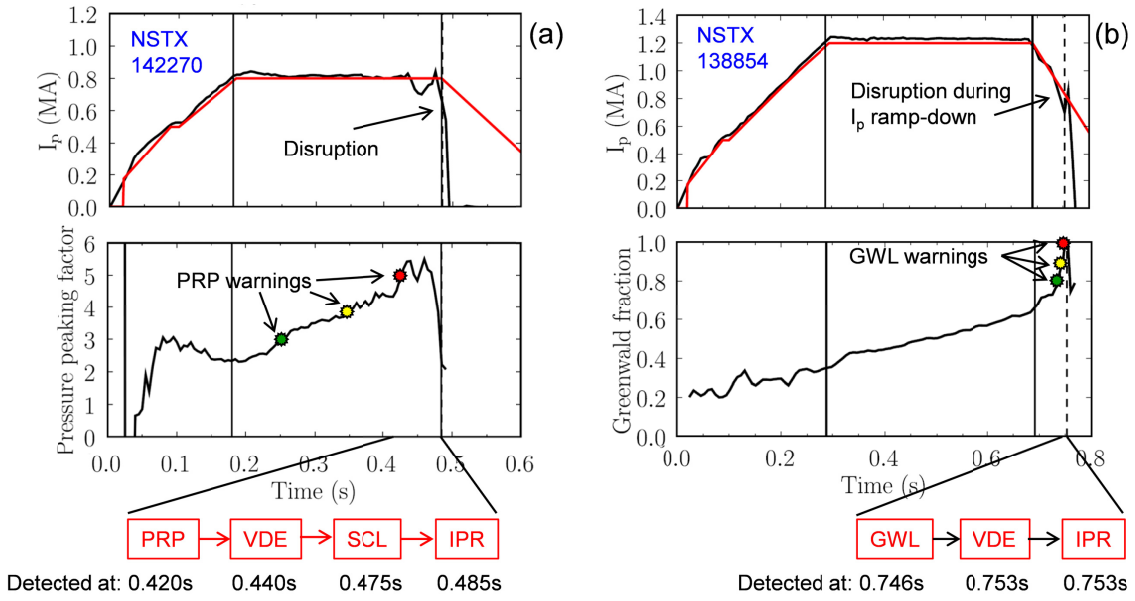

Figure MS-STA-5: *Initial DECAF code results showing disruption events chains for two NSTX plasmas.*

NSTX-U CD-4 Plasma Equilibrium

Since the early days of NSTX it has been known that modeling of the evolution of the device wall current is essential for accurate equilibrium reconstructions, especially in the current ramp-up phase of the discharge [MS-STA-16]. In addition, magnetic diagnostics with sufficient stray field compensation are essential for such reconstructions. Both of these key elements were prepared and available for NSTX-U CD-4 plasmas. The NSTX-U EFIT reconstructions performed during the CD-4 plasma operation period helped guide plasma operations to optimize the plasma at low current (significantly less than the currents induced in the vessel walls), with a subset of the plasma shaping coils, and only pre-programmed control of the shaping coil currents. Figure MS-STA-6 shows results of the reconstruction of the first NSTX-U plasmas (prepared to completion of DOE CD-4 for the device). These plasmas were ohmically-heated, using a subset of the device's shaping coils with pre-programmed waveforms only, and with no special wall conditioning (including no bakeout of the device). Nevertheless, the goal of reaching plasma current, I_p = 50 kA under these conditions was significantly surpassed. Reaching this goal was verified by the computed I_p from the equilibrium reconstructions. Results from the reconstructed I_p using the full magnetic diagnostic set and a detailed conducting wall model compared very well to the (independent) time evolution of I_p from plasma rogowski measurements where wall current effects were subtracted. The high loop voltage (over 4V) used to start up these initial plasmas generated a correspondingly large vessel current of over 420 kA computed in the equilibrium reconstructions. The reconstructions also identified or confirmed important specific details in the poloidal distribution of the wall current including the significant current (~15 kA) generated in the new center stack crown regions (the slanted sections of the center stack) and the PF1a coil mandrels (assembly and mounting components of the PF1a coils), and the relatively small current (~ 1kA) in the vessel bellows.

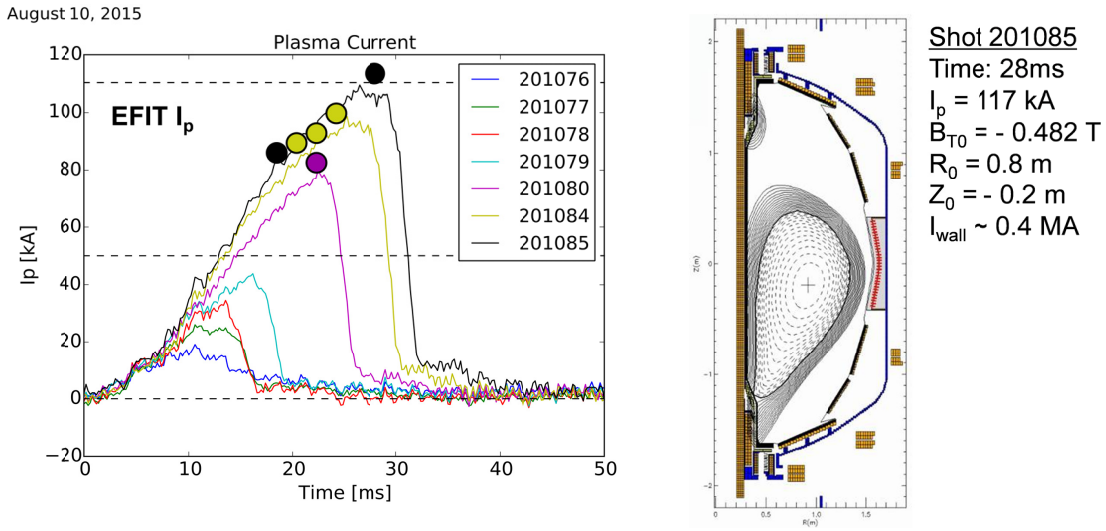

***Figure MS-STA-6**: Reconstruction of plasma current, flux contours, and wall current for the first NSTX-U plasmas.*

Further optimization of the initial CD-4 plasmas in NSTX-U was accomplished by altering the relative timing of the main equilibrium vertical field (generated by the PF5 coil) and the PF3 shaping coil, as well as the relative balance of current in the PF3 upper/lower shaping field coils. The NSTX-U EFIT reconstructions showed the expected relative imbalance of the current running in the PF1a upper/lower mandrel elements. This imbalance was countered by a suitable imbalance in the programmed PF3 upper/lower coil currents. Iteration between the examination of the reconstructed results and the pre-programming of the shaping field currents led to a further increase of I_p as the plasma was better centered in the vessel before moving toward either an upper or lower single null configuration, two examples of which are shown in Figure MS-STA-7. The maximum I_p computed in reconstructions was 138 kA. The maximum plasma volume reconstructed in these plasmas exceed 9 m^3 (compared to a typical highly-shaped equilibrium volume of about 13 m^3.)

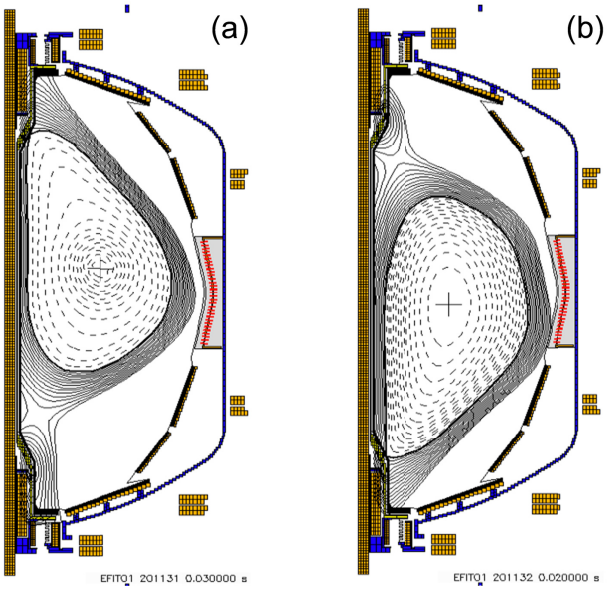

***Figure MS-STA-7**: Initial NSTX-U ohmically-heated plasmas reaching I_p = 138 kA.*

KSTAR Research at High Normalized Beta Significantly Above the n = 1 No-wall Limit

Joint collaborative research on the Korean Superconducting Tokamak Advanced Research facility (KSTAR) reached further milestones through the Columbia U.-NSTX-U collaboration by creating plasmas with maximum normalized beta on the device. The most compact representation of the significantly expanded high normalized beta stability operational space can be expressed in a plot of (l_i, β_N). This is shown below, with comparisons to results from prior years. Figure MS-STA-8 shows the newly achieved β_N and l_i values from discharges dedicated to explore $\beta_N > \beta_N^{no\text{-}wall}$ overlaid on the equilibrium performance obtained previously [MS-STA-17-19]. Note that all of the points shown in this plot represent a fully-converged KSTAR EFIT equilibrium reconstruction performed by the US collaboration for the KSTAR Research Team. The β_N above 4 (max. $\beta_N > 4.3$) has been achieved in discharges having toroidal magnetic field (B_T) in the range 0.9-1.1 T after the plasma reached a flattop current of 0.35-0.4 MA. The total neutral beam heating power (P_{NBI}) from three beam sources was 4 MW. The plasma current was proportionally varied with B_T to get a similar safety factor, $q_{95} \sim 4.5$ for stable plasma operation. The l_i was

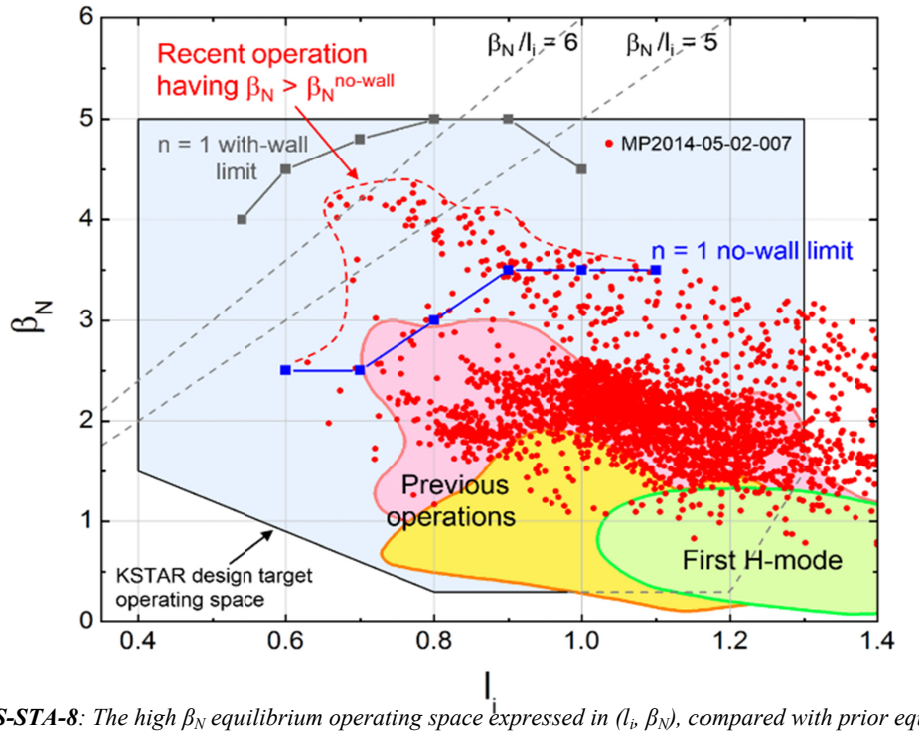

Figure MS-STA-8: *The high β_N equilibrium operating space expressed in (l_i, β_N), compared with prior equilibrium performance. The recent data shown by red points comprises ~3000 current flattop equilibria of 16 shots.*

maintained at low values ranging from 0.66 to 0.86 at $\beta_N > 4.3$ which results in the highest ratio of β_N/l_i up to 6.3 with the energy confinement time, τ_E, of 50-70 ms. As shown in the figure, the plasmas exceed the computed $n = 1$ ideal no-wall β_N limit by 48% - a substantial value. The high $\beta_N > 4$ was sustained for duration longer than a few τ_E in several discharges. Addition of the newly available third neutral beam source helped to increase the peak β_N by more than 10% in these shots, and is also found to lower l_i due to its deposition closer to the plasma edge that apparently leads to a broader current profile, favorable to future advanced tokamak operation.

The increase in β_N by lowering B_T is somewhat saturated at B_T = 1.0 T which is thought to be due to a reduced energy confinement at low B_T.

In these plasmas having $\beta_N >> \beta_N^{\text{no-wall}}$, unstable low-$n$ global kink/ballooning or resistive wall modes are somewhat surprisingly not observed. Rotating q = 1 kink modes and sawteeth are measured by toroidal magnetic probes whereas tearing modes or significant amplitude are absent. The RWM stable plasma operation at this high β_N level may indicate that the mode is stabilized by plasma rotation and kinetic effects [MS-STA-6,12,20,21]. The termination of the discharge around peak β_N commonly occurred in the several other high β_N discharges. The locked mode (LM) sensor signals in the shots that reached high β_N start to show a deviation from zero after ~1 s which indicates the onset of the terminating event, and the current quench occurs when the deviation becomes maximum (Figure MS-STA-9). The pulse lengths before disruption are much longer that the RWM growth time, but maintaining the plasma for longer pulse durations is required to determine if the plasma rotation and q evolution will change mode stability over long pulse, for both RWM and NTM stability. We presently find that data from other LM sensors positioned at different toroidal locations that the radial magnetic field component of the event yield an n = 0 perturbation structure which suggests that the high β_N operation was terminated by a loss of equilibrium control, rather than a mode with n > 0. This apparently is due to an H-L back transition during which the increased vertical field needed to sustain the higher stored energy H-mode plasma is not reduced quickly enough to avoid the plasma from being pushed back to the center column, becoming limited and causing a disruption. This dynamic is verified by both the equilibrium reconstructions and the visible fast camera images. For 2015, a new experiment has been approved that will implement improved plasma control and aim to produce sustained high β_N operation and provide the next step in probing the RWM stability boundary in KSTAR with steady-state equilibrium profiles.

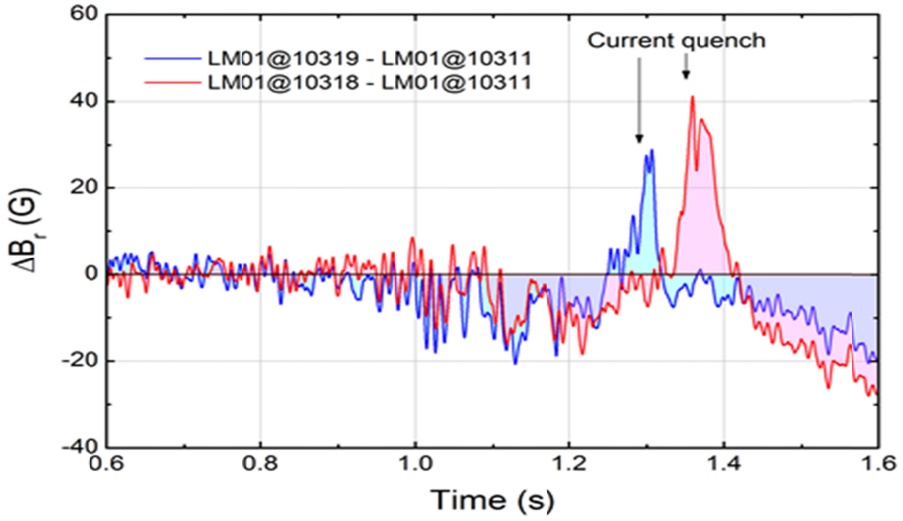

Figure MS-STA-9: *Locked mode (LM) sensor signals from two high β_N discharges terminated by disruption.*

In this area of attaining high β_N in KSTAR, expectations have been greatly exceeded producing plasma with β_N > 4.3 and very high ratio of β_N/l_i up to 6.3, and doing so at reduced toroidal field (not expected to be accessible from past experiments). Additionally, no n = 1 RWMs or other global instabilities are found to limit beta at these high values, and remarkably at up to 50%

above the n = 1 no-wall β_N limit. This is highly encouraging and may indicate that KSTAR may be producing increased stability in part due to reduced $n = 1$ error field in the device along with the usual kinetic stabilization effects. Understanding of these results will improve through upcoming joint experimentation and comparison to high β_N plasmas in NSTX-U.

References

[MS-STA-1] B. Hu et al., Phys. Plasmas **12**, 057301 (2005)
[MS-STA-2] J.W. Berkery et al., Phys. Plasmas **21**, 112505 (2014)
[MS-STA-3] J.W. Berkery et al., Phys. Plasmas **21**, 052505 (2014)
[MS-STA-4] A.H. Glasser and M.C. Chance, Bulletin of the Am. Phys. Society **42**, 1848 (1997)
[MS-STA-5] J.W. Berkery et al., "*Modifications to Ideal Stability by Kinetic Effects in NSTX*", submitted to Nucl. Fusion (2015)
[MS-STA-6] S.A. Sabbagh et al., Nucl. Fusion **53**, 104007 (2013)
[MS-STA-7] J.E. Menard et al., Nucl. Fusion **52**, 083015 (2012)
[MS-STA-8] S.P. Gerhardt et al., Nucl. Fusion **51**, 073031 (2011)
[MS-STA-9] S.P. Gerhardt et al., Nucl. Fusion **52**, 083020 (2012)
[MS-STA-10] W. Howl et al., Phys. Fluids B **4**, 1724 (1992)
[MS-STA-10] J.R. Ferron et al., Phys. Plasmas **20**, 092504 (2013)
[MS-STA-12] J.W. Berkery et al., Phys. Rev. Lett. **104**, 035003 (2010)
[MS-STA-13] E.J. Strait, et al., Phys. Plasmas **14**, 056101 (2007)
[MS-STA-14] P.C. de Vries, et al., Nucl. Fusion **51**, 053018 (2011)
[MS-STA-15] S. P. Gerhardt, et al., Nucl. Fusion **53** 063021 (2013)
[MS-STA-16] S. A. Sabbagh et al., Nucl. Fusion **41**, 1601 (2001)
[MS-STA-17] Y.S. Park, S.A. Sabbagh, J.W. Berkery, *et al.*, Nucl. Fusion **51**, 053001 (2011)
[MS-STA-18] Y.S. Park S.A. Sabbagh, J.M. Bialek, *et al*., Nucl. Fusion **53**, 083029 (2013)
[MS-STA-19] Y.S., Park, S.A. Sabbagh, J.M. Bialek, *et al.*, Phys. Plasmas **21**, 012513 (2014)
[MS-STA-20] B. Hu, R. Betti, and J. Manickam, Phys. Plasmas **12**, 057301 (2005)
[MS-STA-21] S.A. Sabbagh, J.W. Berkery, R.E. Bell, *et al.*, Nucl. Fusion **50**, 025020 (2010)

2. 3D Field Physics Research

Quantification of 3D Plasma Response

Numerical verification and experimental validation of various quantitative aspects in 3D plasma response have been of great interest in the community and investigated jointly with other theory [MS-3D-1] and experimental groups [MS-3D-2]. In particular, the efforts under JRT14 were successfully extended, by validating ideal plasma response in more details with the upgraded DIII-D magnetic sensors in both high and low field side [MS-3D-3], but also by showing the importance of kinetic effects in high-β NSTX plasmas beyond the no-wall limit.

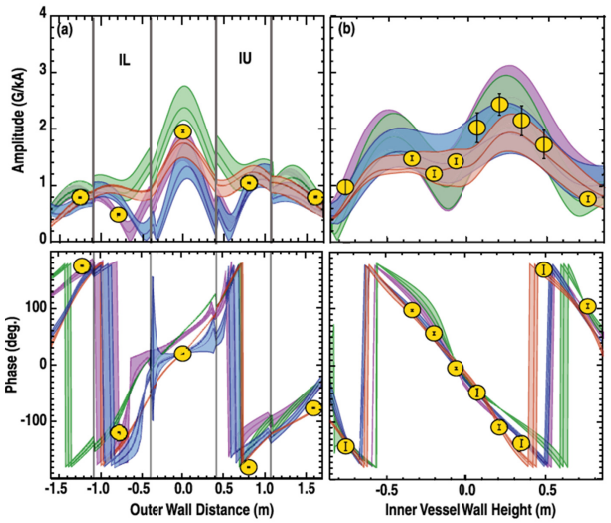

Figure MS-3D-1 *The amplitude (top) and phase (bottom) of n=1 plasma response measured by (a) LFS sensors and (b) HFS sensors (circles), compared to predictions by IPEC (green), MARS-F (blue), VMEC (red), and M3D-C1 (purple).*

Figure MS-3D-1 shows the comparison of experimentally measured response in DIII-D for n=1 field amplitude and phase, to 4 different codes, IPEC, MARS-F, VMEC, and M3D-C1. While slight differences exist, the agreement shown between four unique physical and numerical formalisms is indeed remarkable. The joint efforts indicated that in many circumstances linear ideal MHD provides a good representation of tokamak 3D responses. However, it is also shown that the linear model can locally break down when the applied field strength is significant, and that the ideal approximation can become poor when plasma is close to the ideal stability limit. Indeed MARS-K applications to NSTX high-β plasmas confirmed the importance of kinetic effects by thermal ions in 3D response, similarly to DIII-D high-β plasmas [MS-3D-4].

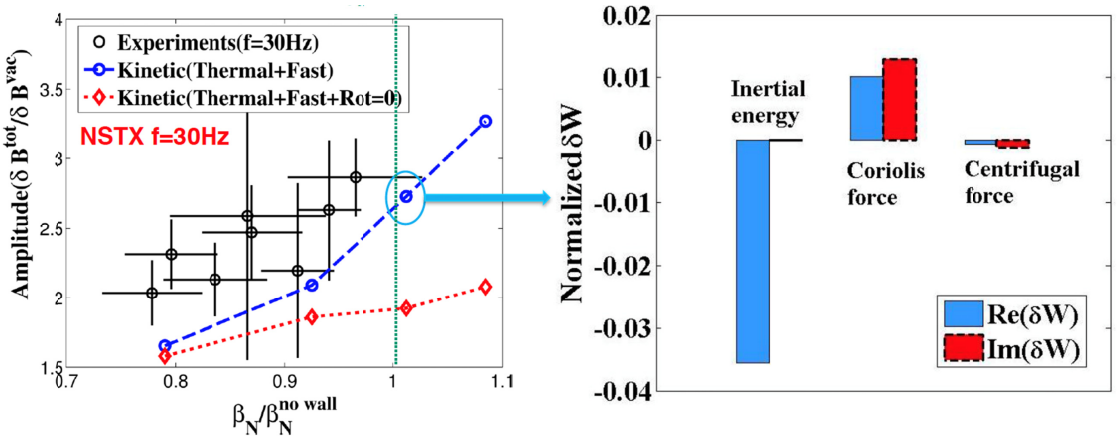

Figure MS-3D-2 *Amplitude measured by sensors and predicted by MARS-K with (blue) and without (red) fluid rotation (Left figure). Energy analysis shows the inertial energy associated with fluid rotation is most important and destabilizing to plasma.*

In the case of NSTX additionally, the effects associated with fluid rotation were important to explain the measured plasma response [MS-3D-5]. As shown in Figure MS-3D-2, particularly inertial energy by rotation is the largest and destabilizing, which leads to the larger amplification of plasma response.

Self-consistent 3D equilibrium and transport

Neoclassical transport in the presence of 3D fields modifies the radial electric field by non-ambipolar fluxes, accompanied by toroidal rotation change as predicted by neoclassical toroidal viscosity (NTV) theory [MS-3D-6-9]. The non-ambipolarity also induces the radial currents, implying that 3D equilibrium $j \times B = f$ can be significantly modified, which will then reestablish the non-ambipolar transport in closed loop. This self-consistent process for both equilibrium and transport has been tested in MARS-K code, but a new general perturbed equilibrium code (GPEC) has also been successfully developed to verify and validate the self-consistent calculations as well as apply for 3D optimization with full eigenmodes and response structures. GPEC is upgraded from IPEC, by solving non-Hermitian and inhomogeneous force balance equation rather than Hermitian and homogeneous equation in the ideal case.

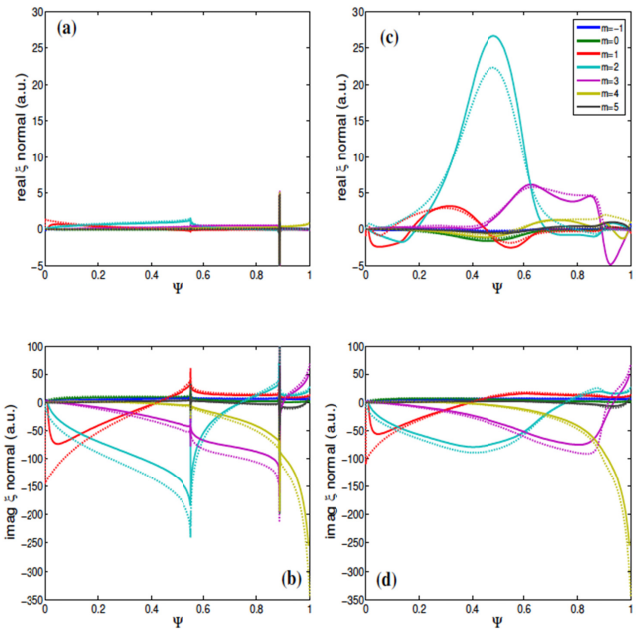

Figure MS-3D-3. *Normal displacements solved by GPEC (solid) and MARS-K (dotted). (a) and (c) are cosine and sine components for ideal case, and (b) and (d) are cosine and sine components for kinetic case including thermal trapped ions.*

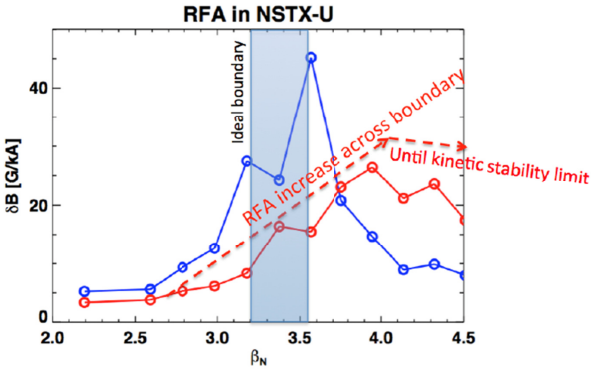

Figure MS-3D-4 *Magnetic field response in a virtual sensor at the plasma boundary, to n=1 field by midplane coils, predicted by IPEC (blue) and GPEC (red) as a function of β.*

Figure MS-3D-3 shows the successful benchmarking of the solutions between GPEC and MARS-K. In particular (c) illustrates an entirely new structure of plasma displacements by self-consistent process, as predicted by both GPEC and MARS-K. Furthermore, GPEC application to NSTX-U configuration predicted the well-known trends of resonant field amplification (RFA) across the ideal no-wall limit, but also a new trend in higher β as shown in Figure M3-

3D-4. Plasma ultimately hits "kinetic no-wall" limit as pressure becomes higher, and the response can be maximized near the kinetic no-wall limit but its amplitude is limited by toroidal torque. More detailed formulations, numerical benchmark and experimental applications of GPEC and upgraded MARS-K have been documented in the final technical report of the Early Career Research Program project entitled "Self-consistent calculations of pedestal modification by 3D fields in tokamaks" and separately submitted to FES [MS-3D-10].

The toroidal torque required to perturb plasma modifies not only the response amplitude, but also produces the phase shift in response. Another interesting technique to understand these two important aspects in the self-consistent plasma response is to investigate their frequency dependency and resulting Nyquist diagram. Figure MS-3D-5 shows the predicted Nyquist diagram by MARS-K, with various model combinations of kinetic and rotational effects. Comparisons of the characteristic shapes and poles with experiments in details will offer the better chance of model validation, as well as physics understanding of multi-mode response characteristics, as will be tested in the coming DIII-D and/or NSTX-U campaign.

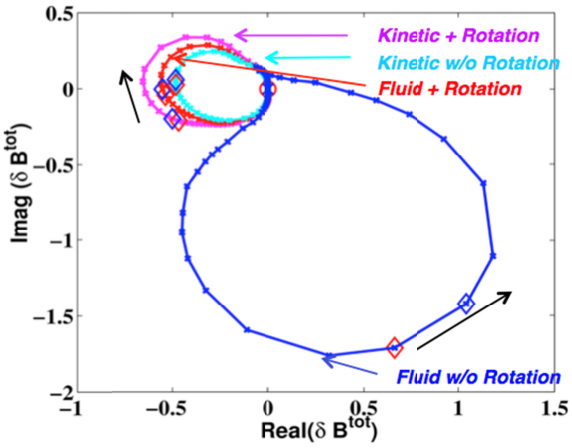

Figure MS-3D-5 *Nyquist diagrams simulated by MARS-K depending on the indicated models, by varying frequency of applied n=1 field by midplane coils in NSTX-U.*

Development of plasma rotation control algorithm utilizing NBI and NTV actuators

In the FY14 NSTX-U Year End Report, the initial success of a unique plasma rotation control algorithm using NTV as an actuator for the first time in closed-loop feedback was reported. In FY15, the algorithm has now been successfully expanded utilizing both NBI and NTV in combination to control plasma rotation [MS-3D-11,12]. In the FY14 results, the action of the NTV torque occured directly in the outer region of the plasma, then relied on momentum diffusion to alter the rotation profile in the core to reach the target rotation profile. More rapid alteration of the plasma rotation frequency, ω_ϕ, in the core and more generalized ω_ϕ profile alteration can be affected by combining NBI and NTV actuators. An example of the combined use of NBI and NTV for plasma rotation control is shown in Figure MS-3D-6. In this case, the desired ω_ϕ profile has greater peaking with higher core ω_ϕ.

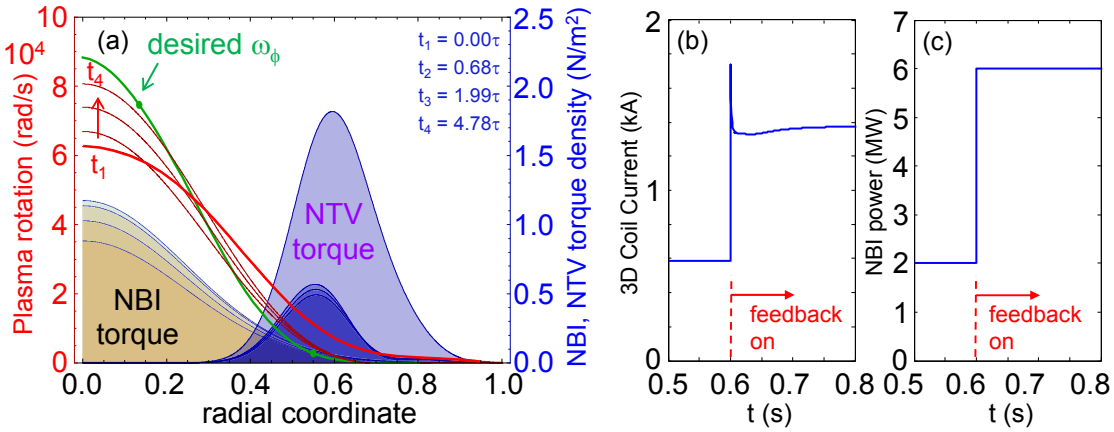

Figure MS-3D-6*: Plasma rotation controller with NBI and NTV as actuators: (a) evolution of NBI and NTV torque profiles, and ω_φ toward the target profile, (b) 3D coil current, and (c) NBI power evolution.*

The addition of the NBI actuator allows the increased core ω_ϕ, but the desired reduction of ω_ϕ in the outer part of the plasma requires greater T_{NTV} not only to drive the rotation lower, but also to create a larger steady-state NTV torque to balance the increased momentum input from the increased NBI power.

The strength of NTV in NSTX has been shown to be strongly dependent on ion temperature, $T_i^{2.5}$ [MS-3D-13] consistent with the expectation of the "1/ν" regime scaling in NTV theory [MS-3D-14]. The NTV model used in the control algorithm results shown in Figure MS-3D-6 does not include this dependence. Inclusion of this improved NTV model under closed-loop feedback control was examined with results summarized in Figure MS-3D-7. The first important result is that the closed-loop feedback algorithm generally controlled the plasma rotation profile moving toward the desired target profile as the ion temperature was rapidly changed in the modeling, first increased, then decreased by about a factor of two. These can be envisioned as fairly extreme, but credible changes in T_i on axis as might occur during L-H transitions, or back-transitions. The lowest value of T_i on axis chosen was done so to simulate plasma conditions significantly below those produced in a standard high performance target plasma on NSTX, therefore well outside of a typical bounded operational range for this parameter. Perhaps more profound is the second key element found in the simulation – the dynamics of the NTV actuator and control response during this T_i variation. The lower right panel of Figure MS-3D-7 shows the time evolution of the on-axis T_i value, which the profile scaled self-similarly along with this variation. Three time points labeled t_1 – t_3 are shown indicating times at different T_i values with sufficient time to allow the plasma rotation profile to reach a steady-state. The rotation profile evolution, including the desired target rotation profile are shown in the upper left frame, and the response of the actuators is shown in the upper right frames. At t_1, the desired plasma rotation is generally reached as NBI torque increases the core rotation and NTV reduces the rotation in the outer part of the plasma. Increasing T_i is not an issue for the controller, which produces nearly the same NTV torque profile by reducing the 3D field coils (here, an n = 3 applied field configuration is assumed). Most interesting is the result at reduced T_i. The NTV torque is significantly weakened and the 3D coil current is increased to compensate. The NTV torque also broadens significantly and the desired rotation profile does not match the desired profile over the majority of the profile. This

result is a product of the actuator limitations. Present studies are investigating the greater control capability provided by the newly available 6 NBI sources in NSTX-U, and the 3D coil upgrade (NCC) planned. More detail on the NCC physics design is given in the next section.

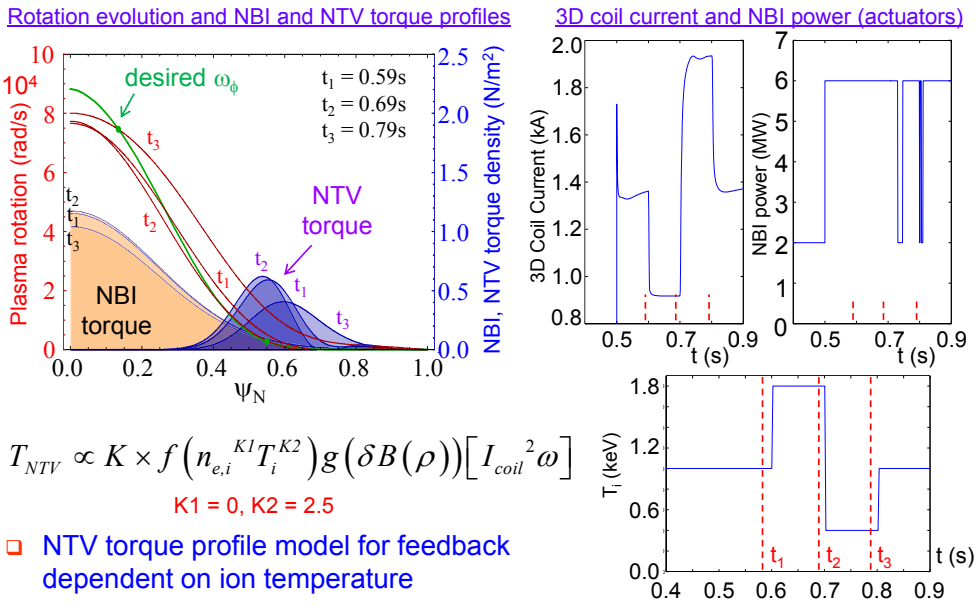

$$T_{NTV} \propto K \times f\left(n_{e,i}{}^{K1} T_i^{K2}\right) g\left(\delta B(\rho)\right)\left[I_{coil}{}^2 \omega\right]$$

***Figure MS-3D-7**: Successful demonstration and ramifications of closed-loop plasma rotation control simulation using an NTV model scaling as $T_i^{2.5}$.*

Design and physics analysis of non-axisymmetric control coil (NCC)

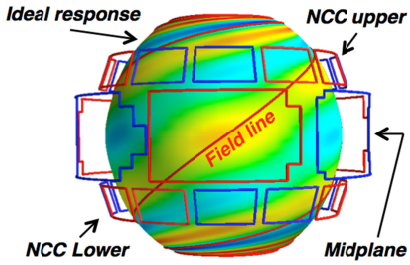

***MS-3D-8:** Full NCC, midplane coils, field lines with a NSTX-U target, and IPEC response field on the boundary. The coils and fields are color-coded (+:red, -:blue).*

Non-axisymmetric control coil (NCC) design and physics analysis have been continued and extended, to most efficiently achieve error field correction, NTV control, ELM modification, and RWM active control in NSTX-U. Previously it was shown that NCC alone can provide much more flexibility and greater figures of merit than the present midplane coils, but furthermore that NCC in NSTX-U can be unique in the world for its geometric coverage and plasma coupling efficiency when the midplane coils are combined and optimized together. This is because midplane coils are close enough to plasma and thus effectively constitute three rows of internal coils when the two off-midplane NCC coils are combined. Figure MS-3D-8 shows that the relative phase of upper NCC, midplane coil, and lower NCC can be arranged to produce n=3 following the helical pitch of the magnetic field lines at the outboard section in NSTX-U, which maximizes the width of stochastic field region when the NCC field is superposed. This coherent perturbation to the field lines without a gap between the coils is possible for n=1-2 even with the partial set of NCC (6 upper and 6 lower) and up to n=3 with the full set. No other device or coils can produce such a high degree of the pitch alignment except the KSTAR internal coils for n=1, and the ITER RMP coils.

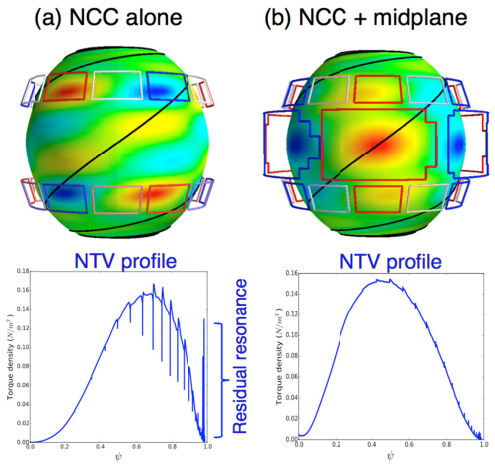

MS-3D-9: *(a) NCC-only optimization and (b) NCC + midplane coil optimization for core NTV with the resonant fields strongly minimized. NTV torque density (N/m^2) profiles are also shown (normalized to 1Nm).*

This ability for the coherent perturbations at the outboard section becomes also very useful in optimizing NTV. Figure MS-3D-9 shows the comparison of the optimized n=3 NTV profile for the core by IPEC-PENT, for NCC alone vs. NCC with midplane coils. The spiky peaks shown in the NTV profile indicate the residual resonant fields, and from them one can see clearly that (b) NCC + midplane provides non-resonant braking with higher purity than (a) when NCC alone is used. This configuration was found first by IPECOPT, which incorporated the advanced optimization tools developed for stellarators [MS-3D-15], but later by utilizing IPEC coupling matrix and minimizing first a few dominant modes. Figure MS-3D-10 shows the optimized n=1-6 NTV profiles, with the indicated ratio of the current amplitude (NCCF:MID) and relative phases. Note that the resonant peaks remain for the optimized n=4 and n=6 in the edge, as midplane coils are not practically capable of n=4 or n=6. One can see that NCC can provide local NTV in different locations if optimized, which will be greatly useful to control rotation and rotational shear in NSTX-U.

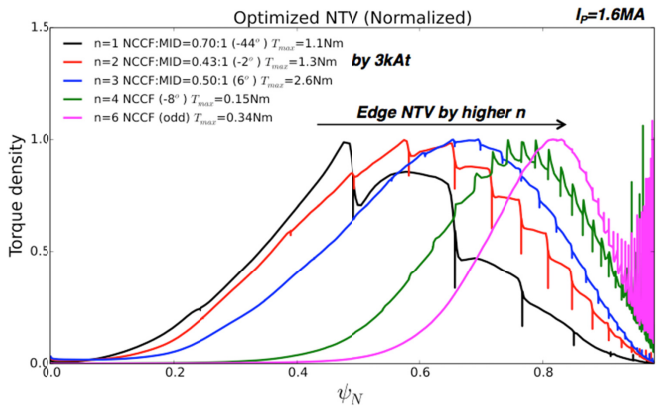

Figure MS-3D-10: *Torque density profiles created by core-optimized NCC and midplane coil combinations for each n in an I_P=1.6MA NSTX-U target. NCCF:MID indicates the ratio of coil currents, and (angle) indicates the relative phase from upper NCC, midplane, to lower NCC.*

NCC is also very useful for RWM active control. The previous VALEN3D analysis showed that RWM control performance increases as NCC coils are added, and operation close to the ideal-wall limit is achievable when the idealized sensors are used. The sensor optimization has been therefore one of important issues, especially since exciting RWM B_P sensors driving neighboring NCC coils yielded relatively poor performance. 3D analysis of extended MHD sensors found new good location near the upper divertor, and VALEN3D with these optimized sensors and gains almost recovered the control performance predicted with the idealized sensors as shown in Figure MS-3D-11.

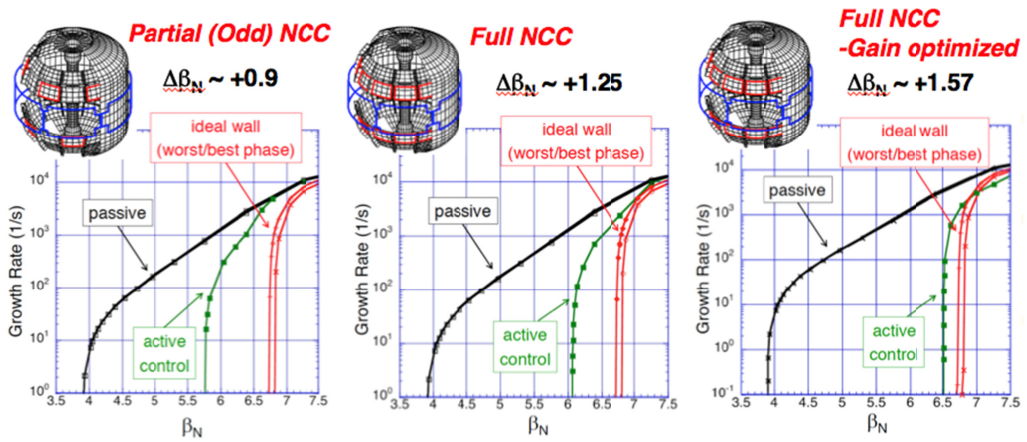

Figure MS-3D-11: *RWM growth rates predicted by VALEN-3D, when partial and full NCC are used as actuator and the optimized sensors near the upper divertor are utilizied. The $\Delta\beta_N$ gains are shown compared to passive stabilization, and one can see RWM active control may provide an opportunity of near ideal-wall operation for NSTX-U if feedback gain is additionally optimized.*

Another continuing effort in NCC physics analysis is to apply the Vacuum Island Overlap Width (VIOW) method [MS-3D-16] to characterize ELM modification capability. TRIP3D calculations showed that the 2x6 partial NCC could produce thick enough VIOW with optimized in a large range of q_{95}. Interestingly, it was shown that one additional array 2x7 can greatly improve VIOW by n=2,4,9 island overlapping. Of course this indicates that there will be a lot more interesting configurations if the full 2x12 set is available and if a sufficient number of power supplies is equipped. These physics analyses are being used for NCC conceptual design and engineering, and in parallel will be continued with advanced 3D codes GPEC, MARS-K, and M3D-C[1].

References

[MS-3D-1] A. Reiman, N. Ferraro, A. Turnbull, J.-K. Park et al., Nucl. Fusion **55**, 063025 (2015)

[MS-3D-2] E.J. Strait, J.-K. Park, E.S. Marmar, "Quantify plasma response to non-axisymmetric (3D) magnetic fields in tokamaks", Final Report for FES 2014 JRT (2014)

[MS-3D-3] J. D. King, E. J. Strait, S. A. Lazerson et al., Phys. Plasmas **22**, 072501 (2015)

[MS-3D-4] Z. Wang, M. Lanctot, Y. Liu, J.-K. Park et al., Phys. Rev. Lett. **114**, 145005 (2015)

[MS-3D-5] Z. Wang, "Drift kinetic effects on 3D plasma response in high-beta tokamak resonant field amplification experiments", TI1.00003, The 56th APS DPP meeting (2014)

[MS-3D-6] K. C. Shaing, Phys. Fluids **26**, 3315 (1983)

[MS-3D-7] K. C. Shaing, Phys. Plasmas **10**, 1443 (2003)

[MS-3D-8] K. C. Shaing, S. A. Sabbagh and M. S. Chu, Nucl. Fusion **50**, 025022 (2010)

[MS-3D-9] J.-K. Park, A. H. Boozer and J. E. Menard, Phys. Rev. Lett. **102**, 065002 (2009)

[MS-3D-10] J.-K. Park and Z. R. Wang, "Self-consistent calculations of pedestal structure modifications by 3D fields in Tokamaks", Final technical report of the Early Career Research Program project 34205 (2015)

[MS-3D-11] S.A. Sabbagh, R.E. Bell, T.E. Evans, et al., IAEA FEC 2014, paper EX/1-4

[MS-3D-12] I. Goumiri, C. Rowley, S.A. Sabbagh, et al. submitted to Nuclear Fusion (2015)

[MS-3D-13] S.A. Sabbagh, J.W. Berkery, R.E. Bell, *et al.*, Nucl. Fusion **50**, 025020 (2010)

[MS-3D-14] K.C. Shaing, Phys. Plasmas **13**, 052505 (2006)
[MS-3D-15] S. Lazerson, J.-K. Park, N. C. Logan and A. H. Boozer, "Numerical optimization of three-dimensional coils for NSTX-U", Plasma Phys. Control. Fusion, In Press (2015).
[MS-3D-16] M. E. Fenstermacher, T. E. Evans et al., Phys. Plasmas **15**, 056122 (2008)

3. Disruption Studies

Massive Gas Injection System

Predicting and controlling disruptions is an important and urgent issue for ITER. Methods to rapidly quench the discharge after an impending disruption is detected are also essential to protect the vessel and internal components of an ST-FNSF. In support of this activity, NSTX-U will employ three Massive Gas Injection (MGI) valves that are very similar to the double flyer plate design being considered for ITER. NSTX-U will be the first device to operate this valve design in plasma discharges. These valves have been tested off-line and deliver the required amount of gas (~ 200 – 400 Torr.L) to support NSTX-U experiments, which will offer new insight to the MGI data base by studying gas assimilation efficiencies for MGI gas injection from different poloidal locations, with emphasis on injection into the private flux region. The valve has also been successfully operated in external magnetic fields of 1 T.

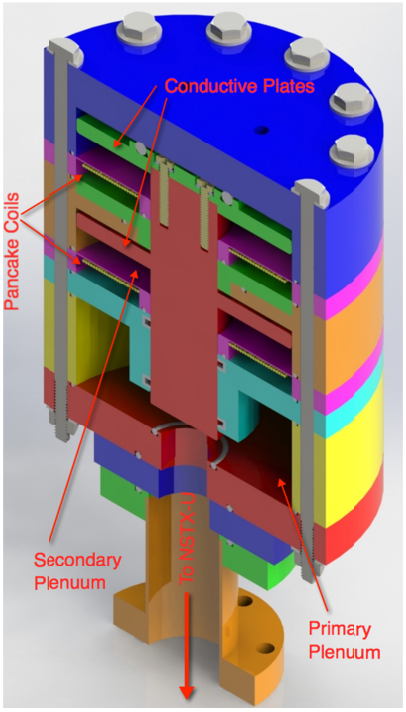

Figure MS-DIS-1: *Internal component drawing of the double solenoid MGI valve for NSTX-U. The valve uses two solenoids, with currents driven in opposite directions so that there is no net J x B force on the valve when it is operated in an external magnetic field.*

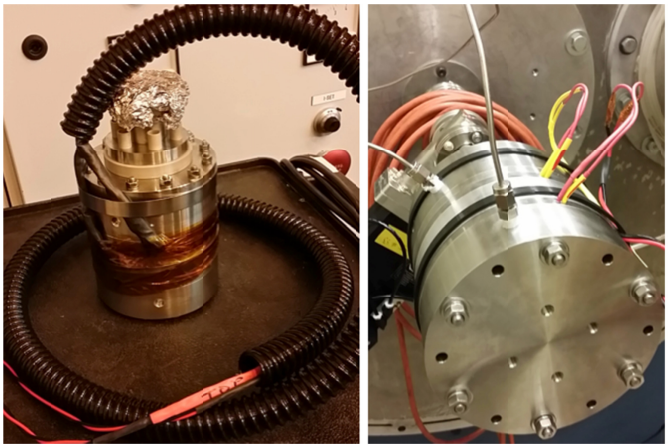

Figure MS-DIS-2: *Photo showing the MGI valve for NSTX-U and the valve undergoing off-line tests on a University of Washington test stand.*

As described in the 2014 Annual report, an external magnetic field can interact with the currents flowing in the coil and the conducting disk to generate forces that act on these components. The most recent improvements to the valve design were motivated by the work of Baylor et al., for the ITER test valve [MS-DIS-1] currents in both coils are driven in opposite directions, which results in the J x B force that generates a torque on the in which a double solenoid configuration was

adopted. The advantage of this configuration is that valve from cancelling. Figure MS-DIS-1 shows the internal components of this valve. A photo of this valve is shown in Figure MS-DIS-2.

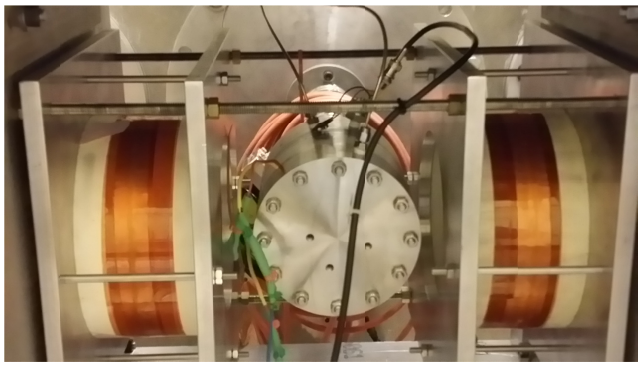

Figure MS-DIS-3: *Setup used for MGI valve testing in an external magnetic field. The valve is located between two solenoid coils.*

Experimental results obtained from the operation of the valve with the single solenoid are described in in the 2014 Annual report and also now published in the Review of Scientific Instruments [MS-DIS-2]. Here we briefly summarize results obtained from the operation of the new valve with the double solenoid.

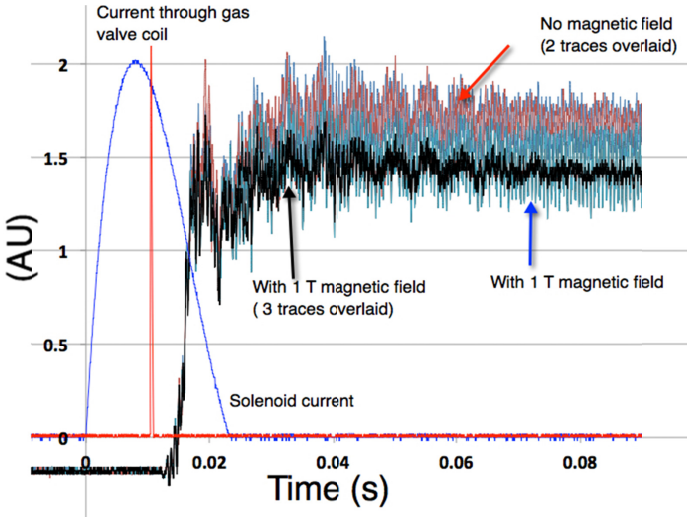

Figure MS-DIS-4: *Experimental traces from the operation of the valve with and without the presence of an external magnetic field. Shown are the current pulse duration through the solenoid and the current pulse through the gas valve pancake coils. The gas valve is discharged 10 ms after the solenoid discharge is initiated. Shown are two gas pressure traces for cases in which there was no external magnetic field. Shown also are four gas pressure traces during the presence of a 1 T external magnetic field in a configuration in which the field is parallel to the pancake solenoid surface. One of the gas pressure traces is noisy.*

The initial important observation was that adding a second solenoid did not substantially increase the size of the capacitor bank power supply or the operating voltage for injecting the same amount of gas (~27 Pa.m^3 nitrogen) with similar gas pressure rise times in the 1.3 m^3 test chamber. The double solenoid valve was also operated with the coils connected in a parallel configuration and series configuration using a 4.57 m (15 feet) long extension cable, such as would be required for a NSTX-U installation. Including the 3 m (10 feet) long wire from each coil, the distance from the coil to the power supply for this case is about 7.62 m (25 feet). In this case for similar amounts of injected gas, the operating voltage was about 700 V for the series configuration and 900 V for the parallel configuration. The current through each coil was 1 kA for the series configuration, and about 1.3 kA for the parallel configuration. The total current through the SCR switch for the parallel configuration was therefore about 2.6 kA. The slightly higher current through each valve for the parallel configuration is offset by a shorter current pulse width, because the system inductance is new reduced.

Figure MS-DIS-3 shows the experimental arrangement that was used to perform these tests. The valve is located between two solenoids that are separated from each other by 21 cm. For an operating voltage of 1.1 kV, the current in the solenoid is 2 kA, which generates 1 T fields in the region where the valve is located.

Figure MS-DIS-4 shows gas pressure traces for operation without an external magnetic field, and for operation with 1 T field. The valve operation is not affected by fields of 0.8 T or less. As the field increases to 1 T, there is a 10% reduction in the amount of injected gas over the long duration. However, from the fast baratron signals it is not clear if there is any change on the short timescale, during the first peak in the gas pressure signal. It is not know at this time if this is related to faster valve closing time at 1 T fields, or if in fact less gas is initially injected. Nevertheless, this small change can be easily compensated by adjusting the valve operating voltage. Initial experiments on NSTX-U will limit the magnetic field at the valve vicinity to the 1 T level.

Electromagnetic Particle Injector System

While the MGI system may be adequate for most disruptions, the warning time for the onset of some disruptions could be much less than the MGI system response time. To address this important issue, a novel system based on the rail-gun concept has been designed, and plans for an off-line experimental test are in progress. The device referred to as an Electromagnetic Particle Injector (EPI) is fully electromagnetic, with no mechanical moving parts, which ensures high

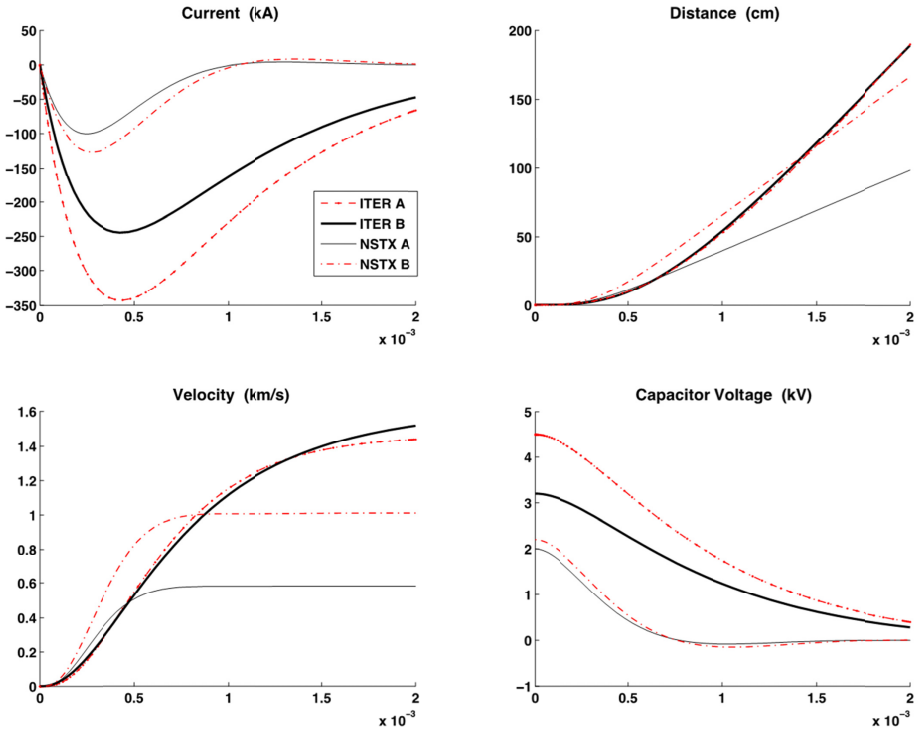

Figure MS-DIS-5: *Shown are traces from simulation results showing injector current, pellet velocity, distance traveled by the projectile, and capacitor bank voltage, all as a function of time.*

reliability after a period of long standby. In addition to responding on the required fast time scale, its performance substantially improves when operated in the presence of high magnetic fields [MS-DIS-3]. The system is also suitable for installation in close proximity to the reactor vessel. The 2014 Annual report describes this concept in some detail.

During 2015 we examined in more detail the effect of the external magnetic field on injector operation. The main results are briefly summarized here in Figure MS-DIS-5. ITER-A case is for a capacitor bank charging voltage of 4.5 kV, and ITER-B is for a capacitor bank voltage of 3.2 kV, but with $B_T = 2$ T, the external magnetic field augmentation. There are a number of important observations that can be made from the simulation results. First, for a projectile mass of 15 g, a 100 mF capacitor bank charged to 4.5 kV can accelerate the capsule to about 1.5 km/s in about 1.5 ms. During this time the projectile travels about 1.2 m, so the injector electrode length is about 1.2 m for this operating scenario. Approximately 1.5 ms after the system is triggered, the capsule traveling at about 1.5 km/s exits the injector. If the system is located 5 m away from the edge of plasma, the projectile should begin to penetrate it in about 7.5 ms after a command is issued to activate this DM system. Because of external magnetic field augmentation, the ITER-B case attains similar parameters, but with a capacitor bank that is about half the size of the ITER-A case. Alternatively, if the original capacitor bank size is retained; a 25 g projectile would achieve similar acceleration parameters. Simulations also show that at a slightly higher operating voltage of 5.5 kV, but without external field augmentation, the projectile can reach velocities of over 2 km/s in 1.5 ms, in an accelerator that is 1.7 m long. Figure MS-DIS-6, shows a conceptual layout of the system in reference to the ITER mid-plane port plug.

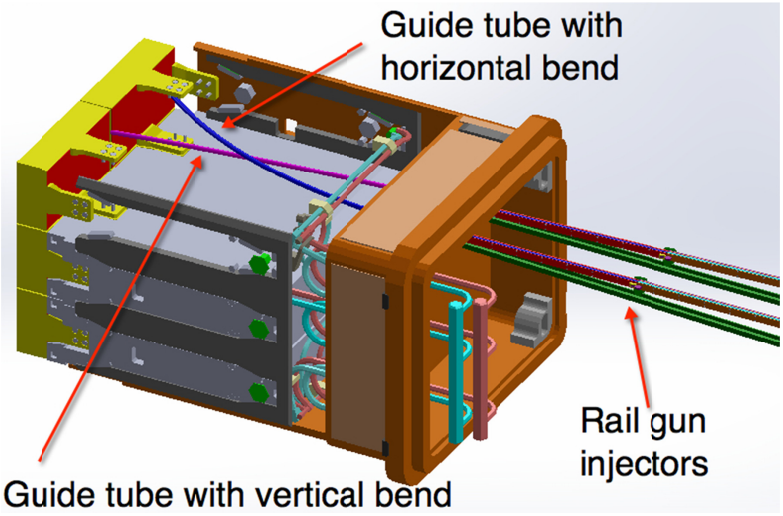

Figure MS-DIS-6*: Hypothetical installation configurations for the injector being located behind a mid-plane port plug. Shown are configurations with the pellet guide tube having a vertical bend for radial injection, and with a horizontal bend for tangential injection to allow an un-fragmented pellet to exit the vessel through a suitable port at the end of the pellet trajectory. The second configuration may not be suitable for ITER, but could be incorporated into the design of future devices.*

Because of the compact nature of the injector and its simple geometry, a test of the concept could be conducted on NSTX-U or on a large tokamak. Parameters for such a device, whose primary objectives are to verify the system response time, attainable velocity parameters and successful dispersion of the capsule payload inside the tokamak plasmas are also shown in Figure MS-DIS-5. Case A is for a low-power test to verify the system response time. A 20 mF capacitor bank charged to 2 kV accelerates a 1.5 g projectile to over 0.5 km/s in about 0.7 ms in an accelerator

that is 30 cm long. As the operating voltage is increased to 2.2 kV and the bank size increased to 30 mF, the velocity increases to about 1 km/s in 1 ms, in an accelerator that is about 60 cm long. NSTX Case A should be adequate for a test on NSTX-U, while Case-B would serve as an intermediate off-line test towards developing a larger-scale injector. The voltage waveform for all these cases shows that for the chosen capacitor bank size, the energy in the capacitor is depleted on the acceleration time scale. The peak acceleration currents for the four cases range from 80 kA for the low-power NSTX-U case to a maximum of about 350 kA for the ITER-A case.

3D Nonlinear modeling of NSTX VDE with M3D-C1

Nonlinear free-boundary 3D tokamak resistive wall instabilities have been calculated using a new resistive wall model [MS-DIS-4] in the two-fluid M3D-C1 [MS-DIS-5] 3D magnetohydrodynamics code. In this model, the resistive wall and surrounding vacuum region are included within the computational domain. This implementation contrasts with the method typically used in fluid codes in which the resistive wall is treated as a boundary condition on the computational domain boundary using the thin-wall approximation. Besides allowing a finite thickness, and possibly a non-axisymmetric wall, this approach has the advantage of maintaining purely local coupling of mesh elements. This new capability has now been used to simulate the fully 3D nonlinear evolution of vertical displacement events (VDEs) in NSTX.

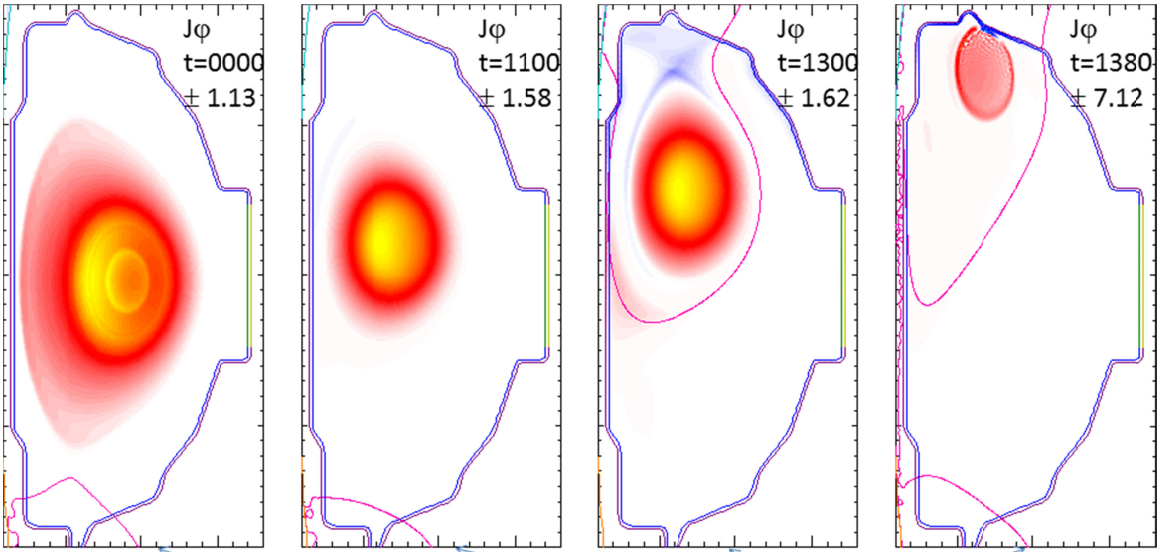

Figure MS-DIS-7: *Toroidal current density at 4 times at a given toroidal location during a NSTX 3D VDE simulation with M3D-C1. Yellow and red are positive, blue is negative.*

The VDE calculations are performed in diverted tokamak geometry, at physically realistic values of dissipation, and with resistive walls of finite thickness. When the vertical control system is switched off, the plasma begins to drift, initially axisymmetrically, with a vertical growth rate proportional to the wall resistivity. After a brief period, as the plasma drifts and deforms, a toroidal mode number n=1 resistive wall mode with dominant poloidal mode number m=2 begins to appear, and it too initially grows with a growth rate proportional to the wall resistivity.

Eventually, as the plasma becomes limited by the first wall, the growth rate of the n=1 mode increases dramatically leading to a rapid thermal and current quench.

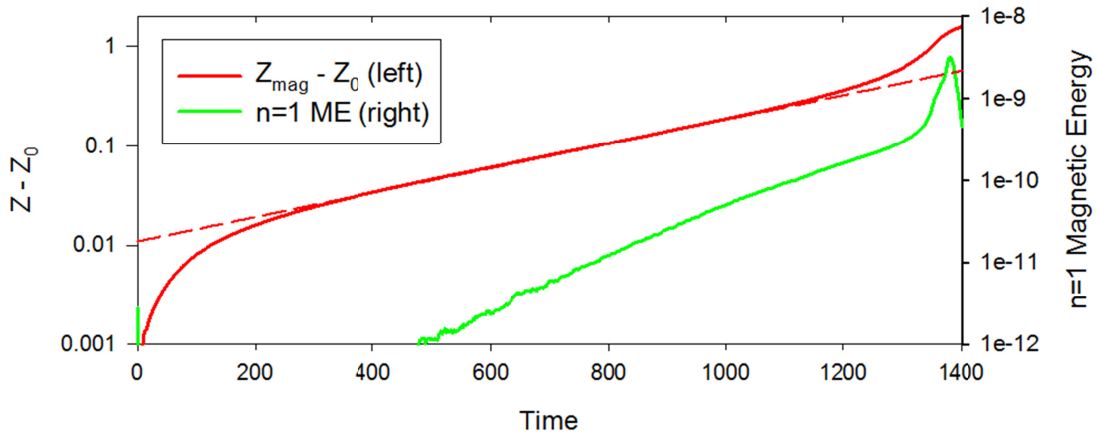

Figure MS-DIS-8: *Magnetic axis position (red) and energy in n=1 mode (green) during NSTX VDE simulation shown in Figure 1. Note sharp increase in slope of n=1 energy after t=1300* τ_A.

Strong (induced) currents are observed to flow in the wall and between the plasma and the wall (halo). New diagnostics are being implemented to facilitate comparisons between these results, previous M3D and TSC simulations, and NSTX magnetics data.

Multi-machine analysis of non-axisymmetric and rotating halo currents

Halo currents measured during tokamak disruptions exhibit non-axisymmetric and rotating features in several machines including Alcator C-Mod [MS-DIS-6], ASDEX Upgrade [MS-DIS-7], and NSTX [MS-DIS-8]. Such non-axisymmetries are of great interest to ITER because they can increase mechanical stresses during a disruption, especially if the rotation resonates with the natural frequencies of the vessel [MS-DIS-9]. In conjunction with the ITPA Working Group on Non-Axisymmetric Halo Currents, a multi-machine analysis of these phenomena has been initiated at PPPL. The ITPA non-axisymmetric halo current database presently includes data from NSTX, DIII-D, AUG, and C-Mod. These data are analyzed within a common numerical framework. Emphasis is placed on the evolution of the $n = 1$ component of the halo current over the course of the disruption, as well as on how the non-axisymmetries and rotation depend on the equilibrium plasma parameters at the start of the disruption.

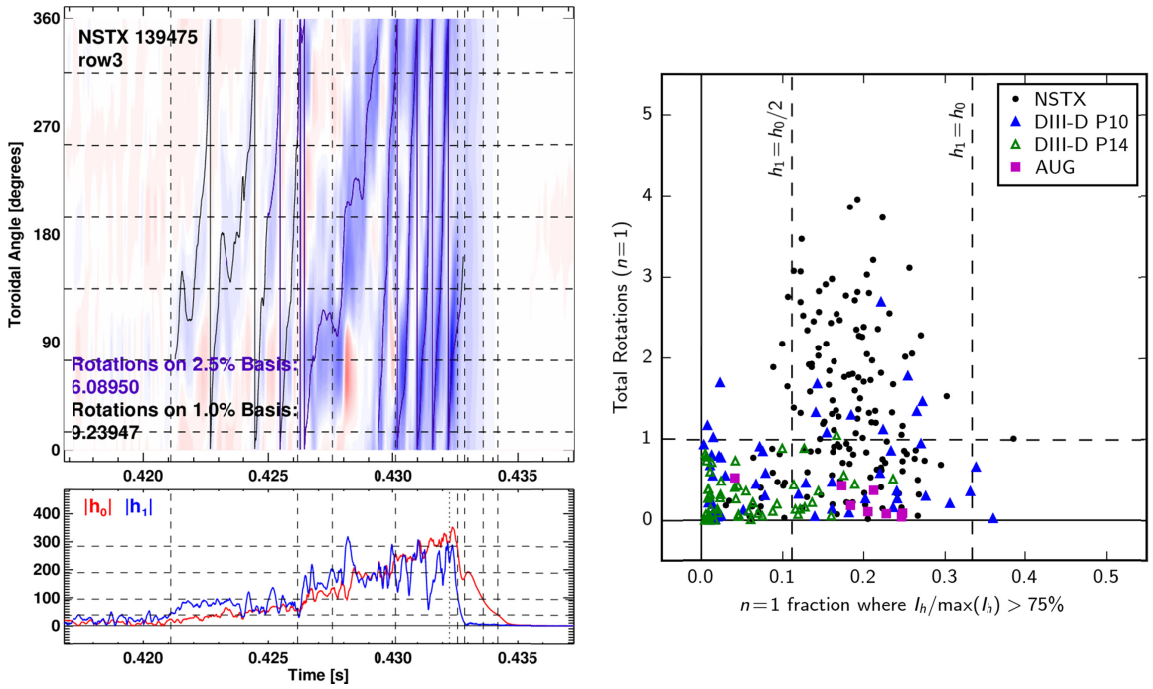

Figure MS-DIS-9*: Non-axisymmetric and rotating halo current analysis. Left: Representative halo current rotation pattern in NSTX [MS-DIS-8]. The n = 0 and n =1 components of the halo (h_0 and h_1) are tracked throughout the disruption. Data from NSTX, DIII-D, AUG, and C-Mod have now been analyzed using these techniques. Right: Rotation vs. non-axisymmetry (here called the "n = 1 fraction") for four sensor arrays in three different devices [MS-DIS-10].*

A progress report on the PPPL-led multi-machine halo current analysis was presented at the Theory and Simulation of Disruptions Workshop held in Princeton, NJ, in July 2015 [MS-DIS-10]. Sample results from the progress report are shown in Figure MS-DIS-9. On the left is a sample analysis of non-axisymmetric and rotating halo currents during a representative NSTX disruption. The non-axisymmetry of the halo current pulse is assessed by fitting the toroidal profile of the halo current to an $n = 0/1$ function of the form $I_h = h_0 + h_1 \sin(\phi - h_2)$. The rotation of the halo current is tracked by integrating the time evolution of h_2, which is the phase of the $n = 1$ halo current lobe. This analytical framework has been applied halo current pulses from NSTX, DIII-D, AUG, and C-Mod. The aggregate results from three of the machines are shown on the right of Figure MS-DIS-9. This preliminary scatterplot reveals several trends such as NSTX having the highest rotation and DIII-D having the highest axisymmetry (although different halo current sensor arrays, P10 and P14, give differing measurements of the non-axisymmetry and rotation in DIII-D). Moving forward, additional AUG data and C-Mod data will be added to this scatterplot, and the various trends will be formally identified and analyzed in order to explore the underlying physics that drives halo current non-axisymmetry and rotation in tokamaks.

References

[MS-DIS-1] L.R. Baylor, C.C. Barboer, J.R. Carmichael, et al., "*Disruption mitigation system developments and design for ITER*," accepted for publication in Fusion Science and Technology (2015)

[MS-DIS-2] R. Raman, T.R. Jarboe, B.A. Nelson, et al., Rev. of Sci. Instruments **85**, 11E801 (2014)

[MS-DIS-3] R. Raman, T.R. Jarboe, J.E. Menard, et al., "*Fast time response electromagnetic disruption mitigation concept*", accepted for publication in Fusion Science and Technology (2015)

[MS-DIS-4] N.M. Ferraro, S.C. Jardin, L.L. Lao, M. Shephard, and F. Zhang, "*Multi-Region Approach to Free-Boundary 3D Tokamak Equilibria and Resistive Wall Instabilities*", submitted to J. Comp. Phys. (2015)

[MS-DIS-5] S. C. Jardin et al., Computational Science and Discovery **5** 014002 (2012)

[MS-DIS-6] R. S. Granetz, I. H. Hutchinson, J. Sorci, J. H. Irby, B. LaBombard, et al., Nucl. Fusion **36**, 545 (1996)

[MS-DIS-7] G. Pautasso, L. Giannone, O. Gruber, A. Herrmann, M. Maraschek, et al., Nucl. Fusion **51**, 043010 (2011)

[MS-DIS-8] S.P. Gerhardt, Nucl. Fusion **53**, 023005 (2013)

[MS-DIS-9] T.C. Hender, J.C. Wesley, J. Bialek, A. Bondeson, A.H. Boozer, et al., Nucl. Fusion **47**, S128 (2007)

[MS-DIS-10] C.E. Myers, S.P. Gerhardt, N. Eidietis, G. Pautasso, R.S. Granetz, et al., "*Multi-machine analysis of non-axisymmetric and rotating halo currents*," Theory and Simulation of Disruptions Workshop, Princeton, NJ, July 13–15, 2015.

B. Transport and Turbulence TSG Research Highlights

NSTX-U transport and turbulence studies in FY2015, in the preparation of upcoming NSTX-U operations, have focused on analyzing existing NSTX data, performing experiment-theory comparisons, and collaborating with other tokamaks on NSTX-U relevant physics topics.

1. Thermal Transport

Understanding the source of anomalous electron thermal transport in NSTX/NSTX-U is one of the highest priority transport and turbulence research topics. A number of results have been obtained in the last year to advance our understanding in this area. It should be noted that the unique features of ST operation, in particular strong toroidal rotation, large $\rho_* = \rho_i/a$, high beta, and strong toroidicity and shaping, result in plasma regimes distinct from that of conventional aspect ratio tokamaks.

Dissipative trapped electron mode turbulence (DTEM)

To investigate the importance of finite-ρ_* effects, nonlinear global electrostatic gyrokinetic simulations using the GTS code [TT-1] have recently focused on a NBI-heated NSTX H-mode discharge [TT-2] where there are strong electron gradients. In particular, both the density gradient and toroidal rotation shear (and corresponding E×B shear) are very large in the core region. Previous nonlinear local ETG simulations for this discharge were unable to account for the experimental transport fluxes in this region [TT-3]. On the other hand, the global GTS simulations predict that the strong density gradient drives the dissipative trapped electron mode (DTEM) unstable [TT-4, TT-5]. The DTEM is distinguishable from the collisionless TEM (CTEM) through differences in the linear mode structure and the unique response to collisions. When electron collisions are set to be zero the predicted instability is CTEM (Figure TT-1), and the most unstable mode occurs for $k_\theta\rho_s \sim 0.5$. With electron collisions, the resulting unstable DTEM modes exhibit much larger structures with growth rates that peak at $k_\theta\rho_s \sim 0.1$. Perhaps the most remarkable feature discovered is that the E×B shear stabilization effect on the DTEM is surprisingly weak. In contrast, the E×B shear can reduce the CTEM growth rate by a factor of ten. The robustness of DTEM may allow it to be a major turbulence source in STs.

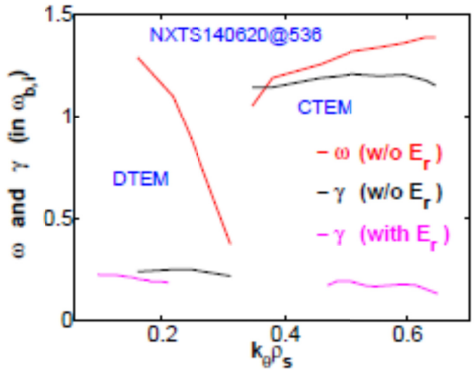

Figure TT-1: *Linear growth rate γ and real frequency ω (normalized by ion bounce frequency $\omega_{b,i}$) vs poloidal wavenumber k_θ for CTEM ($v_e = 0$) and DTEM ($v_e = 1$).*

Saturated DTEM turbulence from nonlinear simulations show large scale, quasi-coherent eddy structure as seen in a potential contour plot (Figure TT-2, left), with a narrow spectrum consisting of a few dominant modes at a low-n range corresponding to $k_\theta\rho_s \sim 0.02-0.08$ (Figure TT-2, right). This characteristic is in contrast to the broad-band fluctuations in typical ITG and CTEM turbulence, and can be utilized for DTEM's identification in experiments.

The quasi-coherent DTEM fluctuations are found to drive significant plasma transport in multiple channels. As shown in Figure TT-3 (left), DTEM-generated ion energy flux is quite close to the experimental value, and DTEM-induced particle and momentum transport (Figure TT-3, middle) are also at experimental level in the central core region where DTEM is unstable. However, the density gradient driven DTEM in this case appears not to produce enough transport to account for highly anomalous electron energy flux in experiments. It should be noted that DTEM can also drive significant electron thermal transport for other discharges with stronger electron temperature gradients.

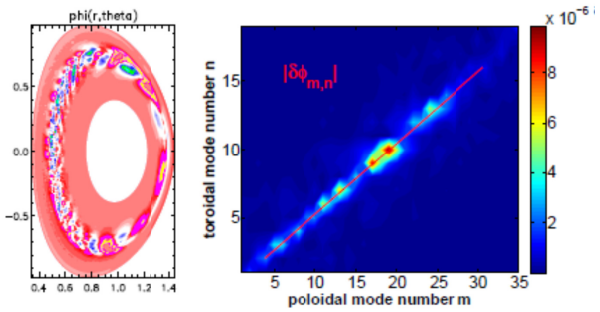

Figure TT-2: *(left) A snapshot of fluctuation potential and (right) m,n spectrum from a nonlinear DTEM simulation for an NSTX H-mode.*

Another very unique feature of DTEM is that the predicted transport increases with increasing collision frequency. As shown in Figure TT-3 (right), increasing electron collision frequency causes a turbulence transition from CTEM (at unrealistically low collision frequency) to DTEM (relevant to NSTX/NSTX-U). These DTEM simulations were based on a discharge that has a larger density gradient than in those used for energy confinement scaling studies. The DTEM is unstable over a wide range of density gradients, and it does provide an additional theoretical microturbulence mechanism (in addition to microtearing modes [TT-6]) that could be at least partially responsible for the observed energy confinement scaling in NSTX, $\tau_E \sim 1/\nu_*$ [TT-7].

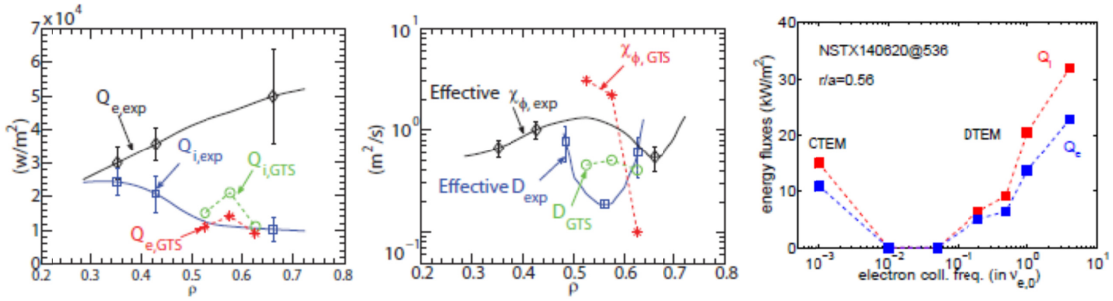

Figure TT-3: *Simulated DTEM driven (left) energy fluxes and (middle) particle and effective momentum diffusivities, in comparison with experimental values inferred from TRANSP analysis. (right) Simulated TEM-driven energy fluxes as a function of electron collision frequency.*

Thermal transport due to Alfven eigenmodes

Recent ORBIT modeling of compressional and global Alfven eigenmodes (CAE, GAE) effects on electron orbits shows that in addition to the inferred diffusion caused by orbit stochastization [TT-8], the modes also cause a net radial convection. The ratio of convection velocity to diffusion coefficient is ~ 10 – 25 m^{-1} for the conditions modeled. This implies convective transport will dominate diffusive transport for $L_{Te} >$ ~ 4 - 10 cm, typical of core plasmas where anomalously large χ_e have been inferred (assuming classical beam behavior). The ratio of convection velocity to diffusion coefficient seems to be roughly constant as the GAE & CAE mode amplitudes are rescaled, even when the diffusion coefficient changes several orders of magnitude (from

negligible to ~ 100 m^2/s), so the amplitude threshold for significant transport may be lower than what was previously found. For the conditions modeled, the trapped electrons were largely responsible for the transport, possibly because the bounce frequencies were comparable to the mode frequencies.

The modeling was performed using a 1 keV isotropic electron population deposited at $\psi_{norm}^{1/2} = 0.15$ in shot 141398, t = 580 ms, using measured mode frequencies and toroidal mode numbers and approximate amplitudes, and estimated poloidal mode numbers from that shot and time. Simulations for the same conditions showed that using only two modes can cause significant transport if the amplitudes are scaled large enough to have the same total amplitude as the experimental spectrum (i.e. rms radial displacement for the pair is ~ 3 mm). Figure TT-4 shows the population averaged radial displacement vs. time for two GAEs with (*f,n,m*) = (563 kHz,-6,2) & (567 kHz,-8,1) and rms E×B radial displacements of ~ 2.5 mm & 1 mm. The amount of transport very much depends on how close the modes are in frequency, as the convection velocity (and diffusion coefficient) vary roughly inversely with the frequency difference between the modes. Simulations with a single mode produced no significant transport, as expected since single modes cannot cause orbit stochastization.

In simulations using the full set of experimental modes, but at zero frequency, neither the diffusion nor the convection was eliminated. Rather, they were reduced by a factor of ~ 5. In the zero frequency limit, the transport is essentially ripple transport, which indicates that ripple transport can cause net convection of an isotropic thermal electron population.

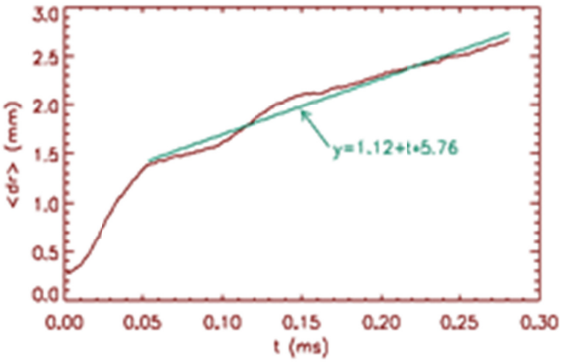

Figure TT-4: *Population averaged radial displacement in the presence of two GAEs with with (f,n,m) = (563 kHz,-6,2) & (567 kHz,-8,1) and rms E×B radial displacements of ~ 2.5 mm & 1 mm. Straight line is a linear fit.*

A potentially significant implication of the convection observed in the simulations is that CAEs and GAEs may play a role in establishing the radial electric field. Repeating the simulation using the full experimental spectrum of modes, but using a 1 keV isotropic population of deuterons at $\psi_{norm}^{1/2} = 0.15$, showed that convection was reduced by a factor of ~ 20, while the ratio of convection to diffusion decreased to ~ 5. An important piece of future work is to investigate how CAE/GAE induced electron transport changes in the presence of an equilibrium radial electric field.

Suppression of ETG turbulence at high density gradient

Following previous observations [TT-2, TT-3] researchers from Alcator C-Mod (MIT), in collaboration with NSTX-U researchers, have recently investigated further the role of linear vs. nonlinear stabilization of ETG turbulence due to large density gradients. Figures TT-5(a) & (b)

show the spectrogram and total integrated scattered power from one channel of the high-k collective microwave scattering diagnostic [TT-9]. Early in the discharge (t<0.3 s), little fluctuation power is measured, consistent with the local normalized electron temperature gradient ($R/L_{Te}=-R/T_e \cdot \nabla T_e$) having not surpassed the linear threshold for ETG instability (as given by [TT-10] and verified for this case using GS2, Figure TT-5d). However, for t > 0.32 s, density fluctuations grow as R/L_{Te} exceeds the ETG threshold (Figure TT-5c). While the temperature gradient remains above the linear ETG threshold throughout the discharge, the measured fluctuation power drops dramatically after t > 0.42s, suggesting there is an additional effect (beyond linear threshold effects) that influences the measured high-k turbulence. An increase in local density gradient (R/L_n, Figure TT-5d) throughout the later part of the discharge suggests it may influence the fluctuation amplitudes.

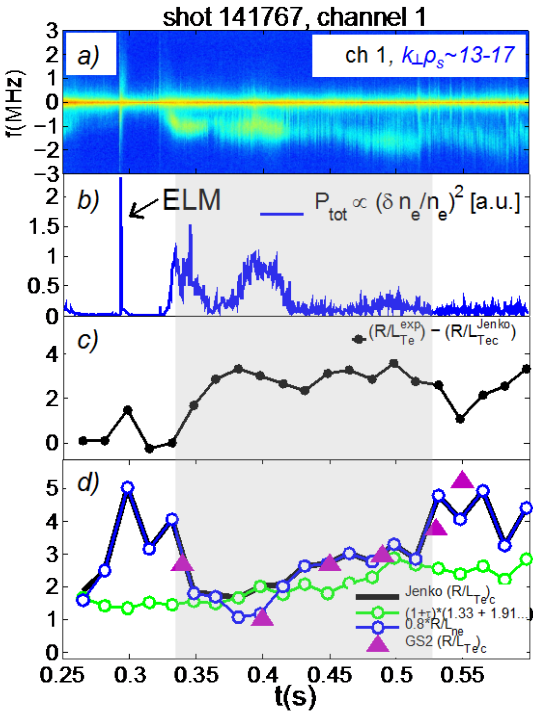

Figure TT-5: *(a) Fluctuation spectrogram from channel 1 of high-k scattering diagnostic. (b) Total scattered power from channel 1. (c) Difference in normalized electron temperature gradient between experimental measurement and ETG linear threshold gradient (R/L_{Te}-$R/L_{Te,crit}$). (d) Components of ETG threshold gradient due to MHD equilibrium (green circles) and density gradient (blue circles), from Ref [TT-10]. ETG threshold calculated by GS2 shown by triangles.*

As shown in Figure TT-6a, the high density gradient (at t = 565 ms) appears to shift the measured spectra to higher $k_\perp$, resulting in a reduction of amplitude at lower $k_\perp$. While there is uncertainty in this observation due to possible refraction effects of the density gradient on the microwave scattering probe beam, the trend is qualitatively reproduced both in the calculated linear growth rate spectra (Figure TT-6b) and the nonlinear electron heat flux spectrum (Figure TT-6c). In particular, dedicated scans show that increasing the density gradient shifts the most unstable linear ETG modes and the nonlinear turbulent spectra to higher-k_θ (and therefore $k_\perp$), similar to previous simulation results [TT-3,TT-11]. This qualitative connection supports the experimental observation of nonlinear density gradient stabilization of high-k turbulence. Future work will strive to clarify the measurement uncertainty due to refraction effects, and to establish a more direct comparison of simulation and measurement through the development and use of a synthetic diagnostic.

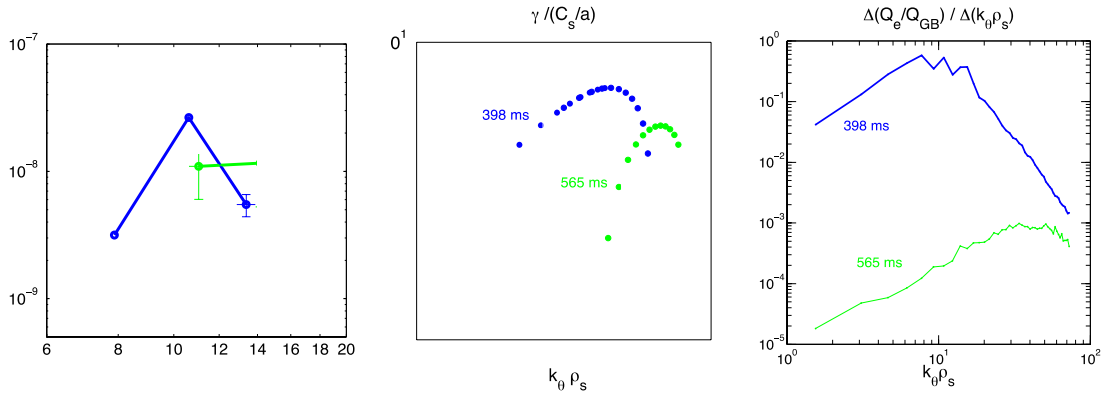

Figure TT-6: *(a) Experimental amplitude of electron density fluctuations from the high-k scattering diagnostic, (b) linear growth rates predicted by GS2 linear simulations, and (c) fractional electron heat flux spectrum predicted by GYRO electron scale nonlinear simulations for low R/L_n (blue) and high R/L_n (green).*

Non-local transport

Highly non-linear electron thermal transport was observed in a set of RF-heated L-mode plasmas [TT-12]. It was observed that electron-scale turbulence spectral power, as measured by the high-k scattering system at r/a~0.6, was reduced significantly following the cessation of RF heating. Linear stability analysis has shown that both ion- and electron-scale microinstabilities are unstable in the high-k measurement region, and that, linearly, the profiles are well above marginal stability. Three explanations are possible for this non-linear response. The first one is high profile stiffness, so that even nearly-negligible changes in driving gradients can lead to large changes in turbulence and transport. The second one is profile variation since the equilibrium profile changes outside of the high-k measurement region may affect turbulence and thus electron thermal transport in the high-k measurement region, e.g. from turbulence spreading [TT-13]. The third one is flux-driven transport, which would inherently be a non-local phenomenon. A decrease in local heat flux, due to changes in some other region of the plasma, leads to a decrease in the turbulence responsible for the transport [TT-14].

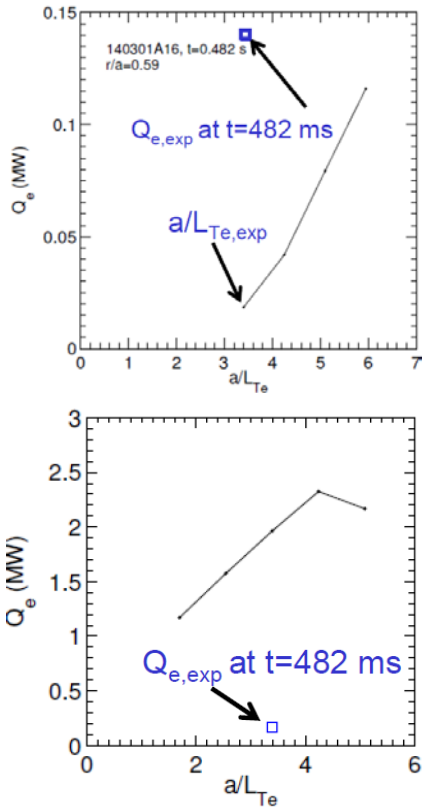

Figure TT-7: *Upper panel: total electron heat flux predicted by the electron-scale simulations as a function of a/L_{Te}; lower panel: total electron heat flux predicted by the ion-scale simulations as a function of a/L_{Te}.*

Nonlinear local gyrokinetic simulations using GYRO code [TT-15] have been carried out to address possible profile stiffness for both electron-scale and ion-scale. These nonlinear simulations include electromagnetic effects, electron and ion collisions and carbon impurity. The upper panel of Figure TT-7 shows the total electron heat flux predicted by the electron-scale

simulations as a function of a/L_{Te} together with experimental-evaluated electron heat flux from TRANSP. It shows that a 75% increase in a/L_{Te} is needed for ETG turbulence to explain observed electron heat flux at t=482 ms (after the RF cessation) and at least a 20 % change in a/L_{Te} is needed to double Q_e, e.g. from 0.02 MW to 0.04 MW (still well below the experimental Q_e). It can be seen that neither the magnitude nor the stiffness of electron thermal transport driven by ETG turbulence is able to explain experimental observation, which is consistent with our expectations from linear stability analysis. On the other hand, ion-scale nonlinear simulations produce larger electron thermal transport as shown in the lower panel of Figure TT-7, much larger than what is needed to explain experimental electron heat flux. The lower panel of Figure TT-7 shows that a 25% increase in a/L_{Te} only leads to an 18% increase in Q_e and thus the stiffness in electron thermal transport cannot explain observed reduction in transport and turbulence, which is also expected from linear analysis showing that ion-scale modes are far from marginal stability.

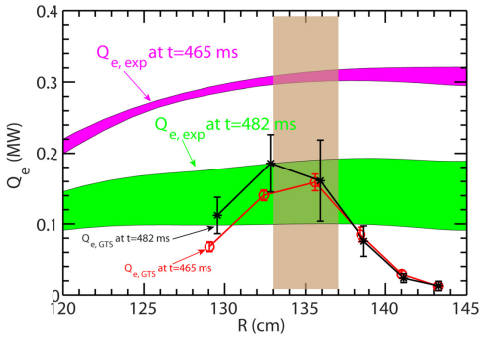

Figure. TT-8 *Red circles: electron energy flux, $Q_{e,GTS}$, at t=465 ms (before the RF cessation) as a function of major radius from nonlinear GTS simulation (averaged over a quasi-steady saturation period); black asterisks: $Q_{e,GTS}$ at t=482 ms (after the RF cessation) from nonlinear GTS simulation (averaged over a quasi-steady saturation period); magenta band: experimental $Q_{e,exp}$, radial profile at t=465 ms from experiment power balance analysis; green band: $Q_{e,exp}$ radial profile at t=482 ms from experiment power balance analysis. Note that the vertical widths of the magenta and green bands denote the experimental uncertainties. The errorbars of Q_e from nonlinear GTS simulations are the standard deviation of Q_e in the quasi-steady saturation periods of the simulations. The width of dashed rectangular denotes the high-k measurement region, i.e. from R=133 to 137 cm.*

Ion-scale global nonlinear gyrokinetic simulations are carried out with the GTS code for t=465 ms (before the RF cessation) and for t=482 (after the RF cessation) with experimental equilibrium profiles to assess effects from profile variation on electron thermal transport in the high-k measurement region. These global simulations cover a radial domain from Ψ_N=0.25 to 0.8 (R ~ 120 cm to 147 cm), where Ψ_N is the square root of the normalized toroidal flux. The size of grids on poloidal planes is about local ρ_i, and 80 particles per cell·species are used. The experimental equilibrium E×B shear is turned-on from the beginning of the simulations. Figure TT-8 compares electron energy flux, $Q_{e,GTS}$, radial profiles at t=465 and 482 ms from GTS simulations with experimental electron heat flux, $Q_{e,exp}$ at the same two time points. It can be clearly seen that while $Q_{e,GTS}$ is essentially the same for both t=465 ms (before the RF cessation) and for t=482 ms (after the RF cessation) at R≳136 cm, $Q_{e,GTS}$ at R≲134 cm is larger at t=482 ms (after the RF cessation) than at t=465 ms (before the RF cessation). We emphasize that the observed change in $Q_{e,GTS}$ before and after the RF cessation opposite to the change in electron heat flux, $Q_{e,exp}$, before (t=465 ms) and after (t=482 ms) the RF cessation from power balance analysis as shown in Figure TT-8, i.e. $Q_{e,exp}$ at t=465 ms (before the RF cessation) is about a factor of 2 higher than $Q_{e,exp}$ t=482 ms (after the RF cessation). On the other hand, the GTS simulation result is consistent with our expectation from local linear stability analysis described above. Thus we conclude that global effects from profile variation, e.g. turbulence spreading, are not likely able to explain the observed reduction in electron thermal transport after the RF cessation and also the reduction in

electron-scale turbulence if we consider the possible nonlinear interaction between ion-scale and electrons-scale turbulence as suggested in [TT-16,TT-17]. We also note that $Q_{e,GTS}$ at t=465 and 482 ms are both in good agreement with $Q_{e,exp}$ at t=482 ms (after the RF cessation) but not with $Q_{e,exp}$ at t=482 ms (before the RF cessation). This shows that even global nonlinear gyrokinetic simulations taken into account not only the temporal variation but also the spatial variation of the equilibrium profiles before and after the RF cessation cannot explain the observed drop in electron thermal transport and turbulence. We conclude that neither local or global gradient-driven simulations seem are able to explain the experimental observations.

2. Momentum Transport

Previous perturbation experiments in NSTX H-modes indicated the existence of a significant inward momentum pinch [TT-18,TT-19], which is roughly consistent with the theoretical Coriolis pinch mechanism for electrostatic ITG turbulence. However, linear gyrokinetic simulations for those discharges predict that electromagnetic microtearing or kinetic ballooning modes (KBMs) dominate in these high-beta H-mode plasmas, with a corresponding small outward pinch (RV_φ/χ_φ) which is insensitive to parameter variations [TT-20]. A number of additional effects have been investigated in 2015 to clarify this apparent discrepancy.

In collaboration with MAST researchers, similar perturbative momentum transport experiments were run in MAST L-modes (during their last run campaign in 2013) to avoid the complications from theoretical electromagnetic effects in high beta H-mode plasmas. Initial analysis of this data has just recently commenced, assuming that the momentum flux (Π) is composed of only diffusive (χ_φ) and convective (V_φ) contributions, $\Pi \sim -\chi_\varphi\Omega + V_\varphi\Omega$ (where Ω is the angular rotation rate). The results shown in Figure TT-9 indicate the existence of a momentum pinch, with a pinch parameter $RV_\varphi/\chi_\varphi \approx$ (-2) – (-12) that is comparable the values inferred in the NSTX H-modes. Gyrokinetic predictions are proceeding to determine whether the predicted Coriolis pinch is consistent with the experimental interpretation. This work also provides the basis for NSTX-U L-mode experiments that will be performed in FY2016.

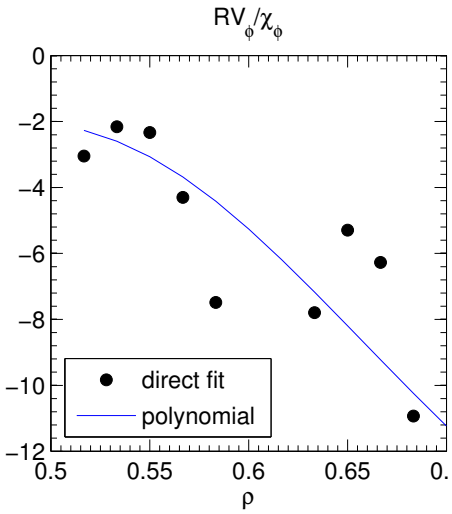

Figure TT-9: *Inferred pinch parameter (RV_φ/χ_φ) from perturbative momentum experiments in MAST L-mode plasma, using two different analysis methods.*

In addition to the Coriolis pinch, there are a number of other effects that could be important in the interpretation of momentum transport [TT-21]. More generally, the momentum flux can be decomposed into additional contributions, including those due to a residual stress (Π_{RS}), such as those resulting from profile shearing effects at finite-ρ_*, and centrifugal effects that can become important as the Mach number approaches unity:

$$\Pi \sim \chi_\varphi \left[u' + \left(R V_\varphi / \chi_\varphi \right) u + C_{cf} \nabla \left(u^2 / 2 \right) \right] + \Pi_{RS}$$

The residual stress effects can occur independent of rotation ($u=R\Omega/c_s$) or rotation gradient ($u'=-R^2\nabla\Omega/c_s$). Indeed, nonlinear global simulations for an NSTX L-mode plasma indicated that there can be a non-negligible residual stress contribution when both rotation and rotation gradient are set to zero ($u=u'=0$) [TT-22]. The influence of centrifugal effects depends on the gradient of the rotation energy, $\nabla(u^2/2)$. This complicates the experimental interpretation as this is equivalent to the product of rotation and rotation gradient, $u \cdot u'$, and the resulting decomposition of momentum flux is no longer simply linear in u or u′. Linear gyrokinetic simulations using the GKW code (collaboration with U-Bayreuth) were run with many combinations of u and u′ to infer C_{cf} specifically for NSTX H-mode plasmas [TT-23]. In those case, the resulting centrifugal coefficient $C_{cf} \sim (-0.5)$ was found to be stronger than the predicted pinch coefficient $RV_\varphi/\chi_\varphi \sim (-0.1) - (-0.2)$, suggesting it may play a non-negligible role in the momentum transport. Future work will further investigate this prediction of centrifugal effects on momentum transport and its parametric dependencies.

Finally, recent work (in collaboration with an Indiana University summer undergraduate student, as part of the DOE SULI 2015 program) has focused on revisiting the interpretation of the momentum transport experiments. This work has focused on implementing a more sophisticated analysis method, which relies upon integrating the momentum transport equation for assumed $[\chi_\varphi, V_\varphi]_{fit}$ profiles, and then using this function within a nonlinear least-squares fitting algorithm to determine the best fit transport parameters. This method was established and was tested comprehensively by generating synthetic data over a broad range of assumed $[\chi_\varphi, V_\varphi]_{synthetic}$. This forward-modeling approach will be used in FY16 to further test the experimental interpretation of momentum transport, specifically to determine if centrifugal and/or residual stress contributions can be inferred from the experimental data.

3. Particle and Impurity Transport

Impurity transport with triggered ELMs

The consistency between experimental impurity transport levels and neoclassical estimates was studied in NSTX discharges with triggered ELMs in otherwise naturally ELM-free H-mode discharges. In NSTX H-mode discharges, ion thermal transport was typically close to the neoclassical levels. Intrinsic carbon transport was found to be consistent with neoclassical estimates in ELMy discharges with boronized PFCs. Changes in main ion profiles due to the application of lithium led to changes in carbon neoclassical convection (NCLASS, NEO). However, a deviation of carbon transport from neoclassical estimates was observed at the top of the pedestal, where a predicted inward pinch was not observed experimentally [TT-24]. The application of 3D-field triggered ELMs (up to 60 Hz) [TT-25] to naturally ELM-free lithium-conditioned discharges led to changes in n_e, n_C, T_i, v_ϕ for normalized volumetric radii $R_{VOL} \geq 0.5$. In particular, n_C was reduced by up to 50% while the T_i and v_ϕ normalized gradients increased by up to a factor of 3 at $R_{VOL} \sim 0.6$. The changes in T_i and main ion density profiles due to triggered

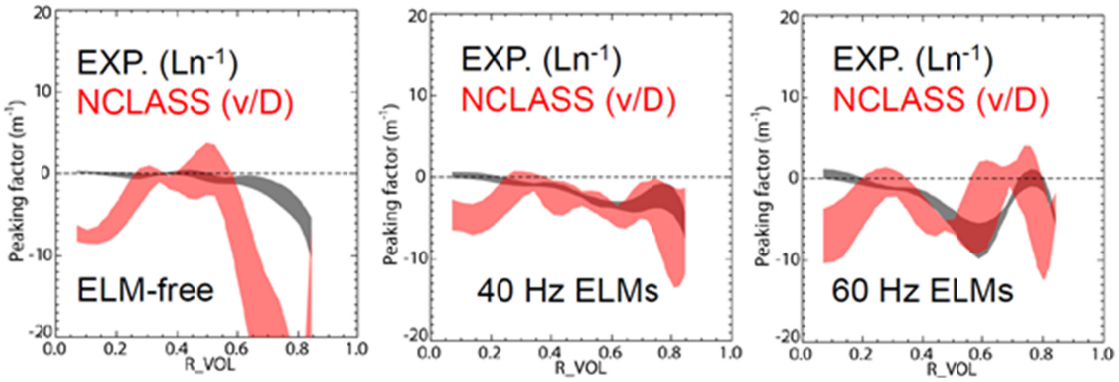

Figure TT-10: *Experimental peaking factors (black) and neoclassical predictions for the v/D ratio for lithium conditioned discharges: ELM-free (left) and with triggered ELMs at 40 and 60 Hz (right).*

ELMs led to changes in the estimates of carbon neoclassical transport coefficients comparable and opposite to those observed with the transition from ELMy boronized discharges to ELM-free lithium-conditioned discharges. Concomitantly, better agreement between the neoclassical transport predictions and experimental impurity density profile shapes was observed in lithium-conditioned discharges with triggered ELMs in a similar way to the naturally ELMy discharges. In Figure TT-10, experimental peaking factors (Ln_C^{-1}) in black and neoclassical predictions for the v/D ratio based on NCLASS calculations are shown for lithium-conditioned discharges: ELM-free (left) and with 40 Hz and 60 Hz triggered ELMs (right).

Centrifugal effects on impurity transport

As mentioned above and noted previously [TT-24], there appears to be a discrepancy in the measured carbon peaking and neoclassical prediction in the region of ρ~0.7 for ELM-free H-modes. Linear gyrokinetic simulations were run to investigate the possible influence of micro-instabilities on the carbon profile. The gyrokinetic simulations again show the presence of electromagnetic microtearing and hybrid ITG-KBM modes in these high-beta H-mode plasmas. The corresponding carbon particle flux for ITG-KBM, and its dependence on rotation and rotation gradient (including centrifugal effects), was investigated systematically using GKW (collaboration with University of Bayreuth) [TT-23].

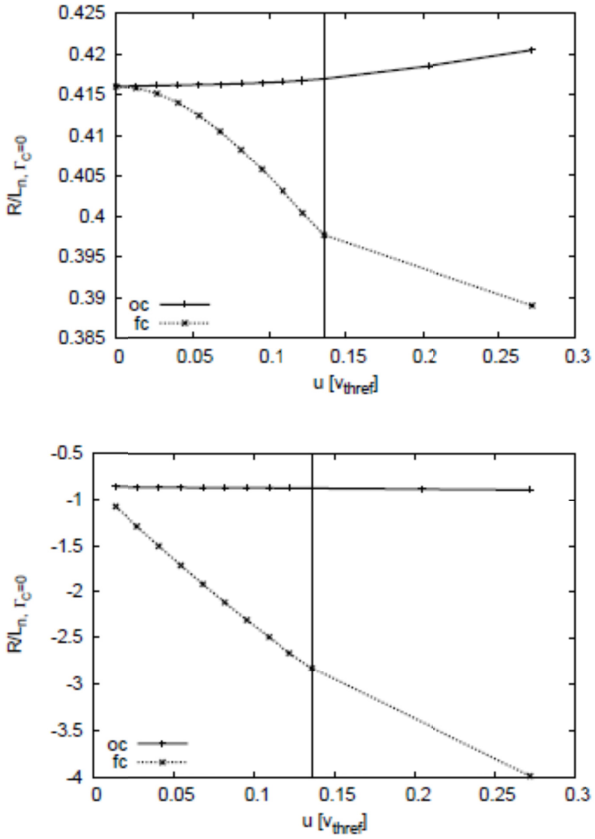

Figure TT-11: *Density gradient length for zero carbon particle flux with (top) zero rotation gradient (u'=0) and (bottom) experimental rotation gradient (u'=0.91), for the case with only Coriolis effects (oc, without centrifugal effects), and full rotation effects (fc, with centrifugal effects).*

Figure TT-11 shows the calculated density gradient length, $R/L_{n,c}$, needed for zero carbon particle flux from the hybrid ITG-KBM mode for various values of rotation and rotation shear. The zero flux state reflects a steady-state condition with no local carbon source. In the absence of a rotation gradient ($u'=0$, top panel) the simulations predict a peaked carbon profile ($R/L_{n,c}>0$), regardless of rotation and centrifugal effects. The picture changes significantly if also the rotation gradient is included (bottom panel). In this case, roto-diffusion (impurity flux driven by rotation gradient) provides a strong outward particle flux. Therefore, a locally hollow profile ($R/L_{n,c} < 0$) is needed to obtain zero particle flux. If centrifugal effects are neglected (Coriolis only), the predicted gradient is $R/L_{n,c} \approx -0.85$ and is largely independent of rotation (u). Including centrifugal effects leads to an enhancement in the hollowing that increases with toroidal rotation. For the experimental rotation u=0.14, the predicted $R/L_{n,c} \approx -2.8$ is nearly three times bigger, which is notably similar to the experimental value $R/L_{n,c,exp} = -3.5$. If this effect is manifested in nonlinear simulations, it suggests that the locally inverted carbon profile (in this source-free region) is a due to a balance between diffusive effects and the strong outward transport from both roto-diffusion and centrifugal effects for the ITG-KBM instability.

Interpretative modeling of impurity transport diagnostics

In order to quantify transport quantities from the newly built and installed edge/core Multi-Energy Soft X-ray (ME-SXR) system, the JHU group has developed a new python-based interface to the STRAHL impurity transport code. This code is used to model neo-classical/anomalous transport, in order to determine ion fractional abundances of plasma impurities. Using this transport code in combination with atomic data from the ADAS database, ME-SXR synthetic emission is obtained for different X-ray thin-metal filters and a bolometric channel. These synthetic calculations will be compared and fitted to ME-SXR measurements at the edge/core of NSTX-U in order to determine transport coefficients.

The Johns Hopkins group has also prepared models to quantify impurity densities from the beam plasma charge-exchange and the background Bremsstrahlung emission, measured in the XUV spectral range (50-700 Å) using the upgraded Transmission Grating Imaging Spectrometer (TGIS). Impurity densities are estimated by fitting the modeled synthetic spectra to TGIS measurements.

The JHU group has also contributed to collaborative work with RFX-mod by modeling helium line emission and line ratio, towards the determination of electron temperatures and densities in the edge of NSTX-U. The RFX-mod line ratio system measures helium emission from thermal beam into plasma for three different wavelengths (667.8, 706.5, and 728.1 nm). The system is schedule to be installed and operated on NSTX-U, where it will enable to extend fast Te measurements with the JHU ME-SXR diagnostic, to the far edge plasma.

4. Collaboration with DIII-D relevant to NSTX-U transport & turbulence physics

A significant amount of analysis has been performed in collaboration with DIII-D which has helped NSTX-U researchers develop experience and provide the starting basis for a number of transport and turbulence topics to be studied on NSTX-U.

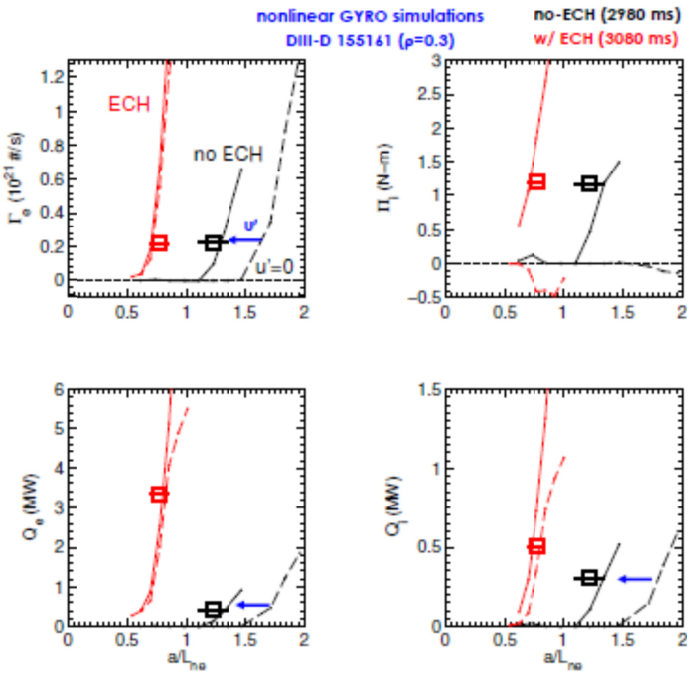

Figure TT-12: *Solid lines show electron particle (Γ_e), ion momentum (Π), electron and ion heat fluxes (Q_e, Q_i) predicted from GYRO simulations for various density gradients in DIII-D QH mode plasmas. Black lines are for the case with NBI-only, red lines are for the case with NBI+ECH. The squares show the experimental values from TRANSP analysis. The dashed lines are from simulations that set the parallel velocity gradient to zero ($u'=0$) while keeping finite E×B shearing.*

NSTX-U researchers contributed substantial nonlinear gyrokinetic analysis the DIII-D QH-mode experiments National Fusion Science Campaign experiment "Controlling H-mode particle transport with ECH" led by D. Ernst (MIT). Gyrokinetic simulations show density gradient driven trapped electron modes (TEM) are the only unstable drift modes in the inner half-radius. Particle transport driven by TEMs increases strongly with electron temperature when local ECH is applied, reducing the core electron density gradient. The simulated heat, particle & momentum fluxes all agree with the measurements (Figure TT-12), and illustrate that with ECH, the increased T_e/T_i, and decreased collisionality lead to enhanced density gradient driven TEM turbulent transport [TT-26]. Ongoing analysis will contribute to upcoming presentations and publications by Ernst (MIT) and NSTX-U researchers, and also provides a basis for studying density profile control in NSTX-U using RF heating.

As part of this work, simulations also showed that, without ECH (NBI only), the parallel velocity gradient (PVG, ~u′) provides substantial instability drive (via the Kelvin-Helmholtz instability), and is critical to include in the simulations to obtain agreement with the measured fluxes (Figure TT-12, dashed lines) [TT-27]. In contrast, when ECH is applied, the rotation and rotation gradient are decreased (due to enhanced TEM activity) and the effect of the parallel velocity gradient drive becomes negligible. It was also found that including finite beta electromagnetic effects was crucial in obtaining quantitative agreement. This work, in conjunction with previous global GTS simulations of Kelvin-Helmholtz instability in an NSTX L-mode [TT-4,TT-5], provides the basis for investigating PVG-driven instabilities in NSTX-U.

NSTX researchers were also instrumental in the development and implementation of a DBS synthetic diagnostic to apply to the DIII-D QH-mode GYRO simulations [TT-28]. The corresponding change in measured DBS spectra from the addition of enhanced TEM due to ECH was reproduced through the synthetic DBS fluctuation spectra (Figure TT-13). The development of the synthetic DBS diagnostic provides the basis for analysis of DBS measurements expected to be developed during NSTX-U operations.

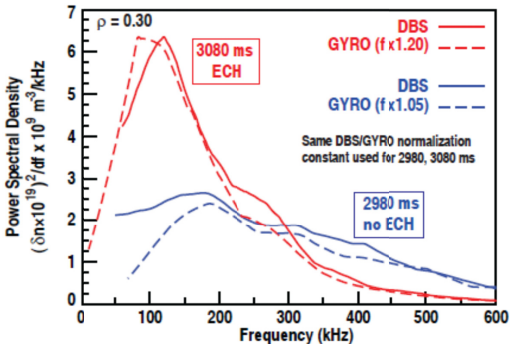

Figure TT-13: *Measured Doppler backscattering spectra (DBS, solid lines) and synthetic DBS from GYRO simulations (dashed) for NBI-only (blue) and NBI+ECH (red) DIII-D QH mode.*

Additional gyrokinetic analysis has been performed by NSTX-U researchers for DIII-D high non-inductive fraction discharges that exhibit ITBs [TT-29]. The simulations predict that inside the ITB radius ($\rho<0.6$) the large parallel velocity gradient provides substantial instability drive where temperature and density gradients are relatively weak [TT-27]. In addition, both gyrokinetic and infinite-n MHD ballooning stability simulations show the profiles are near the KBM threshold in this region. These two mechanisms (PVG and KBM, depending on rotation gradient and beta, respectively) may be at least responsible for limiting core pressure gradients. This work provides the basis for studying core transport in high non-inductive fraction NSTX-U discharges at high beta and significant beam heating.

References

[TT-1] W.X. Wang et al., Phys. Plasmas, **17**, 072511 (2010).
[TT-2] Y. Ren et al., Phys. Rev. Lett. **106**, 165005 (2011).
[TT-3] Y. Ren et al., Phys. Plasmas **19**, 056125 (2012).
[TT-4] W.X. Wang et al., Phys. Rev. Lett (submitted).
[TT-5] W.X. Wang et al., Phys. Plasmas (submitted).
[TT-6] W. Guttenfelder et al., Phys. Plasmas **19**, 056119 (2012).
[TT-7] S.M. Kaye et al., Nucl. Fusion **53**, 063005 (2013).
[TT-8] N. N. Gorelenkov et al., Nucl. Fusion **50** 084012 (2010).
[TT-9] D. R. Smith et al., Rev. Sci. Instrum. 79, 123501 (2008)
[TT-10] F. Jenko et al., Phys. Plasmas **8**, 4096 (2001).
[TT-11] W. Guttenfelder et al., Nucl. Fusion **53**, 093022 (2013).
[TT-12] Y. Ren et al., "Experimental Observation of Nonlocal Electron Thermal Transport in NSTX RF-heated L-mode plasmas", Proc. 25th Int'l. Atomic Energy Agency Fusion Energy Conference, EX/P6-43, St Petersburg, Russia Federation, October 13-18, 2014
[TT-13] W. X. Wang et al., Phys. Plasmas 14, 072306 (2007)
[TT-14] S.-I. Itoh and K. Itoh, Sci. Rep. 2, 860 (2012)
[TT-15] J. Candy and R. E. Waltz, Phys. Rev. Lett. 91, 045001 (2003)
[TT-16] F. Jenko, J. Plasma Fusion Res. SERIE 6, 11 (2004)
[TT-17] Y. Ren et al., Nucl. Fusion 53, 083007 (2013)
[TT-18] W.M. Solomon et al., Phys. Rev. Lett., **101**, 065004 (2008).
[TT-19] S.M. Kaye et al., Nucl. Fusion, **49**, 045010, (2009).
[TT-20] W. Guttenfelder et al., EU-US TTF, Santa Rosa, CA (2013).
[TT-21] A.G. Peeters et al., Nucl. Fusion **51**, 094027 (2011).
[TT-22] W. Guttenfelder et al., US TTF, San Antonio, TX (2014).
[TT-23] R. Buchholz et al., Phys. Plasmas (in press).
[TT-24] F. Scotti, et al., Nucl. Fusion **53**, 083001 (2013).
[TT-25] J.M. Canik et al., Nucl. Fusion **50**, 064016 (2010).
[TT-26] D.R. Ernst et al., IAEA-FEC EX/2-3, St. Petersburg (2014).
[TT-27] W. Guttenfelder et al., US-EU TTF, Salem, MA (2015).
[TT-28] D.R. Ernst et al., US-EU TTF, Salem, MA (2015).
[TT-29] A.M. Garofalo et al., IAEA-FEC PPC/P2-31, St. Petersburg (2014); US-EU TTF (2015).

C. Energetic Particles TSG Research Highlights

The main drivers for Energetic Particle (EP) research in FY-15 have been the fulfillment of the NSTX-U Milestone R(15-2) and contributions to the FY-15 Joint Research Target (JRT-15). The main goals, directly related to EP physics, are:

- Milestone R(15-2): "Assess the effects of neutral beam injection parameters on the fast ion distribution function and neutral beam driven current profile"
- JRT-15: "Conduct experiments and analysis to quantify the impact of broadened current and pressure profiles on tokamak plasma confinement and stability"

Specific EP activities related to these goals are summarized in the Milestone R(15-2) and JRT-15 notable outcome reports. Milestone R(15-2) also describes EP activities in preparation for the upcoming NSTX-U run campaign, e.g. diagnostic work and planning of experiments. In addition, new results have been obtained from experiments and theory/modeling studies of EP-driven instabilities in the Alfvén frequency range (AEs), as summarized below. (Note that contributions from the EP Topical Science Group to studies of thermal transport by high-frequency Alfvénic instabilities are described in the Turbulence and Transport Research Section).

1. Classification and understanding of unstable AE regimes

The development of parametric scaling laws for plasma confinement, ELM stability, and for the H-mode threshold have helped to guide theory towards a better understanding of those phenomena. A similar semi-empirical approach towards characterizing the stability boundaries for some common EP-driven instabilities as seen on NSTX has been applied to NSTX data. Understanding the conditions under which beam-driven instabilities arise, and the extent of the resulting perturbation to the fast ion population, is important for predicting and eventually demonstrating non-inductive current ramp-up and sustainment in NSTX-U, as well as the performance of future fusion plasma experiments such as ITER and FNSF. A database has been constructed, based on shots from the 2010 experimental campaign for which TRANSP runs were done. Each shot was divided into 50 ms intervals. The dominant beam-driven activity was characterized (see Figure EP-1), and plasma parameters were collected into a database [EP-1]. It is found that TAE avalanches are present for $\beta_{fast} / \beta_{total} > 0.3$ and quiescent plasmas only for $\beta_{fast} / \beta_{total} < 0.3$. Recent work has focused on including MSE-constrained q-profile and rotational shear information in the database. Preliminary analysis has found that the q-profile information further separates the parameter regimes of the previously

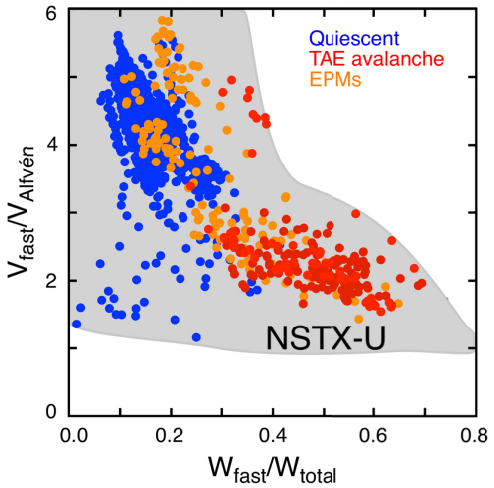

Figure EP-1: *Stability diagram for various EP-driven instabilities on NSTX (from Ref. [EP-1]). The expected parameter range for NSTX-U is shown by the shaded area.*

identified type A and B energetic particle modes. Specifically, the type B EPMs occur in plasmas with $q_{min}>1$, whereas the fishbone-like (type A) EPMs occur in plasmas with $q_{min}\approx 1$. Further, much of the initial fast frequency chirp of the type B EPMs can be attributed to flattening of the toroidal rotation profile in the core.

Several theories have been proposed in the past to explain the different regimes of EP-driven instabilities observed in NB-heated plasmas. A common paradigm is the nonlinear behavior of fast ion phase space structures in connection with fast ion transport mechanisms. The nonlinear behavior can lead to the formation of structures like "holes" and "clumps" in the distribution function, whose evolution is then locked to a chirping frequency of instabilities. The structures are non-perturbative modes, whose existence is linked to the kinetic response of resonant particles. They can seriously degrade fast ion confinement by allowing instabilities to tap energy from gradients in the EP distribution over a phase space range much wider than the original resonance regions. The energy balance of chirping structures is explained by an interplay between the background dissipation, γ_d, which constantly takes energy out of the mode, and the fact that the frequency sweeping allows for the structure to access phase space regions with distribution function gradients otherwise inaccessible. This provides a continuous source of free energy for the instability. In other words, the phase space structures seek lower energy states to compensate losses due to γ_d, thus holes move upwards and clumps move downwards in momentum coordinate space. As they move, they leave an irreversibly modified distribution behind.

The onset of phase-space holes and clumps has been theoretically shown to be associated with an explosive solution of an integro-differential, nonlocal cubic equation that governs the early mode amplitude evolution in the weakly nonlinear regime. The existence and stability of the solutions of the cubic equation have been theoretically studied as a function of Fokker-Planck coefficients (cf. M. K. Lilley et al., Phys. Rev. Lett. 102, 195003 (2009)) for the idealized case of a single resonant point of a localized mode. From realistic computations of NSTX mode structures and resonant surfaces using the NOVA code, the effective pitch angle scattering and slowing down (or *drag*) collisional coefficients can be calculated. They are now included in the standard output of the NOVA-K kinetic MHD code. NSTX discharges have been analyzed for different cases with respect to chirping experimental observation [EP-2, 3]. Those results are compared with the theory that predicts the parameters region that allow for chirping to take place (Figure EP-2). This constitutes a novel study, since the experimental study of conditions for chirping onset in terms of collisional

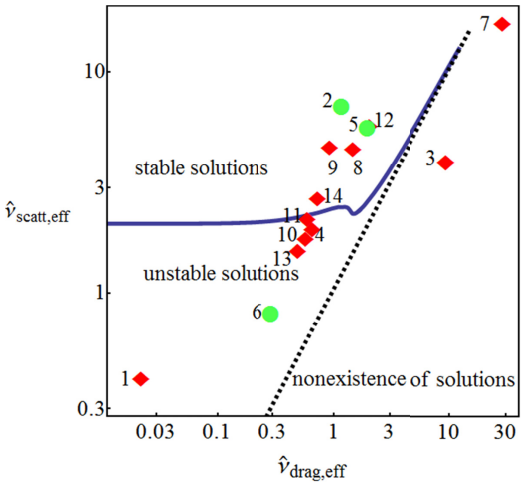

Figure EP-2: *Points corresponding to TAE modes for NSTX shot #141711 are plotted in terms of the effective scattering and drag collisional coefficients. Diamonds represent modes that presented chirping while the disks stand for non-chirping ones. The graph is divided according to different types of solutions of the equation that represents the stability boundary obtained in [M. K. Lilley et al., Phys. Rev. Lett. 102, 195003 (2009)] for the idealized case of a single resonant point of one localized mode.*

parameters had not been tackled before. The results indicate that, although it may give important physical insights, an idealized case with single-point resonance is not enough to properly predict the onset of a frequency chirping regime for experimental NB-heated scenarios. For this reason, the next step of this work will be aimed at extending the criterion in order to take into account mode structure information, as well as resonance profiles spread over phase space.

Besides their relevance for fast ion transport, Alfvénic instabilities also play an important role for thermal electron power balance. Following previous work, an energy-channeling mechanism is proposed to explain flattening of the electron temperature profiles at a high beam power in NB-heated NSTX plasmas [EP-4]. The hybrid code HYM [EP-5] has been used to investigate properties of beam-ion-driven compressional Alfvén eigenmodes (CAEs) in NSTX. The HYM code is a 3D nonlinear global stability code in toroidal geometry, which treats the beam ions using full-orbit, delta-f particle simulations, while the one-fluid resistive MHD model is used to represent the background plasma. Results of self-consistent HYM simulations of CAEs in NSTX demonstrate strong coupling of CAEs to kinetic Alfvén waves (KAW) near the Alfvén resonance location, cf. Figure EP-3. The beam-driven CAE can mode convert to KAW, thus channeling energy from the beam ions at the injection region - near the magnetic axis - to the location of the resonant mode conversion at the edge of the beam ion density profile. This mechanism can explain the reduced heating of the plasma center in NSTX inferred from the experiments. Moreover, it has been found that strong CAE/KAW coupling follows directly from the dispersion relation, and will occur for any unstable compressional mode.

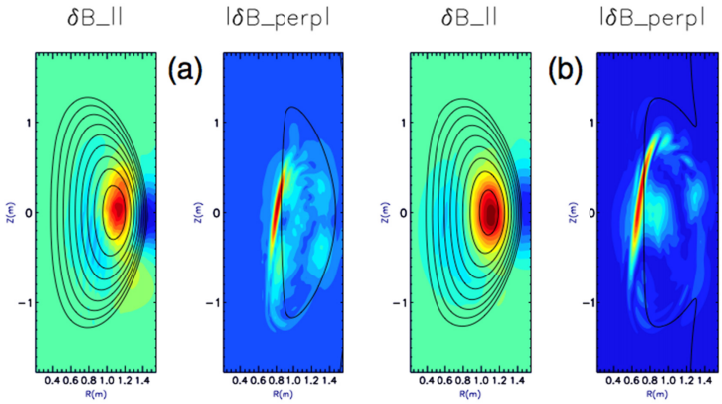

Figure EP-3: *Contour plots of magnetic field perturbation for (a) n=8 and (b) n=4 CAE modes, showing resonant coupling to KAWs. The solid contour line on the δB_{perp} plots indicates the location of the Alfvén resonance. (From Ref. [EP-4]).*

2. Predictions of mode stability and saturation

Energetic particle modes and Alfvén modes driven by super-Alfvénic beam ions were routinely observed in neutral beam heated plasmas on the National Spherical Torus Experiment (NSTX). These modes can significantly impact beam-ion transport, thus causing beam-ion redistribution and losses. Recent simulation results of TAEs show mode radial structure consistent with the reflectometer measurements of electron density fluctuations [EP-6]. More recently, nonlinear simulations of multiple TAEs in NSTX plasmas have been carried out through the M3D-K code. The model is self-consistent, with mode structure determined non-perturbatively including effects of energetic particles and plasma toroidal rotation. NSTX experimental results show that multiple low-amplitude beam-driven TAEs with weak frequency chirping can transit to mode avalanche with much larger amplitudes and stronger frequency chirping. In order to explore mechanisms of avalanche, M3D-K nonlinear simulations of multiple beam-driven TAEs and the n=1 fishbone

have been carried out. The simulation results show strong interaction between TAEs and fishbone that either enhances or reduces saturation level of individual modes depending on mode number and other parameters. As beam ion beta increases beyond a threshold, mode saturation levels are found to increases sharply. Correspondingly, the locally flattening regions merge together resulting in global particle transport and substantial particle loss. These results are similar to the TAE avalanche observed in NSTX.

Using a different approach, a combination of analytic models and the particle-following numerical simulation code ORBIT is being developed to find the saturation levels of unstable Alfvén modes and the resulting effect on beam and alpha particle distributions [EP-7]. The initial unstable mode spectrum and eigenvalues are supplied by the NOVA code, then time evolution of these modes to saturation is performed with the guiding center code ORBIT. Solving the drift kinetic equation with a guiding center code in the presence of Alfvén modes driven unstable by a distribution of high energy particles requires the use of a δf formalism. The initial distribution, f_0, is assumed to be a steady state high energy particle distribution in the absence of the modes, and $f=f_0+\delta f$ describes the particle distribution in the presence of the modes. The Hamiltonian is written as $H=H_0+H_1$ with H_0 giving the unperturbed motion, conserving particle energy E, toroidal canonical momentum P_ζ, and magnetic moment μ. By writing the initial particle distribution in terms of these variables, a simple means of calculating mode-particle energy and momentum transfer results, providing a very accurate δf formalism. The numerical beam deposition code NUBEAM in TRANSP produces a list of particles, giving energy, pitch, and location, which can be used to find the unperturbed distribution $f_0(E,P_\zeta,\mu)$. The effect of unstable Alfvén modes on high-energy particle distributions is being examined for NSTX [EP-7], and will then be extended to DIII-D and ITER scenarios.

3. Suppression of energetic particle driven instabilities via HHFW heating

In beam-heated plasmas in the National Spherical Torus Experiment (NSTX) heated with neutral beams, the beam ions typically excite Energetic Particle Modes (EPMs or fishbones), and Toroidal, Global or Compressional Alfvén Eigenmodes (TAE, GAE, CAE). These modes can redistribute the energetic beam ions, altering the beam driven current profile and the plasma heating profile, or they may affect electron thermal transport or cause losses of the beam ions. Analysis of NSTX data has found cases where multiple instabilities driven by the super-thermal beam ions, are seen to be suppressed with the application of High Harmonic Fast Wave heating [EP-8]. Toroidal Alfvén Eigenmodes, Global Alfvén Eigenmodes and fishbones were all suppressed, even though the resonant drive mechanisms for these classes of modes are very different. The experiments were at relatively low plasma current (300 kA), relatively low density and with neutral beam power of 2 MW. In these experiments, the modes were reproducibly stabilized for long periods of time. A threshold power of about 1.5 MW was found for stabilization to occur, but that may scale with density and beam power. The abrupt return of mode activity following HHFW heating suggests that the modifications to the fast ion distribution were relatively small, or that the HHFW more directly interferes with the resonant drive of the modes. These results strongly motivate future experiments to determine whether this stabilization mechanism can be extended to more typical operational conditions, that is, higher currents, higher densities and more beam power.

4. Validation of Critical Gradient Model and extension to non-perturbative regime

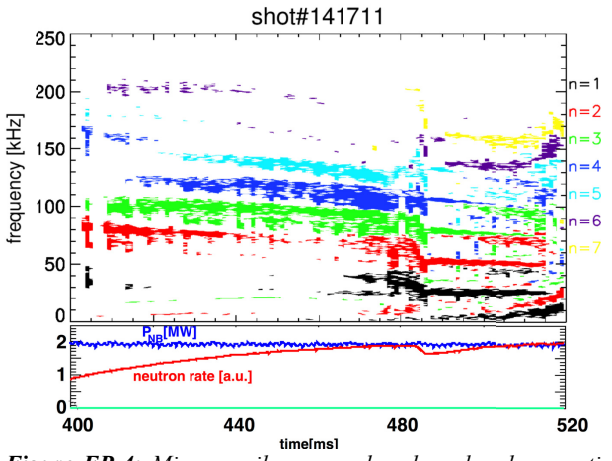

Figure EP-4: *Mirnov coil measured and analyzed magnetic field oscillations spectrum vs time in NSTX discharge #141711. Shown to the right is the color coding for toroidal mode numbers. Bottom insert depicts the NBI injected power (blue curve) and neutron flux evolution (red curve).*

A "critical gradient" model (CGM) is being validated against NSTX experiments in addition to its preliminary validations against DIII-D data [EP-9, 10]. Among the NSTX plasmas available for the analysis, discharge #141711 with reversed magnetic shear profile was chosen. It is characterized by the presence of several instabilities driven by beam ions in the TAE range of frequencies [EP-11]. Instabilities have low to medium toroidal mode number ($2<n<6$) and feature characteristic frequency chirps on a millisecond time scale.

Figure EP-4 shows the evolution of different signals. Toroidal mode numbers are color coded in the figure as indicated. The observed modes are not virulent instabilities, despite the chirping behavior toward the end of the discharge when a TAE *avalanche* event occurs. The choice of this shot is made due to its relatively benign AE activity for NSTX, which transforms to the avalanche at t=480 ms. Note that the CGM is not applicable beyond t=480 ms, as the physics of EP transport in the avalanche is far more complicated than the model implies (see previous paragraph on the chirping mode physics comparison).

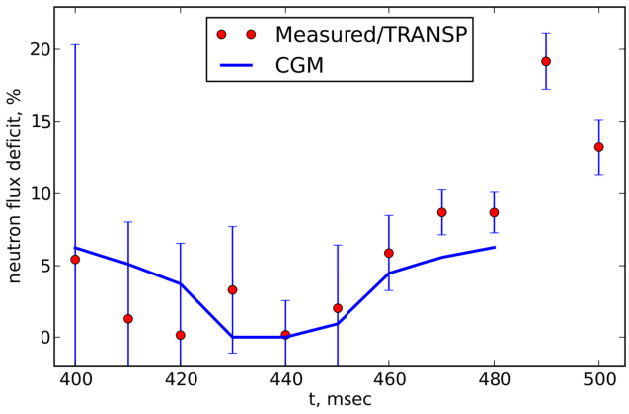

Figure EP-5: *Neutron deficit as computed by the TRANSP code for NSTX #141711. It compares this deficit with the predictions by the CGM. At t=480 ms, a TAE avalanche occurs (cf. Figure EP-2) beyond which CGM could not be applied.*

In the application of CGM to the NSTX data, a version of the model based on the normalization of the AE growth rates to NOVA-K [EP-9] computed increments was used. The nomalization constants are derived using the TAE mode structures at four to five radial points, r/a ~ 0.1, 0.3, 0.5, 0.7 and 0.9. They are chosen by finding the locations of the maximum values of the growth rates. Between those locations, a linear interpolation formula was used. An analytic expression for growth and damping rates is employed outside that range. Figure EP-5 presents the results of the model predictions against the NSTX data. Considering experimental uncertainties in the absolute calibration of the neutron detectors, the CGM predictions are within the error bars of the

measurements. Overall, the CGM validation exercise against the NSTX experimental results looks promising and warrants a confidence in its possible predictions. The validating exercise ensures that the quasilinear approach targeted within PPPL is an appropriate method for future research in the EP area.

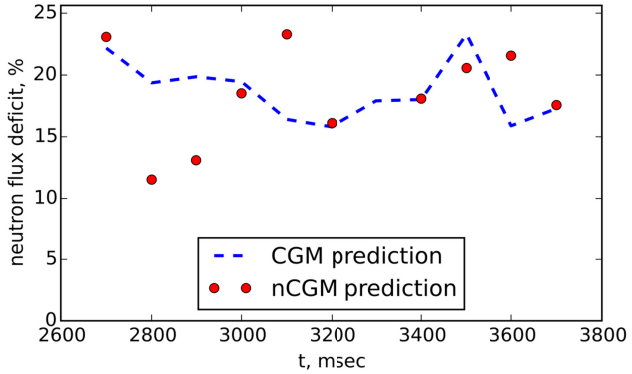

Figure EP-6: *Comparison of the CGM and nCGM predictions for DIII-D test case, discharge #153072. The deficit should be compared with the experimentally obtained deficit using classical computations by the TRANSP code.*

As shown in the R(15-2) Milestone report, CGM in the perturbative regime could not be applied to DIII-D since it underpredicts the neutron deficit by the factor of ~2. The question emerges whether the model is applicable, since earlier studies suggest that non-perturbative explanations should be brought [EP-10]. A new version of CGM is developed to account for the non-perturbative excitation of various modes including TAEs when their drive is strong. The HINST code (HIgh-N STability code, [EP-11, 12]) is available for that purpose and was applied. The code solves the system of equations in the ballooning variable to find the mode structure and its net growth rate non-perturbatively. As an example, it is applied to a DIII-D plasma where the drive reaches $\gamma/\omega < 0.3$ locally and the application of the perturbative NOVA-K results is questionable. HINST computed net growth and damping rate are used for nCGM normalization where the linear interpolation was used again between the computed values of the growth rates. Here 20 radial points provided the growth and damping normalization points. Beam ion neutron flux deficit profiles are computed by the 1.5D code and are plotted on Figure EP-6. The results of the DIII-D validation show that the predictions of both CGM and nCGM are close to each other. They are also close to the "kick" model neutron flux deficit (see R(15-2) Milestone report, Figure 2b). The non-perturbative CGM cannot be used in NSTX though since nCGM normalization is based on HINST code results which is a high-n ballooning code and cannot be justified for typical NSTX conditions.

5. Diagnostic development

Key diagnostics for the experimental characterization of the fast ion distribution function on NSTX-U are fast-ion D-alpha (FIDA) systems and arrays of solid-state neutral particle analyzers (ssNPA). Analysis and interpretation of FIDA and ssNPA data is challenging, since the systems sample only a portion of the entire distribution. The FIDAsim code [R15-2-4] is used for forward-modeling of experimental data to infer the actual distribution function based on predictions from the TRANSP/NUBEAM code and comparison to experimental data. Recent development of a FIDA analysis technique will enable accurate interpretation of data from the upgraded FIDA and ssNPA systems available on NSTX-U (see below for details on the diagnostics). To test the technique, measured fast-ion D-alpha (FIDA) data from an extensive NSTX database have been

compared to "classical" predictions that neglect transport by instabilities [R15-2-5]. Even in the absence of detectable MHD, in virtually all cases, the profile peaks at smaller major radius and the profile is broader than the predictions. Abrupt large-amplitude MHD events flatten the FIDA profile, as do most toroidal Alfven eigenmode (TAE) *avalanche* events. Generally, the onset of a long-lived mode also flattens the FIDA profile. There is a shortfall of high-energy ions at large major radius in discharges with repetitive TAE bursts.

To improve the interpretation of both FIDA and ssNPA data, a new 3D "halo" model previously implemented in TRANSP has undergone extensive verification for NSTX and projected NSTX-U scenarios [R15-2-6]. The 3D halo neutral code uses a "beam-in-a-box" model that envelopes both injected beam neutrals and resulting halo neutrals. Upon deposition by charge exchange, a subset of the beam energy components produces first generation halo neutrals that are tracked through successive generations until an ionization event occurs or the descendant halos exit the box. The 3D halo neutral model and Neutral Particle Analyzer (NPA) simulator in the TRANSP code have been benchmarked with the Fast-Ion D-Alpha simulation (FIDAsim) code. When using the same atomic physics database, TRANSP and FIDAsim simulations get excellent agreement on the spatial profile and magnitude of beam and halo neutral densities, as well as the NPA energy spectrum. The simulations show that halo neutrals remain in the vicinity of the neutral beam footprint as expected and that halo neutral density can be comparable with beam neutral density. Future comparisons between measurements, FIDAsim and TRANSP modeling will benefit from this important improvement for NSTX-U scenarios with complex NB injection patterns.

References

[EP-1] E.D. Fredrickson et al., Nucl. Fusion **54** (2014) 093007.

[EP-2] V. N. Duarte et al., *Nonlinear chirping structures and the regions of applicability of quasilinear theory*, Sherwood Fusion Theory Conference, March 16-18th, 2015.

[EP-3] V. N. Duarte et al., to be presented at 57th APS-DPP Meeting, Savannah GA (2015)

[EP-4] D. Liu et al., Phys. Plasmas **22**, 042509 (2015)

[EP-5] R. B. White et al., to be presented at 57th APS-DPP Meeting, Savannah GA (2015)

[EP-6] K. Ghantous et al., Phys. Plasmas **19**, 092511 (2012).

[EP-7] W. W. Heidbrink et al., Nucl. Fusion **53**, 093006 (2013).

[EP-8] M. Podestà et al., Nucl. Fusion **52**, 094001 (2012).

[EP-9] N. N. Gorelenkov et al., Phys. Plasmas **6**, 2802 (1999).

[EP-10] Z. Wang et al., Phys. Rev. Lett. **111**, 145003 (2013).

[EP-11] C. Z. Cheng et al., Nucl. Fusion **35**, 1639 (1995).

[EP-12] C. Z. Cheng and N. N. Gorelenkov, Phys. Plasmas **11**, 4784 (2004).

III. Integrated Scenarios Research Highlights

The integrated scenarios group is tasked with understand the following elements within the NSTX-U program:

- ST startup & ramp-up
- HHFW heating and current drive
- neutral beam current drive
- axisymmetric plasma control
- fully non-inductive plasma scenarios
- Integration of the above elements amongst themselves, and with the scientific understanding achieved in the other science groups.

The science group is led by Stefan Gerhardt (PPPL), with Roger Raman (U. of Washington) as the deputy. The science group is divided into three topical science groups (TSGs), as follows:

A. The **Solenoid Free Plasma Startup** (SFPS) TSG is tasked with understanding solenoid free startup-up and ramp-up. The TSG leader is Dennis Mueller (PPPL) with Roger Raman as the deputy. Fatima Ebrahimi (Princeton University) acts as the theory and modeling representative.

B. The **Wave Heating and Current Drive** (RF) TSG is tasked with understanding the physics and technology of HHFW, ECH, and potentially EBW, in the unique plasma conditions and geometry of the ST. The group is lead by Rory Perkins (PPPL), with Joel Hosea (PPPL) as the deputy. Nicola Berteli (PPPL) is the theory and modeling representative, and Paul Benoli (MIT) is the university representative.

C. The **Advanced Scenarios and Control** (ASC) TSG is tasked with understanding axisymmetric plasma control, scenarios with very high non-inductive current fraction or very long pulse, and discharge scenario development in general. The TSG leader is Devon Battaglia (PPPL), with Stefan Gerhardt as the deputy. Francesca Poli (PPPL) is the theory/modeling representative, and Egemen Kolemen (Princeton University) is the University representative.

A. Solenoid-Free Start-up and Ramp-up TSG Research Highlights

1. SFPS and Ramp-up experiments planned FY16 operation on NSTX-U

The Solenoid-Free Start-up and Ramp-up (SFPS) group has 3 primary objectives for FY16:

1. Establish the capability for generating closed flux plasma currents without reliance on the central solenoid. During FY2016, the method of Transient Coaxial Helicity (CHI) injection will be employed to establish this capability. Eventually closed flux plasma currents of about 400 kA are required to enable non-inductive current ramp-up using neutral beams, ECH, and HHFW. For FY2016, the goal is to achieve currents in the range of about 200 kA. Supporting experiments will also study the flux closure mechanisms using the NIMROD code, and

improved diagnosing of the CHI injector region to support the simulations. Results related to this are described at the end of this section.

2. Demonstrate coupling of the CHI produced current to inductive operation. An important objective of this goal is to assess the quality of the CHI produced target, and to compare to the quality of similar discharges obtained on NSTX.

3. Study non-inductive current fraction in low current inductively produced discharges. In these experiments the requirements for NBI and HHFW parameters to enable current overdrive will be studied so that these methods could be applied to a CHI target during later years.

The following experimental proposals have SFPS Priority-1 run time planned for the FY16 run. Unlike experiments in other groups that could be run very early after start of NSTX-U operations, experiments from the SFPS group will take place towards the second half of the NSTX-U run campaign in order to benefit from good vessel conditions that are essential for CHI plasma start-up, and to benefit from some understanding of the coupling capability of the new tangential neutral beams to NSTX-U high current inductively generated targets.

Transient CHI Plasma Start-up on NSTX-U
XP # not assigned
Run time: 1.5 day during second half of NSTX-U run. Priority 1a
Milestone: R18-3
Status: Not reviewed

TSC simulations have identified the required coil currents to initiate transient CHI discharges on NSTX-U. All hardware components to enable Transient CHI operations are installed on NSTX-U. An important external system required for initiating CHI discharges is the CHI 2 kV, 40 mF Capacitor Bank. Old components were replaced and the design for the capacitor bank current limiting resistor assembly was revised and improved. Discharging the charged bank at full voltage into a dummy load then successfully tested the re-furbished capacitor bank. These tests also verified that the fairly involved Control System for the bank worked as required. These tests were conducted by operating the system from a local computer that is located near the capacitor bank system. An upgrade of the control software from the present Windows XP to Windows 7 is needed to allow it to be operated remotely from the NSTX-U Control Room. This work is in progress. Immediately following this computer upgrade, the capacitor bank will be used to generate plasmas in a condition referred to as “Stuffed Mode”, a procedure during which the elongation of the CHI plasma is severely controlled and restricted to the region near the injector. This is part of the commissioning procedure, and is used to establish and test conditions that are required to support the primary XP for transient CHI start-up. These tests will be conducted during the first half of the NSTX-U run, and will be necessary to formulate the detailed Transient CHI XP.

Non-inductive Flux Savings of Inductively Driven Targets
XP # not Assigned

Run time: 0.5 day during second half of NSTX-U run. Priority 1b
Milestone: R18-3
Status: Not reviewed

A necessary step after establishing transient CHI start-up is to see if it is compatible with conventional inductive operation. This is a measure of the quality of the target discharge and is a step that is required for any new plasma start-up method. The procedure for this will largely follow the procedure developed for a similar XP on NSTX. Measuring the inductive flux savings will assess the quality of the CHI plasma, and this will be compared to the flux savings obtained on NSTX.

Low Plasma Current, Fully Non-Inductive, HHFW H-Mode Plasmas
XP # not assigned
Run time: 0.5 day during second half of NSTX-U run. Priority 1b
Milestones: R18-3
Status: Not reviewed

This experiment benefits from very successful studies on NSTX in which HHFW at a power of much less than 1 MW was able to heat a 300 kA inductive plasma from about 200 eV to over 1 keV in 20 ms. This aspect of HHFW is very desirable to increase the temperature of ECH heated CHI discharges to the temperatures needed for efficiently coupling NBI power to achieve current overdrive. Recent TRANSP-TORIC simulations predict that 4-6 MW of RF power may ramp low current inductive plasma to over 400 kA, and that it can heat these plasma as on NSTX. RF power of the appropriate phasing will be applied to a 250 kA inductively generated target in which the central solenoid current is clamped.

NBI Overdrive Without RF
XP # not assigned
Run time: 0.5 day during second half of NSTX-U run. Priority 1c
Milestones: R17-4
Status: Not reviewed

Eventually, NBI is anticipated to be the primary system to provide non-inductive current ramp-up from about 400 kA to 1 MA, where it will be sustained using NBI and Bootstrap current drive. In support of this, we plan to begin initial tests to study the coupling of NBI to low current inductively generated targets. Because non inductive current sustainment of high current discharges is easier and much more important for the early phase of NSTX-U operations, and because these studies will provide helpful information related to NBI coupling to low current discharges, these studies will begin after a reasonable data set is obtained from several early XPs on NSTX-U that will use NBI.

2. NIMROD Simulations

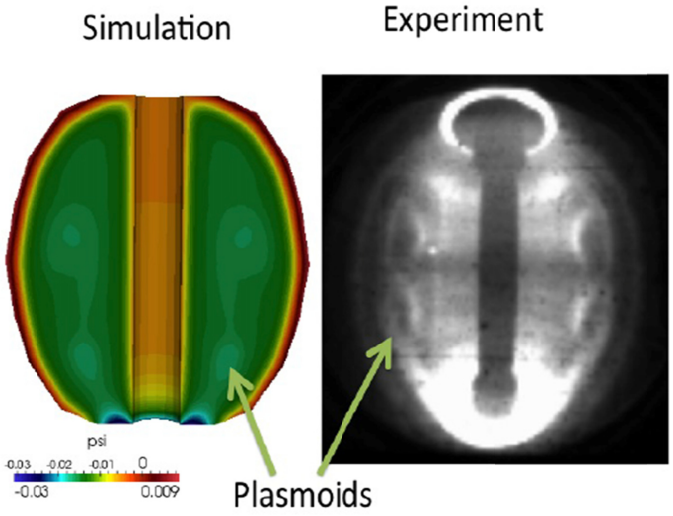

Figure IS-SFPS-1: *Left: Plasmoid formation in MHD simulations of NSTX during CHI Right: Camera image in NSTX shows two discrete bubble plasmoid-like structures. [1,2]*

This first section describes NIMROD simulations conducted by F. Ebrahimi that has identified a possible new mechanism for fast flux closure during CHI discharges.

Magnetic reconnection, which energizes many processes in nature, has been shown to have a fundamental role in the plasma start up and current formation in NSTX/NSTX-U. In a recently published paper, [IS-1,2] it was recognized that transient Coaxial Helicity Injection (CHI) discharges in NSTX/NSTX-U may provide a rich platform for investigating fundamental reconnection physics, in particular reconnecting plasmoids physics. Plasmoids can form under different circumstances in fusion and astrophysical plasmas. Anytime oppositely directed magnetic field lines in a plasma are pushed together and reconnect via some dynamical process and form a long current sheet, the plasmoid instability might occur and cause plasmoids to form. For the first time we have simulated plasmoid instability in a realistic tokamak geometry and have shown that plasmoids can even form during helicity injection in a large fusion device when no other dynamical process (or instability) is initially present. Through resistive MHD simulations, it is demonstrated that during transient CHI discharges at high Lundquist number, the elongated current sheet formed through a Sweet-Parker forced reconnection process [IS-3,4] breaks up, and a transition to spontaneous reconnection (plasmoid instability) occurs. Motivated by the simulations, experimental camera images have been revisited and suggest the existence of reconnecting plasmoids in NSTX (see Figure IS-SFPS-1). As CHI is a promising candidate for plasma start-up and may ultimately also have the potential for steady-state current drive, it is thus important to understand the CHI physics to be able to correctly model it in simulations of NSTX/NSTX-U and to be able to extrapolate its viability to a reactor. Our simulations show that plasmoid-mediated reconnection may be the leading mechanism for fast flux closure.

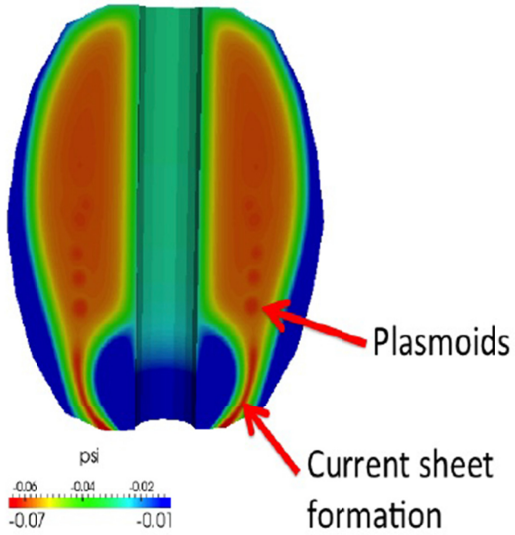

Figure IS-SFPS-2: *Plasmoid formation in MHD simulations of NSTX-U*

One of the novel characteristics of the global NIMROD simulations of CHI in NSTX is that they have been performed in a realistic experimental geometry that includes currents driven in the external toroidal and poloidal field coils. These simulations showed that large-scale system-sized plasmoids are formed and cause fast reconnection in a fusion plasma. Consistent with the theory, fundamental characteristics of the plasmoid instability including 1) the break up the elongated current sheet, 2) the increasing number of plasmoids with Lundquist number, and 3) the reconnection rate, as it becomes nearly independent of S, have been observed in these simulations. We have also performed MHD simulations in the NSTX-U configuration. The coil currents in these simulations are optimized to give a very narrow injector flux footprint width. Plasmoid instability with continued injection of plasmoids (up to eight) are observed during the injection phase as shown in Figure IS-SFPS-2.

These results along with future experiments with high-resolution diagnostics could improve our understanding of guide field reconnection with strong implications for astrophysical plasmas. The direct detection of plasmoids in large fusion devices during magnetic reconnection would have a significant impact as these large-scale plasmoids are similar to the plasmoids on the surface of the sun. To detect and measure all the signatures of reconnection (such as plasma flows and current sheets) high resolution cameras (full spatial and temporal diagnostics) are required. In NSTX- U, transient CHI may have the potential to vary the electron temperature, density and the local reconnecting magnetic field strength over a very wide range, thus providing a well-diagnosed test bed for basic reconnection studies, which may not be possible on any of the smaller devices in existence at this time. At every stage advanced nonlinear 3-D single and two fluid global MHD simulations are required to provide support for understanding the physics and to predict the experimental observation.

In short, through experimental measurements, along with the numerical simulations, we may find out how reconnection, in particular plasmoids, would affect the maximum flux closure and CHI-generated current for optimal startup. Understanding reconnection physics may be necessary to predict how transient CHI scales as it is extrapolated to future (larger) devices, such as the ST-FNSF.

This second section summarizes the work of by E.B. Hooper, which are results from resistive MHD simulations using NIMROD, the primary goal of which is to obtain a better match of the experimental results and improving the physics understanding for future experiments in NSTX-U. When impurity radiation used to match the measured electron temperatures is greatly reduced, a high-poloidal number mode which was observed in previous simulations [IS-5] is much stronger and affects flux-surface closure unlike the previous results.

The work reported here is directed to understanding the mode physics and its consequences.

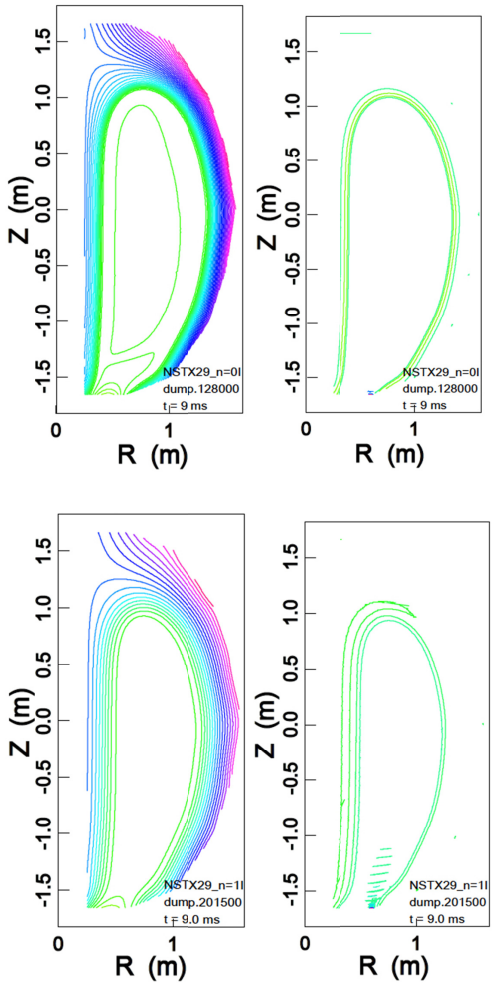

Figure IS-SFPS-3: *Axisymmetric (top) and non-axisymmetric (bottom) poloidal flux (left) and RB_ϕ ~ $I_{poloidal}$ (right) contours at 3 ms after start of injection*

The reduction in radiation results in higher temperatures (> 100 eV). The mode undergoes a series of relaxation oscillations that broaden the poloidal flux distribution and the current and plasma flow along the surface of the injected flux bubble relative to a stable, axisymmetric simulation (Figure IS-SFPS-3). A series of linear, non-axisymmetric simulations were performed starting from a nonlinear, axisymmetric injection. The linear mode consists of velocity vortices and magnetic-field surfaces with axes oriented along the background magnetic field (toroidal plus injected poloidal); the perturbed current flows predominantly along the field. The mode is strongest outside the strong plasma flow just inside the surface of the flux bubble; it lies instead in the region of poloidal current flow that generates the increase in toroidal field pressure that expands the bubble.

The linear calculations find the instability growth rate to be high (~ 1 μs^{-1}). The growth rate is insensitive to the resistivity, viscosity, and particle diffusion. If the axisymmetric (background) plasma flow is set to zero, the mode is still unstable although the growth rate is decreased by a factor of two. A model of the Kelvin-Helmholtz mode [IS-6] predicts growth rates more than an order-of-magnitude slower and a perturbation localized in the strong plasma-flow region. The conclusion is that dissipation and velocity shear are not primary drivers for the instability.

The mode is likely an ideal MHD, current-driven instability. A model is being developed of this instability in the slowly-evolving flux and current configuration during helicity injection in a ST and will be compared with the simulations when complete. Eventually the results of these simulations will need to be compared to the experimental parameters and to experimental observations.

3. CHI Activities in Support of an ST-FNSF

A conceptual design study of CHI for a ST-FNSF has identified two possible design configurations, as described in a recent paper [IS-7]. One of these configurations will soon undergo an experimental test on the QUEST ST at Kyushu University. During the past year all necessary CHI hardware were incorporated into the QUEST vessel. Figure IS-SFPS-4 shows the inner CHI electrodes on QUEST and the US procured CHI insulator sections that are located beneath the electrodes that are visible in inner vessel view of QUEST. The CHI activity on QUEST is led by the NSTX-U CHI effort.

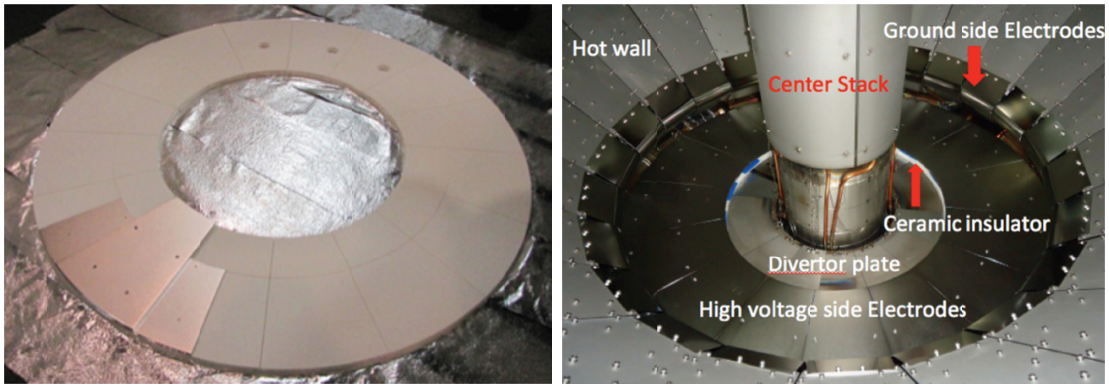

Figure IS-SFPS-4: *(Left) Photo showing the 16 sections of the US procured primary CHI insulators for QUEST. (Right) Photo of the interior lower divertor region of the QUEST vessel showing the CHI electrodes. The insulators are located below the electrode plates, as shown by one of the red arrows.*

During FY15 we also wrote a Topical Review Paper on solenoid-free plasma start-up in spherical tokamaks, that summarizes the state of research in all of the solenoid-free plasma start-up methods that are being tested in all the STs and tokamaks [IS-8].

B. Wave Heating and Current Drive TSG Research Highlights

1. Experimental Proposals for the FY-16 Run

Four experimental proposals and one machine proposal were allocated runtime for the first NSTX-U campaign. The Wave Heating and Current Drive Topical Science Group will initially focus on characterizing the scrape-off layer (SOL) losses of high harmonic fast wave (HHFW) power in H-mode plasmas [IS-9, IS-10] and verifying the predicted decreases of these losses at larger magnetic fields. Subsequent experiments will study the absorption of HHFW power by fast and thermal ions and generating low-current fully non-inductive plasmas powered with HHFW. A novel technique for obtaining two-dimensional images of the HHFW wavefield has also been proposed and allocated runtime.

HHFW antenna conditioning and performance evaluation
XMP-026
Runtime Allocation: 2.25 days Weeks 5-8, 0.75 days Weeks 9-16
Status: Submitted for review

In addition to its usual function of checking HHFW system performance (especially relative to wall conditioning) and conditioning the antenna to maximum voltage, this XMP will evaluate the heat load from the second neutral beam onto the HHFW antenna limiter and also improvements gained from the new electrical ground added between the back of each antenna-strap box and the vessel.

Characterizing SOL Losses of Fast Wave Power in H-Mode Plasmas
XP-1510
Runtime Allocation: 0.875 days Weeks 5-8; 0.875 days Weeks 9-16
Milestone: IR(17-1)
Status: Completed Group Review, Team Review scheduled

This experiment seeks to maximize the HHFW heating efficiency in H-mode plasmas by minimizing the amount of power lost to the SOL. Three diagnostic upgrades, a wide-angle infrared (IR) camera view, RF-frequency divertor Langmuir probes, and a SOL reflectometer, will allow for a quantitative assessment of the assertion that the SOL losses are intimately tied to the position of the right-hand cutoff in the SOL and will point to the conditions of optimal coupling for NSTX-U. This XP has undergone Group Review and is scheduled for Team Review in September.

Using 2D BES measurements to resolve the in-situ HHFW wavefield
XP # not assigned
Runtime Allocation: 0.25 days Weeks 5-8
Milestone: IR(17-1)
Status: Not reviewed

We seek to demonstrate 2D imaging of the HHFW density field on NSTX-U with BES measurements, as was demonstrated on the Phaedrus-T tokamak by running two ICRF antennae at slightly different frequencies, resulting in a local density perturbation within the BES detection range. The NSTX-U 2D BES system requires tuning the RF sources with a ~10 kHz offset to enable observations at the beat frequency. If successful, this technique will facilitate a new experimental campaign for HHFW model validation.

HHFW absorption in Neutral-Beam heated plasmas
XP # not assigned
Runtime Allocation: 1.0 days Weeks 9-16
Milestone: R(16-1), R(16-2), IR(17-1)
Status: Not reviewed

HHFW absorption by fast and thermal ions is especially relevant for NSTX-U because (i) for spherical tokamak geometry, ion acceleration to loss orbits constitutes a loss of FW and fast-ion power, and (ii) the increased magnetic field reduces the harmonic number of the FW system, potentially enhancing ion absorption. RF simulations show significant absorption by fast ions in many cases and large thermal-ion absorption when $T_i \geq T_e$. Quantifying the absorption is important to (a) benchmark RF codes, (b) determine the detriment to HHFW performance in beam-heated discharges due to fast-ion absorption, and (c) determine the physics setting the outer gap limit. This experiment will characterize the HHFW absorption as a function of HHFW antenna phases, magnetic field strength, neutral beam mix, and, to the extent possible, the T_e/T_i ratio.

Low Plasma Current, Fully Non-Inductive, HHFW H-Mode Plasmas
XP # not assigned
Lead: Gary Taylor
Milestone: R(18-3)
Runtime Allocation: 1.0 days Weeks 9-16 (0.5 days of SFSU runtime)
Status: Not reviewed

An initial approach to achieving fully non-inductive plasma current (I_P) ramp-up is to heat low I_P (250-350 kA) inductive plasmas with HHFW power. Previous experiments generated and sustained an H-mode discharge with a non-inductive fraction, $f_{NI} \sim 0.65$ but were limited by poor antenna conditioning to a maximum arc-free HHFW power of only ~ 1.4 MW. This experiment aims to achieve $f_{NI} \geq 1$ by coupling 3-4 MW of RF power into an $I_P \sim 300$ kA plasma through expected improved coupling due to the higher $B_T(0)$ and from recent modifications to the HHFW antenna grounding.

2. Ongoing Experimental Analysis

The Potential Role of RF-Rectification in SOL Losses of HHFW Power

NSTX data suggests that RF rectification is present underneath the RF spirals and may be the mechanism underlying the SOL loss of fast-wave power [IS-11, IS-12]. An expression for the heat flux delivered to a material surface in the presence of an RF voltage is developed and applied to Langmuir probe and IR camera data, producing predictions within the range of uncertainty of the data. Upcoming experiments on NSTX-U with better diagnostic coverage and a dedicated power scan will provide more definitive conclusions (See "Proposed Experiments" section above). Also, an experiment is being proposed at the Large Plasma Device at UCLA to test the heat flux derived in this work (see "Collaborations" section below).

Cylindrical Cold-Plasma Model

A cylindrical cold-plasma model of fast-wave propagation in NSTX-like conditions has been benchmarked against previous models. The computed RF voltage in the SOL is roughly consistent with the RF voltages obtained from Langmuir probe data [IS-13]. The model predicts particular modes that propagate a significant fraction of wave power (> 50%) in the edge of the plasma [IS-14], very similar to experimental observations and full-wave simulations using the AORSA code [IS-15]. These results suggest that the SOL losses are directly related to fast-wave propagation in inhomogeneous density profiles, but more work is needed to distinguish these modes from previously studied coaxial modes.

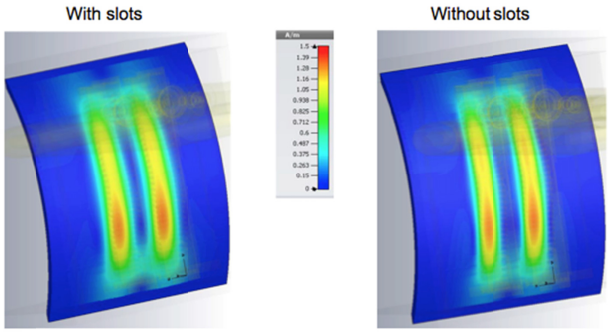

Figure IS-WHCD-1: *Microwave Studio calculation suggests the induced current pattern in sheet is steepened for the Faraday shield wall without slots, raising the wavenumber spectrum and lower coupling. This calculation is run with a copper sheet 5 cm in front of the antenna to mimic the plasma.*

Understanding the Impact of Return Current in Antenna Structures

Previous work on a test stand suggested that large RF return currents are present in the slots of the antenna sidewalls. These currents may be responsible for the large outgassing observed in the test stand [IS-16]. Further work has been done to estimate the impact of these currents on the launched antenna spectrum [IS-17], showing that unslotted sidewalls add higher wavelength components that have lower coupling (Figure IS-WHCD-1). This could have implications for the ICRF system on both KSTAR and EAST (see "Collaborations" section below).

3. Advanced RF Modeling

HHFW NSTX-U simulations and a comparison with "conventional" tokamaks with higher aspect ratios in both HHFW and minority heating regimes

We have examined HHFW power loss in the SOL by using the numerical full wave simulation code AORSA [IS-18], in which the edge plasma beyond the last closed flux surface (LCFS) is included in the solution domain [IS-19]. A collisional damping parameter is used as a proxy to represent the real, and most likely nonlinear, damping processes in order to predict the effects, and possible causes, of this power loss. 2D, single dominant toroidal mode, full wave simulations demonstrated for the first time a direct correlation between the location of the fast wave cut-off layer, the large amplitude RF fields in the SOL, and the observed power losses in the SOL driven by the RF field in the NSTX experiment [IS-15]. In particular, a significant transition to higher SOL power losses was found when the FW cut-off is moved away from in front of the antenna by increasing the edge density in the antenna region (n_{ant}), consistent with the experimental observations [IS-20]. In order to further verify these previous results we have carried out 3D AORSA simulations using several toroidal modes to reconstruct the full antenna spectrum. Figures IS-WHCD-2(a) and (b) show a comparison between the 2D AORSA results (dashed curves) obtained for a single dominant mode corresponding of the antenna phasing of -150° and -90° and the 3D AORSA results (solid curves) where the NSTX antenna spectrum has been reconstructed by using 81 toroidal mode ($-40 \leq n_{\phi} \leq 40$). The 3D AORSA results exhibit similar behavior to that of the dominant mode (2D) runs and, in particular they reproduce a similar transition in SOL power losses as a function of the density in front of the antenna, although it is less pronounced due to the contribution of the several toroidal modes. Larger SOL power losses in 3D runs with respect to the 2D runs are found for low and high n_{ant} and for both antenna phases [IS-21]. These results provide a clear verification of the previous results shown in [IS-15] and allowed us to extend our 2D AORSA simulations to tokamaks with "conventional" geometry and also different heating regime. Therefore, 2D AORSA full wave numerical analysis has been performed for "conventional" tokamaks with higher aspect ratios, such as the DIII-D, Alcator C-Mod, and EAST devices, in order to estimate the behavior of the RF power losses in "standard" geometry experiments, similar or different heating regime and compare them with NSTX/NSTX-U results. DIII-D results are found to be in agreement with the results obtained for NSTX/NSTX-U and they are also in agreement with previous experimental observations [IS-22]. In contrast, numerical simulations for Alcator C-Mod and EAST, which operate with ICRH in the hydrogen minority regime in deuterium majority plasma, differ from the simulations results for NSTX/NSTX-U and DIII-D, which operate in the mid/high ICRH harmonic regime [IS-23].

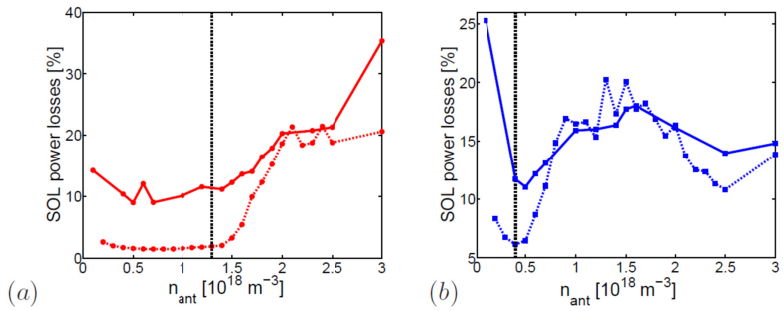

Figure IS-WHCD-2: *Fraction of power lost to the SOL as a function of the density in front of the antenna, comparing the 3D AORSA runs (solid curves) where the antenna spectrum has been reconstructed for $-40 \leq n_\phi \leq 40$ and the single toroidal mode runs (dashed curves) $n_\phi = -21$ (a) and $n_\phi = -12$ (b) corresponding to the dominant mode of the antenna spectrum for -150◦ and -90◦ phasing between antenna straps, respectively. The vertical lines represent the value of the density for which the FW are propagating wave in the SOL.*

Helicon wave simulation in collaboration with RF SciDAC and DIII-D

Recent efforts have shown that helicon waves (fast waves at > $20\omega_{ci}$) may be an attractive option for driving efficient off-axis current drive during non-inductive tokamak operation for DIII-D, ITER and DEMO [IS-24]. For DIII-D scenarios, the ray tracing code, GENRAY, has been extensively used to study helicon current drive efficiency and location as a function of many plasma parameters [IS-24]. The full wave code, AORSA, which is applicable to arbitrary Larmor radius and can resolve arbitrary ion cyclotron harmonic order, has been recently used to validate the ray tracing technique at these high cyclotron harmonics [IS-25]. If the SOL is ignored, the GENRAY and AORSA calculated current drive profiles are comparable for the envisioned high beta advanced scenarios for DIII-D, where there is high single pass absorption due to electron Landau damping and minimal ion damping [IS-26]. These AORSA simulations are extremely difficult in the helicon regime due to: (i) very large numerical grids required (short λ) (ii) very high harmonic IC resonances in the plasma. However, AORSA calculations of helicon waves have also been extended to include the SOL for the first time, where possible SOL effects are highlighted [IS-21]. Figure IS-WHCD-3 shows the total electric field magnitude for Helicon case in DIII-D with $\omega/2\pi = 476$ MHz, $n_\phi = -94$ (corresponding to $N_{||} = -4$) and different values of the density in front of the antenna (n_{ant}) shown in the plots. These initial results show a behavior/trend of the electric field in the SOL similar to NSTX/NSTX-U/DIII-D results [IS-15, 21]. Initial estimates of the fraction of power absorbed to the SOL indicate larger SOL losses when waves can propagate in the SOL as found previously. Work is still underway / in progress in order to quantify the RF SOL losses and the antenna-plasma loading. This work is done in collaboration with E. F. Jaeger (XCEL), C. Lau (ORNL), D. Green (ORNL), R. Pinsker and R. Prater (DIII-D).

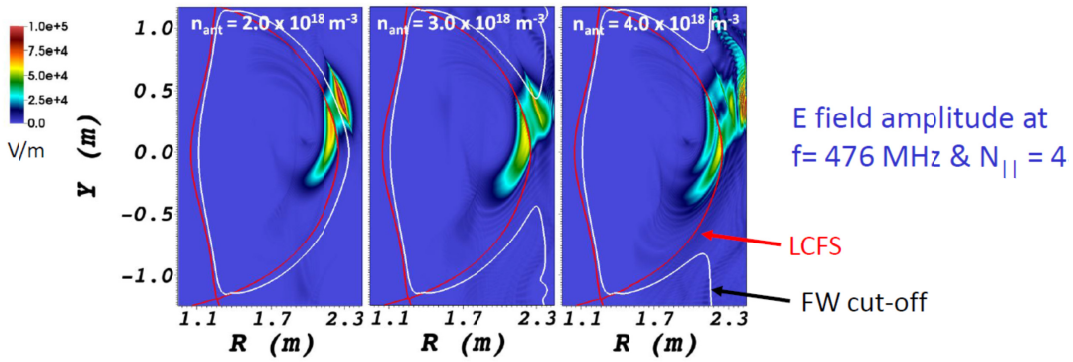

Figure IS-WHCD-3: *Total electric field amplitude for different density values in front of the antenna (n_{ant}) (shown in the plots) with toroidal mode numbers $n_\phi = -94$ ($N_{||} = -4$) and $\omega/2\pi = 476$ MHz for a DIII-D helicon case. The white and red curves indicate the FWcut-off layer and the LCFS, respectively.*

Benchmark activity of ICRF full-wave codes with EUROfusion WPCD & US code AORSA

A detailed comparison between four European ICRH full-wave codes, namely CYRANO [IS-27], EVE [IS-28], LION [IS-29], and TORIC v.6 [IS-30] together with U.S. code AORSA [IS-18] have been performed for ICRF-heating scenarios foreseen in ITER [IS-31, 32]. Two main operational phases are foreseen in ITER. In the first, called non-activated (half-field, ≈ 2.65T on axis) phase, the main ion species is He4. In the second phase, called activated (only at full-field, ≈ 5.3T on axis), the main ion species are D and T. The ICRF system can operate with frequencies ranging from ≈ 40 MHz up to ≈ 55 MHz allowing to have $2f_{He4}$ (≈ 40 MHz for the half-field phase) and $2f_T$ (≈ 53 MHz for the full-field phase) in the plasma core. In both scenarios, we have performed several parameter scans:

- 10 values of the minority concentration starting from 2% up to 20%. Especially in the case of He3 in ITER, it sounds economically unrealistic to have the minority concentration above a few percent, but it is useful to extend it to test the transition from minority heating to mode conversion regimes.
- The electron temperature (T_e) which is halved and doubled. This is useful to test the electron Landau and transit-time magnetic pumping (TTMP) damping.
- The ion temperature (T_i) of He4 and T, respectively, are also halved and doubled to test the IC harmonic calculations.
- The toroidal wavenumber is scanned and has strong impact on wave propagation and absorption
- The frequency is varied to have IC resonance both on LFS (close to magnetic axis) and HFS.

Figure IS-WHCD-4 shows the power repartition as function of H concentration for the nominal plasma profiles in the case of circular and elliptic equilibria. The higher minority absorption and the lower electron absorption in elliptic w.r.t. the circular equilibrium, is likely due to the larger volume due to ellipticity. These two cases are representative of the quality of the agreement so far achieved: The trends with the minority concentration predicted by the five codes agree reasonably well and the agreement improves for those cases characterized by low electron absorption. In

particular, the effect of electron absorption is clear in figure IS-WHCD-5 which shows the power repartition for the circular equilibrium case with halved (left) and doubled (right) T_e.

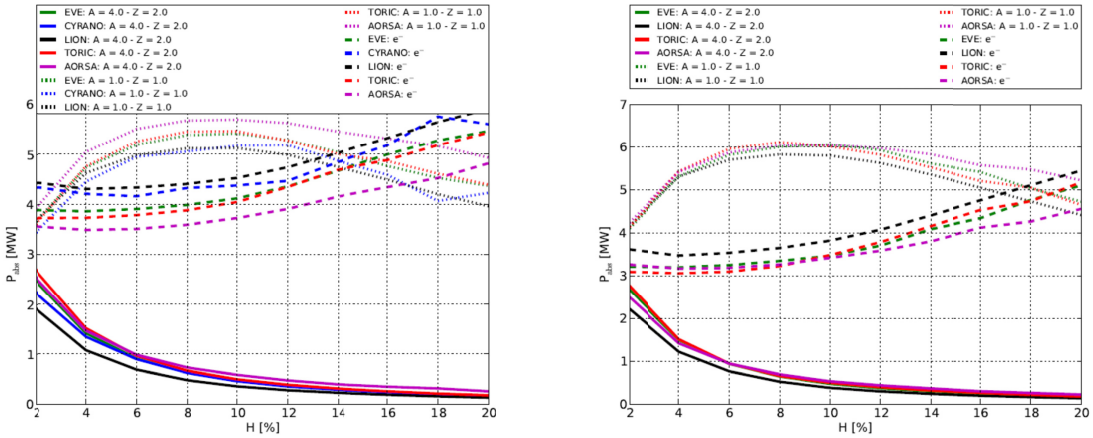

Figure IS-WHCD-4: *Power repartition for the first ten time slices of circular (left) and elliptic (right) cases.*

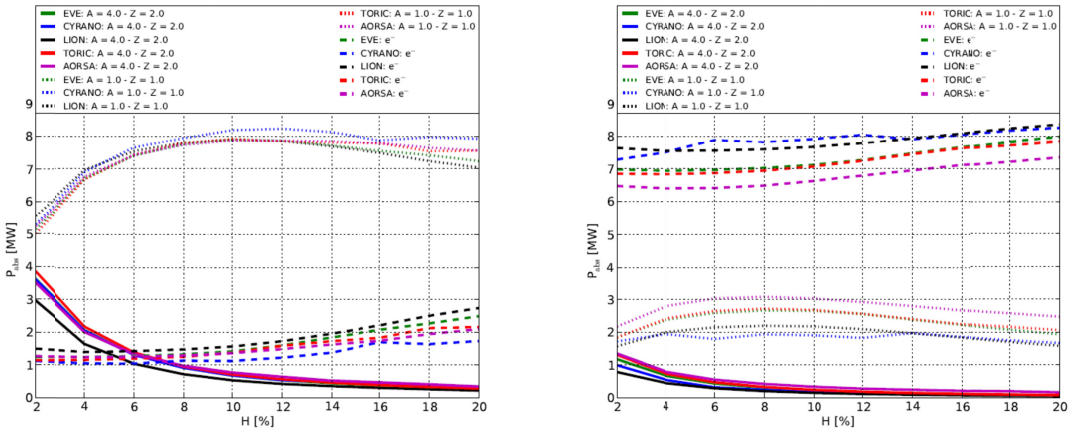

Figure IS-WHCD-5: *Power repartition of the circular case for halved (left) and doubled (right) T_e.*

6. Start-up & Ramp-up Modeling with HHFW and ECH/EBW

A major challenge for ST development is to start-up and ramp-up the plasma current without using a central solenoid. A megawatt-level 28 GHz electron cyclotron (EC) heating system [IS-33] is planned to be operational in 2017-18 and is predicted to heat the initial plasma to $T_e = 400$ eV. HHFW heating will then be added to increase $T_e \sim 1$ keV, and to ramp I_p to 400-500 kA in order to provide enough current to confine fast ions from NBI.

Modeling that combines TRANSP with TORIC or GENRAY demonstrate certain synergisms between the existing HHFW system and the proposed EC system during start-up. These simulations are presented in the Advanced Scenarios section. The results suggest, among other things, that start-up should begin using longer wavelength FW antenna phasing during the EC pre-heating to maximize electron heating and then transitioning to shorter wavelength phasing to reduce fast ion absorption and to maximize electron absorption [IS-34, 35].

4. Collaborations Relevant to RF Research on NSTX-U

Long-Pulse ICRH Heating for KSTAR and EAST

Studies of FW power loss to the SOL are being extended to KSTAR and EAST for the minority-heating regime due to their implications for high-power long-pulse operation in ITER. In an ICRF experiment on KSTAR [IS-36], significant core heating was observed with a coupling efficiency of ~67% at a 600 kW ICRF power level; a follow-on XP is planned for September 2015 to increase the power level. For EAST, stored energy analysis indicates that only ~20% of the ICRH power is heating the core plasma. Proposals for increasing the coupled power include improving RF feedthrough design and slotting the antenna sidewalls and septa, both of which have been explored at PPPL using the QuickField and Microwave Studio codes respectively. Also, two experimental proposals for the EAST ICRF system, "Partition of ICRH power absorption as a function of T_e / T_i" and "Interactions of Fast Waves with the SOL Plasma," have been drafted and will be submitted for the upcoming physics campaign and would complement experiments planned on NSTX-U.

Long-Pulse ECRH Heating and Current-Drive for KSTAR

In an experiment conducted on KSTAR [IS-37], initial ECH beam steering results were obtained to begin the development of feedback tracking and stabilization of NTMs. N. Bertelli implemented the TORBEAM code for placing the ECH beam deposition at the NTM surface. This effort was reported on at the KSTAR Conference in February 2015 [IS-38], and a follow-on XP will be performed in September 2015. Also, PPPL engineering has designed and fabricated a fixed water-cooled steady-state mirror for the existing ECH launcher and has undertaken the conceptual design of an advanced steady-state water-cooled two-channel 2 MW ECH launcher to support the increase of ECH power delivered to KSTAR for NTM stabilization [IS-39].

Other Collaborations

Data processing for the C-Mod Chromex spectrometer for Mo I lines in the spectral window 375 – 395 nm has been done to produce the time-dependence of the Mo I line brightness, which could be a convenient tool for erosion studies. This type of analysis might be important for NSTX-U in understanding erosion of antenna components at higher NBI power.

R. J. Perkins attended the UCLA Basic Plasma Science User Group Meeting and presented a brief talk on the potential impact of RF rectification on SOL losses NSTX (see Ongoing Analysis section above). A white paper is being drafting to propose an experiment on the UCLA Large Plasma Device (LAPD) to study the heat flux to a divertor-like surface in the presence of RF fields.

C. Advanced Scenarios and Control TSG Research Highlights

1. Developing the Plasma Scenarios for the Center-Stack Upgrade KPP

Inductive startup scenario development for NSTX-U

The process for inductive startup of the plasma discharge on NSTX-U required development beyond the startup scenarios used in NSTX due to the fact that the flux and vertical fringe field from the ohmic solenoid is about three times larger, the initial plasma must form at larger major radius and the induced currents in the vessel structures are different. In FY15, a time-dependent magnetic field model (LRDFIT) was employed to develop initial scenarios for plasma startup on NSTX-U and one of the scenarios was successfully used to produce the test plasma that satisfied the CD-4 construction milestone.

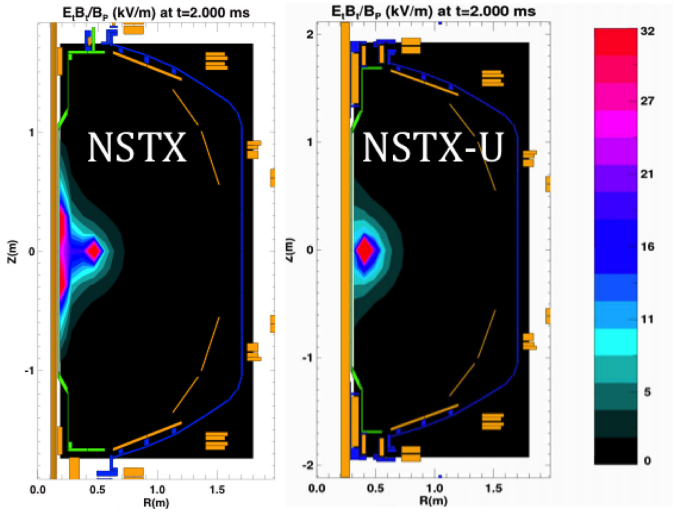

Figure IS-ASC-1: *Lloyd parameter calculated using LRDFIT at +2 ms. NSTX on left, NSTX-U with 0.5T and OH precharge of 8.1 kA and V_{loop} = 4.2V on right.*

On NSTX and NSTX-U the ohmic solenoid is "pre-charged" with positive current that produces a fringe field inside the vacuum vessel. The PF3U and PF3L are also initially pre-charged with positive current in order to cancel (i.e. null) the vertical field near the centerstack inside the vacuum vessel. At the desired breakdown time, an ionized gas is introduced to the vessel by filling the vessel with gas and pulsing a radio frequency antenna. Concurrently, the ohmic solenoid and PF3 coil currents are ramped toward negative current in order to provide a loop voltage across the ionized gas within the magnetic field null. This loop voltage also induces currents in the vessel structure that contribute to the poloidal magnetic field. After a plasma is formed, the confining vertical field is increased by energizing the PF5 coils and continuing to ramp the PF3 coils. The solenoid current continues to ramp toward negative current to provide the loop voltage necessary to increase the plasma current.

LRDFIT is a time-dependent calculation that includes a vessel circuit model and can be used to compute the vacuum magnetic fields. LRDFIT modeling of a typical NSTX startup scenario confirmed that the largest values of the Lloyd parameter (where $E_tB_t/|B_p|$ is a metric for tokamak startup) did correspond to the observed timing and location of the initial breakdown. The calculations also confirmed that the evolution of the fields after breakdown satisfied intrinsic vertical and radial equilibrium and stability for a typical range of plasma currents and boundaries. This result provided confidence that LRDFIT calculations are a suitable tool for developing NSTX-U startup scenarios.

The first scenario developed used the same TF, PF3 and PF5 coil currents from NSTX and modified only the ohmic solenoid current. This required the solenoid precharge current be reduced from 24 kA to 8.1 kA. The modeling suggested that about twice the loop voltage (4.2 V) would be needed at breakdown to match the magnitude of the Lloyd parameter on NSTX due to the increase in the major radius of the breakdown location. Figure IS-ASC-1 compares the Lloyd parameter for the NSTX and NSTX-U scenario at +2 ms, which is the time when the volume-averaged Lloyd parameter is a maximum.

The second scenario investigated using LRDFIT examined the field evolution when starting with a 24 kA precharge in the ohmic solenoid at half toroidal field (B_t = 0.5T). This scenario is required to take advantage of the available volt-seconds required for long pulse discharges on NSTX-U. The calculations identified a viable scenario and some potential challenges with larger fringe field from the ohmic solenoid. The first challenge is that the field null will have a smaller vertical and radial extent, possibly increasing the loop voltage requirements at breakdown. The second challenge is that the relative contribution of the PF3 and PF5 coils compared to the fringe field is small for the initial plasma current ramp to about 100 kA. Consequently, the intrinsic vertical and radial stability is largely determined by the details of the solenoid fringe field and fields due to induced currents in the conducting vessel structures. These fields are significantly more difficult to independently control and optimize than the PF coil currents. These results motivated the development of an XMP for determining the free parameters of a model that could be used to design a startup scenario at arbitrary ohmic pre-charge.

XMP-100 and XMP-131: Initial plasma operation on NSTX-U

Completion of NSTX-Upgrade construction required two operational milestones in order to demonstrate critical components were operational: firing the new neutral beam systems into the vessel armor and forming a test plasma with a plasma current (I_P) exceeding 50kA with a toroidal magnetic field greater than 0.1T. XMP-100 ("Demonstration plasma for CD-4") was completed on August 10, 2015 and satisfied the test plasma milestone by producing a plasma exceeding 100kA with a toroidal field exceeding 0.45T after eleven plasma attempts. XMP-131 ("Increasing the CD-4 I_P") was executed in the two days following XMP-100 and achieved modest improvements in the maximum I_P and duration of the discharge over sixteen plasma discharges.

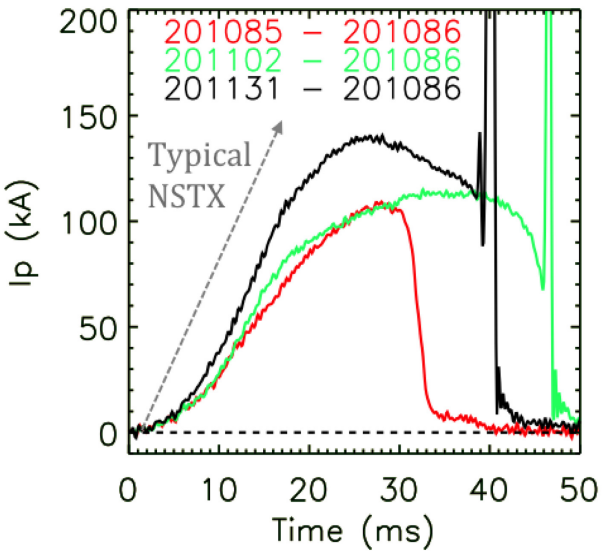

Figure IS-ASC-1*: Plasma current for three discharges during XMP-100 and XMP-131 on NSTX-U. A typical I_p rise in NSTX with well-conditioned walls is shown in gray.*

Figure IS-ASC-2 shows the plasma current from three representative discharges: 201085 (red) was the official CD-4 discharge produced by XMP-100, 201102 (green) was the longest discharge and 201131 (black) was the discharge that achieved the maximum I_P of about 140kA during XMP-131. The I_p was calculated in all three discharges by subtracting a vacuum reference discharge (201086) with the same ohmic current evolution. The plasma current was also in good agreement with the I_P determined using magnetic reconstructions.

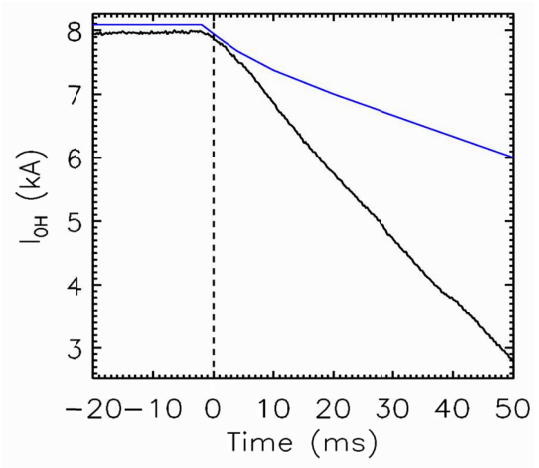

Figure IS-ASC-2: *Ohmic solenoid current for discharges with I_p > 100 kA (black) compared to LRDFIT model scenario (blue).*

The eleven plasma discharge attempts in XMP-100 saw continued improvement in the maximum I_P achieved with each new shot. The largest change made between each shot was in the ohmic solenoid current in order to alter the timing of breakdown and the loop voltage applied after breakdown. Figure IS-ASC-3 shows the ohmic solenoid current for discharge 201085 (and all 16 discharges in XMP-131) compared to the target developed using the LRDFIT modeling described earlier (blue line). One difference is that the ohmic current before +2ms found in the experiment to form a magnetic field null at the correct time and location was about 50 to 100A lower than the model target, suggesting the model slightly underestimated the magnitude of the solenoid fringe field or overestimated the magnitude of the currents induced in the vessel structure. Nevertheless, the model was sufficiently accurate to enable achieving breakdown and the CD-4 target in relatively few shots.

The second difference between experiment and the model is the current ramp is faster after +2 ms in the experiment compared to the target. This is due to the fact that the calculations used assumptions valid for typical wall conditions in NSTX. With these assumptions, it is predicted that after breakdown the loop voltage should be reduced to about 2.5V to achieve the desired I_p ramp rate. However, the initial operations on NSTX-U were performed prior to

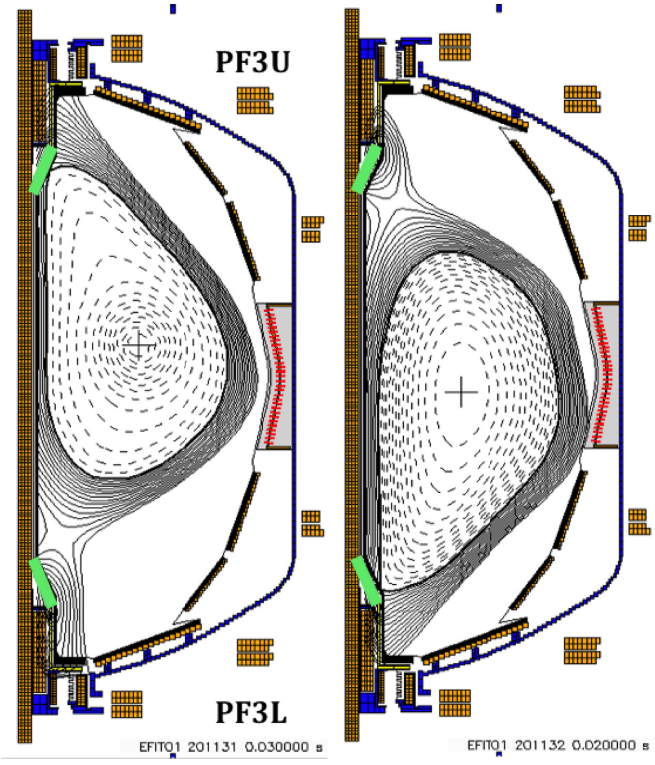

Figure IS-ASC-4: *Magnetic equilibrium reconstruction of 201131 (left) and 201132 (right) when I_p = 120 – 140 kA.*

bake-out and boronization, meaning the plasma impurity content (especially oxygen) and wall outgassing was larger than normal operations. As expected, this increased the required loop voltage to achieve the desired I_p ramp rate by about a factor of two (4.5 – 5 V).

The large loop voltage after breakdown drove significant currents in the NSTX-U vessel structure that made intrinsic vertical stability a challenge when the plasma currents exceed 100 kA. This is illustrated in figure IS-ASC-4, showing the magnetic reconstructions of two discharges near the time of maximum I_p. The large eddy currents in the centerstack "crowns" (green blocks) cause the plasmas to contact the crowns instead of limiting on the centerstack. The PF3U current is 3% larger (more negative) for the discharge in the right panel compared to the left, which leads to the plasma being slightly centered below the midplane and contacting the lower crown.

The goal of XMP-131 was to increase I_p above 100 kA by improving the intrinsic vertical stability and/or reducing the required loop voltage. The intrinsic vertical stability was improved through changes in the balance between the PF3U and PF3L currents, and by reducing the current in PF5. The plasma became more centered in the vessel when the current request for PF3L was larger than PF3U due to sutble differences in the current feedback control of the two coils. The reduction in PF5 increased the plasma volume and the vacuum field index. These changes lead to modest improvements in the maximum I_p and lengthed the discharge (see 201102 in figure IS-ASC-2). The prefill gas fueling was reduced for the last few shots of XMP-131 and the I_p ramp increased, presenting a path forward for reducing V_{loop} (see 201131 in figure IS-ASC-2), although this step was not attempted before the brief startup period ended. These efforts will resume following bake-out and boronization when it is expected that the loop voltage requirements will be significantly reduced with better wall conditions.

2. Experimental Proposals for the FY-16 Run

The Advanced Scenarios and Control topical science group will dedicate a significant amount of run time in the inaugural FY16 campaign to commission control tools that were altered or improved from the NSTX control system due to the new configuration and capabilities of NSTX-U (for example, new PF coils and a 2nd neutral beam). A number of the planned experiments have experimental machine proposals (XMPs) that precede the experiment in order to test the functionality of the control software. Some dedicated time will be spent this run campaign toward experiments that enable new control capabilities for future years, such as current profile control, disruption avoidance and automated plasma ramp down. In addition to control development, significant resources will be dedicated to the TSG mission of demonstrating fully non-inductive operation and stationary long-pulse inductive discharge scenarios. The TSG has emphasized that each experiment proposal develop and demonstrate a connection to testable theories and modeling.

The following experimental proposals have ASC Priority-1 run time planned for the FY16 run, with a number of the proposals approved for operation having completed group and team reviews.

Optimization of vertical control algorithm
XP-1501
Run time: 1 day during first four run weeks
Milestone: R16-3
Status: Completed team and group review

This experiment will determine the plasma elongation limit imposed by vertical stability as a function of the plasma inductance (l_i) and identify limitations in the active vertical control system on NSTX-U. The second half of the experiment will use the previous results coupled with control models to examine the expansion of the elongation limits as a result control model development and optimization.

Tuning of the Automated Rampdown Software
XP-1502
Run time: 0.5 day during first four run weeks
Milestone: JRT2016
Status: Not reviewed

This experiment will make progress in optimizing the free parameters in the disruption detection and automated plasma rampdown software in the plasma control system. Disruption avoidance will be critical in future years as NSTX-U increases its operating envelope.

X-point control integration with shape control
XP-1503
Run time: 1 day during first four run weeks
Milestones: R16-1, R16-3
Status: Completed team and group review

This experiment will test the functionality of controlling the locations of the upper and lower x-point position using the upgraded set of poloidal field coils. Verification of acceptable x-point control is an essential first step toward implementing full plasma shape control capabilities such as advanced magnetic divertor geometries.

Beam power and beta-N control
XP-1504
Run time: 0.5 day during first eight run weeks
Milestones: R16-1, R16-2, R16-3
Status: Completed team and group review

This experiment demonstrates expanded capability to control the timing of the neutral beam injection within the plasma control system to deliver a requested heating power or achieve a particular beta-N.

Maximizing the non-inductive current fraction in NSTX-U H-modes
XP-1507
Run time: 2 days throughout FY16 run
Milestones: R16-2, R16-3, R17-4
Status: Completed team and group review

A primary justification for the upgrade is to operate with 100% non-inductive current drive. Global plasma models provide guidance for the non-inductive plasma current expected for a given toroidal field (TF) and confinement assumptions. This experiment will assess those predictions against the available TF operating space.

Controlled Snowflake Studies
XP-1508
Run time: 2 days throughout FY16 run
Milestones: R16-3, R17-1
Status: Completed team and group review

This experiment will test the functionality of the control of a second x-point near the primary x-point (ie the snowflake divertor) in both the upper and lower-single null configuration. This control capability includes the distance and relative angle separating the x-points, as well as the position of the primary x-point. The goal is to optimize the free parameters of the control algorithm, however the experiment will also contribute the documentation of the impact of the snowflake configuration on the plasma boundary and divertor conditions.

Combined betaN and li feedback control
XP-1509
Run time: 0.75 – 1.25 days throughout FY16 run
Milestones: R16-2, R16-3
Status: Completed team and group review

Simultaneous control of beta-N and li enables safe operation near stability boundaries and experiments where other parameters are varied at fixed betaN and/or li. This experiment will gather a dataset needed to inform model-based control algorithms under development. Plasma current, total and individual beam powers, and mid-plane outer gap size will be considered as actuators. Results will be compared to predictions of closed loop TRANSP simulations to verify the predictive capability of these simulations.

Develop long pulse H-mode for NSTX-U
XP # not assigned
Run time: 1 day near the end of FY16 run
Milestones: R16-1, R16-3
Status: Not reviewed

The goal of the experiment is to make the longest possible H-mode plasma (> 4.5 seconds). This requires scenario development within the constraints of coil heating and neutral beam operation, development of stable plasma shape control through the full swing of the ohmic fringe field, and integrating tools and scenarios that provide adequate MHD stability, particle control, and impurity control.

NB sustainment
XP # not assigned
Run time: 0.5 day near the end of FY16 run
Milestones: R16-2, R17-4
Status: Not reviewed

Following the demonstration of a nearly non-inductive scenario, the time when the flux from the ohmic solenoid is near zero will be moved earlier during the plasma current ramp-up. Neutral beam injection will be varied during the plasma current ramp to compare to model predictions of fully non-inductive operation on NSTX-U.

Current profile controllability scoping study
XP # not assigned
Run time: 0.75 day near the end of FY16 run
Milestones: R16-2, R16-3, R17-4, R18-2
Status: Not reviewed

The goal of this XP is generate data to validate models of the current profile evolution that will be used for designing current profile feedback control algorithms. Actuator modulations (individual beams, outer-gap size, density) will be done in several shots to assess the current profile dynamic response to these changes and the effect of beam pulse-width modulation. Variations in actuator trajectories during the ramp-up will also be done to assess controllability and the applicability of TRANSP and control-oriented reduced models to this phase of the discharge.

Second priority experiments for the FY16 runs are “Closed Loop Density Feedback” aimed at developing active feedback on the plasma density, “Rotation Control” aimed at using neutral beam and 3D fields as actuators to actively control the plasma rotation and, “Reversed Shear Plasma with Relaxed Profiles” that aims to increase the period of reversed shear profiles in NSTX-U via scenario development and control tools.

3. Control and Scenario Modeling

Non-inductive Startup Modeling

Time-dependent, free-boundary calculations have been run with TRANSP to characterize the non-inductive ramp-up phase and the access to sustained fully non-inductive current in the flattop [IS-35].

The simulations use an inductive, 300 kA plasma target plasma as an initial condition and explore how High Harmonic Fast Waves (HHFW) and Neutral Beam Injection (NBI), or a combination of them, affect the scenario.

Simulations indicate that:

(1) NBI alone cannot replace the inductive current after startup, because of the large shine-thru at low density plasma. The beam steering combination and energy affect only marginally the non-inductive driven current, indicating that an additional source is needed to prepare a target plasma for NBI with minimal losses.

(2) HHFW can provide the needed current provided good wave coupling in ensured. In practice, this means that - with standard antenna phasing – a level of 4 MW absorbed power should be achieved within 50 ms to drive a direct fast wave current of about 350 kA.

(3) An interesting synergy is observed between Electron Cyclotron waves and HHFW. At the lowest HHFW phasing the fast wave current drive efficiency is maximized and the minimum HHFW power required is significantly reduced. With 1 MW of EC heating, as planned on NSTX-U, as little of 1 MW of HHFW would be needed to be coupled to the startup plasma in order to drive 300 kA of plasma current.

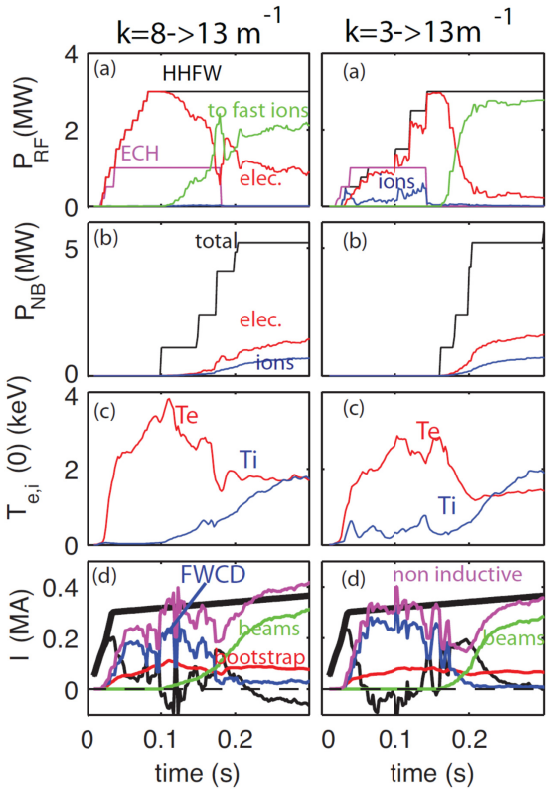

Figure IS-ASC-5: *Simulations with EC, HHFW and NBI at start-up for a dynamic change of phasing in the antenna: transition from $k_{//}$=8 m^{-1} to $k_{//}$=13 m^{-1} at t=0.18 s (left) and from from $k_{//}$=3 m^{-1} to $k_{//}$=8 m^{-1} at 0.14 s (right). (a) EC waveform (magenta), HHFW injected power and power absorbed to the electrons (red), to the ions (blue) and to the fast ions (green). (b) Neutral Beam injected (black) power, and absorbed by the electrons (red) and by the ions (blue). (c) Central value of electron and ion temperature. (d) current waveform (thick black) and contributions: FWCD (blue), beam current (green), ohmic (black) and bootstrap (red), the total non-inductive current is also shown for comparison (magenta).*

The path to fully non-inductive ramp-up on NSTX-U should include all three sources: the EC to pre-heat the CHI start-up plasma, the HHFW to maximize non-inductive current at low density and NBI to ramp-up the current after the L-H transition, when the current drive efficiency of the HHFW is reduced. Simulations indicate that, if the HHFW antenna phasing is changed dynamically, NSTX-U will benefit from the synergy with EC at startup to maximize the direct current and from reduced fast ion absorption later (see Figure IS-ASC-5). This would provide a smooth transition between the non-inductive startup and the NBI driven phase.

Control Modeling with TRANSP

PPPL Control Modeling

Closed loop simulations of control algorithms with the integrated modeling code TRANSP continue to serve as a tool for design and testing of control algorithms planned for NSTX-U. The capability of conducting closed loop simulations was first added to the TRANSP code last year, and work continues on developing the framework. The approach relies on the "Expert file" mechanism, which allows custom run specific code to be injected into the production TRANSP code. Development efforts have made the control framework more flexible, modular, and user-friendly, which will facilitate wider application and the addition of more capabilities. In modularizing the framework, efforts have been made to mirror the structure of the NSTX-U Plasma Control System (PCS) software, to maximize the framework's utility for tuning PCS parameters and for testing proposed PCS modifications.

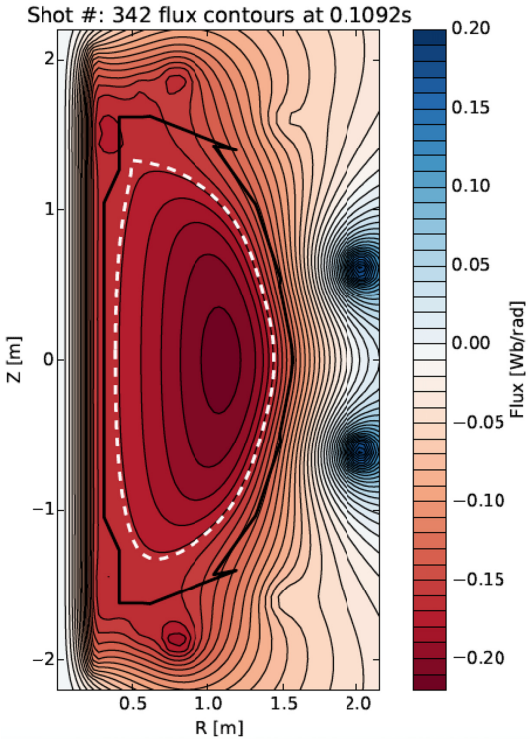

Figure IS-ASC-6: *rtEFIT calculation of an NSTX-U equilibrium. The calculation is constrained by magnetic field "measurements" taken from TRANSP calculations*

Control simulations in TRANSP have begun to fully exploit the capabilities of ISOLVER, TRANSP's free-boundary equilibrium solver, by including the coupled evolution of coils and conducting structures of the vessel in the plasma equilibrium calculation. Based around this capability, a new module is in development to allow feedback control of the coils that determine the plasma shape in TRANSP, adding another important axisymmetric control problem to the list of problems that can be studied with TRANSP. The full set of NSTX-U magnetic diagnostics that are used for axisymmetric control have been included in ISOLVER, allowing synthetic diagnostics to be obtained from predictive TRANSP runs. These synthetic diagnostics have been used for stand-alone verification of updates and improvements to rtEFIT (the real-time equilibrium reconstruction code in the PCS, see Figure

IS-ASC-6) and ISOFLUX (the real-time shape control algorithm in the PCS). In addition, a set of scripts have been developed that use the ISOLVER equilibrium solver to generate control-oriented models of the evolution of the plasma equilibrium, based around the results of a predictive TRANSP run. These models have been used for shape and vertical stability control designs, simplified (faster than TRANSP) simulations, and are planned for use in studying how system parameters (e.g., vertical growth rates) evolve during a discharge to assess controller robustness.

Lehigh University Control Development

New actuators and diagnostics capabilities planned for NSTX-U will enable the control and optimization of the current profile in a way that was not possible with NSTX. In order to make use of these new capabilities to their fullest, new control algorithms are needed to manipulate not only the bulk plasma properties but also the plasma profiles by synergistically combining diagnostics and actuators. The objective of the work currently carried out by members of the Lehigh University Plasma Control Group is to understand the current profile dynamics in NSTX-U and to develop current-profile control algorithms that enable the efficient and optimal use of actuators and diagnostics by using modern model-based control approaches.

Motivated by the coupled, nonlinear, multivariable, distributed-parameter plasma dynamics, the first step towards current-profile control design has been the development of a physics-based, control-oriented model for the current profile evolution in response to non-inductive current drives and heating systems. For this purpose, the nonlinear magnetic-diffusion equation has been coupled with empirical models for the electron density, electron temperature, and non-inductive current drives (neutral beams). The resulting first-principles-driven, control-oriented model has been tailored to NSTX-U based on TRANSP predictive simulations [IS-40]. As NSTX-U starts operation, further refinement of this model is expected based on TRANSP analysis simulations.

A feedforward + feedback control scheme for the regulation of the current profile has been constructed by embedding the proposed nonlinear, physics-based model into the control design process. Firstly, nonlinear optimization techniques have been used to design feedforward actuator trajectories that steer the plasma to a desired operating state with the objective of supporting the traditional trial-and-error experimental process of advanced scenario planning. Experimental testing of these optimal feedforward control laws has been proposed at the 2016 NSTX-U Research Forum. The experiment will allow not only to evaluate the performance of the proposed feedforward controllers but also to validate the control-oriented models for current, temperature and density profile evolution used for control synthesis. The evaluation of control feasibility through use of feedforward trajectories and the validation of the control-oriented models are both key prerequisites for the next step, which is to implement a feedback controller to regulate the safety factor profile around a desired target. Moreover, the experiment will assess the potential of model-based optimal feedforward profile control as a systematic approach for scenario planning in NSTX-U. Secondly, a time-variant, linear-quadratic-integral, optimal, feedback controller capable of regulating the safety factor profile around a desired target profile while rejecting disturbances [IS-41] has been developed with the goal of adding robustness to the overall control

scheme. Neutral beam injectors and the total plasma current are used as actuators to shape the current profile. The effectiveness of the proposed controller in regulating the safety factor profile in NSTX-U has been demonstrated via closed-loop predictive simulations based first on the developed nonlinear response model [IS-42] and later on TRANSP [IS-43]. This latter simulation work, which is still on progress, exploits the availability of the recently developed TRANSP's capability of integrating closed-loop control algorithms and represents the last simulation stage before experimental implementation and testing.

Figure IS-ASC-7 shows initial results from a recent closed-loop iota-profile control simulation in TRANSP. The goal is to track a target state trajectory after the feedback controller is turned on at 1 s., while rejecting perturbed initial conditions and constant input disturbances. Further modeling work based on new NSTX-U data followed by control re-design and TRANSP-based closed-loop simulation studies (including implementation of more sophisticated feedback control algorithms) are planned for the upcoming year.

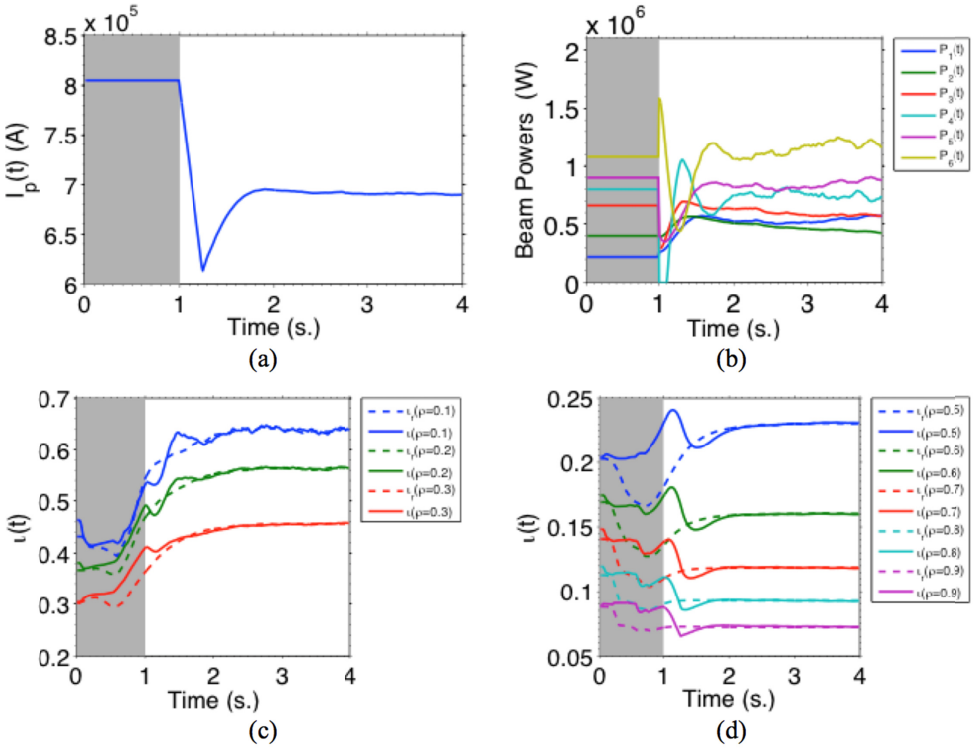

Figure IS-ASC-7: *Feedback control simulation results from TRANSP: (a) plasma current, (b) beam powers, (c)-(d): actual (solid) and target (dashed) iota profile at selected spatial locations. The controller is off in the grey region.*

References

[IS-1] F. Ebrahimi and R. Raman, PRL, **114**, (205003), 2015.

[IS-2] This work appeared on:
https://www.iter.org/whatsnew/2015/06/08
http://www.sciencedaily.com/releases/2015/06/150601172838.htm
http://www.innovation-america.org/print/1760
http://science.energy.gov/news/science-headlines

[IS-3] F. Ebrahimi et al. Phys. Plasmas **20**, (090702) 2013.

[IS-4] F. Ebrahimi et al. Phys. Plasmas **21**, (056109), 2014.2

[IS-5] E. B. Hooper, C. R. Sovinec, R. Raman, F. Ebrahimi and J. E. Menard, Phys. Plasmas, **20**, 092510 (2013).

[IS-6] W. Horton, T. Tajima, and K. Kamimura, Phys. Fluids **30**, 3485 (1987).

[IS-7] R. Raman, T. Brown, L.A. El-Guebaly, et al., "Design description for a co-axial helicity injection plasma startup system for a ST-FNSF," Accepted for publication in Fusion Sci. and Technology (2015)

[IS-8] R. Raman and V.F. Shevchenko, "Solenoid-free plasma start-up in spherical tokamaks," Plasma Phys. Controlled Fusion **56** 102001 (October 2014)

[IS-9] J. C. Hosea *et al.*, "High harmonic fast wave heating efficiency enhancement and current drive at longer wavelength on the National Spherical Torus Experiment," *Phys. Plasmas* **15**, 056104 (2008)

[IS-10] R. Ellis, C. Brunkhorst, J. Hosea, "Upgrades to the NSTX HHFW antenna," *AIP Conf. Proc*. **1580**, 350 (2014)

[IS-11] R. J. Perkins, J. C. Hosea, M. A. Jaworski *et al.*, "The contribution of radio-frequency rectification to field-aligned losses of high-harmonic fast wave power to the divertor in the National Spherical Torus eXperiment," *Phys. Plasmas* **22,** 042506 (2015)

[IS-12] C. Lau, J. B. Wilgen, J. B. Caughman *et al.*, "Using X-mode L, R and O-mode reflectometry cutoffs to measure scrape-off-layer density profiles for upgraded ORNL reflectometer on NSTX-U," *Rev. Sci. Instrum.* **85**, 11D815 (2014)

[IS-13] R. J. Perkins, *et al*., "The Potential Contribution of RF Sheaths to Field-Aligned SOL Losses on NSTX." *APS DPP Meeting Abstracts* (2014)

[IS-14] R. J. Perkins *et al.*, "Searching for Enhanced RF Field Amplitudes in the SOL Using a Simplified Cold-Plasma Model," 42nd EPS Conference on Plasma Physics, Lisbon (2015)

[IS-15] N. Bertelli *et al.,* "Full wave simulations of fast wave heating losses in the scrape-off layer of NSTX and NSTX-U," *Nucl. Fusion* **54** 083004 (2014)

[IS-16] R. J. Perkins *et al.*, "High Voltage Test-Stand Research Done on ICRF Antenna Elements of the High-Harmonic Fast-Wave System of NSTX," 21st Topical Conference Radio-Frequency Power in Plasmas, Lake Arrowhead, US (2015)

[IS-17] J. C. Hosea *et al.*, "High Voltage Research on ICRF Antenna Elements and Improved Coupling for ICRF Antennas," JA-EU-US RF Heating Technology Workshop, Tokyo, Japan (2015)

[IS-18] E.F. Jaeger *et al*, *Phys. Plasmas* **8**, 1573 (2001).

[IS-19] D.L. Green et al, *Phys. Rev. Lett.* **107**, 145001 (2011).

[IS-20] C.K. Phillips *et al*, *Nucl. Fusion* **49**, 075015 (2009).
[IS-21] N. Bertelli, Invited talk at the 21st Topical Conference on Radiofrequency Power in Plasmas, UCLA Conference Center at Lake Arrowhead, California, April 27 - 29, 2015. To be published to AIP Conf. Proc. (2015).
[IS-22] C. C. Petty and et al. Nucl. Fusion, 39:1421, 1999.
[IS-23] N. Bertelli et al., 25 IAEA FES Conf. (2014) TH/P4-14.
[IS-24] R. Prater et al, "Application of very high harmonic fast waves for off-axis current drive in DIII-D and FNSF-AT tokamaks", Nuclear Fusion, V.54, No.8, 2014.
[IS-25] C. Lau, E. F. Jaeger, N. Bertelli, et al., 21st Topical Conference on Radiofrequency Power in Plasmas, UCLA Conference Centerat Lake Arrowhead, California, April 27 - 29, 2015. To be published to AIP Conf. Proc. (2015).
[IS-26] R.I. Pinsker, N. Bertelli, et al. , 42nd European Physical Society Conference on Plasma Physics (Lisbon, 22-26 June 2015) P5.107
[IS-27] P.U. Lamalle, PhD thesis - Université de Mons (1994) LPP-ERM/KMS Laboratory Report 101.
[IS-28] R. Dumont, *Nuclear Fusion* **49**, 075033 (2009).
[IS-29] L. Villard, S. Brunner, and J. Vaclavik, *Nuclear Fusion* **35**, 1173 (1995).
[IS-30] M. Brambilla and R. Bilato, *Nuclear Fusion* **46**, S387 (2006).
[IS-31] R. Bilato, N. Bertelli et al, Status of the benchmark activity of ICRF full-wave codes within EUROfusion WPCD and beyond; International Tokamak Physics Activity (ITPA) - Energetic particles physics, 25 March 2015 (Cadarache, France).
[IS-32] R. Bilato, N. Bertelli, et al, 21st Topical Conference on Radiofrequency Power in Plasmas, UCLA Conference Center at Lake Arrowhead, California, April 27 - 29, 2015. To be published to AIP Conf. Proc. (2015).
[IS-33] G. Taylor *et al.*, "A megawatt-level 28 GHz heating system for the National Spherical Torus Experiment Upgrade,**"** EPJ Web of Conferences 87 , 02013 (2014).
[IS-34] G. Taylor *et al.*, "Development of Fully Non-Inductive Plasmas Heated by Medium and High-Harmonic Fast Waves in the National Spherical Torus Experiment Upgrade," 21st Topical Conference Radio-Frequency Power in Plasmas, Lake Arrowhead, US (2015)
[IS-35] F. Poli *et al.*, "Simulations of non-inductive current ramp-up and sustainment in the National Spherical Torus Experiment Upgrade", submitted for publication (2015).
[IS-36] G. Taylor, N. Bertelli, J. C. Hosea, R. Perkins, H. J. Kim, S. J. Wang, B. H. Park, J-G, Kwak, "Edge power deposition during ICRF heating." XP executed on KSTAR
[IS-37] N. Bertelli *et al.*, "Optimization of NTM stabilization by ECCD and ECRH/ECCD efficiency in advanced scenario." XP submitted to KSTAR and combined with other ECH XP's.
[IS-38] M.H.Woo *et al.*, "Current status of MHD mode feedback control system using ECH in KSTAR," KSTAR conference, Daejon, Korea (2015) P1-28
[IS-39] R. Ellis and J. Hosea, "Additive Manufacturing Techniques for ECH Launcher Components," KSTAR Conference, Daejon, Korea (2015).
[IS-40] Z.O. Ilhan, J.E. Barton, W. Shi, E. Schuster, D.A. Gates, S. Gerhardt, E. Kolemen and J. Menard, "Physics-based Control-oriented Modeling of the Current Profile Evolution in NSTX-Upgrade", 55th Division of Plasma Physics (DPP) Annual Meeting of the American Physical Society (APS), Denver, Colorado, USA, November 11-15, 2013.

[IS-41] Z.O. Ilhan, J.E. Barton, W.P. Wehner, E. Schuster, D.A. Gates, S. Gerhardt, E. Kolemen and J. Menard, “First-Principles-Driven Model-Based Optimal Control of the Current Profile in NSTX-U”, 56th Division of Plasma Physics (DPP) Annual Meeting of the American Physical Society (APS), New Orleans, Lousiana, USA, October 27-31, 2014.

[IS-42] Z.O. Ilhan, W. P. Wehner, J. E. Barton, E. Schuster, D.A. Gates, S. Gerhardt and J. Menard, “First-Principles-Driven Model-Based Optimal Control of the Current Profile in NSTX-U”, proceedings of the IEEE Multi-Conference on Systems and Control, Sydney, Australia, September 21-23, 2015.

[IS-43] Z.O. Ilhan, W.P. Wehner, E. Schuster, M.D. Boyer, D.A. Gates, S. Gerhardt and J. Menard, “Performance Assessment of Model-Based Optimal Feedforward and Feedback Current Profile Control in NSTX-U using the TRANSP Code”, 57th Division of Plasma Physics (DPP) Annual Meeting of the American Physical Society (APS), Savannah, Georgia, USA, November 16-20, 2015.

Papers Published by NSTX-U Researchers (Oct. 2014 - Sept. 2015)

1. RAMAN R and Shevchenko VF
   Solenoid-free plasma start-up in spherical tokamaks
   PLASMA PHYS. CONTROLLED FUSION **56** 102001 (October 2014)

2. VAN ECK NJN, Abrams T, van den Berg MA, et al.,
   Operational characteristics of the high flux plasma generator Magnum-PSI
   FUSION ENGINEERING AND DESIGN **89** 2150 (October 2014)

3. MAINGI R,
   Enhanced confinement scenarios without large edge localized modes in tokamaks: control, performance, and extrapolability issues for ITER
   NUCLEAR FUSION **54** 114016 (November 2014)

4. BERKERY JW, Betti R, Sabbagh SA, et al.
   The effect of an anisotropic pressure of thermal particles on resistive wall mode stability
   PHYSICS OF PLASMAS **21** 112505 (November 2014)

5. STAGNER L and Heidbrink WW
   On geometric factors for neutral particle analyzers
   REV. SCI. INSTRUM. **85** 11D803 (November 2014)

6. LUCIA M, Kaita R, Majeski R, et al.,
   Development progress of the Materials Analysis and Particle Probe
   REV. SCI. INSTRUMENTS **85** 11D835 (November 2014)

7. FAUST I and Heidbrink WW
   Two-dimensional AXUV-based radiated power density diagnostics on NSTX-U
   REV. SCI. INSTRUM. **85** 11D856 (November 2014)

8. DELGADO-APARICIO L and Heidbrink WW
   High-resolution tangential absolute extreme ultraviolet arrays for radiated power density measurements on NSTX-U
   REV. SCI. INSTRUM. **85** 11D859 (November 2014)

9. LIU D, Heidbrink WW, Tritz K, et al.,
   Design of solid state neutral particle analyzer array for National Spherical Torus Experiment-Upgrade
   REV. SCI. INSTRUM. **85** 11E105 (November 2014)

10. Bell RE
Development and operation of a high-throughput accurate-wavelength lens-based spectrometer
REV. SCI. INSTRUM. **85** 11E404 (November 2014)

11. RAMAN R, Jarboe TR, Nelson BA, et al.,
Design and operation of a fast electromagnetic inductive massive gas injection valve for NSTX-U
REV. SCI. INSTRUMENTS **85** 11E801 (November 2014)

12. GERHARDT SP, Erickson K, Kaita R, et al.,
Magnetics for equilibrium reconstruction and realtime plasma control in NSTX-Upgrade
REV. SCI. INSTRUMENTS **85** 11E807 (November 2014)

13. MUELLER D, Roquemore AL, Jaworski, M, et al.,
In situ measurement of low-Z material coating thickness on high Z substrate for tokamaks
REV. SCI. INSTRUMENTS **85** 11E821 (November 2014)

14. SCHWARTZ JA, Jaworski MA, Mehl J, et al.,
Electrical detection of liquid lithium leaks from pipes
REV. SCI. INSTRUMENTS **85** 11E824 (November 2014)

15. MENARD JE, Wang Z, Liu Y., et al.,
Rotation and kinetic modifications of the tokamak ideal-wall pressure limit
PHYS. REV. LETT. **113** 255002 (December 2014)

16. AHN J-W, Maingi R, Canik JM, et al.,
Broadening of divertor heat flux profile with increasing number of ELM filaments in NSTX
NUCLEAR FUSION **54** 122004 (December 2014)

17. HAHM TS, Lee J, Wang WX, et al.,
Turbulent equipartition pinch of toroidal momentum in spherical torus
NUCLEAR FUSION **54** 123012 (December 2014)

18. ONO M, Jaworski MA, Kaita R et al.,
Active radiative liquid lithium divertor concept
FUSION ENGINEERING AND DESIGN **89** 2838 (December 2014)

19. ABRAMS, T, Jaworski MA, Kaita R, et al.,
Erosion and re-deposition of lithium coatings on TZM molybdenum and graphite during high-flux plasma bombardment
FUSION ENGINEERING AND DESIGN **89** 2857 (December 2014)

20. FREDRICKSON ED, Taylor G, Bertelli N, et al.,
Suppression of energetic particle driven instabilities with HHFW heating
NUCL. FUSION **55** 013012 (January 2015)

21. LEPSON JK, Beiersdorfer P, Bitter M, et al.
Charge exchange produced emission of carbon in the extreme ultraviolet spectral region
J. PHYS: CONF SER **583** 012012 (January 2015)

22. ONO M and Kaita R
Recent progress on spherical torus research
PHYS. PLASMAS **22** 040501 (April 2015)

23. PERKINS RJ, Hosea JC, Jaworski MA, et al.,
The contribution of radio-frequency rectification to field-aligned losses of high-harmonic fast wave power to the divertor in the National Spherical Torus experiment
PHYS. PLASMAS **22**, 042506 (April 2015)

24. LIU D, Fu G-Y, Crocker NA, et al.,
Hybrid simulation of toroidal Alfvén eigenmode on the National Spherical Torus Experiment
PHYS. PLASMAS **22** 042509 (April 2015)

25. KAITA R, Abrams T, Jaworski M, et al.
Addressing the challenges of plasma-surface interactions in NSTX-U
IEEE TRANS. on PLASMA SCI. **43** 965 (April 2015)

26. EBRAHIMI F and Raman R
Plasmoids formation during co-axial helicity injection experiments in National Spherical Torus Experiment
PHYS. REV. LETT. **114** 205003 (May 2015)

27. SECHREST Y, Smith D, Stotler DP, et al.
Comparison of beam emission spectroscopy and gas puff imaging edge fluctuation measurements in National Spherical Torus Experiment
PHYS. PLASMAS **22** 052310 (May 2015)

28. BOYER, MD, Andre R, Gates DA, et al.
Central safety factor and betan control on NSTX-U via beam power and plasma boundary shape modification, using TRANSP for closed loop simulations
NUCL. FUSION **55** 053033 (May 2015)

29. BELOVA EV, Gorelenkov NN, Fredrickson ED, et al.,
Coupling of Neutral-Beam-Driven Compressional Alfvén Eigenmodes to Kinetic Alfvén Waves in NSTX Tokamak and Energy Channeling
PHYS. REV. LETT. **114** 015001 (July 2015)

30. ONO M, Chrzanoswki J, Dudek L, et al.
Progress towards commissioning and plasma operation in NSTX-U
NUCL. FUSION **55** 073007 (July 2015)

31. NICHOLS JH, Jaworski MA, Kaita R, et al.,
OEDGE modeling of outer wall erosion in NSTX and effect of changes in neutral pressure
J. NUCL. MATERIALS **463** 276 (August 2015)

32. AHN J-W, Maingi R, Canik JM, et al.,
Impact of ELM filaments on divertor heat flux dynamics in NSTX
J. NUCL. MATERIALS **463** 701 (August 2015)

33. STOTLER DP, Scotti F, Bell RE et al.,
Reconstruction of NSTX midplane neutral density profiles from visible imaging data
J. NUCL. MATERIALS **463** 897 (August 2015)

34. MAINGI R, Osborne TH, Bell MG, et al.,
Dependence of recycling and edge profiles on lithium evaporation in high triangularity, high performance NSTX H-mode discharges
J. NUCL. MATERIALS **463** 1134 (August 2015)

35. SCOTTI F, Soukhanovskii VA, Ahn J-W, et al.,
Lithium sputtering from lithium-coated plasma facing components in the NSTX divertor
J. NUCL. MATERIALS **463** 1165 (August 2015)

36. ABRAMS T, Jaworski MA, Kaita R, et al.
Modeling the reduction of gross lithium erosion observed under high-flux deuterium bombardment
J. NUCL. MATERIALS **463** 1169 (August 2015)

37. CAPECE AM, Roszell JP, Skinner CH, et al.,
Effects of temperature and surface contamination on D retention in ultrathin Li films on TZM
J. NUCL. MATERIALS **463** 1177 (August 2015)

38. MEIER ET, Soukhanovskii VA, Bell RE, et al.,
Modeling detachment physics in the NSTX snowflake divertor physics
J. NUCL. MATERIALS **463** 1200 (August 2015)

39. STOTLER D, Scotti F, Bell RE, et al.,
Midplane neutral density profiles in the National Spherical Torus Experiment
PHYS. PLASMAS **22** 082506 (August 2015)

40. KAYE SM, Abrams T, Ahn J-W, et al.
An overview of recent physics results from NSTX
NUCL. FUSION **55** 104002 (October 2015)

Papers Accepted or Submitted for Publication (as of 9/8/15)

Recently Accepted

1. ZWEBEN, S, et al.,
   Edge and SOL Turbulence and Blob Variations over a Large Database in NSTX
   Accepted for publication in NUCL. FUSION (2015)

2. RAMAN R, Brown T, El-Guebaly LA, et al.,
   Design description for a co-axial helicity injection plasma startup system for a ST-FNSF
   Accepted for publication in Fusion Sci. and Technology (2015)

3. RAMAN R, Jarboe TR, Menard JE, et al.,
   Fast time response electromagnetic disruption mitigation concept
   Accepted for publication in Fusion Sci. and Technology (2015)

Submitted

1. SZALKOWSKI GA, Darrow DS and Cecil FE
   Design and construction of Faraday cup ion detectors using thin film deposition
   Submitted to REV. SCI. INSTRUM. (2015)

2. ZWEBEN SJ, Davis WM, Kaye SM, et al.,
   Variations in edge and SOL turbulence in NSTX
   Submitted to NUCL. FUSION (2015)

3. LAZERSON SA, Park J-K, Logan N, et al.
   Numerical optimization of three-dimensional coils for NSTX-U
   Submitted to PLASMA PHYS. CONT. FUSION (2015)

4. POLI FM, et al.
   Simulations of non-inductive current rampup and sustainment in the National Spherical Torus Experiment Upgrade
   Submitted to NUCL. FUSION (2015)

5. MEIER E, et al.,
   Modeling divertor concepts for spherical tokamaks NSTX-U and ST-FNSF
   Submitted to NUCL. FUSION (2015)

6. BERTELLI N, et al.
   Full wave simulations of fast wave efficiency and power losses in the scrape-off layer of tokamak plasmas in mid/high harmonic and minority heating regimes
   Submitted to NUCL. FUSION (2015)

7. PODESTA M, et al.
   Effect of MHD instabilities on neutral beam current drive
   Submitted to NUCL. FUSION (2015)

8. SMITH, D., et al.
   Evolution patterns and parameter regimes in edge localized modes on the National Spherical Torus Experiment
   Submitted to NUCL. Fusion (2015)

9. BANERJEE S, et al.,
   Analysis of turbulence imaging data in NSTX Ohmic plasmas
   Submitted to NUCL. FUSION (2015)

10. MUNOZ BURGOS J, et al.,
    Applications of advanced kinetic collisional radiative modeling and Bremsstrahlung emission to quantitative impurity analysis on NSTX
    Submitted to NUCL. FUSION (2015)

11. WANG W, et al.,
    Distinct Turbulence Sources and Confinement Feature in Spherical Tokamak Plasma Regime
    Submitted to PHYS. REV. LETT. (2015)

12. HEIDBRINK W, et al.,
    Analysis of fast-ion Dα data from the National Spherical Torus Experiment
    Submitted to NUCL. FUSION (2015)

13. WANG W, et al.,
    Identification of new turbulence contributions to plasma transport and confinement in spherical tokamak regime
    Submitted to PHYS. PLASMAS (2015)

14. DARROW D., et al.,
    Optimization of the angular orientation for a fast ion loss detector in a tokamak
    Submitted to REV. SCI. INSTRUMENTS (2015)

15. SCOTTI F, et al.,
    A dual wavelength imaging system for plasma-surface interaction studies on the National Spherical Torus Experiment Upgrade
    Submitted to REV. SCI. INSTRUMENTS (2015)

16. SOUKHANOVSKII V, et al.,
    Developing snowflake divertor physics basis in the DIII-D, NSTX and NSTX-U tokamaks aimed at the divertor power exhaust solution
    Submitted to IEEE TRANS ON PLASMA SCI (2015)

17. RUSSELL D, et al.,
    Modeling the effect of lithium-induced pedestal profiles on scrape-off-layer turbulence and the heat flux width
    Submitted to PHYS. PLASMAS (2015)

18. MUNOZ BURGOS J, et al.,
    Evaluation of thermal helium beam and line-ratio fast diagnostic on NSTX-U
    Submitted to PLASMA PHYS. AND CONT FUSION (2015)

19. BUCHOLTZ R, et al.
Influence of centrifugal effects on particle and momentum transport in NSTX
Submitted to PHYS. PLASMAS (2015)

20. SECHREST Y, et al.,
Cross-diagnostic Characterization of Edge Fluctuations in NSTX
Submitted to PHYS. PLASMAS (2015)

21. DAVIS WM, Tchilinguian GJ, Carroll T, et al.,
Control and data acquisition upgrades for NSTX-U
Submitted to FUSION ENG. and DESIGN (2015)

Invited / Oral Presentations at Scientific Conferences

IAEA Fusion Energy Conference in St. Petersburg, Russian Federation held October 13-18, 2014 (includes NSTX-U researchers working on other/collaborating facilities)

1. "Overview of recent physics results from NSTX" , S. Kaye (PPPL)
2. "Physical Characteristics of Neoclassical Toroidal Viscosity in Tokamaks for Rotation Control and the Evaluation of Plasma Response", S.A. Sabbagh (Columbia University)
3. "Configuration Studies for an ST-Based Fusion Nuclear Science Facility", J.E. Menard (PPPL)
4. "Effects of MHD Instabilities on Neutral Beam Current Drive", M. Podesta (PPPL)
5. "Developing Physics Basis for the Radiative Snowflake Divertor at DIII-D", V. Soukhanovskii (LLNL)
6. "Edge Instability Limiting the Pedestal Growth on Alcator C–Mod Experiment and Modeling", A. Diallo (PPPL)
7. "Burning Plasma Relevant Control Development: Advanced Magnetic Divertor Configurations, Divertor Detachment and Burn Control", E. Kolemen (Princeton University)

Review/invited talks at 56th APS-DPP meeting, New Orleans, LA on Oct. 27-31, 2014

8. Review talk: "Recent progress on spherical torus research and implications for fusion energy development path", M. Ono (PPPL)
9. "Broadening of the divertor heat flux footprint with increasing number of ELM filaments in NSTX", Joon-Wook Ahn (ORNL)
10. "Simulation of 3D effects on partially detached divertor conditions in NSTX and Alcator C-Mod", Jeremy Lore (ORNL)
11. "Drift Kinetic Effects on 3D Plasma Response in High-beta Tokamak Resonant Field Amplification Experiments", Z.R. Wang (PPPL)
12. "Unification of Kinetic Resistive Wall Mode Stabilization Physics in Tokamaks", S.A. Sabbagh (Columbia University)
13. "Energy Channeling and Coupling of Neutral-beam-driven Compressional Alfven Eigenmodes to Kinetic Alfven Waves in NSTX", Elena Belova (PPPL)

Talks at American Nuclear Society 21st Topical Meeting on the Technology of Fusion Energy (TOFE) held November 9-13, 2014, Anaheim, CA

14. "NSTX Upgrade for Establishing Physics and Technology Basis for FNSF", M. Ono (PPPL)
15. "Configuration Studies for an ST-based Fusion Nuclear Science Facility", J. Menard (PPPL)
16. "Engineering Challenges and Opportunities with Liquid Metal Plasma-Facing Components", M. Jaworski (PPPL)

Invited presentations at 21st Topical Conference on RF Power in Plasmas held at Lake Arrowhead, California on April 27- 29, 2015

17. "Effect of the Scrape-Off Layer in AORSA Full Wave Simulations of Fast Wave Minority, Mid/High Harmonic, and Helicon Heating Regimes", N. Bertelli (PPPL)

Oral presentations at 26th IEEE Symposium on Fusion Engineering (SOFE), 5/31-6/4, 2015 in Austin, TX

18. "The NSTX-U Program for Closing Gaps to Fusion Energy", by J. E. Menard (PPPL)
19. "Developing Snowflake Divertor Physics Basis in the DIII-D, NSTX, and NSTX-U Tokamaks Aimed at the Diverter Power Exhaust Solution" by V. A. Soukhanovskii (LLNL)
20. "Prospects for Power and Particle Exhaust with High-Temperature Liquid Lithium Divertors" by M. A. Jaworski (PPPL)
21. "NSTX-U Digital Coil Protection System Integration with Existing Plasma Control System" by K. G. Erickson (PPPL)
22. "NSTX Upgrade Power Supply System" by W. Que (PPPL),
23. "Tensile Strain Mitigation During the NSTX-U OH Coil Cooldown" by P. H. Titus (PPPL)

Oral presentations at 7th IAEA topical meeting on theory of plasma instabilities (March 4-6, Frascati, Italy)

24. "Distinct turbulence sources and confinement feature in spherical tokamak plasma regime", W.X. Wang (PPPL)

Oral presentations at US/EU TTF Workshop held in Salem, MA from 4/28-5/1, 2015

25. "Non-preturbative critical gradient model for Alfvenic fast ion relaxation using HINST code" by N. Gorelenkov (PPPL)
26. "Validation of a new fast ion transport model for TRANSP" by M. Podesta (PPPL)
27. "Physical mechanisms setting the divertor heat-load width seen from the XGC1 gyro kinetic simulations" by S. Ku (PPPL)
28. "Experimental studies of electron-sclae turbulence on NSTX and NSTX-U: present status and future plans" by Y. Ren (PPPL)
29. "Nailing down the bootstrap current physics in steep pedestal plasma from advanced numerical simulation" by R. Hager (PPPL)

Invited oral presentations at IEA Workshop on the Theory and Simulation of Disruptions hosted by PPPL July 13-15, 2015

30. "Tearing Mode Control for ITER" by E. Kolemen (Princeton University)
31. "M3D-C1 Simulation of a NSTX Disruption Induced by Rapid Current Ramp-down" by S. Jardin (PPPL)

32. “Wall Current Calculations for an NSTX VDE” by J. Breslau (PPPL)
33. “Multi-Machine Analysis of Non-Axisymmetric and Rotating Halo Currents” by C. Myers (PPPL)
34. “The Tokamak Density Limit – a Thermo-Resistive Disruption” by D. Gates (PPPL)
35. “Simulation of Radiation Driven Islands at the Density Limit” by D. Brennan
36. “Theory and Modeling Needs For Improved Kinetic Treatments of High-Beta Pressure Limits” by J. Menard (PPPL)
37. “Global MHD Mode Stabilization for Disruption Avoidance in Tokamaks” by S. Sabbagh. (Columbia University)

Oral presentations at 4th International Symposium on Lithium Applications in Fusion Devices (ISLA) held in Granada, Spain from Sept. 28-30, 2015

38. “Liquid lithium applications for solving challenging fusion reactor issues and NSTX-U contributions” by M. Ono (PPPL)
39. “Incremental upgrades toward high-heat flux, liquid lithium PFCs in the NSTX-U” by M.A. Jaworski (PPPL)
40. “Lithium granule ablation and penetration during ELM pacing experiments at DIII-D” by R. Lunsford (PPPL)
41. “The effect of progressively increasing lithium conditioning on edge transport and stability in high triangularity NSTX H-mode discharges” by R. Maingi (PPPL)

Seminars and Colloquia

1. Y. Ren (PPPL) gave a seminar entitled “Recent Progress in Studying High-k Turbulence in NSTX” at ASIPP, Hefei, China on August 5, 2014.

2. M. Ono (PPPL) gave a seminar entitled “NSTX Upgrade for Establishing Physics and Technology Basis for FNSF” at UCLA on November 14, 2014.

3. J. Menard (PPPL) presented “Scientific Opportunities and Challenges in the Upgraded National Spherical Torus Experiment" by at the PPPL Science on Saturday series on March 14, 2015

4. R. Kaita (PPPL) gave a colloquium lecture on fusion energy to science and engineering faculty and STEM (Science, Technology, Engineering, and Mathematics) students at Union University in Jackson, TN on March 19, 2015.

5. R. Maingi (PPPL) presented a guest lecture at Cornell University on the “Principles of Magnetic Fusion and the Plasma-Material Interface” on 4/20/15. The trip was supported by the APS Distinguished Lectures in Plasma Physics program.

6. R. Kaita (PPPL) gave a colloquium lecture on magnetic fusion that included a description of NSTX-U research at Messiah College in Mechanicsburg, PA on April 23.

7. Charles Skinner (PPPL) visited the Yale Climate and Energy Institute, New Haven, CT on April 24th to attend the Conference on Climate Change and the Future of Nuclear Energy and gave a special invited talk on '*Fusion: Energy for the Future*'.

8. J. Menard (PPPL) gave a seminar presentation to NFRI/KSTAR scientists entitled "NSTX-U Research Highlights and Program Status and Plans" following the KSTAR PAC meeting held April 27-29, 2015 at the National Fusion Research Institute (NFRI) in Daejeon, South Korea.

9. J. Menard (PPPL) presented "Confinement And Stability Discoveries From High-Beta Spherical Tori," at the Norman Rostoker Memorial Symposium on August 24, 2015 in Newport Beach, CA

10. R. Maingi (PPPL) presented a colloquium at the Dept. of Physics and Astronomy, West Virginia University on September 3, 2015: "The Benefit of Coating the Plasma Facing Surfaces of Fusion Research Chambers with Low-Atomic-Number Materials in Keeping Plasma Hot, Confined, and Fusing."

11. Devon Battaglia (PPPL) presented "The Mission of NSTX-U Toward the Development of Fusion Energy" at the University of Rochester's Laboratory for Laser Energetics on September 4.

Major Awards by NSTX-U Researchers

- L. Delgado-Aparicio, Early Career Research Award, DOE Office of Science.

Hosted Meetings and Workshops

1. An international TRANSP User's Group meeting organized by S. Kaye was hosted by PPPL on March 23-24, 2015.

2. PPPL hosted the 21st meeting of the ITPA Divertor and Scrape-off Layer Topical Group on June 9-12th, and the meeting was organized by C. Skinner (PPPL)

3. IEA Workshop on the Theory and Simulation of Disruptions hosted by PPPL July 13-15, 2015.

NSTX-U PPPL Employee Leadership in Venues Outside of PPPL

1. Bell, R., Expert, ITPA Diagnostics Topical Group
2. Darrow, D., Chair, ITPA Diagnostics, Fusion Products Working Group
3. Darrow, D., Expert, ITPA Diagnostics Topical Group
4. Diallo, A., Expert, ITPA Pedestal and Edge Physics Topical Group
5. Ferraro, N, Expert, ITPA Pedestal and Edge Physics Topical Group
6. Fredrickson, E., Member, ITPA Energetic Particle Physics Topical Group
7. Gerhardt, S. Member, APS DPP Rosenbluth Award Committee 2015
8. Gerhardt, S., Member, Alcator C- Mod/Magnetic Fusion Experiments Program Advisory Committee
9. Gerhardt, S., Member, ITPA Integrated Operating Scenarios Group
10. Gorelenkov, N., Deputy Leader, USBPO Energetic Particles Topical Group
11. Gorelenkov, N., Expert, ITPA Energetic Particle Physics Topical Group
12. Guttenfelder, W., Expert, ITPA Transport and Confinement Topical Group
13. Hosea, J., Co-chair, US-Japan RF Physics Workshop
14. Hosea, J., Member, ORNL ICH COV Review for DOE
15. Jaworski, M., Member, ITPA scrape-Off-Layer and Divertor Topical Group
16. Kaye, S., Expert, ITPA Pedestal and Edge Topical Group
17. Kaye, S., Member, ITPA Transport and Confinement Topical Group
18. Kolemen, E., Assistant Professor, Princeton University
19. Kolemen, E., Group Leader, USBPO Operations and Control
20. Kolemen, E., Local Organizer MHD Control Workshop at Princeton
21. Maingi, R., Chair, ITPA Pedestal and Edge Physics Topical Group
22. Maingi, R., Expert, ITPA DiagnosticsTopical Group
23. Maingi, R., Group Leader, USBPO Pedestal, SOL and Divertor Physics
24. Maingi, R., Leader, FES-sponsored community-led PMI strategic workshop activity
25. Maingi, R., Member, Alcator C- Mod/Magnetic Fusion Experiments Program Advisory Committee
26. Maingi, R., Member, APS/DPP Distinguished Lecturers in Plasma Physics
27. Maingi, R., Member, ITPA Coordinating Committee
28. Maingi, R., Member, of the MIT PSFC Program Advisory Committee
29. Maingi, R., Technical Program Co-chair, TOFE 2014 Meeting
30. Maingi, R., Technical Program Committee Member, of the H-mode Workshop
31. Maingi, R., Technical Program Committee Member, SOFE 2015 Meeting
32. Menard, J., Chair of Local Organizing Committee for 18th International Spherical Torus Workshop
33. Menard, J., Co-chair of International Advisory Committee for China Fusion Engineering Test Reactor (CFETR)
34. Menard, J., Chair of Executive Committee of IEA Implementing Agreement for Cooperation on Spherical Tori
35. Menard, J., Member, Culham Centre for Fusion Energy Advisory Committee
36. Menard, J., Member, Alcator C-Mod Magnetic Fusion Experiments Program Advisory Committee

37. Menard, J., Member, USBPO Council
38. Menard, J., Expert, ITPA MHD, Disruptions and Control Topical Group
39. Menard, J., Member, Princeton University C7 Committee
40. Menard, J., Member, Program Advisory Committee, KSTAR Program
41. Menard, J., Member, Research Council UK Fusion Advisory Board
42. Ono, M., Member, APS DPP Program Committee 2015
43. Ono, M., Member, ISLA Program Committee 2015
44. Ono, M., Member, ISTW Program Committee 2015
45. Ono, M., Member, ICPP Program Committee 2015
46. Park, J-K., 2015 Co-chair, MHD Control Workshop at PPPL, 2015
47. Park, J-K., Committee Member, MHD Control Workshop, 2014
48. Park, J-K., Expert, ITPA MHD, Disruptions and Control Topical Group
49. Park, J-K., Panel Member, FES Transient Workshop: 3D-MPs
50. Park, J.K., Lecturer, Princeton University
51. Perkins, R., Committee Member, 21st Topical Conference on Radiofrequency Power in Plasmas 2015
52. Podesta, M., Expert, ITPA Energetic Particle Physics Topical Group
53. Podesta, M., Member, TTF Executive Committee 2015
54. Podesta, M., Member of the Editorial Advisory Board of Review of Scientific Instruments
55. Poli, F., Deputy Leader, BPO Topical Group on Integrated Scenarios
56. Poli, F., Member, US ITPA-IOS
57. Poli, F., Panel Member, FES Integrated Modeling Workshop
58. Ren, Y., Expert, ITPA Transport and Confinement Topical Group
59. Skinner, C., Expert, ITPA Diagnostics Topical Group
60. Stratton, B., Chair, PDR for ITER UV Spectroscopy Systems at ITER
61. Stratton, B., Member, ITPA Diagnostics Topical Group
62. Stratton, B., Deputy Group Leader, USBPO Diagnostics
63. Taylor, G., Expert, ITPA Diagnostics Topical Group
64. Zweben, S., Resident Associate Editor, Physics of Plasmas